Evaluation of settlement models for sand under the influence of cyclic loads induced by automatic stacking cranes

G.G.L. Simon

Delft University of Technology
Faculty of Civil Engineering and Geosciences

cover figure: Automatic stacking cranes at the Rotterdam Water Gateway container terminal. On the left an autonomous guided vehicle. In the back more automatic stacking cranes, ship-to-shore cranes and a large container ship. Source photo: `https://www.flickr.com/people/rotterdamworldgateway/` [Online; accessed March 10, 2020]

Evaluation of settlement models for sand under the influence of cyclic loads induced by automatic stacking cranes

By

G.G.L. Simon

in partial fulfilment of the requirements for the degree of

Master of Science
in Applied Earth Science
Master track Geo-Engineering

at the Delft University of Technology
to be defended publicly on Thursday June 24, 2021 at 09:15 AM.

Student number:	4178467	
Thesis committee:	Prof. Dr. C. Jommi,	TU Delft, chair
	Dr. F. Pisanò,	TU Delft
	Dr. Ir. R. C. Lanzafame,	TU Delft
	Dr. Ir. F. Bisschop,	Arcadis Nederland B.V., company supervisor

An electronic version of this thesis is available at `http://repository.tudelft.nl/`.

TU Delft Delft University of Technology

ARCADIS Design & Consultancy for natural and built assets

Preface

I would like to start off by expressing my appreciation for your interest in my Master thesis. If you have a question about my work or are interested in having a discussion about the results, feel free to contact me. I am sure you will be able to find me. I hope you will enjoy reading my Master thesis report.

This Master Thesis is the final work to fulfill my Master of Science program in Applied Earth Sciences at Delft University of Technology. The research is a collaboration between Arcadis Nederland B.V. and Delft University of Technology. I would like to thank Arcadis Nederland B.V. for this interesting graduation topic and the resources that were made available to me to carry out this research. It has been a great experience to study in the Arcadis office in Rotterdam and join the online team meetings. I will always remember the project site visit at the Rotterdam World Gateway container terminal, the scale of container terminal and the size of the container cranes are really impressive. I would also like to thank Delft University of Technology. During my Bachelor and Master I learnt a lot from the best professors about many topics in Applied Earth Sciences and Geo-engineering. Although my study has now come to an end, I will continue to specialise myself in both fields. At Delft University of Technology I had the opportunity to go on multiple study trips to Belgium, Luxembourg, Germany, France, Norway, Austria and Switzerland and on an exchange to Denmark. These were all great experiences, but they would not have been half the fun without my peers. It was a pleasure to work together with the smartest students I have met in my life and some of them became my friends. All together, Delft University of Technology has become a big part of my life. I am looking forward to come back some day.

Secondly, I want to thank my Thesis committee: Prof. Dr. C. Jommi, Dr. F. Pisanò, Dr. Ir. R. C. Lanzafame and Dr. Ir. F. Bisschop for their help and feedback throughout this period. I learned a lot from you. A special thank you goes out to Dr. Ir. F. Bisschop, the weekly meetings we helped me a lot. And a special thank you goes out to Prof. Dr. C. Jommi. During our frequent meetings you introduced me to methods and theories in the field of geotechnical engineering that helped me finding my conclusions.

I would also like to thank my friends. Having coffees together at the faculty with my peers from Geo-engineering, cooking amazing meals with the coolest housemates after a day of studying or a having a few beers at one of the annual village festivals in Twente. These moments make me really happy and I am really lucky to have you.

Finally, I would like to thank my family for all their love and support. My sister, Brecht, I look up to her because she is one of the smartest persons I know. My mom, I admire her because she has followed her dream and it made her very successful. Meanwhile she always made sure that my sister and I always had everything we needed. And my father, who taught me how to make the biggest sand castles on the beautiful beaches of Brittany when I was a little boy. Unwittingly this may have sparked my interest in geotechnics.

G.G.L. Simon
Delft, June 2021

Summary

Six cyclic settlement models for sand are evaluated to analyse the settlement of automatic stacking crane (ASC) rail tracks at the Rotterdam World Gateway (RWG) container terminal. During Phase 1 of the RWG container terminal settlement of the rail tracks occurred at multiple locations after the ASCs became operational. This has repeatedly led to (unplanned) downtime of parts of the RWG container terminal due to rail track maintenance. Settlements are caused by densification of the sand fill, which is a result of the cyclic load applied by ASCs moving continuously over their rail tracks.

The aim of this research is to contribute to prevent unplanned downtime in Phase 2 of the RWG container terminal due to rail track settlements. Also, reliable settlement predictions can be used to determine the intensity and extent of the ground compaction that are needed to meet the settlement requirement of 20 mm for ASC rail tracks.

The cyclic settlement models, which have been validated to predict the cyclic settlement of rail tracks and shallow foundations, are obtained from literature. The available soil data include CPT's, boreholes and standard laboratory soil testing. In addition, settlements of the ASC rail tracks in Phase 1 had been measured for a period of almost one year. The cyclic settlement models are evaluated at six different locations, where the sand is medium to very dense and settlements up to 32 mm have been measured. The load is modelled as a quasi-static load equivalent to a vertical stress of 60 to 90 kPa applied to the ballast-sand interface. The model parameters of the cyclic settlement models are determined by correlation, (FE) modelling of the first load cycle, extrapolation and estimation.

The zone of influence was found to reach around 6 m below the shallow foundation. Densification of the sand fill is substantial within the entire zone of influence. The maximum densification was found not to coincide with the minimum void ratio, it is a variable that depends on the initial state of the sand and the loading and soil conditions. After order 10^4 load cycles densification of the sand was found to become negligible. To meet the settlement requirement for ASC rail tracks the sand fill must consist of sand layers with a minimum and average relative density of at least 65% and 85%, respectively.

Cyclic settlement increases with the number of load cycles, amplitude of the load and extent of the zone of influence and decreases with relative density, stiffness of the sand and volumetric threshold strain. However, correlations used to calibrate the model parameters lead to model predictions that are over- or insensitive to parameters that affect the cyclic settlement. The cyclic settlement predictions of the terminal density model are most reliable and match best with the settlement measurements, for loose and medium dense sand the model predictions underestimate the settlement.

Instead of using correlations to obtain the model parameter values and decrease their uncertainty it is recommended to measure the:

- disturbance of the sand fill underneath the ASC rail tracks due to construction;
- maximum densification of the sand underneath ASC rail tracks in Phase 1 at locations where rail track settlement has stopped, i.e. where the sand reached its maximum densification;
- model parameters that characterise the cyclic densification behaviour of sand in cyclic soil tests.

This will improve the reliability of the cyclic settlement predictions of ASC rail tracks constructed on a sand fill. To validate the cyclic settlement models for ASC rail tracks on sand, measurements of the settlement with depth as function of the number of load cycles are needed.

Samenvatting

Zes cyclische zakkingsmodellen voor zand zijn geëvalueerd om de zakking van automatic stacking crane (ASC) rails op de Rotterdam World Gateway (RWG) container terminal te voorspellen. Tijdens Fase 1 van de RWG container terminal zijn op meerdere plekken rails verzakt nadat de ASCs in bedrijf werden genomen. Hierdoor moest er (ongepland) onderhoud worden uitgevoerd aan de rails waardoor de container terminal meerdere keren (gedeeltelijk) uit bedrijf is geweest. Zakkingen van de rails worden veroorzaakt door verdichting van het zandpakket, dit is het resultaat van de cyclische belasting die wordt uitgeoefend door de continu passerende ASCs.

Doel van dit onderzoek is om (ongepland) onderhoud aan ASC rails in Fase 2 van de RWG container terminal, veroorzaakt door verzakkingen, te voorkomen. Betrouwbare zakkingsvoorspellingen kunnen worden gebruikt om de intensiteit en diepte van de grondcompactie te bepalen die moet worden uitgevoerd om te voldoen aan de zakkingseis van 20 mm voor ASC rails.

De cyclische zakkingsmodellen zijn afkomstig uit de literatuur en zijn gevalideerd om zakking te voorspellen van rails of funderingen op staal. De beschikbare gronddata omvat sonderingen, grondboringen en data uit standaard geotechnisch laboratorium onderzoek. Daarnaast zijn zakkingen van de ASC rails in Fase 1 gemeten voor een periode van bijna één jaar. Zes locaties in Fase 1 zijn uitgekozen om de cyclische zakkingsmodellen te evalueren, het zand is hier matig tot zeer vast gepakt en er zijn zakkingen gemeten tot 32 mm. De belasting is gemodelleerd als een quasi-statische belasting gelijk aan een verticale spanning tussen 60 en 90 kPa aangebracht op het grensvlak van het ballastbed en de zandlaag. De waarden van de model parameters van de cyclische zakkingsmodellen zijn bepaald door correlatie, (EE) modelleren van de eerste belastingwisseling, extrapolatie en te schatten.

De zone van invloed reikt tot ongeveer 6 m onder de fundering. De diepte neemt toe met de amplitude van de belasting en neemt af met de stijfheid van het zand en de drempelwaarde van de schuifrekamplitude. Verdichting van het zandpakket is aanzienlijk in de hele zone van invloed. Het stopt zodra de maximale verdichting bereikt is. Het is bepaald dat dit niet overeen komt met het minimum poriëngetal. Verdichting van het zand na meer dan 10^4 belastingswisselingen is verwaarloosbaar. Om aan de zakkingseis voor ASC rails te voldoen moet het zandpakket in de zone van invloed bestaan uit zand met een minimale en gemiddelde relatieve dichtheid van ten minste 65% en 85%, respectievelijk.

Cyclische zakking neemt toe met het aantal belastingwisselingen, amplitude van de belasting en omvang van de zone van invloed en neemt af met de relatieve dichtheid, stijfheid van het zand en de drempelwaarde van de schuifrekamplitude. De zakkingsvoorspellingen door het 'terminal density model' zijn het betrouwbaarst en corresponderen het best met de zakkingsmetingen, echter voor los- en matig gepakt zand worden de zakkingen onderschat. De correlaties die zijn gebruikt om de waarden van de model parameters te bepalen zorgen ervoor dat zakkingsvoorspellingen over- of ongevoelig worden.

In plaats van gebruik te maken van correlaties om de waarden van model parameters te bepalen en om de onzekerheid ervan te verminderen wordt aanbevolen om:

- verstoring van het zandpakket onder de ASC rails door de constructiewerkzaamheden te bepalen;
- maximale verdichting van het zand onder de ASC rails te meten op plekken in Fase 1 waar het zakken van de rails is gestopt, oftewel waar het zand de maximale verdichting heeft bereikt;
- model parameters te meten in cyclische oedometer- en triaxiaaltesten.

Dit resulteert in betrouwbaardere zakkingsvoorspellingen van ASC rails geconstrueerd op zand. Om de cyclische zakkingsmodellen te valideren voor ASC rails op zand moeten zakkingen met de diepte en het aantal belastingwisselingen gemeten worden.

Contents

List of Figures

List of Tables

1 Introduction

Settlement is the vertical downward movement of the ground. Settlement occurs when for instance a static load is applied onto the ground, e.g. settlement induced by the weight of an embankment or a building. Periodically recurring or cyclic loads can also induced settlement, e.g. the settlement underneath rail tracks induced by train movements. The structure itself and its foundation settle along with the deformation of the soil. Uneven settlement between two adjacent points is referred to as differential settlement and it might lead to tilting of a structure. The maximum allowable (differential) settlement of a structure mainly depends on the type of structure. Eventually, settlements can become too large and it is no longer possible to (safely) operate the structure. The structure needs to be maintained or demolished and rebuild, which can lead to high costs. For container terminals also costs of downtime must be considered, which are especially high for unplanned downtime. A reliable prediction of the settlement with time is required in order to design a construction that can operate safely and efficiently throughout its lifetime.

At the Rotterdam World Gateway (RWG) container terminal in the Port of Rotterdam automatic stacking cranes (ASCs) move over one million containers per year [8]. The moving cranes apply a cyclic load to the soil underneath ASC rail tracks. A result is that the ground is settling. The container terminal, officially open since September 2015, has already been taken out of service several times for maintenance of the ASC rail tracks. This has led to high costs. Recently an expansion of the container terminal was proposed. This expansion will include the addition of multiple ASC rail tracks. Before the ASC rail tracks are designed a better understanding of cyclic settlement of sand underneath ASC rail tracks is desired. An improved geotechnical design of the ASC rail tracks should reduce maintenance costs and (unplanned) downtime of the container terminal. This study is about the prediction of the settlement of the sand layer underneath rail tracks for ASCs induced by a high number of load cycles as a result of the movements of ASCs.

1.1. Rotterdam World Gateway container terminal

Maasvlakte 2 (MV2) is a westward expansion of the Port of Rotterdam into the North Sea. It is a reclaimed land mass with a surface area of 2000 hectares in front of the coast of Rotterdam. MV2 is connected to Maasvlakte 1 (MV1), an area reclaimed from the North Sea during the 1970s (Figure 1.1). Construction of MV2 started in 2008, in 2011 the project was completed. MV2 is developed for port related industries, primarily container terminals. The RWG container terminal is one of the new container terminals located at MV2. In Figure 1.1 the RWG container terminal is indicated in green.

The RWG container terminal is a state-of-the-art container terminal. World's biggest container ships moor here to load and unload containers. At the land-side trains and trucks arrive to load and unload containers. Located in between is an area where the containers are temporarily stored by ASCs. In this area settlement of the ASC rail tracks accumulated. The area is divided into container stacks. The RWG container terminal consists of 25 stacks and each stack is about 330 meters long, 10 or 12

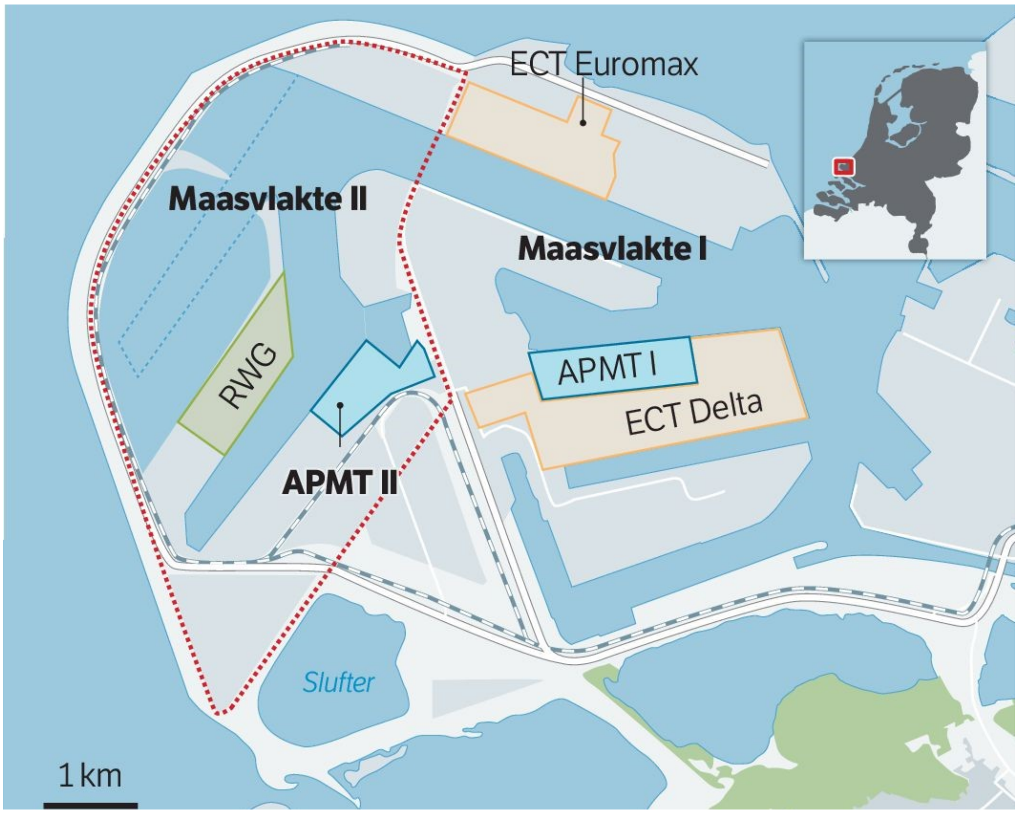

Figure 1.1: MV1 and MV2. The RWG container terminal is indicated by the green bottom-side-up left trapezoid [22] .

containers wide, and can be up to 5 containers high.

The entire process is automated and managed from a control room. After a container is unloaded from a ship by a ship-to-shore (STS) container crane, it is lifted onto an autonomous guided vehicle (AGV). The AGV transports the container over a small distance to an ASC. The ASC stores the container temporarily in its stack. Figure 1.2 shows a photo of a few container stacks and ASCs at a terminal similar to the RWG container terminal. At each stack two ASCs are installed. The second ASC will lift the container from the stack and moves it to the other end of the ASC rail track. Here the container is loaded onto a truck or train and transported inland. A container that arrives at the container terminal by truck or train will undergo the same process, but in the opposite order. The system at the RWG container terminal is designed by Kalmar [6], an info graphic of this system can be found in Appendix F.

The RWG container terminal has reached its full capacity of 2.35 million TEU (twenty-foot equivalent unit) per year. A result of the container market volume growth in the Port of Rotterdam [7]. Consequently, RWG has been looking to expand its container terminal, preparations commenced recently. The expansion of the container terminal is referred to as Phase 2. Figure 1.3 presents an aerial view of the current lay-out of the RWG container terminal, referred to as Phase 1 (Fase 1), and the location for Phase 2 (Fase 2).

During the test and start-up period of Phase 1, settlement underneath the rail tracks was observed at multiple locations after the ASCs started moving. However some settlements were expected, the magnitude of the (differential) settlements that occurred made maintenance of the crane rail tracks necessary. The rails had to be levelled in order to enable the operations of the ASCs. It was concluded by several investigations that cyclic loads as a result of the movements of the ASCs (partially) induced the settlements of the rail tracks. It is known that cyclic loads can induce densification of a sand packing (see Figure 1.4). Compaction work has been carried out before construction of the rail tracks, this was however, executed locally and only at shallow depths. Due to strict (differential) settlement re-

Figure 1.2: Photo of a few stacks at the Dubai Ports World London Gateway terminal. Each stack contains two ASCs. The containers are temporarily stacked underneath the ASCs. The same system is employed at the RWG container terminal [6].

Figure 1.3: Aerial view of the RWG container terminal, Phase 1 (Fase 1) and Phase 2 (Fase 2) are indicated. Phase 1 was completed in 2014, preparations for Phase 2 have started [32]

quirements for ASC rail tracks, maintenance was required several times during the terminal's start-up period. Currently the ASC rail tracks are maintained annually to prevent derailment. The amount of settlement has become less with time.

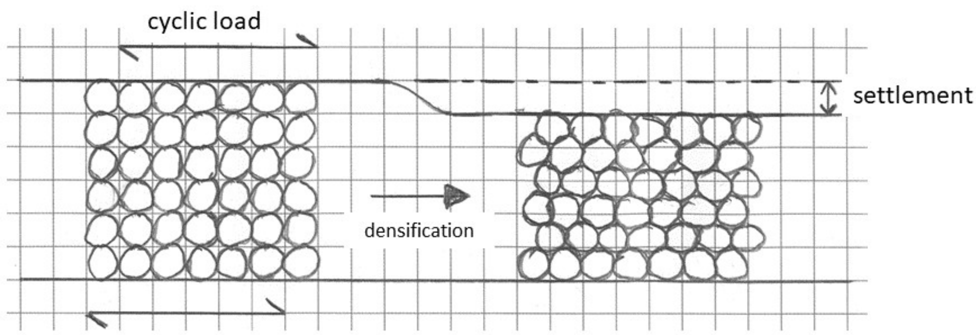

Figure 1.4: Densification of a sand layer induced by a cyclic load.

To improve operation of the ASCs in Phase 2 compaction of the first $5m$ of the sand fill is foreseen in order to decrease the (differential) settlements and to keep them within the limits set by the requirements for ASC rail tracks. A small part of the area of Phase 2 has recently been improved using the Cofra dynamic compaction (CDC) method 1.5. The CDC method and its effect on a sand packing are illustrated by Figures 1.6 and 1.7. Application of this method involves dropping a heavy weight 20 to 60 times per minute onto a metal footing for a maximum of a few minutes. Impact of the weight onto the footing generates a vibration into the subsurface. The sand particles contract which causes compaction of the sand layer. This method is also known as the rapid impact compaction (RIC) method.

Figure 1.5: Compaction of the Phase 2 area at the RWG container terminal with the CDC-method. In the background the operating RWG container terminal (Phase 1).

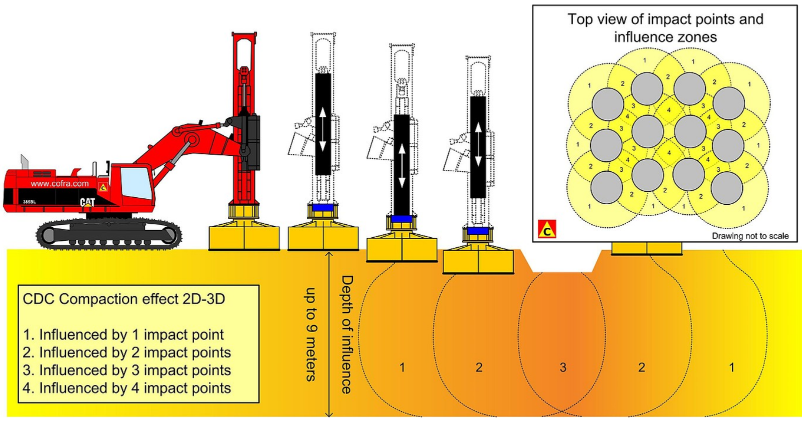

Figure 1.6: The CDC-method [5].

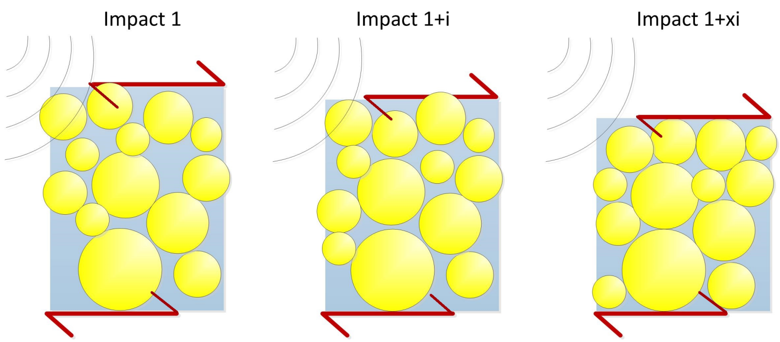

Figure 1.7: Compaction mechanism in sand during application of a CDC-method [5].

1.2. Problem

In order to decrease maintenance of ASC rail tracks as a result of (differential) settlements in Phase 2, influence of an ASC's movements on the settlement was predicted using different cyclic settlement models. Existing cyclic settlement models however, are still in development. The models used show a wide range in settlement predictions.

Arcadis used two different cyclic settlement models to predict the settlement in Phase 2. The compaction / liquefaction (C/L) model [46] and the Hergarden model [25]. These models have been selected because they are relatively simple to implement and validated for applications involving cyclic loads. Both methods are strongly empirical. Based on the model predictions compaction of the first $5m$ of the sand fill underneath ASC rail tracks was suggested.

Although both models predict that settlement induced by cyclic loads will occur, variation between the model predictions is relatively large. Furthermore, reliability of the predictions are unknown. This is caused by uncertainties related to the sensitivity of the cyclic settlement models. As a consequence it is not possible to accurately determine the extent (depth) and intensity of compaction that is needed to meet the (differential) settlement requirements for ASC rail tracks.

1.2.1. Settlement requirements

The very strict (differential) settlement requirements that apply to ASC rail tracks make a reliable prediction of the cyclic settlement important. Settlement requirements for ASC rail tracks are based on the operation tolerances defined in Table 7 of ISO 12488-1: tolerances for wheels and travel and traversing tracks of cranes [26]. Table 7 and also Table 1 of ISO 12488-1 are attached in Appendix F. This document describes tolerances for safe operation, or the serviceability state, of crane rail tracks. These are stricter than the tolerances for ASCs that define the serviceability and ultimate limit state of an ASC.

The operation tolerances for crane rail tracks are therefore decisive in this research.

ASC rail tracks belong to tolerance class 1. This class consists of rail tracks for cranes travelling over 50.000 km during their lifetime. For ASC rail tracks that fall in tolerance class 1 the 'tolerance of horizontal straightness of rail head at each point of the rail track' and the 'tolerance of height related to opposite measuring points at right angles at each point of the track' are both $\pm 10\ mm$. The tolerances are indicated by symbols B_{w1} and E_{w1} in Table 7 of ISO 12488-1, respectively. They are translated to an absolute settlement requirement for the whole length of the ASC rail tracks of 20 mm.

1.2.2. Densification and compaction

Densification and compaction both mean the permanent decrease in porosity of a sand as a result of rearranging grains under the influence of a load [49]. The result is an increase of the density of the sand. In this report the term densification is used to describe the increase in density of the sand underneath the ASC rail tracks induced by a cyclic load as a result of the movements of the ASCs. Compaction will be used to refer to an increase in density of the sand as a result of construction works and ground improvements.

1.2.3. Cyclic behaviour of sands

A sand subjected to a (cyclic) load deforms. Strains accumulate in the sand. Behaviour of sand under the influence of a cyclic load depends on the level of strain induced by the applied load. Below the elastic threshold strain this leads to elastic strains at the sand grain contacts. When the load is removed (at the end of a load cycle) the sand grains take their original shape and position. Fabric of the sand has not changed. For strains larger than the elastic threshold strain and below the volumetric threshold strain, fabric of the sand changes permanently. This is caused by rearrangement of the sand grains but without permanently changing the volume of the sand [55]. Vertical plastic strain, and consequently settlement, might accumulate under these conditions as a result of accumulation of deviatoric plastic strain. This will be a relatively small amount of settlement. For strain levels, above the volumetric threshold strain, volume of the sand changes permanently. Volumetric plastic strains accumulate. This results in settlement of the sand [39]. The threshold strain values depend on the type of sand and are independent of the density of the sand.

Long-term behaviour with regards to shear strain accumulation in sands is described by shakedown or ratcheting. Shakedown means that shear strain accumulation within a load cycle decreases till zero with increasing number of load cycles. In contrast, ratcheting is the continuous accumulation of shear strains in sand [39].

Density of a sand evolves asymptotically towards a stable value under the influence of a constant cyclic load. At this density the strain level induced by a constant cyclic load becomes smaller than the volumetric threshold strain. The volumetric plastic strain within a load cycle becomes zero [37]. In a ratcheting state shear strains will continue to accumulate while density of the sand remains stable. In a shakedown state also shear strains within a load cycle become zero.

1.3. Objective and research questions

The aim of this research is to contribute to prevent unplanned downtime in Phase 2 of the RWG container terminal due to rail track settlement. The main research objective is to evaluate a cyclic settlement model that can make reliable predictions of the settlement induced by a cyclic load as a result of the movements of ASCs at the RWG container terminal. This cyclic settlement model will be used to predict settlement of ASC rail tracks of the Rotterdam World Gateway container terminal Phase 2. Based on this settlement prediction the extent and intensity of the compaction of the sand layer is determined in order to minimise (differential) settlement of the sand layer and decrease (unplanned) downtime at the RWG container terminal.

The following questions will have to be answered to carry out the research objective:

1. Which parameters (soil properties, load parameters) affect densification of a sand layer (and resulting cyclic settlement) induced by a cyclic load as a result of the movements of automatic stacking cranes?
2. How reliable are the cyclic settlement predictions made by the evaluated model for the Rotterdam World Gateway container terminal Phase 2 and how do the results compare to the (differential) settlement requirements for automatic stacking crane rail tracks?
3. How should the cone penetration test profile of a sand fill look like in order to meet the (differential) settlement requirements for automatic stacking crane rail tracks?

1.4. Methodology and approach

In this study three research methods are combined, a literature study, data analysis and modelling. In Figure 1.8 the work flow adopted in this research is schematised.

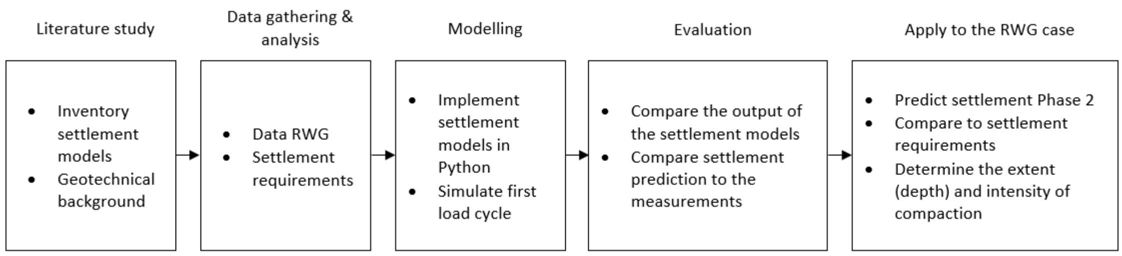

Figure 1.8: Flowchart of this research.

1.4.1. Literature study

A lot of research related to cyclic settlement of sand has been carried out in the (recent) past. Numerous cyclic settlement models are described in literature. These models have been developed for various applications including vibratory sheet piling, seismically-induced settlements and settlement underneath roads, highways, runways and rail tracks. The literature study consists of an inventory of existing cyclic settlement models and a study of the relevant background information. A summary of the literature study is added to the report. It describes six cyclic settlement models that are evaluated during this research to predict settlement of sand underneath ASC rail tracks.

1.4.2. Data analysis

The data that describe the local conditions at the RWG container terminal is acquired from site investigations that were carried out years ago for the purpose of constructing MV2 and the RWG container terminal. It is made available for this research and consist primarily of soil investigation data and reports, design reports, internal memo's and measured rail track settlement. The gathered data from the RWG container terminal are analysed in order to determine the local conditions and to estimate the model parameter values of the cyclic settlement models. Secondly, model predictions from the six cyclic settlement models are analysed and compared with the settlement measured in Phase 1 of the RWG container terminal. Finally, one of the cyclic settlement models is used to predict the settlement in Phase 2 of the RWG container terminal. Based on the results the extent (depth) and intensity of compaction of the sand in Phase 2 of the RWG container terminal is determined.

1.4.3. Modelling

The modelling part of this research consists primarily of implementation of the cyclic settlement models from the inventory. For each model its equations are converted into a computational method which outputs a prediction of the settlement. Additionally, small improvements are implemented in the models. The first load cycle is simulated in an FE model and with the improved Schmertmann method. The improved Schmertmann method is a settlement model for sands under the influence of a static load [52]. The cyclic settlement models and improved Schmertmann method are implemented in Python, a computer programming language [3]. During this research Python version 3.7 is used in a Spyder environment [4].

1.5. Thesis outline

This thesis report is a summary of the research that is conducted in order to give a reliable prediction of the cyclic settlement underneath ASC rail tracks as a function of the number of load cycles. Six cyclic settlement models are evaluated in this research. They are implemented in Python and the model parameter values are estimated based on the input data. The current chapter gives an introduction of the problem and the research.

Chapter 2 summarises six cyclic settlement models that are obtained during the literature study that is carried out. These models are developed to determine settlement of sand induced by a cyclic load. The improved Schmertmann method is explained.

In Chapter 3 the gathered data are described. Data are gathered during several site investigations that have been carried out for the purpose of constructing MV2 and the RWG container terminal. Model parameter values are determined by the data.

Chapter 4 starts with a discussion about the uncertainty of the input data, model parameter values and model predictions of the cyclic settlement models. Preliminary results that follow from the literature study, gathered data and simulation of the first load cycle are presented and discussed. Subsequently, model predictions of the cyclic settlement models is presented and discussed. Model predictions of the cyclic settlement models is compared to settlement measurements. One cyclic settlement model is selected to predict the settlement underneath the ASC rail tracks of Phase 2. Based on the settlement predictions extent and intensity of compaction of the sand fill is determined.

Finally, in Chapter 5 the research questions are answered and recommendations are presented. A distinction is made between recommendations related to the research objective and recommendations related to construction and operation of ASC rail tracks at the RWG container terminal. The first group of recommendations focuses on gathering data in order to decrease uncertainty of the model parameters of the cyclic settlement models in order to obtain more reliable model predictions. The second group gives recommendations related to the extent and intensity of compaction of the sand before construction of ASC rail tracks.

2

Settlement models for cyclic loaded sand

Many (cyclic) settlement models have been developed and validated specifically for one, or possibly a few, applications. To the author's knowledge no specific models have been developed for settlement underneath rail tracks of ASCs. The cyclic settlement models that are evaluated in this research have been initially developed for different applications. The concept behind each of the selected cyclic settlement models is summarised in this chapter.

Whether a model is suitable to predict the settlement is case dependent and is determined by multiple factors, including:

- soil conditions;
- loading conditions;
- desired output;
- available data.

For example, there are models suitable to predict the settlement underneath an embankment on top of a saturated clay with a low hydraulic conductivity. Other models are more suitable to predict the settlement in (dry) sands under drained conditions near vibratory sheet piling. When the settlement is the result of a cyclic load, a prediction of the settlement as a function of the number of load cycles is desired and not just the total settlement. Moreover, in engineering practice, the choice for a settlement model is also driven by the available data. When a model parameter of the settlement model cannot be determined from the available data its value will be estimated. This will increase the uncertainty of the settlement prediction.

Each settlement calculation involves roughly three steps [49]:

1. determine the zone of influence;
2. determine the stress within the zone influence;
3. calculate the plastic strain according to the selected settlement model.

The amplitude of the load is related to the applied load. Due to damping the amplitude of the load decreases with distance from its source and at a certain distance becomes too small to induce plastic strains. The extent of the domain wherein plastic strains occur induced by the load is the zone of influence. Its depth is called the depth of influence. The final step involves applying the settlement model to calculate the plastic strains inside the zone of influence and subsequently the settlement.

This research focuses on cyclic settlement models for sands. These models are developed to predict the response of sands to a large number of load cycles. For this research they are evaluated to predict the settlement of the sand underneath the ASC rail tracks as a result of the cyclic load applied by the ASCs at the RWG container terminal. Cyclic settlement models can be divided into three groups based on their approach [35]:

1. density increase until the maximum densification is reached;
2. calculate the strain within each load cycle;
3. calculate the plastic strain at the end of each load cycle.

The first group of cyclic settlement models assumes a maximum increase in density as a result of the applied load cycles. These cyclic settlement models output the total plastic strain (as the number of load cycles $N \rightarrow \infty$), but not as a function of the number of load cycles. This is indicated in Figure 2.1 by the black dot. Depending on the model the maximum density is a function of the initial state of the soil, soil conditions including the minimum and maximum void ratio, stiffness and volumetric threshold strain and the loading conditions. The cyclic settlement models in the second group compute the behaviour of the sand within each load cycle based on the evolution of the stresses and strains. Advanced numerical soil models are used to compute this behaviour. The strain generated in the loading phase is partially reversed in the unloading phase. With increasing number of load cycles the plastic strain increases. The wave form of the solid line in Figure 2.1 represents the evolution of strain within each load cycle, which consists of elastic and plastic strains. This approach involves multiple computational steps per load cycle. Especially in problems that involve a large number of load cycles this costs substantial computational effort. Secondly, in each computational step a small numerical error is introduced, for a large number of load cycles this error becomes significantly large and the output becomes unreliable. The third group of cyclic settlement models does not consider the strain within each load cycle but only describes the plastic strain at the end of each load cycle. This is displayed in Figure 2.1 by the dashed line. The plastic strain is given as a function of the number of load cycles. The majority of the cyclic settlement models evaluated in this research belongs to the third group. The Hergarden model, described in Section 2.2, belongs to the first group. No cyclic settlement models from the second group are considered in this research due to the large number of load cycles involved in this problem, the numerical error would become too large.

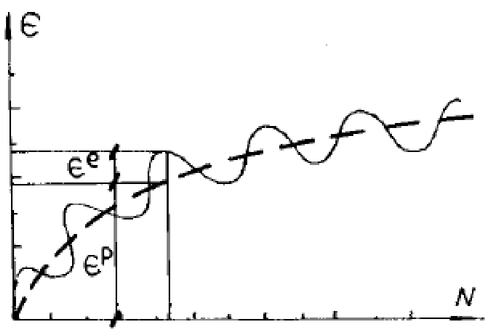

Figure 2.1: Cyclic densification of a dry sand modelled by the three different groups of cyclic settlement models. The maximum plastic strain at $N \rightarrow \infty$ is indicated by the black dot (group 1), the strain within each load cycle by the solid line (group 2) and the plastic strain at the end of each load cycle by the dashed line (group 3) [46].

The total plastic strain consists of the volumetric plastic strain and the deviatoric plastic strain. The cyclic settlement models output is given either in terms of vertical plastic strain, which is related to the settlement, or in volumetric plastic strain. In the latter case, the vertical component of the volumetric and deviatoric plastic strain will need to be determined. Combined they make up the vertical plastic strain which is needed to calculate the settlement.

In the upcoming sections the plastic strain calculations of six selected cyclic settlement models is described. The settlement models are described each in its own section. This is followed by a description of the improved Schmertmann method. This method is used to calculate the vertical strain in a sand as a result of a static load. This method is used to estimate the vertical plastic strain after one load cycle. In the final section the cyclic settlement models are compared to each other and an overview of the model parameters of the six models is given.

2.1. Compaction / Liquefaction model

A cyclic load applied to a sand induces densification of the sand. Densification is defined as the permanent decrease in porosity:

$$\Phi = \frac{\Delta n}{n_0} \tag{2.1}$$

with

Φ = densification, [-],
$\Delta n = n_0 - n$ = change in porosity, [-],
n_0 = initial porosity, [-].

The Compaction / Liquefaction (C/L) model describes densification of dry and saturated sands in drained conditions as a function of the number of load cycles (for saturated sands in undrained conditions it describes the pore pressure generation as a function of the number of load cycles) [46]. The C/L model is based on the analysis of the mechanical behaviour of several different particulate materials, such as sands, in cyclic simple shear and cyclic oedometer tests. A result is that two versions of the C/L model exist. The C/L model for cyclic shear describes densification of sands induced by cyclic (simple) shearing [45] [46]. The C/L model for cyclic oedometer compression describes the densification of sands under cyclic uni-axial lateral constrained compression [48] [49]. In both versions densifiction increases with increasing number of load cycles and amplitude of the load. The rate of densification decreases with the number of load cycles. This is described by:

$$\frac{d\Phi}{dN} = D_1 J e^{-D_2 \Phi} \tag{2.2}$$

with

N = number of load cycles, [-],
D_1, D_2 = material constants, [-],
J = second invariant of the strain or stress tensor, [-].

In the C/L model for cyclic shear J becomes the second invariant of the strain tensor. In the C/L model for cyclic oedometer compression J becomes some invariant of the stress tensor. Integration of Equation 2.2 over N gives:

$$\Phi = c_1 ln(1 + c_2 z) \tag{2.3}$$

with

$c_1 = \frac{1}{D_1}$ = material constant related to D_1, [-],
$c_2 = D_1 D_2$ = material constant related to D_1 and D_2, [-],
$z = JN$ = variable related to the invariant J and the number of load cycles, [-].

In Figure 2.2a the results from three cyclic oedometer tests on a medium dense 'Leighton Buzzard' sand with varying vertical stress amplitude are plotted as a function of the number of load cycles. In Figure 2.2b the same data is plotted in the Φ, z-plane. In this plane it is possible to fit one curve through all the data, called the 'common compaction curve'. The same can be done with data from cyclic simple shear tests with varying cyclic shear strain amplitude. The 'common compaction curve' characterises the densification properties of a sand. The material constants c_1 and c_2 (and D_1 and D_2) are determined by fitting Equation 2.3 to the 'common compaction curve'.

The 'common compaction curve' and the values of the material constants c_1 and c_2 of the same sand type vary between the two versions of the C/L model. The behaviour of a sand in cyclic simple shear tests is different compared to its behaviour in cyclic oedometer tests, as a result of the different loading and boundary conditions. The material constants should therefore be determined with a cyclic test that best mimics the loading and boundary conditions of the case analysed. According to the C/L model densification of a sand is uniquely determined by the type of sand, its initial relative density, the type of loading and the boundary conditions. This does not include the amplitude of the load. The

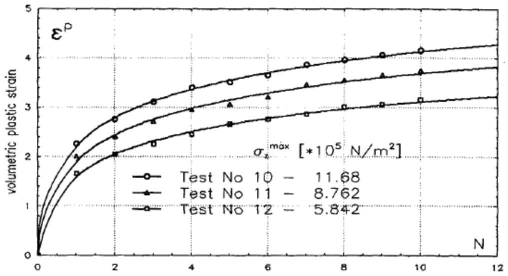

(a) Densification plotted as a function of the number of load cycles.

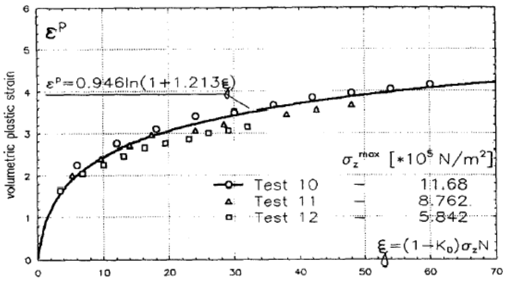

(b) Densification plotted in the Φ, z-plane together with the 'Common compaction curve'.

Figure 2.2: Densification of a medium dense 'Leighton Buzzard' sand in three cyclic oedometer tests with varying vertical stress amplitude [48]. In this figure Φ and z from Equation 2.3 are indicated with ε^p and ξ, respectively.

C/L model assumes that densification of a sand under the influence of a load with a large amplitude is the same under the influence of a load with a small amplitude but after a larger number of load cycles.

2.1.1. C/L model for cyclic shear

In the C/L model for cyclic shear the second invariant of the strain tensor J in Equation 2.3 becomes a function of the cyclic shear strain amplitude:

$$J = \frac{1}{4}\gamma_0^2 \tag{2.4}$$

with

J = second invariant of the strain tensor, [-],
γ_0 = cyclic shear strain amplitude, [-].

The cyclic shear strain amplitude is half of the difference between the maximum shear strain during the loading and unloading phase. The strains and also the cyclic shear strain amplitude, induced by a cyclic force can be determined with a finite-element method (FEM) computation [46]. Note that the cyclic shear strain amplitude and the invariant have a unit 10^{-3} and 10^{-6}, respectively. Substitution of the second invariant J into Equation 2.3 gives:

$$\Phi = c_1 ln(1 + c_2\frac{\gamma_0^2 N}{4}) \tag{2.5}$$

with

Φ = densification, [-].

The volumetric plastic strain as a result of the densification is calculated as follows:

$$\varepsilon^p_{vol,N} = -\Phi \cdot \frac{n_0}{1-n_0} = -\Phi \cdot e_0 \tag{2.6}$$

with

$\varepsilon^p_{vol,N}$ = volumetric plastic strain after N load cycles, [-],
e_0 = the initial void ratio, [-].

Densification and volumetric plastic strain both have unit 10^{-3}.

Equation 2.5 shows that densification increases with the number of load cycles, the cyclic shear strain amplitude and the material constants c_1 and c_2. The first two model parameters comprise the load parameters. The cyclic shear strain amplitude increases with the amplitude of the load. The material constants comprise the soil parameters. The material constants increase with decreasing initial relative density, reflecting that densification is larger for loose sands than for dense sands. To obtain the volumetric plastic strain the densification is multiplied by the initial void ratio in Equation 2.6. The volumetric plastic strain increases with increasing void ratio, again reflecting that the settlement is larger for loose materials. The initial void ratio gives the initial state of the sand.

2.1.2. C/L model for cyclic oedometer compression

In this version of the C/L model the invariant J from Equation 2.3 becomes a function of the vertical stress amplitude:

$$J = \sigma_z - \sigma_x \tag{2.7}$$

with

J = invariant of the stress tensor, $[10^2\ kPa]$,
σ_z = the stress in the vertical direction, $[10^2\ kPa]$,
σ_x = the stress in the horizontal direction, $[10^2\ kPa]$.

Due to the zero-lateral strain boundary condition only vertical strains accumulate. Densification is therefore equal to the vertical plastic strain. Substituting $\varepsilon_{v,N}^{p}$ and Equation 2.7 into Equation 2.3 gives:

$$\varepsilon_{v,N}^{p} = c_1 ln(1 + c_2(\sigma_z - \sigma_x)N) \tag{2.8}$$

The vertical plastic strain has unit 10^{-3} and the stresses unit $10^2\ kPa$.

The total vertical plastic strain calculated in Equation 2.8 increases with the number of load cycles, the amplitude of the stresses and the material constants c_1 and c_2. The number of load cycles and the amplitude of the stresses comprise the load parameters. The amplitude of the stresses increases with the amplitude of the load. The material constants comprise the soil parameters of the sand. The material constants increase with decreasing initial relative density, reflecting that densification is larger for loose sands than for dense sands. The material constants can be determined with a cyclic oedometer test. Implicitly they incorporate the initial state of the sand. Equation 2.8 does not contain a parameter which explicitly defines the initial state of the sand.

2.2. Hergarden model

The Hergarden settlement model is developed by R. Hergarden to predict the settlement of the surrounding ground level during vibratory sheet piling [25]. This model is described by CUR166 [17] and is evaluated by Meijers [34]. The third step of the settlement calculation, the plastic strain calculation, is based on work from D.D. Barkan [11]. In the Netherlands the Hergarden model is used to predict the settlement of sandy soils induced by the vibrations generated during installation or removal of sheet pile walls [38].

A propagating vibration causes deformation of the sand, which returns partially to its original shape after the vibration has passed. Figure 2.3 shows a wave generated by an ASC propagating vertically through the sand. A large number of vibrations can cause significant deformation of the sand surrounding the vibratory source. To calculate the corresponding densification the magnitude of the vibration is expressed in terms of acceleration. This is the acceleration of the sand grains induced by the propagating vibration. At depths at which the amplitude of the acceleration, normalised by the acceleration of gravity, lies above the threshold acceleration an increase in the relative density will occur:

$$\Delta D_R = \begin{cases} e^{-\alpha_B \eta_0} - e^{-\alpha_B \eta}, & \text{if } \eta_0 < \eta \\ 0, & \text{if } \eta_0 \geq \eta \end{cases} \tag{2.9}$$

with

ΔD_R = increase in relative density, [-],
α_B = Barkan parameter (value varies between 3 to 5), [-],
η = amplitude of the acceleration of the vibration normalised by the acceleration of the gravity, [-],
η_0 = threshold acceleration, [-].

The amplitude of the acceleration of the vibration normalised by the acceleration of the gravity (η) and the threshold acceleration (η_0) are defined below:

$$\eta = \frac{a}{g} \tag{2.10a}$$

$$\eta_0 = \frac{ln(1 - D_{R,0})}{\alpha_B} \tag{2.10b}$$

with

$D_{R,0}$ = initial relative density, [-],
a = amplitude of the acceleration of the vibration, $[m \cdot s^{-2}]$,
g = acceleration of the gravity, $[m \cdot s^{-2}]$.

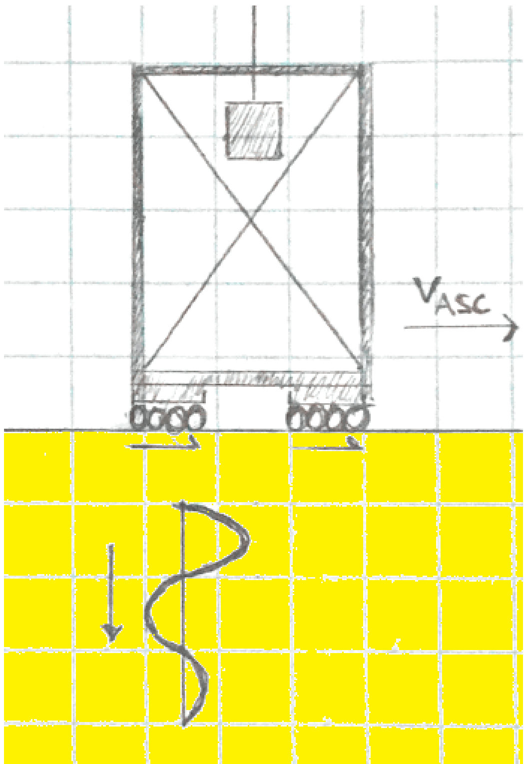

Figure 2.3: A vibration generated by an ASC vertically propagating through a sand layer. The amplitude of the acceleration of a vibration is decreasing with distance from its source due to material and geometric damping.

The Hergarden model assumes that the vibration continues until densification is complete. The sand evolves to a denser state and additional densification can only be induced by vibrations that are stronger compared to the initial vibrations. Based on the increase in relative density induced by the vibrations the volumetric plastic strain is determined:

$$\varepsilon_{vol}^p = \Delta D_R \frac{e_{max} - e_{min}}{1 + e_0} \tag{2.11}$$

with

ε_{vol}^{p} = volumetric plastic strain, [-],
ΔD_R = change in relative density, [-],
e_{max} = maximum void ratio, [-],
e_{min} = minimum void ratio, [-],
e_0 = initial void ratio, [-].

The Hergarden model differs from the other models discussed in this chapter because it is the only model that does not determine the densification as a function of the number of load cycles and therefore only outputs the maximum densification. Moreover, it is the only cyclic settlement model described here which considers the dynamic effects of a load. This can be recognised by the different terminology and model parameters that describe the model, such as amplitude of the acceleration of the vibration instead of amplitude of the load. The dynamic effects of the load are incorporated in the amplitude of the acceleration of the vibration. The other cyclic settlement models model the load as a quasi-static (cyclic) load and neglect the dynamic effects.

Densification (increase in relative density) increases with the amplitude of the acceleration of the vibration, according to Equation 2.9. The amplitude of the acceleration is a load parameter and it increases with the amplitude of the load applied by the ASC and its velocity and acceleration. The Hergarden model assumes that the amplitude of the load uniquely determines the densification, in contrast to the C/L models. The threshold acceleration in Equation 2.10b becomes more negative with increasing initial relative density. This results in less densification. The initial relative density gives the initial state of the sand. Further, the threshold acceleration decreases (densification of the sand increases) with increasing Barkan parameter. This parameter varies between 3 and 5. A Barkan parameter equal to 3 corresponds to high stress levels and strengths of the sand; its value is equal to 5 for low stress levels and strengths of the sand. The studied literature about the Hergarden model does not specify what is considered as low or high stress levels and strengths. The Barkan parameter is considered a soil parameter because it determines the soils resistance against deformation. The volumetric plastic strain corresponding to the change in relative density is calculated with Equation 2.11. The volumetric plastic strain increases with increasing difference between the minimum and maximum void ratios. Together with the Barkan parameter, the minimum and maximum void ratios comprise the soil model parameters of the Hergarden model.

2.3. Terminal density model

The terminal density of a soil is defined as the density at which the soil under the given loading and boundary conditions remains constant (terminal stands for final in this context and is not related to container terminal). The density of a soil at its terminal density does not change as long as these remain constant. The terminal void ratio is the void ratio corresponding to the terminal density. The range of terminal densities of a granular material is defined by its boundaries, the very dense state, and the state that is very loose. Examples of known soil states that fall under this definition of the terminal density are the minimum and maximum void ratio [16] [37] [39].

Under the influence of a cyclic load the density of a sand will evolve asymptotically with number of load cycles towards the corresponding terminal density, this is displayed in Figure 2.4. It shows the densification as a function of the number of load cycles of a medium dense (initial relative density is 44%) and a dense (initial relative density is 86%) sand sample in a cyclic oedometer test. The void ratios of the two samples decrease with the number of load cycles. The change in void ratio in the first load cycle is significantly larger compared to the other load cycles, for both samples. With increasing number of load cycles the rate at which the void ratio evolves towards the terminal void ratio decreases, i.e. the plastic strain per load cycle decreases with increasing number of load cycles. A sand reaching its terminal density under the influence of a cyclic load will display zero plastic strain during the subsequent load cycles. The data also shows that the initial void ratio influences the terminal void ratio. The dense sample has a lower terminal void ratio compared to the medium dense sample. However, the change in void ratio to reach the terminal void ratio is smaller for the dense sample, i.e. densification of the dense sample is smaller

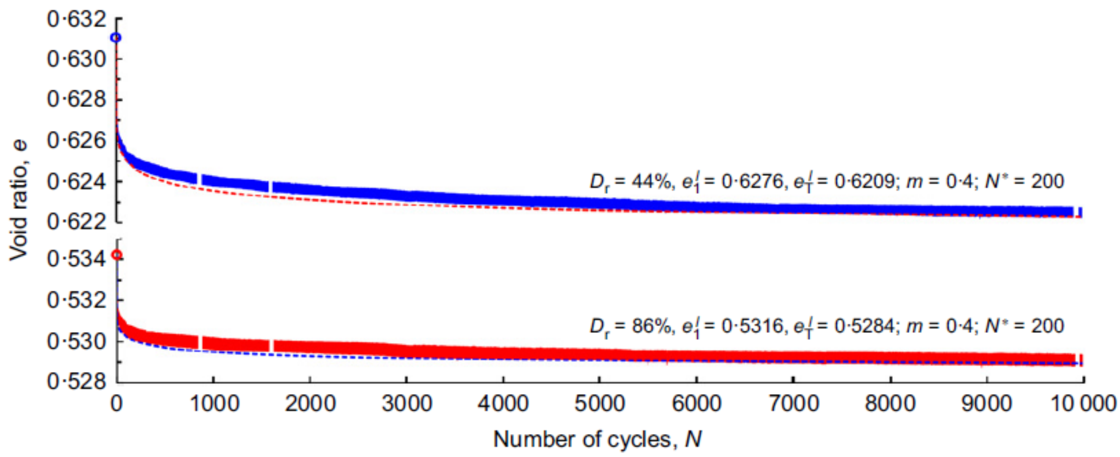

Figure 2.4: The evolution of the void ratio with the number of load cycles in a cyclic oedometer test of a medium dense sand (blue), initial relative density is 44%, and a dense sand (red), initial relative density is 86% [39].

The terminal density model is based on the mechanical behaviour of sand in a stress-controlled cyclic oedometer tests [39]. It describes the evolution of the void ratio towards the terminal void ratio with increasing number of load cycles:

$$e_N = e_T + (e_1 - e_T)[1 + (\frac{N-1}{N^*})^m]^{-1} \tag{2.12}$$

with

e_N = void ratio after N load cycles, [-],
e_T = terminal void ratio, [-],
e_1 = void ratio after one load cycle, [-],
N = number of load cycles, [-],
N^* = characteristic number of load cycles, [-],
m = fitting parameter, [-].

Equation 2.12 calculates the void ratio after N load cycles, which lies in between the initial and the terminal void ratio. The volumetric plastic strain after N load cycles is:

$$\varepsilon_{vol,N}^{p} = \frac{e_o - e_N}{1 + e_0} \tag{2.13}$$

with

$\varepsilon_{vol,N}^{p}$ = volumetric plastic strain after N load cycles, [-],
e_0 = initial void ratio, [-].

Densification increases (void ratio decreases) with the number of load cycles, according to Equation 2.12. The number of load cycles is the only explicitly defined load parameter in the terminal density model. The amplitude of the load is implicitly incorporated in the terminal density model. The void ratio after one load cycle and the terminal void ratio decrease with increasing amplitude of the load. The amplitude of the load therefore uniquely determines the densification. The void ratio after one load cycle and the terminal void ratio also depend on the initial state of the sand, they decrease with decreasing initial void ratio. However, in this model these void ratios are considered as soil parameters, because they characterise the densification behaviour of the sand. The terminal void ratio can be determined in a cyclic soil test. The model given in Equation 2.12 is based on oedometer tests. In order to use this equation the terminal density can best be determined from a cyclic oedoemeter test. The terminal density is reached when the plastic strain in a load cycle becomes zero. Note that this is the terminal density under the given conditions. For a different amplitude of the load or under the influence of different loading and boundary conditions the terminal density will be different. The parameters m and N^* determine the rate at which the void ratio evolves towards the terminal void ratio and are therefore also soil parameters. m is a fitting parameter, its value is $m = 0.45 \pm 0.05$. At $N = N^* + 1$ the sand has reached half of its total densification. In very loose sands $N^* \rightarrow 1000$ and in very dense sands $N^* \rightarrow 1$ [39]. In a very dense sand the total densification is small, half of the densification occurs in the first two load cycles. In looser sand the total densification is larger and the number of load cycles before half of the densification has occurred increases. Note that the densification in the first load cycle in the loose sand will be larger compared to the dense sand. The difference between the initial void ratio and the terminal void ratio defines the maximum densification. The initial void ratio gives the initial state of the sand.

2.4. Seismic induced strain model

During a number of strain-controlled cyclic simple shear tests with varying cyclic shear strain amplitudes on several types of sand it was observed that [21]:

1. vertical plastic strain increases with the number of load cycles;
2. vertical plastic strain per load cycle decreases;
3. most of the total vertical plastic strain accumulates during the first few load cycles;
4. during the first 10 to 15 load cycles the shear stress has to increase in order to maintain a constant cyclic shear strain amplitude, thereafter the cyclic shear stress remains constant.

This behaviour is displayed in Figure 2.5 which shows three plots of the cyclic shear strain, cyclic shear stress and the total vertical plastic strain versus the number of load cycles of a typical dry sand in a strain-controlled cyclic simple shear test.

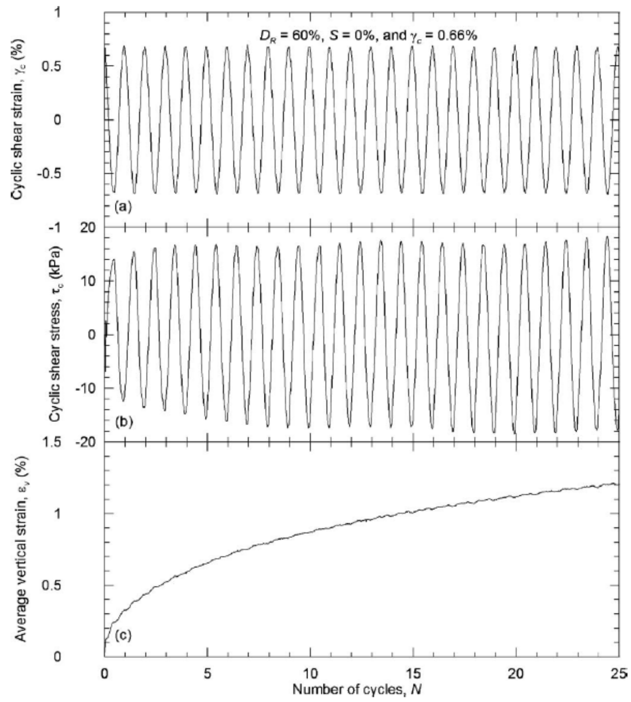

Figure 2.5: Behaviour of a dry Silica No.2 sand with a relative density of 60% in a strain-controlled cyclic simple shear test during the first 25 load cycles; a) cyclic shear strain vs. number of load cycles; b) cyclic shear stress vs. number of load cycles; and c) vertical strain vs. number of load cycles [21].

Accumulation of the vertical plastic strain in Figure 2.5c is described by two equations, which have been used to estimate the settlement of a sand layer induced by seismic shaking [54]. The first equation gives the relation between the vertical plastic strain after 15 load cycles and the cyclic shear strain amplitude:

$$\varepsilon^p_{v,N=15} = a(\gamma_0 - \gamma_{tv})^b \tag{2.14}$$

with

$\varepsilon^p_{v,N=15}$ = vertical plastic strain after 15 load cycles, [-],
γ_0 = cyclic shear strain amplitude, [-],
γ_{tv} = volumetric threshold strain, [-],
a = material constant depending on the type of sand and its relative density, [-],
b = material constant depending on the type of sand and its relative density, [-].

The vertical plastic strain after 15 load cycles depends on the applied cyclic shear strain amplitude, the type of sand and the initial relative density of the sand. It increases with the cyclic shear strain amplitude and decreasing relative density. The second equation is a relation between the vertical plastic strain after 15 load cycles and the total vertical plastic strain after N load cycles:

$$C_N = \frac{\varepsilon^p_{v,N}}{\varepsilon^p_{v,N=15}} = R \cdot ln(N) + c \tag{2.15}$$

with

$\varepsilon^p_{v,N}$ = vertical plastic strain after N load cycles, [-],
N = number of load cycles, [-],
C_N = strain ratio after N load cycles, [-],
R = slope parameter, [-],
c = intercept parameter, [-].

C_N increases with the number of load cycles, its value increases from 0 to 1 in the first 15 load cycles. For $N > 15$ the value of C_N continues to increase at a decreasing rate. The plot of C_N as a function of the number of load cycles in a loglinear plot is a straight line. The slope of this line gives the value of parameter R. Because for $N = 15$ the ratio between ε^p_N and $\varepsilon^p_{N=15}$ becomes 1, the value of parameter $c = 1 - R \cdot ln(15)$. This is the value where the line with slope R intersects the $N = 1$ vertical axis. Substitution of parameter c into Equation 2.15 gives:

$$C_N = 1 + R \cdot ln(\frac{N}{15}) \tag{2.16}$$

Rewriting Equation 2.15 and substituting Equations 2.14 and 2.16 results in an equation for the vertical plastic strain after N load cycles:

$$\varepsilon^p_{v,N} = \begin{cases} C_N \cdot \varepsilon^p_{v,N=15} = (1 + R \cdot ln(\frac{N}{15})) \cdot (a(\gamma_0 - \gamma_{tv})^b), & \text{if } \gamma_0 > \gamma_{tv}, \\ 0, & \text{if } \gamma_0 \leq \gamma_{tv}. \end{cases} \tag{2.17}$$

Vertical plastic strain increases with the number of load cycles and the cyclic shear strain amplitude, which comprise the loading parameters. Vertical plastic strain will only accumulate when the cyclic shear strain amplitude is larger than the volumetric threshold strain. Only elastic volumetric strains develop during a load cycle when its value lies below the volumetric threshold strain. The volumetric threshold strain depends on the type of soil. Its value is estimated at 10^{-4}, a typical value for sands [55]. Together with parameters a, b and R, the volumetric threshold strain comprises the soil parameters. Parameters a and b are material constants that can be determined during cyclic simple shear tests. Their values depend on the type of sand and its initial relative density. The vertical plastic strain of loose sands after 15 load cycles is larger than of dense sands, therefore the values of a and b decrease with increasing initial relative density, reflecting that densification is larger in loose sands (Equation 2.14). The initial state of the sand is implicitly incorporated in this model through these parameters. For most of the tested sands parameter R has a value between 0.24 and 0.34 [21].

2.5. Cumulative plastic strain model

The cumulative plastic strain model is developed to predict the contribution of subgrade soils to the total plastic deformation of a pavement system (e.g. rail tracks or highways) induced by a cyclic load [36]. The pavement structure consists of a ballast-, subballast- and subgrade layer. On top of the ballast the rail track is constructed. A granular material such as sand is typically used as subballast material, the subgrade layer normally consists of the in-situ soil. The cumulative plastic strain model calculates the vertical plastic strain of a (subgrade) soil as a function of the number of load cycles. It is based on the results from cyclic triaxial tests with varying amplitudes of the cyclic load on a silty clay, a typical subgrade soil. The vertical plastic strain increases with the number of load cycles and the amplitude of the load. The vertical plastic strain per load cycle decreases with the number of load cycles and is largest in the first load cycle. A power model relationship of the vertical plastic strain as a function of the number of load cycles can be fitted through the data from the cyclic triaxial tests using a least-squares method:

$$\varepsilon_{v,N}^{p} = AN^{b} \tag{2.18}$$

with

$\varepsilon_{v,N}^{p}$ = vertical plastic strain after N load cycles, [-],
N = number of load cycles, [-],
A = material constant depending on the soil type, initial state and deviatoric stress, [-],
b = material constant depending on the soil type ($0 < b < 1$), [-].

For $N = 1$ parameter A becomes equal to the vertical plastic strain after one load cycle ($A = \varepsilon_{v,N=1}^{p}$), substitution into Equation 2.18 gives:

$$\varepsilon_{v,N}^{p} = \varepsilon_{v,N=1}^{p} N^{b} \tag{2.19}$$

with

$\varepsilon_{v,N=1}^{p}$ = vertical plastic strain after one load cycle, [-].

Parameter b is determined in cyclic triaxial tests. The results of a large number of cyclic triaxial tests on various types of soils conducted by several researchers have been compiled [30]. It was concluded that parameter b depends on the soil type. Its value ranging between 0.06 and 0.29, with the smaller values corresponding to silts and sandy soils and the larger values to clays. The vertical plastic strain after one load cycle depends on the soil type, its initial state and the deviatoric stress applied to the soil, which increases with the amplitude of the load. Parameter b and the vertical plastic strain after one load cycle are considered soil parameters in this model, their values depend on the type of soil and they characterise its densification behaviour. However, the vertical plastic strain after one load cycle also implicitly incorporates the initial state of the soil and the amplitude of the load. It increases with decreasing initial relative density, reflecting that densification is larger in loose sands, and with the amplitude of the load. The number of load cycles is the only explicitly defined load parameter in the cumulative plastic strain model.

2.6. The improved Schmertmann method

The Schmertmann method [50] is not a cyclic settlement model. The Schmertmann method is developed to determine the vertical strain as a result of a static load:

$$\varepsilon_{z} = \frac{p}{E} I_{z} \tag{2.20}$$

with

ε_{z} = vertical strain at depth z, [-],
p = stress on the foundation, [kPa],
E = stiffness of the sand, [kPa],
I_{z} = strain influence factor at depth z, [-].

Similar to the elastic theory, the vertical strain depends on the applied stress and the stiffness of the sand. However, in contrast to this theory, the Schmertmann method assumes a different distribution of the vertical strain with depth compared to the equations governing traditional stress distribution curves, like the Boussinesq stress distribution [15]. According to the Schmertmann method the vertical strain directly underneath the shallow foundation has a value (close to) zero, which increases till it reaches its maximum value at a depth that can be related to the width of this foundation. After the vertical strain reached its maximum value it decreases with depth to zero. This distribution of the vertical strain is observed during (computer) modelling of static loaded shallow foundations on sand [50].

The vertical strain distribution assumed by the improved Schmertmann method is defined by the improved strain influence factor diagrams [52]. Figure 2.6 shows the simplified I_z distributions of a square and a rectangular shallow foundation with a length-width ratio larger than 10. The vertical axis represents the depth below the shallow foundation normalised by its width. The depth below the foundation at which the simplified I_z distribution reaches its maximum or peak value varies between a half and one time the width of the foundation. The depth below the foundation to which vertical strains occur as a result of the stress p on the foundation (depth of influence) varies between two and four times the width of the foundation. Both depths depend on the dimensions of the foundation. The peak value of the simplified I_z distribution depends on the applied stress on the foundation and the initial effective vertical stress (before construction of the foundation) at the depth corresponding to the peak value:

$$I_p = 0.5 + 0.1\sqrt{\frac{p}{\sigma'_{v,p}}} \tag{2.21}$$

with

I_p = peak value of the influence factor, [-],
$\sigma'_{v,p}$ = Initial effective vertical stress at the depth corresponding to I_p, [-].

The two distributions in Figure 2.6 define the boundaries of the simplified I_z distribution. A shallow foundation with different dimensions ($1 < L/B < 10$) will have a simplified I_z distribution which will lie in between these two distributions, in Figure 2.6 an example is indicated by the green line.

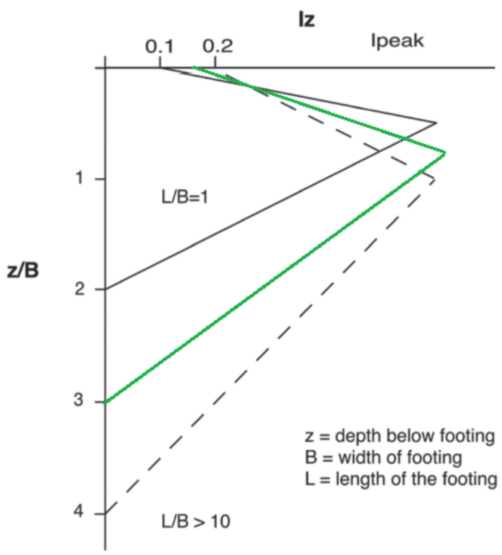

Figure 2.6: The boundaries (indicated by the two black lines) and an example (indicated by the green line) of the simplified I_z distribution below the center of a loaded shallow foundation on sand. Figure obtained from Gavin et al. [42].

According to Equation 2.20 the vertical strain decreases with stiffness of the sand. It increases with foundation stress, which increases with the amplitude of the load, and with the strain influence factor.

The strain influence factor depends on the dimensions of the foundation. With increasing width of the foundation it becomes more square, consequently the depth of the influence factor (depth of influence) decreases from four times (for $L/B > 10$) towards two times (for $L/B = 1$) the width of the foundation. However, at the same time the depth of the influence factor increases with the width of the foundation. Further, the applied foundation stress decreases with increasing foundation size, because the load is divided over a larger area. This will decrease the peak value of the strain influence factor according to Equation 2.21. Although it is not directly obvious from the formulation of strain influence factor, it is expected that an increase in the width of the foundation will lead to less vertical strain, considering that the amplitude of the load and the stiffness of the sand remain fixed.

The Schmertmann method will be used to estimate the vertical plastic strain with depth after one load cycle. This is one of the model parameters of the cumulative plastic strain model. The vertical plastic strain after one load cycle is also used to determine the void ratio after one load cycle, which is one of the model parameters of the terminal density model. Note that the improved Schmertmann method is a static method, therefore it determines the total vertical strain, which also includes the elastic vertical strain. Furthermore, the total vertical strain is the sum of the vertical strain components of the volumetric strain and the deviatoric strain.

2.7. Comparison cyclic settlement models

In Table 2.2 (at the end of this chapter) the six cyclic settlement models discussed in this chapter are summarised. The main equations, model parameters and output are given together with the concept of each cyclic settlement model. The cyclic settlement models differ from each other in model parameters, equations, output, method to determine the depth of influence, whether densification continues indefinitely with increasing number of load cycles or evolves to a maximum density, the laboratory experiments that constitute their theoretical basis, loading conditions and in their applications.

Between the cyclic settlement models also similarities exist. Each model assumes densification increases with increasing number of load cycles. The rate of densification decreases with increasing number of load cycles. Consequently, most of the densification is accumulated in the first few load cycles. Although its prediction of the densification is not a function of the number of load cycles this is assumed by the Hergarden model as well. Furthermore, rate of densification increases with the amplitude of the load. All six cyclic settlement models assume that densification decreases with (initial) relative density of the sand. Densification is larger in a loose sand compared to a dense sand.

The model parameters of the six cyclic settlement models evaluated in this research can be divided into three groups: load parameters, initial state or soil parameters. In Table 2.1 the model parameters of the cyclic settlement models are assigned to these groups. Load parameters (grey row) describe the loading conditions, for example the number of load cycles or a parameter that is related to the amplitude of the load. Initial state parameters (top yellow row) describe the initial state of the soil. In the evaluated cyclic settlement models this is described by the initial relative density or the initial void ratio. The soil parameters (bottom yellow row) describe the densification properties of the soil, for example material constants or the minimum and maximum void ratios. Their values are often determined in cyclic laboratory tests and depend on the type of sand and sometimes its initial state. The material constants c_1 and c_2 in both C/L models for example. These constants describe the densification characteristics of the sand. However, their values depend also on the initial relative density. Besides the densification properties, some of the soil parameters also describe the initial state of the soil. Moreover, not every cyclic settlement model has a model parameter in each of the three groups. The C/L model for oedometer compression, seismic induced strain model and cumulative plastic strain model do not have a model parameter that explicitly describes the initial state of the soil. The soil parameters that depend on the initial relative density implicitly incorporated the initial state. Furthermore, the Hergarden model is not a function of the number of load cycles. Therefore the amplitude of the acceleration of the vibration is the only load parameter in this model. In the terminal density model and the cumulative plastic strain model the number of load cycles is the only load parameter. The amplitude of the load is implicitly incorporated in the soil parameters of these models.

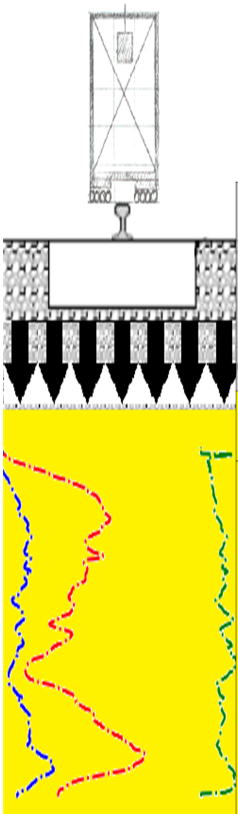

	Cyclic settlement models					
	C/L model for cyclic shear	C/L model for cyclic oedometer compression	Hergarden model	Terminal density model	Seismic induced strain model	Cumulative plastic strain model
Load Parameters	N $\gamma_0{}^{(2)}$	N $\sigma_z{}^{(2)}$ $\sigma_x{}^{(2)}$	$a^{(2)(3)}$	N (1)	N $\gamma_0{}^{(2)}$	N (1)
Initial state	e_0	(4)	$D_{R,0}$ e_0	e_0	(4)	(4)
Soil parameters	$c_1, c_2{}^{(5)}$	$c_1, c_2{}^{(5)}$	e_{min} e_{max} α_B	$N^{*(5)}$ m $e_1{}^{(2)(5)}$ $e_T{}^{(2)(5)}$	γ_{tv} R $a^{(5)}$ $b^{(5)}$	$\varepsilon^p_{v,N=1}{}^{(2)(5)}$ b

N	Number of load cycles
γ_0	Cyclic shear strain amplitude
σ_z	Vertical stress
σ_x	Horizontal stress
a	Amplitude of the acceleration of the vibration
(1)	Amplitude of the load implicitly incorporated in soil parameters
(2)	Depends on the amplitude of the load
(3)	Depends on the ASC's velocity and acceleration
e_0	Initial void ratio
$D_{R,0}$	Initial relative density
(4)	Initial state implicitly incorporated in soil parameters
c_1, c_2	Material constants C/L model
e_{min}	Minimum void ratio
e_{max}	Maximum void ratio
α_B	Barkan parameter
N^*	Characteristic number of load cycles
m	Fitting parameter
e_1	Void ratio after one load cycle
e_T	Terminal void ratio
γ_{tv}	Threshold volumetric strain
R	Slope parameter
a	Material constant seismic induced strain model
b	Material constant seismic induced strain model
$\varepsilon^p_{v,N=1}$	Vertical plastic strain after the first load cycle
b	Material constant cumulative plastic strain model
(5)	Depends on the initial relative density

Table 2.1: Overview of the model parameters per cyclic settlement models that are evaluated in this research.

The terminal density model and the Hergarden model determine a maximum density as a function of the load and soil parameters and the initial state of the sand. The density of the sand evolves towards this maximum density during densification. Densification stops when this maximum density is reached. Due to changing loading and / or boundary conditions the maximum density might increase and densification proceeds until the new maximum density is reached. The other cyclic settlement models assume that densification continues indefinitely with increasing number of load cycles. At depths where the amplitude of the load is larger than the threshold value settlement accumulates indefinitely. According to the C/L model for cyclic shear and the seismic induced strain model settlement will accumulate indefinitely at depths where the cyclic shear strain amplitude is larger than the volumetric threshold strain of the sand, also in case the initial relative density is (more than) 100%. Eventually densification per load cycle becomes negligible because the rate of densification decreases with the number of load cycles. According to the C/L model for cyclic oedometer compression and the cumulative plastic strain model, which do not include a threshold value, accumulation of the settlement will occur when the amplitude of the load is larger than zero, regardless of the relative density of the sand. According to these models cyclic settlement will accumulate indefinitely within the zone of influence, even under the influence of a small load and in sands with a relative density that is (more than) 100%. Eventually densification per load cycle becomes negligible because the rate of densification decreases with the number of load cycles.

The C/L model for cyclic shear and the seismic induced strain model are based on strain-controlled cyclic simple shear tests. The cumulative plastic strain model is based on stress-controlled cyclic triaxial compression tests. The C/L model for cyclic oedometer compression and the terminal density model are based on cyclic oedometer tests. During these laboratory tests a quasi-static cyclic load is applied to the samples that are tested. The cyclic settlement models that are based on the mechanical behaviour of the soil samples do not consider dynamic effects of the load. Consequently, the load parameters in these models only depend on the amplitude of the load or the number of load cycles. It is unclear which (laboratory) tests the Hergarden model is based on, the model does however include the dynamic effects of a load. The acceleration of the amplitude of the vibrations depends on the amplitude of the load and the velocity and acceleration of an ASC.

The C/L models, seismic induced strain model and cumulative plastic strain model assume that densification of the sand can continue indefinitely with increasing number of load cycles. In theory any given amount of densification can be reached, regardless of the amplitude of the load. According to these cyclic settlement models the amount of densification is therefore not uniquely determined by the amplitude of the load, i.e. densification of a sand under the influence of a load with a large amplitude will also occur under the influence of a load with a small amplitude but after a larger number of load cycles. Note that the depth of influence increases with the cyclic shear strain amplitude, which increases with the amplitude of the load, the settlement output from the C/L model for cyclic shear and the seismic induced strain model is therefore uniquely determined by the amplitude of the load. The terminal density model and the Hergarden model determine a maximum density which increases with the amplitude of the load. The amplitude of the load uniquely determines the densification, i.e. under the influence of a load with a large amplitude more densification occurs compared to a load with a smaller amplitude. For all six cyclic settlement models densification is not independent of the amplitude of the load, the rate of densification increases with the amplitude of the load.

One of the reasons why the cyclic settlement models differ from each other is that they have been developed for different applications. Most of the cyclic settlement models have been applied to estimate the settlement of a shallow foundation and / or a pavement system. Both correspond more or less to the problem that is considered in this research, the settlement of ASC rail tracks. Rail tracks are a typical example of a pavement system. The ASC rail tracks are constructed on concrete rail road ties on a ballast bed, this represents a shallow foundation.

2.7.1. Depth of influence

Different methods are adopted by the cyclic settlement models to estimate the depth of influence of the cyclic load. The Hergarden model determines the depth of influence as the largest depth where the acceleration of the amplitude of the vibration is larger than the threshold acceleration. The seismic induced strain model compares the cyclic shear strain amplitude to the volumetric threshold strain. The largest depth where the cyclic shear strain amplitude is larger than the volumetric threshold strain is the depth of influence. The C/L model for cyclic oedometer compression estimates the depth of influence based on the friction angle of the sand and half the width of the foundation. For 30° friction angle, typical value for sands, this becomes around 1.7 times half the width of the foundation. The depth of influence determined with the improved Schmertmann method is adopted by the cumulative plastic strain model. The vertical strain after one load cycle estimated with the improved Schmertmann method is one of the model parameters of the cumulative plastic strain model. In the improved Schmertmann method the depth of influence is related to the width of the foundation. Based on the dimensions of the shallow foundation the depth of influence varies between two and four times the width of the foundation. That is thus at least more than twice and up to five times the depth of influence determined by the C/L model for cyclic oedometer compression. The literature about the C/L model for cyclic shear and the terminal density model do not specify a method to determine the depth of influence. The C/L model for cyclic shear adopts the method that is used by the seismic induced strain model. In both models the cyclic shear strain amplitude is a model load parameter. The output of the improved Schmertmann method is used to determine the void ratio after one load cycle, one of the model parameters of the terminal density model. The terminal density model will therefore adopt the depth of influence determined by the improved Schmertmann method, like the cumulative plastic strain model.

2.7.2. Cyclic settlement

The C/L model for cyclic shear, Hergarden model and terminal density model output the volumetric plastic strain. The C/L model for cyclic oedometer compression, seismic induced strain model and cumulative plastic strain model output the vertical plastic strain. The settlement in a soil element (or layer) related to the vertical plastic strain is:

$$S = \varepsilon_v^p \cdot \Delta H \tag{2.22}$$

with

S = settlement, $[m]$,
ΔH = layer thickness, $[m]$.

Note that the vertical plastic strain output of the C/L model for cyclic oedometer compression has unit 10^{-3}. The settlement in a soil element becomes:

$$S = \varepsilon_{v,N}^p \cdot 10^{-3} \cdot \Delta H \tag{2.23}$$

with

S = settlement, [m],
$\varepsilon_{v,N}^p$ = vertical plastic strain, [-],
ΔH = layer thickness, [m].

The total settlement is equal to the combined settlement of all elements over the same vertical.

The volumetric plastic strain is not directly related to the settlement. For the cyclic settlement models that output the volumetric plastic strain, first the vertical plastic strain needs to be determined before the settlement can be calculated. The vertical plastic strain consists of the vertical component of the volumetric and the deviatoric plastic strain:

$$\varepsilon_v^p = \varepsilon_{v,vol}^p + \varepsilon_{v,dev}^p \tag{2.24}$$

with

$\varepsilon_{v,vol}^p$ = vertical component of the volumetric plastic strain, [-],
$\varepsilon_{v,dev}^p$ = vertical component of the deviatoric plastic strain, [-].

Practically it is difficult to determine the vertical components of the volumetric and the deviatoric plastic strain. Instead the vertical plastic strain could be estimated. For example, determine the ratio between the vertical and the volumetric plastic strains, the 'vertical-volumetric strain ratio' (VVSR), based on a FEM analysis. The vertical plastic strain is then approximated by multiplying this ratio with the volumetric plastic strain:

$$\varepsilon_v^p = VVSR \cdot \varepsilon_{vol}^p \tag{2.25}$$

with

$VVSR$ = ratio between the vertical and the volumetric strains, [-],
ε_{vol}^p = volumetric plastic strain, [-].

After the vertical plastic strain is determined based on the volumetric plastic strain, Equation 2.22 is used to calculate the settlement. Note that the volumetric plastic strain of the C/L model for cyclic shear has unit 10^{-3}, Equation 2.23 must be used to calculate the settlement.

		Cyclic settlement models					
		C/L model for cyclic shear	C/L model for cyclic oedometer compression	Hergarden model	Terminal density model	Seismic induced strain model	Cumulative plastic strain model
Calculation	Input parameters	N: Number of load cycles γ_0: Cyclic shear strain amplitude c_1, c_2: Material constants e_0: Initial void ratio	N: Number of load cycles σ_z: Vertical stress σ_x: Horizontal stress c_1, c_2: Material constants	a: Amplitude of the acceleration of the vibration $D_{R,0}$: Initial relative density e_0: Initial void ratio α_B: Barkan parameter e_{min}: Minimum void ratio e_{max}: Maximum void ratio	N: Number of load cycles e_0: Initial void ratio e_1: Void ratio after one load cycle e_T: Terminal void ratio N^*: Characteristic number of load cycles m: Fitting parameter	N: Number of load cycles γ_0: Cyclic shear strain amplitude γ_{tv}: Volumetric strain threshold R: Slope parameter a, b: Material constants	N: Number of load cycles $\varepsilon^p_{v,N=1}$: Vertical plastic strain after the first load cycle b: Material constant
	Equation(s)	▪ $\phi = c_1 \cdot \ln\left(1 + c_2 \frac{\gamma_0^2 N}{4}\right)$ ▪ $\varepsilon^p_{vol,N} = -\phi \cdot e_0$	▪ $\varepsilon^p_{v,N} = c_1 \cdot \ln(1 + c_2(\sigma_z - \sigma_x)N)$	▪ $\Delta D_R = \begin{cases} e^{-\alpha_B \eta_0} - e^{-\alpha_B \eta}, & if\ \eta < \eta_0 \\ 0, & if\ \eta_0 \geq \eta \end{cases}$ ▪ $\eta = \frac{a}{g}$; $\eta_0 = \frac{\ln(1-D_{R,0})}{-\alpha_B}$ ▪ $\varepsilon^p_{vol} = \Delta D_R \frac{e_{max}-e_{min}}{1+e_0}$	▪ $e_N = e_T + (e_1 - e_T)\left[1 + \left(\frac{N-1}{N^*}\right)^m\right]^{-1}$ ▪ $\varepsilon^p_{vol,N} = \frac{e_0 - e_N}{1+e_0}$	▪ $\varepsilon^p_{v,N=15} \approx (a(\gamma_0 - \gamma_{tv})^b)$ ▪ $C_N = (1 + R \cdot ln\left(\frac{N}{15}\right))$ ▪ $\varepsilon^p_{v,N} = \begin{cases} C_N \cdot \varepsilon^p_{v,N=15}, & if\ \gamma_0 > \gamma_{tv} \\ 0, & if\ \gamma_0 \leq \gamma_{tv} \end{cases}$	▪ $\varepsilon^p_{v,N} = \varepsilon^p_{v,N=1} \cdot N^b$
	Output	Volumetric plastic strain ($\varepsilon^p_{vol,N}$)	Vertical plastic strain ($\varepsilon^p_{v,N}$)	Volumetric plastic strain (ε^p_{vol})*	Volumetric plastic strain ($\varepsilon^p_{vol,N}$)	Vertical plastic strain ($\varepsilon^p_{v,N}$)	Vertical plastic strain ($\varepsilon^p_{v,N}$)
	Depth of influence	Not specified (Estimated as the depth at which $\gamma_0 \leq \gamma_{tv}$)	$b\tan(45° + \frac{1}{2}\theta) \approx 1.7b$ b: half the width of the foundation θ: angle of friction of the sand	Depth at which $\eta_0 \geq \eta$	Not specified (Estimated with the improved Schmertmann method; three times the width of the foundation)	Depth at which $\gamma_0 \leq \gamma_{tv}$	Equal to the depth of influence in the first load cycle (Estimated with the improved Schmertmann method; three times the width of the foundation)
	Max. density	NO* (plastic strain accumulates indefinitely with the number of load cycles)	NO* (plastic strain accumulates indefinitely with the number of load cycles)	YES (vibration induced densification is completed; only stronger vibrations will cause further densification)	YES (asymptotically towards a terminal density with the number of load cycles)	NO* (plastic strain accumulates indefinitely with the number of load cycles)	NO* (plastic strain accumulates indefinitely with the number of load cycles)
Concept	Based on	Strain-controlled cyclic simple shear tests	Stress-controlled cyclic oedometer tests	Dynamic laboratory tests on sand**	Stress-controlled cyclic oedometer tests	Strain-controlled cyclic simple shear tests	Stress-controlled cyclic triaxial compression tests
	Load	Quasi-static cyclic (inertia forces are neglected)	Quasi-static cyclic (inertia forces are neglected)	Dynamic (inertia forces are considered)	Quasi-static cyclic (inertia forces are neglected)	Quasi-static cyclic (inertia forces are neglected)	Quasi-static cyclic (inertia forces are neglected)
	Background	▪ Densification increases with the number of load cycles; The rate of densification decreases with the number of load cycles. ▪ Rate of densification increases with the cyclic shear strain amplitude. ▪ Densification of a sand is uniquely characterised by: - sand type; - initial relative density; - boundary conditions; - type of loading.**	▪ Densification increases with the number of load cycles; The rate of densification decreases with the number of load cycles. ▪ Rate of densification increases with the cyclic stress amplitude. ▪ Densification of a sand is uniquely characterised by: - sand type; - initial relative density; - boundary conditions; - type of loading.**	▪ Densification of sand occurs when the amplitude of the acceleration of the vibration (force) exceeds the threshold acceleration (resistance). ▪ The amplitude of the acceleration increases with amplitude of the load and the velocity and acceleration of an ASC.*** ▪ The threshold acceleration increases with increasing initial relative density and decreasing Barkan parameter. ▪ During densification the relative density increases to the value corresponding to the amplitude of the acceleration of the propagating vibration. Consequently, the threshold acceleration increases to the amplitude of the acceleration of the propagating vibration.	▪ With increasing number of load cycles the void ratio of sand evolves from its initial void ratio towards the terminal void ratio. ▪ The terminal void ratio of a sand is uniquely characterised by: - sand type; - initial relative density; - boundary conditions; - loading conditions*. ▪ Densification increases with the number of load cycles; The rate of densification decreases with the number of load cycles. ▪ Rate of densification increases with the amplitude of the load.	▪ Densification of sand occurs when the cyclic shear strain amplitude is larger than the volumetric strain threshold. ▪ Densification increases with the number of load cycles; The rate of densification decreases with the number of load cycles. ▪ Rate of densification increases with the cyclic shear strain amplitude. ▪ Densification of a sand is uniquely characterised by: - sand type; - initial relative density; - cyclic shear strain amplitude**.	▪ Densification increases with the number of load cycles; The rate of densification decreases with the number of load cycles. ▪ Rate of densification increases with the applied cyclic deviatoric stress. ▪ Densification of a sand is uniquely characterised by: - sand type; - initial relative density.**
	Application(s)	▪ Settlement of a cyclic loaded shallow foundation on sand. ▪ Settlement of sand induced by an earthquake. ▪ Settlement of sand induced by vibroflotation.	▪ Settlement of a cyclic loaded shallow foundation on sand.	▪ Settlement of sand around vibratory sheet piling. ▪ Settlement of a vibrating foundation.	▪ Settlement of a cyclic loaded shallow foundation on sand.	▪ Settlement of sand induced by an earthquake.	▪ Settlement of a pavement structure.
	Comments	* At depths where the cyclic shear strain amplitude is larger than the volumetric strain threshold of the sand volumetric plastic strain accumulates indefinitely, regardless of the density of the sand. ** The same densification can be obtained with a small cyclic shear strain amplitude and a large number of load cycles as with a larger amplitude and fewer number of load cycles. The cyclic shear strain amplitude, which depends on the amplitude of the load, does not uniquely determine the densification. (**Note**: the depth of influence is estimated based on the cyclic shear strain amplitude. The settlement is therefore uniquely characterise by the amplitude of the load.)	* Under the influence of a very small load (vertical stress minus the horizontal stress is larger than zero) the vertical plastic strain accumulates indefinitely within the zone of influence, regardless of the density of the sand. ** The same densification can be obtained with a small cyclic shear stress amplitude and a large number of load cycles as with a larger amplitude and fewer number of load cycles. The cyclic stress amplitude, which depends on the amplitude of the load, does not uniquely characterise the densification.	* The Hergarden model does not calculate the plastic strain as a function of the number of load cycles. It only outputs the maximum volumetric plastic strain. ** It is not explained which devices were used during the laboratory tests. However, it is known that during the tests the void ratio of the sand was measured after being applied to a continuous vibration with a constant amplitude. *** Densification increases with amplitude of the acceleration, which increases with the amplitude of the load. In contrast to the C/L models the densification is uniquely characterised by the amplitude of the load.	* The terminal void ratio decreases with the amplitude of the cyclic load. The total densification therefore increases with the amplitude of the cyclic load. In contrast to the C/L models the densification is uniquely characterised by the amplitude of the load.	* At depths where the cyclic shear strain amplitude is larger than the volumetric strain threshold of the sand vertical plastic strain accumulates indefinitely, regardless of the density of the sand. ** The depth of influence is estimated based on the cyclic shear strain amplitude, which depends on the amplitude of the load. Densification is uniquely characterised by the amplitude of the load.	* Within the zone of influence vertical plastic strain accumulates indefinitely, regardless of the density of the sand. ** The same densification can be obtained with a small cyclic deviatoric stress and a large number of load cycles as with a larger cyclic deviatoric stress and fewer number of load cycles. The cyclic deviatoric stress, which depends on the amplitude of the load, does not uniquely determine the densification.

Table 2.2: Overview of the six cyclic settlement models that are evaluated in this research.

3

Soil profile and relevant data

Data relevant for the prediction of settlement induced by a cyclic load as a result of the movements of ASCs describe the soil conditions and loading conditions. The soil conditions at the RWG container terminal are described by the geotechnical data that is obtained during site investigations. Both in-situ and laboratory tests were executed. In the area of the ASC rail tracks the soil has been investigated more extensively. Due to excavation, construction and compaction that were carried out at container terminal soil conditions underneath the rail tracks have changed. This is described in Section 3.2. The following section the loading conditions at the container terminal are described. Six locations are selected for the evaluation of the cyclic settlement models. At each location the settlement has been measured and a CPT was executed. The CPT-profiles are presented in Section 3.4. Disturbance of the soil after the CPTs were executed is minimal at the six locations.

3.1. Soil conditions underneath the ASC rail tracks

The RWG container terminal is located at MV2, this is a 2000 hectares piece of reclaimed land in the port of Rotterdam (see Figure 1.1). MV2 consists of a hydraulic sand fill extending up to a depth of 20 m, therefore the soil conditions are defined by the construction of MV2. Several soil investigations, in the laboratory and in-situ, have been carried out at the RWG container terminal in order to determine the local conditions.

3.1.1. Construction timeline of MV2 and the RWG container terminal

MV2 is a man-made piece of land, consisting of sand dredged from the North Sea and deposited next to the mouth of the river Meuse in front of the coast of Rotterdam. The RWG container terminal is located on a strip of land at MV2. Figure 3.1 gives a timeline of the construction of MV2 and the RWG container terminal. Below the horizontal axis the milestones of this project are indicated. Above the horizontal axis the most relevant soil investigations and the construction steps that have influenced the local soil conditions are indicated.

Construction of MV2 commenced in 2008, it was completed in 2011. In 2009 and 2010 site investigations were carried out at the RWG container terminal, consisting of shallow and deep cone penetration tests (CPTs), boreholes, sampling and laboratory soil tests. In 2012 construction of the container terminal started. In 2013, just before construction of the rail tracks started, over 300 CPTs till 7 m depth were executed in the area of the ASC rail tracks. Relatively weak shallow sand layers were compacted. In the beginning of 2014 the RWG container terminal was completed and the ASCs could be installed. This was carried out from the beginning of 2014 till the beginning of 2015. After installing each of the ASCs was tested. Settlements underneath the rail tracks of the moving ASCs were observed during the test phase. The first settlements were measured in the summer of 2014. For almost a year, until March 2015, settlements of the ASC rail tracks have been recorded. In September 2015 the RWG container terminal officially opened [8].

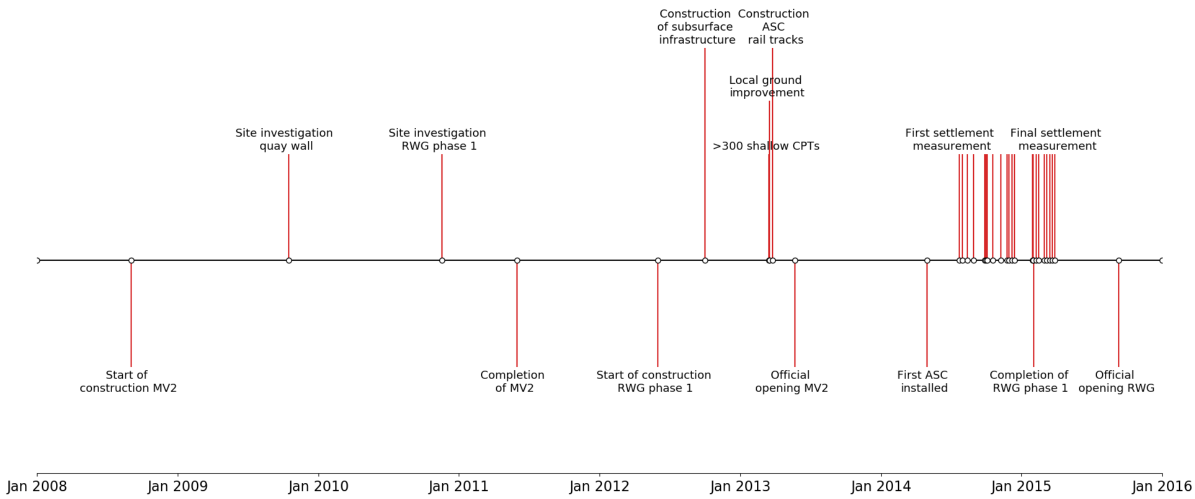

Figure 3.1: Timeline of the construction of MV2 and the RWG container terminal.

3.1.2. Lithology

Before construction of MV2, the area was part of the North Sea and the sea bed level was located at about -12 to -15 $m\ NAP$. During construction the area was raised to about 5 $m\ NAP$. An overview of the layers below the sea bed to a depth of -45 $m\ NAP$ is given by Table 3.1. The first layer, consisting of fine sand, has a thickness between 0 to 5 meters, depending on the initial sea bed level. To raise the area to 5 $m\ NAP$ about 15 to 20 m sand was placed. This sand was dredged from the North Sea [41].

Layer	Geological age	Soil type	Depth [$m\ NAP$]
I	Holocene	fine sand	-10 to -15
II	Holocene	sand, silt, clay	-15 to -20
III	Holocene	clay, peat	-20 to -23
IV	Late Pleistocene	sand, silt, clay	-23 to -25
V	Middle Pleistocene	coarse sand	-25 to -45
VI	Early Pleistocene	clay	below -45

Table 3.1: Lithology of the area before construction of Maasvlakte 2 [14].

3.1.3. Sand fill

After its construction the soil conditions of the sand fill have been investigated to check whether the construction requirements were met. Later additional soil investigation were carried out for the construction of the RWG container terminal. This included twelve boreholes drilled up to 20 meters depth. Their locations are indicated on a map of the RWG container terminal in Figure 3.2. Wet sieve analyses were conducted on 110 samples that were taken from these boreholes at 2 m intervals. In Appendix A documentation of the sieve analysis of two samples is included. The corresponding grain size distribution curves are plotted in Figure 3.3. It is clear that almost all samples contain less than 10% fines, only one of the investigated samples has a larger fines content. The principal fraction of all samples is sand. The average sand fraction percentage of the 110 samples is 96.5%. This means that the soil at RWG can be classified as sand according to the USDA soil texture triangle [9]. The samples contain a (very) small fraction of fines and most also contain a small fraction of gravel. In Table 3.2 a summary of the 110 grain size distributions is given together with their classification. The finest sample is classified as sandy loam, the other samples are classified as sand.

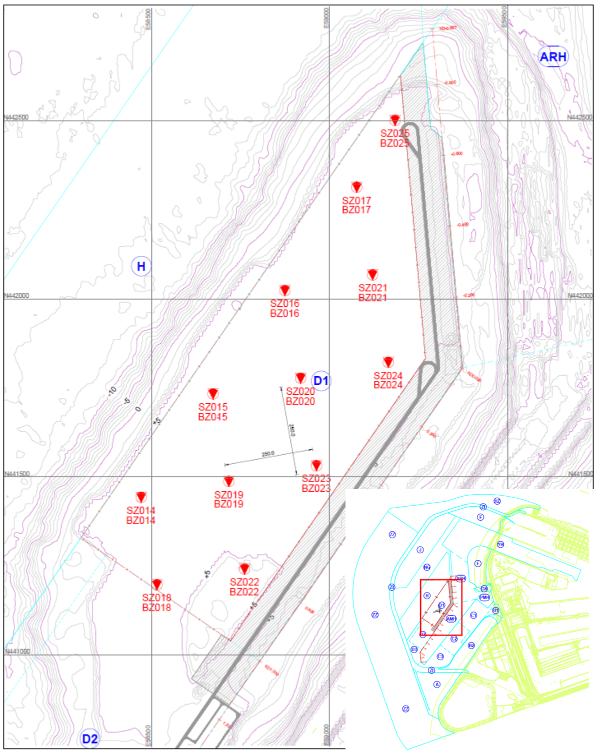

Figure 3.2: Location of the boreholes at the RWG container terminal Phase 1 (indicated with D1). In the small picture: the light green area represents MV1 and the light blue area MV2.

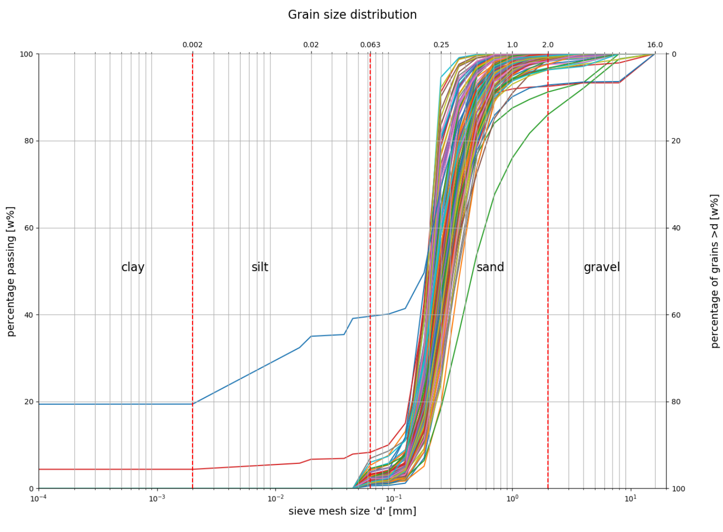

Figure 3.3: Grain size distribution diagrams of 110 soil samples taken at the RWG container terminal.

In Table 3.3 the sand median, the coefficient of uniformity and the coefficient of curvature of the two finest, the coarsest and the average of the 110 samples are given. In the last column their gradation is given. The sand at the RWG container terminal is classified as a medium to coarse uniform (poorly) graded sand.

Sample	Clay [$w\%$]	Silt [$w\%$]	Sand [$w\%$]	Gravel [$w\%$]	Soil class
Finest	19.4	20.2	59.8	0.6	Sandy loam
Second finest	4.4	3.9	91.7	0.0	Sand
Coarsest	0.0	1.7	84.3	14.0	Sand
Average	0.2	2.4	96.5	0.9	Sand

Table 3.2: Percentage by weight of the clay, silt, sand and gravel fractions of the two finest and the coarsest samples and the average of the 110 samples. The corresponding classification is based on the USDA soil texture triangle [9].

Sample	M_{63} [mm]	C_u	C_c	Gradation
Finest	0.252	1.9	-	Medium uniformly graded* sandy loam
Second finest	0.211	2.5	1.2	Medium uniformly graded sand
Coarsest	0.421	3.0	0.9	Coarse uniformly graded sand
Average	0.265	2.0	1.0	Medium uniformly graded sand

* gradation based on the sand fraction.

Table 3.3: The sand median (M_{63}) and the coefficients of uniformity (C_u) and curvature (C_c) of the two finest and the coarsest samples and the average of all samples together with the corresponding gradation [19].

3.1.4. Minimum and maximum void ratio

Near the quay walls, indicated by the grey track in Figure 3.2, an extensive site investigation was carried out. Geotechnical data from this investigation comprises CPT's, borehole data and laboratory test results from a.o. sieve analyses and triaxial testing. Sieve analyses show that the sand near the quay wall with an average $C_u = 2.0$ and $M_{63} = 0.255$ is comparable with the sand at other parts of the container terminal (compared to the values in the bottom row in Table 3.3). Properties of the sand determined for the sand near the quay wall can be extrapolated to the sand underneath the ASC rail tracks. This includes the minimum and maximum void ratio and stiffness of the sand.

The minimum and maximum unit weights of dried samples of the sand fill were measured as part of the triaxial tests that were carried out. Based on these measurements the minimum and maximum void ratio of the sand are determined. In Appendix A documentation of the measurements is presented. Unfortunately, it is not specified which standard has been followed to determine the minimum and maximum void ratios. The range of values for e_{min} and e_{max} are 0.472 - 0.680 and 0.721 - 1.032, respectively. This does not correspond to Figure 3.4. Sand from the North Sea is in general (sub)rounded. For a sand with $C_u = 2.0$ the minimum and maximum void ratio should lie around 0.4 and 0.7, respectively. These values lie outside the range of measured minimum and maximum void ratios. An e_{min} of 0.50 and an e_{max} of 0.80 are selected for this research. This corresponds to sand with subangular grains.

3.1.5. CPT data

At the RWG container terminal a large amount of CPT data has been gathered using standard CPTs. A standard CPT measures the cone tip resistance and the sleeve friction. Especially in the area near the quay wall and at the ASC rail tracks a large amount of CPT data is available. The CPTs carried out near the quay wall extent till a maximum depth of -40 $m\ NAP$. The CPT data validates that the first 20 meter (from 5 till -15 $m\ NAP$) consists of sand. In the top part of the sand layer till a depth of -2 $m\ NAP$ the cone tip resistance is relatively high, indicating well compacted sand, however the cone tip resistance varies strong laterally and also with depth. At some locations less compacted sand layers are present in the top part of the sand fill. In many of the CPTs it is observed that at a depth between 0 and -2 $m\ NAP$ the cone tip resistance decreases significantly, indicating that the sand layer at this depth is less compacted. This sand has been deposited below water level, which could be the reason why it is less compacted compared to the sand deposited above the water level. With depth the cone tip resistance increases gradually. Between -5 and -15 $m\ NAP$ less and well compacted sand layers occasionally occur. At around -15 $m\ NAP$, the initial sea bed level is located and the soil type changes to finer material such as silt and clay. In nine of the CPTs executed near the quay wall also the pore pressures were measured. In the sand fill static pore water pressures are present. In Appendix A three deep CPTs are attached, including one with a pore water pressure measurement.

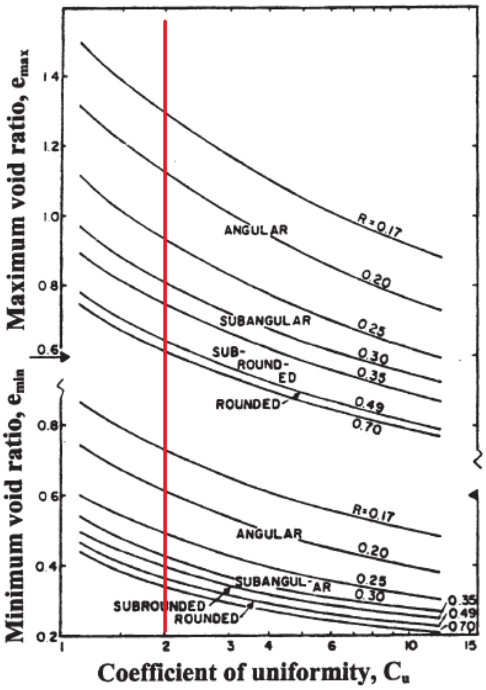

Figure 3.4: Minimum and maximum void ratio as a function of the coefficient of uniformity and the grain shape [57].

To get a better picture of the top layer of the sand fill in the area of the ASC rail tracks, over 300 additional shallow (till a depth of -2 m NAP) CPTs were executed along the proposed ASC rail tracks. The spacing between the shallow CPTs is 25 meters. Some adjacent CPTs showed large differences in the measured cone tip resistance, indicating strong variability of the sand compaction. Note that these shallow CPTs were carried out before construction of the ASC rail tracks, but after construction of the subsurface infrastructure (Figure 3.1). At some locations, variability of the sand compaction can be attributed to the excavation works. Stretches of sand of 8 by 25 m^2around the shallow CPTs that showed low values of cone tip resistance were compacted till a depth of 3 m below the surface level. As a result these CPTs do no longer represent the real state of the sand. For this research six locations are selected that have not been compacted since the corresponding CPT data does not show alarming values of the cone tip resistance. The settlement that was measured after the ASCs started moving was not anticipated. The cone tip resistance, sleeve friction and friction ratio of one of the CPTs corresponding to the selected locations is plotted in Figure 3.5a. Plots of the CPTs corresponding to the other locations can be found in Appendix A.

Relative density

The relative density can be approximated by using a correlation between the cone tip resistance and the relative density. The output of this type of correlation is a (near) continuous profile of the relative density with depth. Figure 3.5b gives a plot of the relative density with depth approximated by the correlation of Baldi[10]:

$$D_R = \frac{1}{3.29} ln(\frac{q_c}{86(\sigma'_{v0})^{0.53}}) \quad (3.1)$$

with

D_R = relative density, [-],
q_c = cone tip resistance, [MPa],
σ'_{v0} = vertical effective stress, [kPa],
C_0, C_1, C_2 = material constants, [-].

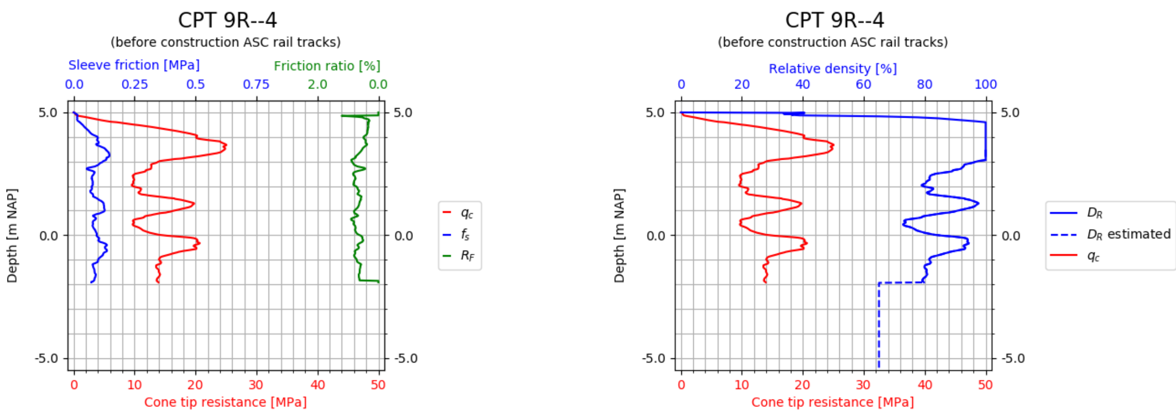

(a) The measured cone tip resistance (q_c), sleeve friction (f_s) and friction ratio (R_F)

(b) The measured cone tip resistance and the relative density (D_R), the dashed line indicates that the relative density is estimated.

Figure 3.5: The measured data by CPT 9R-4 and the relative density determined based on this data using the correlation of Baldi [10].

In Table 3.4 the unit weights of the sand and water that are used to determine the vertical effective stress are given.

Material	Unit weight $[kN/m^3]$	Depth $[m\ NAP]$
Dry sand	18	5 to 0.63
Saturated sand	20	0.63 to -15
Water	10	0.63 to -15

Table 3.4: Estimate of the unit weights of the materials in the sand fill. These values are used to determine the vertical effective stress.

The correlation of Baldi will be used in this research to approximate the relative density of the sand underneath the ASC rail tracks. This correlation has given good estimates of the relative density for a sand with similar minimum and maximum void ratios as determined for the sand fill (0.5 vs. 0.490 and 0.8 vs. 0.821) [43]. Moreover, in Appendix B a few common cone tip resistance - relative density correlations, including the correlation of Baldi given in Equation 3.1, are compared. Especially in dense sands the differences between the correlations become negligible.

Figure 3.5b shows that the initial relative density of the sand in the top 7 meters at the location corresponding to CPT 9R-4 is dense to very dense. It varies between 75 and 100%. Beyond the extent of the CPT, that is deeper than -2 $m\ NAP$, it is assumed that the relative density has a lower value. This is based on the decreasing cone tip resistance at this depth observed in the deeper CPTs taken near the quay wall. The relative density of the sand is estimated at 65%, corresponding to a medium dense sand. This is plotted in Figure 3.5b. To indicate that the relative density is estimated it is plotted with a dashed line.

3.1.6. Stiffness

Stiffness of the sand fill defines its resistance to deformation induced by an applied force, for example the load applied by an ASC. It is measured in a triaxial tests. Samples of the sand fill with varying relative density were tested to determine its stiffness. The samples are taken from varying depths from different boreholes near the quay wall. In total 21 samples were taken. In Appendix A documentation of the results from the triaxial tests of three samples is attached.

Stress-dependent stiffness

Stiffness increases with confining pressure. This dependency is described by a parameter m, rate of stress dependency of the stiffness. For the sand fill parameter m is determined at 0.7. This is the average value of parameter m of the 21 tested sand samples. A typical value for sands is 0.5. In Appendix A is explained how this parameter is determined. In Figure 3.6 the secant stiffness of the sand fill for a reference confining pressure of 100 kPa is plotted as a function of the relative density. Stiffness increases with relative density. The sand has been divided into five groups based on its relative density: loose, medium dense, dense, very dense and densified. For medium dense to very dense sands the values correspond well to a correlation between the relative density and stiffness of another sand [29]. In Table 3.5 the stiffness of the sand for each category for a reference confining pressure of 100 kPa is given.

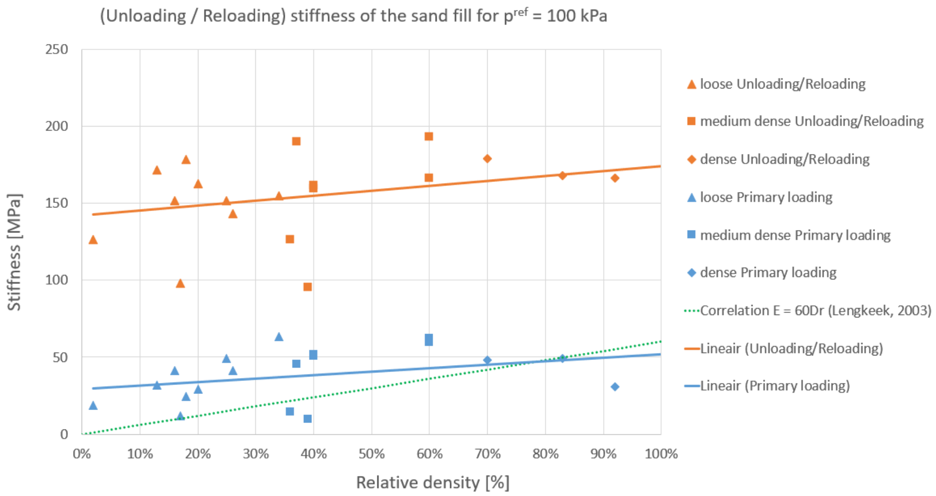

Figure 3.6: Secant stiffness (blue) and unloading/reloading (orange) stiffness for a confining stress of 100 kPa as a function of the relative density for samples from the sand fill. The green line gives a correlation between the relative density and stiffness for a confining stress of 100 kPa [29]. The unloading / reloading stiffness is about 4 times higher than the secant stiffness.

Density sand	D_R [%]	E_{50}^{ref} $[kPa]$	E_{ur}^{ref} $[kPa]$
Loose sand	35	35E3	150E3
Medium dense sand	65	40E3	160E3
Dense sand	80	45E3	165E3
Very dense sand	90	50E3	170E3
Densified sand	100	55E3	175E3

Table 3.5: The secant stiffness and the unloading / reloading stiffness for a confining stress of 100 kPa of the sand fill at different relative densities.

Unloading / reloading stiffness

During the triaxial tests the unloading / reloading stiffness of the sand was measured as well. In Figure 3.6 the unloading / reloading stiffness of the sand fill for a confining pressure of 100 kPa is plotted as a function of the relative density. It is observed that for the sand fill the unloading / reloading stiffness is 3.5 to 4.5 times the secant stiffness. In Table 3.5 the unloading / reloading stiffness of the sand for a reference confining pressure of 100 kPa is given for the five categories. In Appendix A is explained how the unloading / reloading stiffness and the unloading / reloading stiffness for a confining pressure of 100 kPa are determined.

Strain-dependent stiffness

Figure 3.7a shows the dependency of the shear modulus of a soil normalised by its small strain shear modulus (G_0 or G_{max}) on the shear strain level. The shear modulus decreases with increasing shear strain. The S-shaped curve is called the shear modulus reduction curve, it describes the dependency of the shear stiffness on the shear strain. The exact shape of the shear modulus reduction curve is soil type dependent. Figure 3.7b presents two different shear modulus reduction curves of a sand and gravel. The shear modulus reduction curve can be used to determine the dependency of the stiffness of the sand fill on the (shear) strain, because the shear modulus is related to the stiffness:

$$G = \frac{E}{2(1+\nu)} \tag{3.2}$$

with

G = shear stiffness or shear modulus, [kPa],
E = stiffness, [kPa],
ν = Poisson's ratio, [-].

The level of shear strain in conventional soil testing, for example triaxial testing, is larger than the shear strain level typical for (cyclic) loaded foundations. This suggests that the behaviour of the sand underneath the ASC rail tracks will be stiffer compared to its behaviour measured in the triaxial tests.

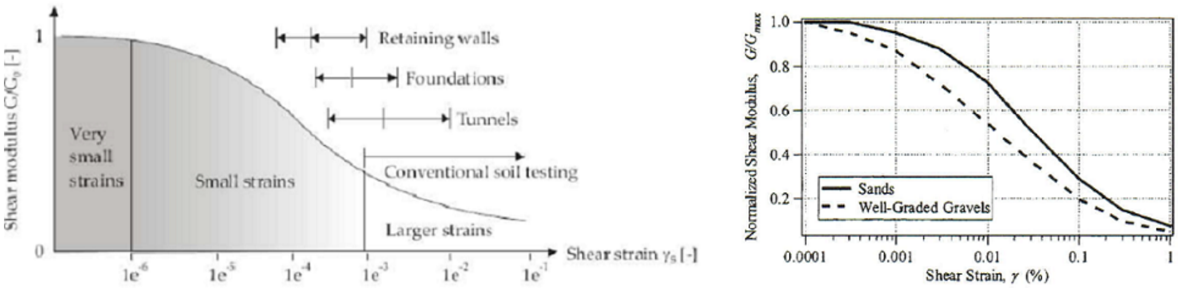

(a) Shear modulus reduction curve, for certain geotechnical applications is the level of shear strain typically involved indicated [12].

(b) Two examples of the shear modulus reduction curve of a sand and a gravel [53].

Figure 3.7: Shear modulus reduction curves.

The shear strain level in the triaxial tests is estimated based on the axial strain and the volumetric strain measured during the triaxial tests:

$$\gamma \approx \varepsilon_a - \frac{\varepsilon_v}{3} \tag{3.3}$$

with

γ = shear strain, [-],
ε_a = axial strain, [-],
ε_v = volumetric strain, [-].

The axial strain and the volumetric strain have an average value of 0.4% and 0.2%, respectively. The shear strain in the triaxial tests is estimated at almost 0.35%. Together with the measured secant stiffness the shear modulus reduction curve can be calibrated to determine the strain dependency of the stiffness of the sand. A shear strain of 0.35% corresponds to a normalised shear modulus of 0.17 ($\approx 1/6$), considering the shear modulus reduction curve for sands in Figure 3.7b. For a shear strain of 0.1%, 0.01%, 0.001% and 0.0001% the sand behaves roughly two, four, five and six times stiffer, respectively. Table 3.6 gives an overview of the estimated stiffness of the sand at different relative densities at different levels of shear strain and corresponding axial strain. In the final column the small strain stiffness, for a shear strain of 0.0001%, is given.

The small strain stiffness can also be determined based on the maximum shear modulus estimated using the graphs plotted in Figure 3.8. The solid line indicated with 0.1 estimates the maximum shear modulus for granular soils with round grains for a confining pressure of 100 kPa as a function of the void ratio [24]. Its value for the range of void ratios 0.5 - 0.8 varies between 70 and 130 MPa. According to

Density sand	D_R [%]	e [-]	E_{50}^{ref} $[MPa]$ $(\gamma \approx 0.35\%)$ $(\varepsilon_a \approx 0.4\%)$	E^{ref} $[MPa]$ $(\gamma \approx 0.1\%)$ $(\varepsilon_a \approx 0.1\%)$	E^{ref} $[MPa]$ $(\gamma \approx 0.01\%)$ $(\varepsilon_a \approx 0.01\%)$	E^{ref} $[MPa]$ $(\gamma \approx 0.001\%)$ $(\varepsilon_a \approx 0.001\%)$	E_0^{ref} $[MPa]$
Loose	35	0.70	35	70	140	175	210
Medium dense	65	0.61	40	80	160	200	240
Dense	80	0.56	45	90	180	225	270
Very dense	90	0.53	50	100	200	250	300
Densified	100	0.50	55	110	220	275	330

Table 3.6: Estimate of the stiffness of the sand at several levels of small strain, in the last column the estimated small strain stiffness is given. These values correspond to a reference stiffness of 100 kPa.

Equation 3.2, this is a stiffness between 170 and 310 MPa, for a Poisson's ratio of 0.2, a typical value for sands. This corresponds well with the small strain stiffness in the final column of Table 3.6.

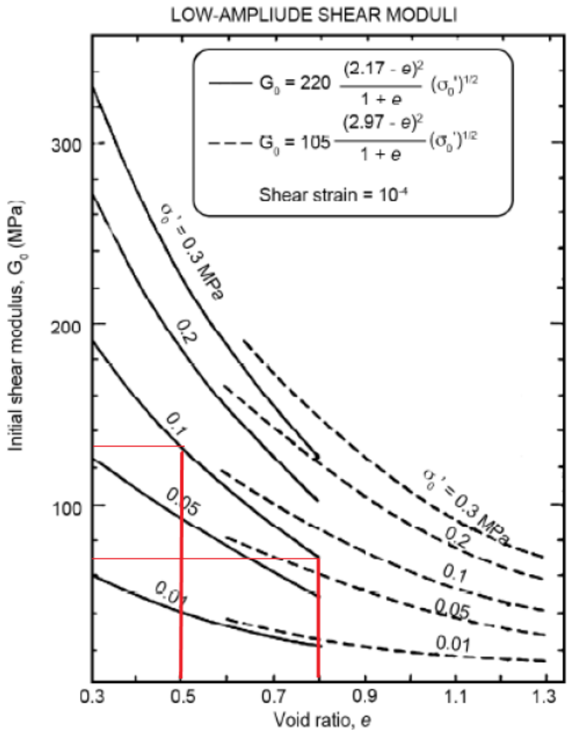

Figure 3.8: Small strain shear modulus as a function of the void ratio. The solid line is for sands with rounded grains and the dashed line is for sands with angular grains [24]

3.1.7. Measured settlement

Despite the local compaction of the less compacted layers the ASC rail tracks have been settling. Settlement accumulated both at locations where local compaction has and has not been carried out. Settlements of the rail tracks were measured from July 2014 till March 2015. At the six locations that are selected to evaluate the cyclic settlement models no local compaction has been carried out. It is assumed that CPT data still represents the soil conditions at these locations. In Table 3.7 the settlement measured at the six selected locations is given. Each value represents a settlement measurement of the rail track. The settlement measurements were taken at the surface. At location 4, corresponding to CPT 8R-4, two settlement measurements of the rail track were taken. The first measured settlement was 11 mm and a month later 21 mm. After each measurement the rail track is maintained and levelled to its original height. The locations of the two settlement measurements seem to overlap, however it is possible that this is not the case. That would mean that the settlement at location 4 is 21 mm and directly adjacent to it 11 mm. Note that only observed settlements are measured. This means that even though no settlement was measured at certain locations, settlement still might have occurred. It is assumed that the settlement at locations where no settlement was measured will lie between 0 and 4 mm, since the smallest settlement that was recorded is 4 mm.

Location	CPT	Settlement [mm]
1	4L-6	14
2	4R-3	27
3	9R-4	- *
4	8R-4	32 (21) **
5	12R-3	- *
6	10L-3	8

* At locations 3 and 6 no settlement was measured
** At the location corresponding exactly to the location of CPT 8R-4 the measured settlement might be 21 mm

Table 3.7: Settlement at the six selected locations during the period July 2014 - March 2015.

Settlement of the rail tracks continued after March 2015, but the settlement measurements were not executed anymore. According to one of the container terminal operators, maintenance of the ASC rail tracks as a result of settlements is still carried out once per year per rail track. The severity of the corrections of the rail tracks has diminished over time (P. Hogesteeger, personal communication, January 20, 2020). It indicates that settlements are still accumulating, but at decreasing rates.

3.1.8. Geohydrology

MV2 is surrounded by seawater, due to groundwater mounding the groundwater level lies above the seawater level. The groundwater level is determined at +0.63 m NAP [33]. Data from the nine CPTu measurements showed static pore water pressures in the 20 m thick sand fill layer. The hydraulic conductivity of the sand fill is estimated at $4 \cdot 10^{-2}$ m/s, this is a typical value for poorly graded medium coarse sand [28].

3.2. Construction of the ASC rail tracks

The ASC rail tracks are constructed on a shallow foundation. Construction commenced not long after the execution of 300 shallow CPTs and the local ground improvements (Figure 3.1). A result of the work that was carried out in the area of the ASC rail tracks is that the soil conditions, at least the top part of the sand fill, have been disturbed.

3.2.1. The ASC foundation

The first step in the construction of the shallow foundations was levelling the sand fill to 5.0 m NAP. At locations where the sand fill surface lied above 5.0 m NAP this meant that up to 1 m of the sand fill had to be removed. This sand was placed at locations where the sand fill surface lied below 5.0 m NAP. At the rail tracks more sand was removed, till a depth of 4.3 m NAP. This sand was replaced by ballast. Before placing the ballast the sand was compacted with a vibratory plate. The ballast bed itself was also compacted by a vibratory roller [33]. This rail track foundation is indicated by 'Gebied I' in Figure 3.9.

The ASCs are installed on a rail track similar to a train rail track. However, only one rail is placed in the middle of a concrete railroad tie, instead of two rails at both ends of the railroad tie for train rail tracks. The other rail is located at a distance equal to the width of an ASC, which 30 m to 40 m. The shallow foundation of an ASC consists of the rail, the concrete railroad ties and the ballast bed. The top of a railroad tie is located at 5 m NAP. Underneath and around the railroad ties ballast is placed. The railroad ties have a length of 1.2 m and a width and height of 0.3 m, the center-to-center (c.t.c.)

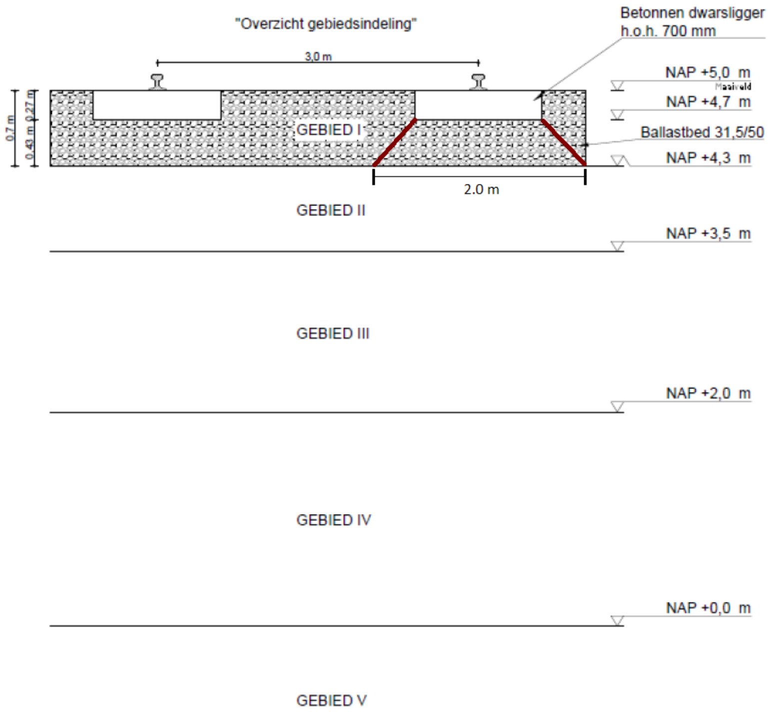

Figure 3.9: Cross-section of the shallow foundation of the rail tracks of two adjacent container stacks and the subsurface underneath. The left rail track is the right rail track belonging to the container stack on the left. The right rail track is the left rail track belonging to the container stack on the right.

distance between two adjacent railroad ties is 0.7 m (into the page). The bottom of the foundation lies at a depth of 4.3 $m\ NAP$. Figure 3.9 shows a cross-section of the foundations of one rail track of two ASCs installed at neighbouring container stacks. The left rail track is the right rail track belonging to the container stack on the left. The right rail track is the left rail track belonging to the container stack on the right. The c.t.c. distance between these two rail tracks is 3.0 m.

3.2.2. Disturbance of the sand

The influence of the compaction works on the state of the sand below the ballast bed has not been measured and therefore needs to be estimated. Relatively simple techniques, a vibratory plate and a vibratory roller, were used to compact the sand. These techniques typically have an extent of around 80 cm [1]. It is assumed that till a depth of 3.5 $m\ NAP$ the ballast bed and the sand reached their maximum compaction as a result of the construction of the ASC rail tracks. This zone comprises 'Gebied I' and 'Gebied II' in Figure 3.9, the relative density is estimated here at 100%. It is assumed that at larger depths the effect of the construction works becomes negligible. Below 3.5 $m\ NAP$ the state of the sand is still represented by the CPT data. The actual extent could be deeper or less deep. Furthermore, the increase in relative density of the compacted sand might have gradually decreased with depth.

In Figure 3.10 the measured cone tip resistance and the correlated relative density of CPT 4L-6 are plotted by the red and blue solid lines, respectively. Till a depth of 3.5 $m\ NAP$ the solid blue line is made transparent, to indicate that the relative density has changed. Above this depth an estimate of the current relative density is plotted by the dark and light brown dashed lines to indicate the ballast bed and the compacted sand, respectively. At depths below the extent of CPT 4L-6 the relative density is estimated at 65%, which is indicated by plotting it with a dashed blue line.

The relative density after construction of the ASCs, but before the ASCs started moving, is thus plotted till a depth of 3.5 $m\ NAP$ by the dark and light brown dashed lines. Below that depth the relative density is plotted by the blue solid and dashed lines. This is the estimated relative density after zero load cycles and is referred to as the initial relative density. The profile of the relative density before construction is plotted over the whole depth by the light and dark blue solid and dashed lines. To distinguish between the two profiles of the relative density, the relative density before construction of the ASC rail tracks will be referred to as the virgin relative density.

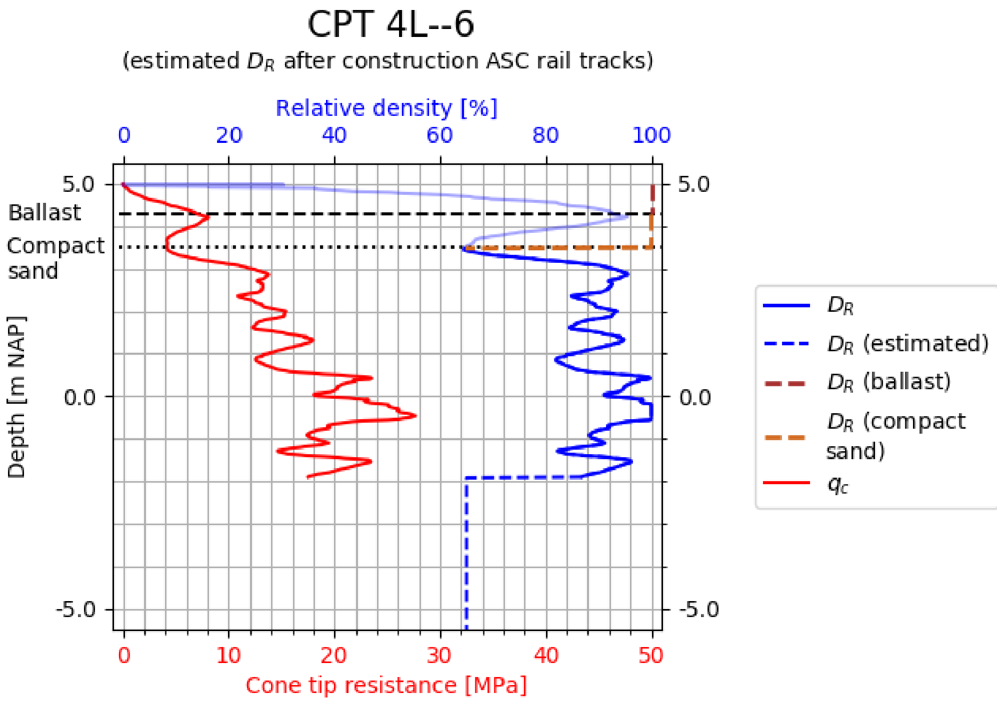

Figure 3.10: The measured cone tip resistance and the relative density correlated with the correlation of Baldi (Equation 3.1) for CPT 4L-6. Above the 'Compact sand'-line the blue line is transparent, indicating that the relative density has changed. The new relative density is indicated by the light and dark brown dashed lines. Below the CPT's extent the relative density is estimated, indicated by the blue dashed line. The ballast bed-sand interface and the estimated depth of the compacted sand lies at 4.3 and 3.5 $m\ NAP$, respectively.

3.3. Loading conditions

The repeated or cyclic load as a result of the movements of ASCs induces densification of the sand and subsequently settlement of the rail tracks. The loading conditions underneath the ASC rail tracks are defined by the amplitude of the load, spreading of the load through the foundation and the sand, the number of load cycles and the frequency of the vibrations that are generated. The hydraulic conductivity of the sand is high and pore water pressure will not accumulate in the sand. The conditions at the RWG container terminal are drained.

3.3.1. Number of load cycles

The c.t.c. wheel distance between two adjacent wheels, part of the same leg of an ASC, is 1.2 m. This distance is small enough to consider the four wheels in the same ASC leg as one linear load. The c.t.c. wheel distance between the rear wheel of the front leg and the front wheel of the rear leg (the two closest wheels of two different legs on the same rail track) is 5.4 m. This distance is large enough to consider them as separate loads. This means that every time an ASC passes, the sand underneath the rail tracks experiences two load cycles. Further, it is assumed that per transported container an ASC is passing twice along the whole container stack. That is one time while carrying a container and one time without. The number of load cycles applied to the sand underneath the ASC rail tracks is in that case equal to four times the amount of transported containers per container stack.

Unfortunately, the number of transported containers per container stack has not been measured, this number will need to be estimated in order to estimate the number of load cycles. A distinction will be made between the settlement measurement period, which took place before the official opening of the RWG container terminal from July 2014 till March 2015 (Figure 3.1), and the period afterwards.

Number of load cycles during the settlement measurement period

Each container stack contains two ASCs. Before an ASC is ready to transport containers it will need to be tested. The testing procedure of an ASC involves driving it multiple times along its rail tracks. The testing procedure included lifting up containers filled with sand weighing up to 40 tonne and transporting them along the container stack. The first settlement underneath the rail tracks was already measured during testing of the ASCs. The number of times an ASC drives along its rail tracks as part of a typical test procedure is unknown.

After testing the ASCs they could start transporting containers. It is unknown how many containers were transported in this period, except that it is a low number. Consequently, the number of load cycles will also be relatively low. In January 2015 the first commercial container ship arrived at the RWG container terminal and 150 containers were transported through the terminal [8]. Towards the end of the settlement measurement period, in February and March of 2015, more containers were transported through the container terminal. The majority of these containers was transported through container stacks 3 to 10, which at the time was referred to as the 'mini-terminal'. The number of load cycles is therefore largest for container stacks 3 to 10.

Unfortunately not much (more) is known about the movements of the ASCs during the settlement measurement period. It is estimated that the number of load cycles as part of the testing procedure lies in the range one thousand. The number of load cycles to transport the first badges of containers is slightly higher. For the container stacks 3 to 10, the 'mini-terminal', the total number of load cycles is estimated between 10 and 50 thousand. For container stacks 11 to 27 the total number of load cycles in this period is estimated between 1 and 10 thousand. This is summarised in Table 3.8.

Container stacks	Number of load cycles
3 - 10	10.000 - 50.000
11 - 27	1.000 - 10.000

Table 3.8: Estimate of the number of load cycles applied to the sand underneath the ASC rail tracks per container stack during the settlement measurement period.

Number of load cycles during operation of the RWG container terminal

During operation of the container terminal the number of load cycles can be estimated as four times the estimated number of the transported containers per container stack. The capacity of the RWG container terminal is 2.35 million TEU (Twenty-foot equivalent) [8]. In 2019 the RWG container terminal was operating almost at its full capacity [20]. It is assumed that on average the container terminal is operating at 90% capacity and that the containers are being distributed evenly over the 25 container stacks. This results in 50.000 containers per container stack per year being transported through the RWG container terminal, which is about 200.000 load cycles per year. About 100.000 load cycles while carrying a container and 100.000 load cycles without a container. The derivation of these numbers is given in Appendix B. In Table 3.9 the estimated number of load cycles for different periods of time are given.

3.3.2. Amplitude of the load

Two types of ASCs are installed at the RWG container terminal, the ASC and the ASC-C. The ASC-C spans more rows of containers stacked next to each other (10 versus 12) and is therefore wider and heavier. The ASC is weighing 236 tonne and the ASC-C 295 tonne. The two ASC types are very

Time [$year$]	Total number of load cycles	Number of load cycles with container	Number of load cycles without container
1	2E5	1E5	1E5
5	1E6	5E5	5E5
10	2E6	1E6	1E6
25	5E6	2.5E6	2.5E6
50	10E6	5E6	5E6

Table 3.9: Estimate of the number of load cycles applied to the sand underneath the ASC rail tracks per container stack after the settlement measurement period.

similar. Both types can carry a container weighing up to 40 tonne. The contact area between the rails and the wheels is the same for both types and therefore their load is spread out over the same surface area. It is assumed that the weight is distributed evenly over the four legs of the ASCs.

In Table 3.10 a few of the specifications of the two ASC types, including the estimated weight of an ASC per leg, are presented. Depending on the ASC type and whether it is carrying a 40 tonne container, the load on one leg varies between 579 and 822 kN. Since containers can weigh less than 40 tonne, the values of the weights given in Table 3.10 represent the range of possible weights. The load is transferred by the track and the railroad ties to the ballast bed. In the ballast bed the load decreases with depth due to spreading of the load. An angle of 1:1 is assumed for the spreading of the load in the ballast bed, this is indicated by the brown lines in Figure 3.9. This results in a loaded surface area beneath one leg of an ASC at the ballast bed-sand interface of 2.0 x 4.6 m^2. If is assumed that the load is distributed evenly over this area the stress will vary between 63 and 89 kPa. In Appendix B is explained how this surface area and the stress are determined.

	Unit	**ASC**		**ASC-C**	
Container stacks	*[-]*	8-11, 14-21, 24-27		3-7, 12, 13, 22, 23	
Width	*[m]*	31.1 (spans 10 containers)		41.1 (spans 12 containers)	
Number of legs	*[-]*	4		4	
Number of wheels per leg	*[-]*	4		4	
Wheel distance (c.t.c. distance two adjacent wheels)	*[m]*	1.2		1.2	
Length of one leg (c.t.c. distance between the two outer wheels)	*[m]*	3.6		3.6	
Distance between two legs (c.t.c. distance between rear wheel of front leg and front wheel of the rear leg)	*[m]*	5.4		5.4	
Velocity of the ASC	*[m/s]*	5		5	
		without container	with container (40 ton)	without container	with container (40 ton)
Total weight	*[ton]*	236	276	295	335
Total weight	*[kN]*	2.32E3	2.71E3	2.90E3	3.29E3
Weight on one ASC leg	*[kN]*	579	677	723	822

Table 3.10: Specifications of the two types of automatic stacking cranes, the ASC and the ASC-C.

In Figure 3.11 three different distributions of the vertical stress increase below the center of a 2 m by 4.6 m shallow foundation are plotted. A uniform vertical stress p is applied to the bottom of the shallow foundation. The vertical stress increase decreases with depth due to spreading of the load in the sand. The estimates of the vertical stress increase with depth are based on the assumption of 1D spreading, 2D spreading and Boussinesq. In either case, the increase in vertical stress is largest directly below the foundation.

The 1D spreading can be used in plane strain conditions, the load spreads out over a width which increases with depth. The 2D spreading or the Boussinesq approximation are used when the load spreads in both lateral and transverse directions. For an estimate of the spreading of the stress below the loaded part of the ASC rail tracks, the 2D spreading under an 1:1 angle is selected. At 4 m depth below the ballast bed, which is two times the width of the shallow foundation, the increase in vertical stress is 10% of its value at the bottom of the foundation, the ballast bed-sand interface. That corresponds to a vertical stress increase of 6 to 9 kPa. With depth the vertical stress increases decreases further and becomes negligible. At 6 m depth below the ballast, equal to three times the width of the foundation, the increase of vertical stress is 5%, which corresponds to 3 to 4.5 kPa.

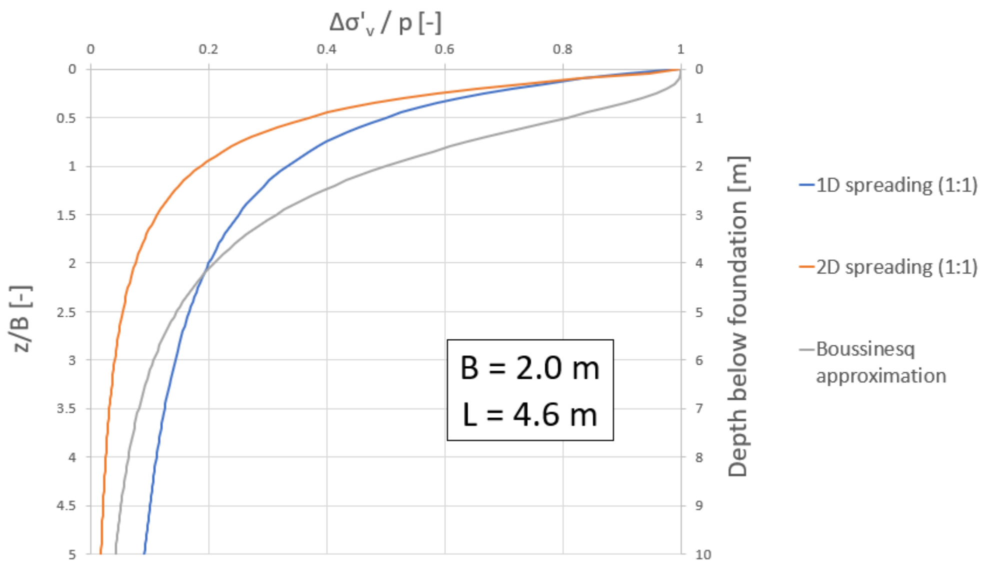

Figure 3.11: Distribution of the vertical stress increase in a dry sand as a result of a stress p applied to a 2 m by 4.6 m interface of the foundation and the sand layer, assuming 1D stress spreading under an angle of 45°, 2D stress spreading under an angle of 45° and an approximation of the Boussinesq stress spreading [18].

3.3.3. Quasi-static cyclic load

A real cyclic load is similar to a sinus-shape. As the ASC is approaching a given point the amplitude of the load applied to that point increases. At the moment the ASC is straight above this point its full load is applied and the amplitude of the load reaches its maximum value. Then the amplitude of the load decreases as the ASC passes. Most of the cyclic settlement models evaluated in this research model the cyclic load as a quasi-static load. That means the applied load is either zero or it has its maximum value, which is equal to the amplitude of the load.

3.3.4. Amplitude and frequency of the vibration

A vibration considers the dynamic effects of the cyclic load, in contrast to a cyclic load modelled as a quasi-static load. This includes acceleration and deceleration of an ASC, lifting containers up and down and shifting them left and right. A vibration can be described by its frequency and the amplitude of the acceleration of the vibration.

The frequency of a vibration generated by an ASC is estimated based on the velocity of an ASC and the distance between two adjacent wheels:

$$f = \frac{v_{ASC}}{s}, \tag{3.4}$$

with

f = frequency, $[Hz]$,
v_{ASC} = velocity of an ASC, $[m \cdot s^{-1}]$,
s = distance or length, $[m]$.

The wheel distance is 1.2 m and the velocity typically varies between 2 and 5 $m \cdot s^{-1}$ (Table 3.10). The dominant frequency of the vibrations generated by an ASC is therefore estimated between 2 and 4 Hz. Note that to determine the frequency of the vibration each of the wheels is considered as an individual load, whereas for the amplitude of the load the wheels in the same ASC leg are considered as one linear load.

The amplitude of the acceleration of a vibration propagating through the sand can be measured with geophones. This was not done at the RWG container terminal. Therefore its value is estimated based on the velocity amplitude of the vibration and the frequency:

$$a = v_{vib} \cdot 2\pi f \tag{3.5}$$

with

a = amplitude of the acceleration of a vibration, $[m \cdot s^{-2}]$,
v_{vib} = velocity amplitude of a vibration, $[m \cdot s^{-1}]$,
f = frequency of a vibration, $[Hz]$.

The velocity amplitude of a vibration is a measure of its energy. It is the velocity of the movements of the grains as the vibration propagates through the sand. The velocity amplitude generated by an ASC is estimated at 0.130 $m \cdot s^{-1}$ at the bottom of the ballast bed. This estimate of the velocity amplitude is about four times the velocity amplitude generated by a train entering a train station [32].

The amplitude of the acceleration of a vibration is estimated between 1.6 and 3.2 $m \cdot s^{-2}$ at the bottom of the ballast bed, depending on the frequency of the vibration. The vibration attenuates with distance from the ASC increases due to material and geometric damping. The amplitude of the acceleration of the vibration with distance is [56]:

$$a(r) = a_0(\frac{r_0}{r})^n \cdot e^{-\alpha(r-r_0)} \tag{3.6}$$

with

a_0 = amplitude of the acceleration at distance r_0 from the source, $[m \cdot s^{-2}]$,
r = distance from the vibration source, [m],
α = attenuation coefficient, $[m^{-1}]$,
n = geometric damping, [-]; n = 1.0 for vertically propagating waves.

In Figure 3.12 the normalised amplitude of the acceleration of the vibration is plotted with depth ($n = 1$), for a hard and a soft sand. The difference in attenuation of a vibration propagating in a soft or hard sand is negligible. The amplitude of the acceleration of the vibration decreases with depth in a similar way as the increase in vertical stress decreases with depth plotted in Figure 3.11.

The vibration also damps out in lateral direction, the geometric damping parameter n becomes 0.5. Because the rail tracks of a container stack are a few hundred meters long, the vibration at a given point along the ASC rail track has damped out long before the ASC passes by again. The vibration is therefore discontinuous.

3.3.5. Static load applied by the container stack

A large number of containers can be stored in the 25 stacks of the container terminal. The containers can be stacked up to five containers high. Five containers with a maximum weight of 40 tonne can weigh up to 200 tonne. Considering a TEU 1 container, which has a surface area of 2.4 m by 6.1 m, the static load applied by the container stack is equivalent to a stress of 135 kPa. Most of the time less

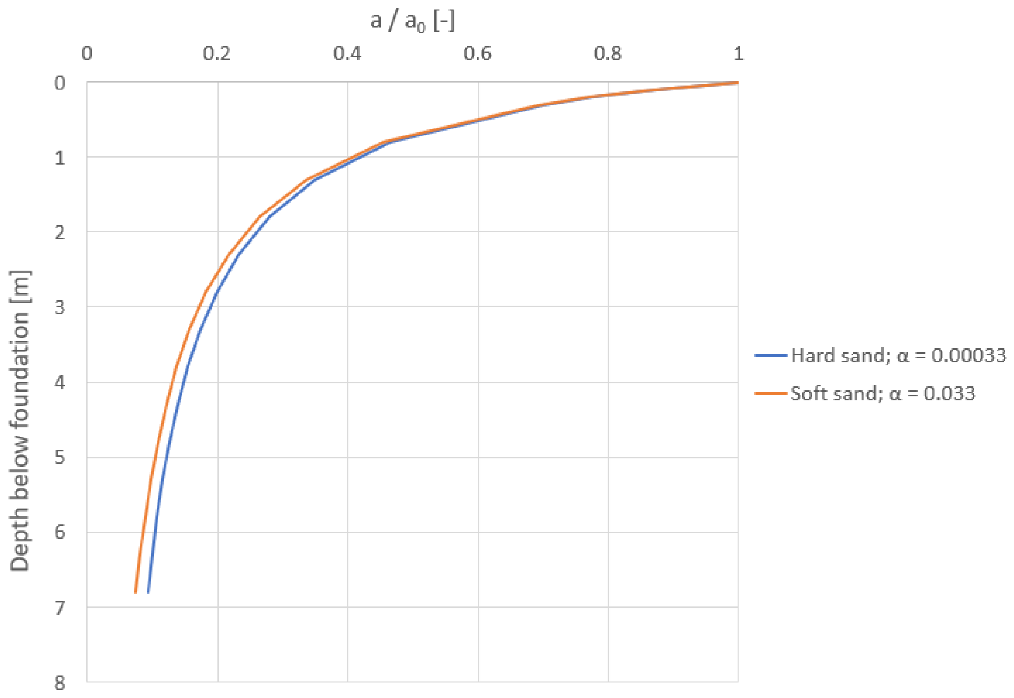

Figure 3.12: Attenuation of a vibration due to geometric and material damping. The normalised amplitude of the acceleration of the vibration in a hard and a soft sand are plotted against depth below the foundation.

than five containers are stacked on top of each other. Furthermore, most containers weigh less than 40 tonne and the majority of the containers consists of the TEU 2 type (Appendix B), which has twice the surface area. The average weight of the containers stored in the container stack is estimated to be equivalent to a static stress of 40 kPa. That would be three containers of 40 tonne stacked on top of each other divided over an area of 2.4 m by 12.2 m (TEU 2 container). That is significant and could affect the stress state underneath the nearby ASC rail tracks.

During the settlement measurement period the number of containers stored in the container stacks was very low. Most of the times no containers were stored in the container stacks and at short moments up to one container high. For the evaluation of the cyclic settlement models the contribution of the weight of the containers to the static load is neglected.

3.4. Summary of the data per location

In Figure 3.13 the six selected locations are indicated on a map of the container stacks at the RWG container terminal. This section summarises the data gathered at the selected locations. This consists of a CPT measurement, which was carried out not more than a few meters distance from the location, the type of crane installed on the rail track above the location, which determines the amplitude of the load, and a settlement measurement. The relative density is correlated to the cone tip resistance. In Figure 3.14 the data is summarised per location. Additionally, a range of the number of load cycles applied by the ASCs is indicated for every location.

3.4.1. Location 1: CPT 4L-6

Location 1 is situated halfway container stack 4, below the left rail track (see Figure 3.13b). At container stack 4 two ASC-C cranes are installed. During the settlement measurement period 14 mm settlement is measured at location 1. The number of applied load cycles is estimated between 10 and 50 thousand. Figure 3.14a shows a plot of CPT 4L-6 and the correlated relative density. Its cone tip resistance

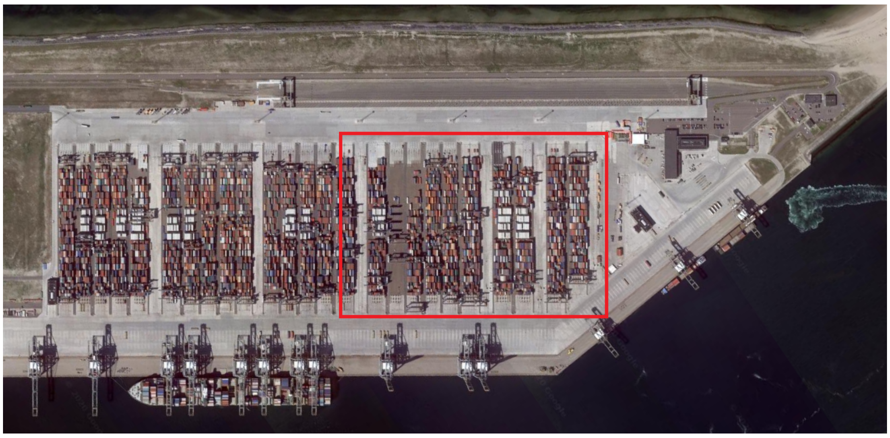

(a) Aerial view of Phase 1 of the container terminal [2]. The red square indicates the container stacks 3 to 13 displayed below.

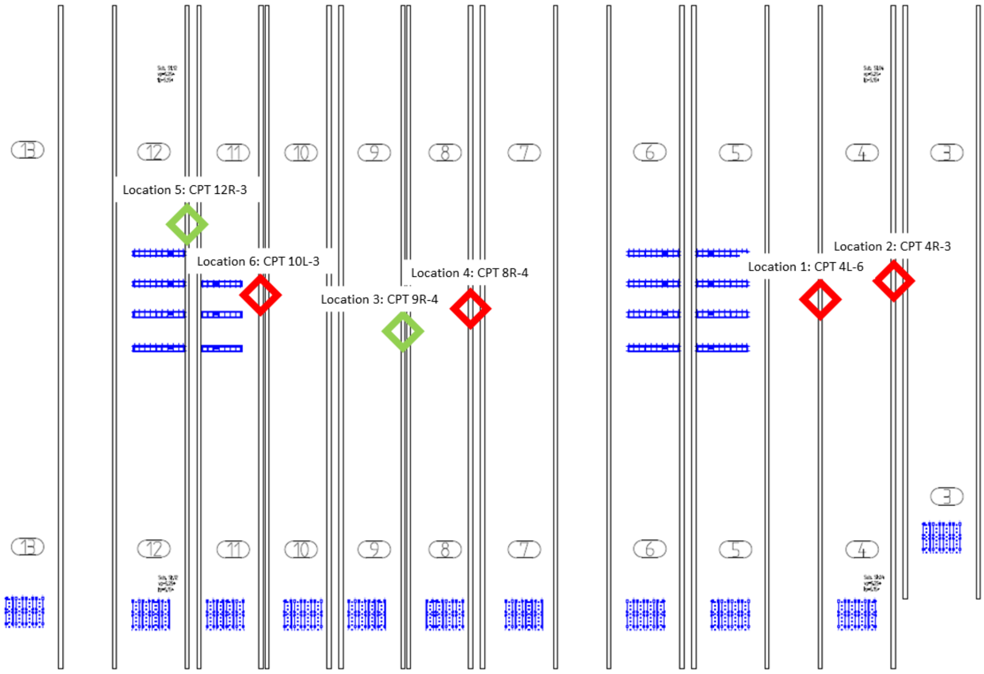

(b) Container stacks 3 to 13 and the six selected locations indicated by the red and green diamonds. Red indicates settlement was observed during the settlement measurement period and green indicates that no settlement was observed during this period.

Figure 3.13: The positions of the six selected locations at the RWG container terminal.

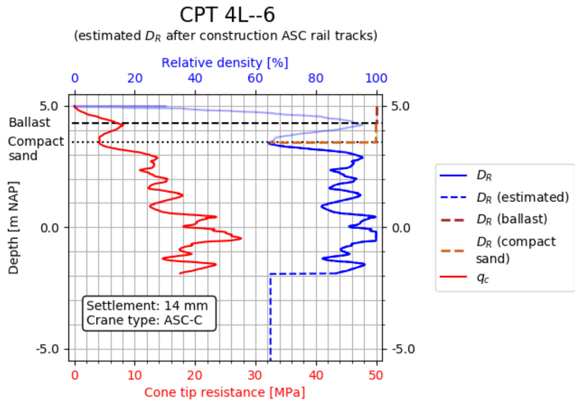

(a) Location 1: CPT 4L-6

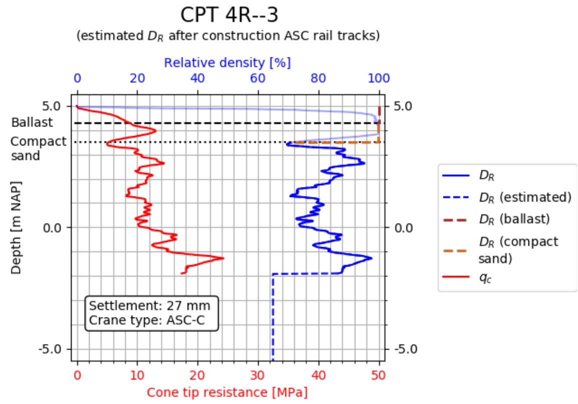

(b) Location 2: CPT 4R-3

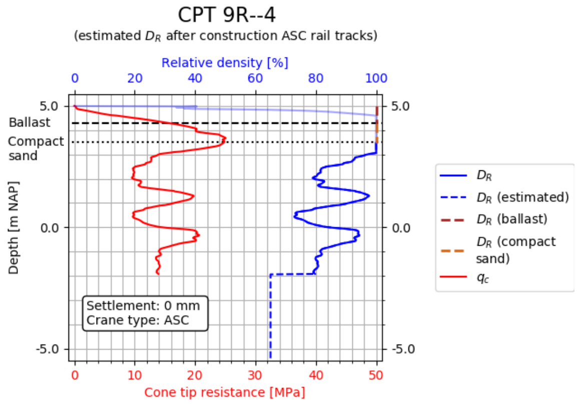

(c) Location 3: CPT 9R-4

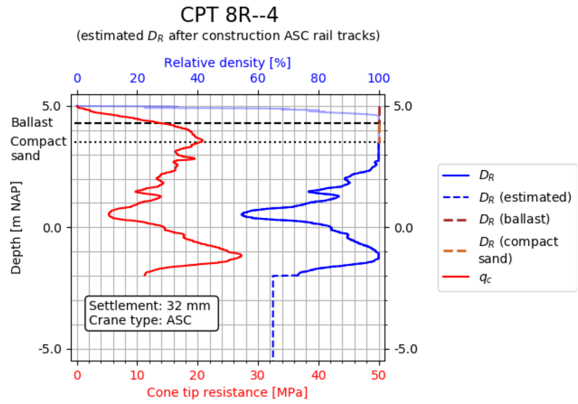

(d) Location 4: CPT 8R-4

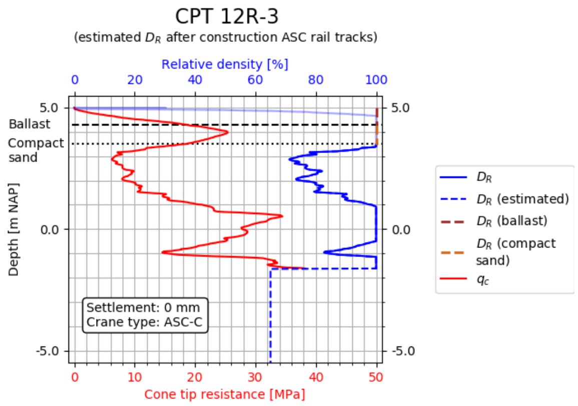

(e) Location 5: CPT 12R-3

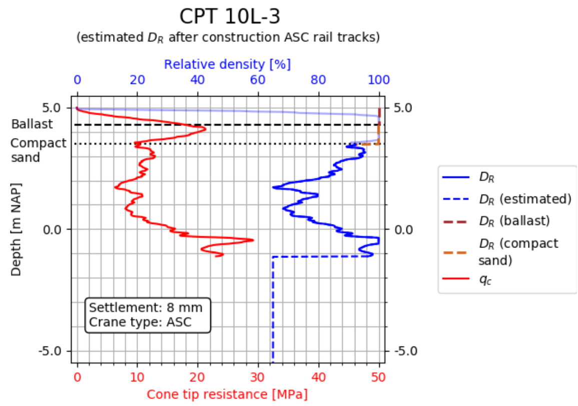

(f) Location 6: CPT 10L-3

Figure 3.14: The measured cone tip resistance and the relative density correlated with the correlation of Baldi (Equation 3.1) for the CPTs corresponding to the six locations. Above the 'Compact sand'-line the blue line is transparent, indicating that the relative density has changed. The new relative density is indicated by the light and dark brown dashed lines. Below the CPT's extent the relative density is estimated, indicated by the blue dashed line. The ballast bed-sand interface and the estimated depth of the compacted sand lies at 4.3 and 3.5 $m\ NAP$, respectively.

gradually increases with depth, between 0 and -2 $m\ NAP$ it decreases. The relative density directly below the compacted sand is around 65%. At larger depths it varies between 80% and 100%, meaning that the sand is medium to very dense.

3.4.2. Location 2: CPT 4R-3

At the other side of container stack 4, below the right rail track, almost at the same height, location 2 is situated (see Figure 3.13b). The lateral distance between location 1 and 2 is around 35 m. Because location 2 is situated at the other side of the same container stack as location 1, it is assumed that the sand underneath the rail track at this location has experienced the same loads as the sand at location 1, i.e. the same number of load cycles of the same amplitude. That is 10 to 50 thousand load cycles applied by an ASC-C. At this location 27 mm settlement is measured. Location 2 corresponds to CPT 4R-3, its cone tip resistance and the correlated relative density are plotted in Figure 3.14b. The cone tip resistance gradually increases with depth, similar to the cone tip resistance measured at location 1. However, over the length of the CPT the cone tip resistance has a lower value than at location 1, except directly below the compact sand. Consequently, under the same loading conditions more settlement occurred at location 2 compared to location 1. In the domain below the compact sand till the extent of the CPT the relative density varies between 70% and 95%.

3.4.3. Location 3: CPT 9R-4

Location 3 is one of the two locations where no settlement was measured during the settlement measurement period. Location 3 is situated below the right rail track of container stack 9 (see Figure 3.13b). At this container stack two standard ASCs are installed. The number of load cycles at this location is estimated between 10 and 50 thousand. CPT 9R-4 is executed at this location. The cone tip resistance and the correlated relative density are plotted in Figure 3.14c. Its cone tip resistance varies with depth. Directly below the compact sand it has a large value and the relative density of the sand is high. At larger depths the cone tip resistance varies. Below 0 $m\ NAP$ it decreases. The relative density of the sand varies between 70% and 100% over the length of the CPT.

3.4.4. Location 4: CPT 8R-4

More settlement was measured during the settlement measurement period at location 4 than at the five other locations: 32 mm. The number of applied load cycles is estimated between 10 and 50 thousand. Location 4 is situated below the right rail track of container stack 8, laterally about 35 m from location 3 (see Figure 3.13b). CPT 8R-4 is executed at this location. The cone tip resistance and the correlated relative density are plotted in Figure 3.14d. The difference between CPTs 8R-4 and 9R-4 emphasises the lateral variability of the compaction of the sand in the top 7 meters. The cone tip resistance also varies strongly with depth. Directly below the compact sand the measured cone tip resistance has a high value. At a depth of 0.5 $m\ NAP$ it reaches its minimum value. Deeper, the cone tip resistance increases strongly and even deeper it decreases again. Although the largest settlement was measured at this location, on average it does not have the lowest cone tip resistance, considering the whole length below the compact sand of the CPTs. At location 4 there is a sand layer at a depth of 0.5 $m\ NAP$ with a relative density of 50%. This is significantly lower than the relative density of the sand fill at the other locations. Densification of this medium dense layer might have primarily contributed to the total settlement.

3.4.5. Location 5: CPT 12R-3

At location 5 also no settlement of the rail tracks was measured, again it is assumed that the settlement at this location lies between 0 and 4 mm. Location 5 lies below the right rail track of container stack 12 (see Figure 3.13b). This container stack was not part of the 'mini-terminal' and therefore less containers have been transported through this container stack during the settlement measurement period. The number of applied load cycles in this period is therefore estimated to be significantly lower, namely between 1 and 10 thousand. At this container stack the heavier ASC-C cranes are installed. The cone tip resistance measured by CPT 12R-3 and the correlated relative density are plotted in Figure 3.14e. It shows strong variability of the cone tip resistance with depth. Directly below the compact sand it has a relatively low value. At 2 $m\ NAP$ its value increases strongly and around 0 $m\ NAP$ it decreases, deeper the cone tip resistance again increases strongly. Over almost its entire length the cone tip resistance of the sand at this location is higher compared to the other locations. The relative density below the compact sand varies between 70% and 100%. Directly below the compact sand the cone tip resistance is lower compared to some of the other locations where settlement was observed. It seems that the first 2 or 3 meter sand below the foundation contributes less to the settlement of the rail tracks than sand at larger depths. That would mean that in this domain densification of the sand is less than at larger depths. Another possibility is that the construction of the ASC rail tracks had a deeper influence on the compaction of the sand than is assumed, for example till at depth of 2 $m\ NAP$ instead of 3.5 $m\ NAP$. A third option could be that settlement did occur at this location but it was not observed and therefore not measured.

3.4.6. Location 6: CPT 10L-3

CPT 10L-3 is executed at location 6. The cone tip resistance and the correlated relative density are plotted in Figure 3.14f. Below the compact sand the cone tip resistance is more or less constant with depth with a relatively low value. Compared to the other locations it has a thick sand layer with a relatively low compaction. Below 1.0 $m\ NAP$ the cone tip resistance increases significantly. The relative density varies between 65% and 100%. Considering the domain starting below the compact sand till the extent of the CPT, location 6 has on average the lowest cone tip resistance. Location 6 is situated below the left rail track of container stack 10 (see Figure 3.13b). At this container stack two normal ASCs are installed. The measured settlement at this location is 8 mm. More settlement would have been expected at this location when its cone tip resistance is compared to the cone tip resistance at other locations where more settlement was measured.

4

Results and discussion

This chapter starts with listing criteria to evaluate the performance of the cyclic settlement models. This is followed by a qualitative discussion about the uncertainty of the input data, summarised in an overview table at the end of Section 4.3. Then assumptions and simplifications about the input data and model parameters to make more reliable model predictions are presented and discussed. To improve reliability of the model predictions an extensive site investigation program is recommended, which is described next. In Sections 4.6 and 4.7 preliminary results based on site conditions and simulations of the first load cycle, made with FE computations in PLAXIS and improved Schmertmann method, are presented and discussed. This is followed by a presentation and discussion of the results obtained with the cyclic settlement models. The results show that the terminal density model gives the best predictions of the cyclic settlement of ASC rail tracks. This model is used to calculate the settlement in Phase 2 of the RWG container terminal. The predicted cyclic settlement is compared to the settlement requirements. Finally, a scenario is presented to compact the sand fill at the RWG container terminal.

4.1. Input data, model predictions & parameters

In the interest of clarity first the definitions of input data, model predictions and model parameters are stated here. These terms are frequently used in this chapter.

Input data are all the data that influence the cyclic settlement. Input data consist of soil properties, soil profile, initial state of the sand, amplitude of the load, number of load cycles and foundation type. Model parameters are defined by the static and cyclic settlement models. Model parameters are divided into three groups: initial state, soil parameters and load parameters. The model parameters of the cyclic settlement models are summarised in Table 2.1. Their values are determined by the input data. Model predictions are a function of the cyclic settlement models and model parameter values, i.e. the output of the cyclic settlement models.

Figure 4.1 gives an overview of the input data that primarily influence cyclic settlement of ASC rail tracks. Soil properties and soil profile determine the model soil parameters and initial state of the sand determines the model initial state parameters. These are indicated in red. Input data that describe the loading conditions, number of load cycles, amplitude of the load and foundation type, are indicated in black. Foundation type determines how the load is transferred onto the soil and is therefore also considered a model load parameter. Model predictions consist of the cyclic settlement and depth of influence. Depth of influence is a model prediction that affects the cyclic settlement model prediction. Therefore, depth of influence is also input data for cyclic settlement models that do not determine it.

Input data and the depth of influence are related to each other, this is indicated in Figure 4.1 by the dashed arrows. Depth of influence depends on the soil properties, soil profile, initial state, amplitude of the load and foundation type. Vice versa, foundation type depends on the depth of influence. Further, it depends on the soil properties, soil profile, initial state and amplitude of the load. The vertical stress

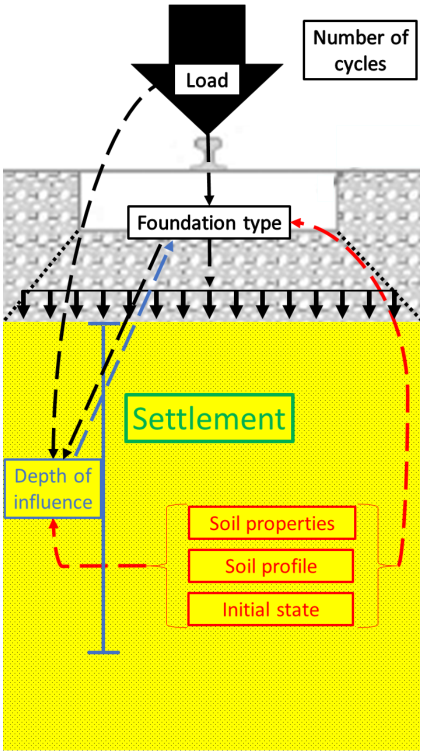

Figure 4.1: Settlement of the rail tracks is expected to be primarily affected by the input data given in the black and red boxes and the depth of influence. Depth of influence is a model prediction that affects the cyclic settlement model prediction. For cyclic settlement models that do not determine the depth of influence it is input data. Settlement is model prediction of the cyclic settlement models. Dashed arrows indicate dependencies between the input data and depth of influence.

at the ballast bed-sand interface depends on the amplitude of the load and spreading of the load in the foundation.

4.2. Evaluation criteria for cyclic settlement models

A good cyclic settlement model considers the relations between the input data and model predictions presented in Figure 4.1. However, uncertainty of the input data causes uncertainty of the model parameters. This influences the performance of cyclic settlement models. Consequently, a good cyclic settlement model might give unreliable model predictions. The main criteria used in this research to evaluate the performance of cyclic settlement models are:

- feasibility data recovery;
- availability data;
- reliability model prediction;
- match with the settlement measurements;
- theoretical and physical correctness.

It is important that input data can be obtained through relatively simple or standard investigation methods, i.e. it is feasible in engineering practice to measure the input data and determine the model parameter values. The input data available for this research are incomplete. Values of the model parameters are estimated and contain uncertainty. Reliable model predictions of the cyclic settlement models is crucial.

Based on the first three criteria the terminal density model and C/L model for cyclic shear are selected. These models are compared with the measured settlement. Secondly, theoretical and physical correctness of the two cyclic settlement models are compared, i.e. which model considers the relations between the input data and model predictions as indicated in Figure 4.1 and is physically correct. For example, indefinite cyclic settlement as $N \rightarrow \infty$ is physically incorrect. Due to uncertainty of the input data it is possible that the cyclic settlement model that is theoretically and physically (most) correct does not coincide with the model that is eventually considered the best.

4.3. Uncertainty of the input data

The available data were gathered for the geotechnical design of the RWG container terminal but never with the intention to evaluate cyclic settlement models. A result is that input data listed in Figure 4.1 are incomplete to determine all model parameter values. Ideally all model parameter values are determined based on soil tests. However, model parameters that characterise cyclic densification properties of sand are determined based on advanced cyclic soil tests, such as a cyclic simple shear or cyclic oedometer tests. Compared to standard soil tests they are more suitable to determine the cyclic densification properties of a sand. However, site investigations executed at the RWG container terminal were limited to standard soil investigation methods, such as CPT's, boreholes and triaxial tests. Input data are completed by:

- estimating data;
- use of correlations;
- inter- or extrapolation of data;
- (FE) modelling of soil behaviour.

Uncertainty of the input data is introduced by (a combination of) the above listed factors. More uncertainty is introduced due to disturbance of soil (samples). In case uncertainty of the model parameters is too large, model predictions become unreliable. Relevant input data that contain uncertainty are:

- CPT data and relative density;
- stiffness of the sand fill;
- minimum and maximum void ratio;
- measured settlement;
- volumetric threshold strain;
- number of load cycles;
- amplitude of the load;
- spreading of the load;
- maximum density;
- cyclic densification properties.

4.3.1. CPT data and the relative density

The soil profile of the sand fill is determined with CPT measurements. With the correlation of Baldi in Equation 3.1 the initial relative density of the sand is determined, which gives the initial state of the sand.

Uncertainty as a result of extrapolation of CPT data over a few meters distance is negligible. The large amount of CPT data makes it possible to select locations where settlements were measured within a few meter distance from a CPT measurement. CPT's show a strong variability of the relative density in the top 7 meter of the sand fill, laterally and vertically. This is demonstrated by the difference between the cone tip resistance at locations 3 and 4, shown in Figures 3.14c and 3.14d, respectively. These two locations are laterally just 35 m apart. Both CPT's also show strong variability of the cone tip resistance with depth. Extrapolation of CPT data over larger distances introduces significant uncertainty.

The soil conditions beyond the extent of a CPT, below around -2 m NAP, do not influence most of the model predictions. For most cyclic settlement calculations the depth of influence lies within the extent of the CPT's. Beyond the extent of a CPT the sand is estimated to be medium dense. This is based on deeper CPT's that were carried out elsewhere at the RWG container terminal. In contrast to the top part of the sand fill, deeper the relative density is less variable and lower.

Conditions in the top part of the sand fill are uncertain. After the CPT's were executed the ASC rail tracks were constructed. State of the sand has not been measured afterwards. The ballast bed and top part of the sand layer underneath are compacted. The relative density is determined at 100% up to a depth of 3.5 m NAP, or 1.5 m depth below the surface. However, it is possible that at certain locations the sand is less compacted and the relative density is lower. Furthermore, influence of the construction works might have been less deep, deeper or gradually decreasing with depth. Together with the depth of influence the extent of the compacted sand layer defines the zone of influence underneath ASC rail tracks.

In this research the correlation of Baldi given in Equation 3.1 is used to correlate the cone tip resistance to the relative density. This introduces a model uncertainty. However, other commonly applied correlations between the cone tip resistance and relative density show similar results, especially for dense sands in the top 10 m of a sand fill. This is shown in Appendix B. The correlation of Baldi gives a good estimate of the relative density of sand underneath the ASC rail tracks.

Disturbance of (the top part of) the sand fill is the main cause for uncertainty of the relative density of the sand. For all cyclic settlement models is assumed that the sand reached 100% relative density till 3.5 m NAP, no settlement occurs above this depth. Increasing the depth of compacted sand results in less settlement. Below the compacted sand an increase of the initial relative density results in a decrease of the settlement.

4.3.2. Stiffness parameters

Stiffness of a sand is a variable soil property. It can be described by the secant stiffness, which is determined in triaxial tests. Unloading / reloading stiffness and stress dependency of the stiffness (parameter m) are also determined in triaxial tests. Small strain stiffness and strain dependency of the stiffness are determined based on the shear modulus reduction curve for sand presented in Figure 3.7b.

Disturbed loose sand is taken from several boreholes executed elsewhere at the RWG container terminal. This sand is comparable to sand underneath the ASC rail tracks, the data have a high extrapolation distance. The sand was used to prepare test samples for the triaxial tests. It is difficult to obtain the in situ relative density in the tests. This is taken care of by determining the secant stiffness of the sand for varying relative density. A correlation between the secant stiffness of the sand and relative density is plotted with the blue solid line in Figure 3.6. The green dotted line is a correlation between stiffness and relative density of another sand type. The two correlations match well, especially for higher relative densities. The secant stiffness values are in the correct order of magnitude.

A correlation between the unloading / reloading stiffness and relative density is plotted with the orange solid line in Figure 3.6. For lower relative densities it is 4.5 times the secant stiffness. For higher relative densities it is 3.5 times the secant stiffness. This is only slightly higher than three times the secant stiffness used as default in the HSsmall model [40].

For sand at the RWG container terminal the value of parameter m is determined at 0.7. Parameter m lies between 0 and 1, a typical value for sands is 0.5 [40]. An increase of parameter m means that the stiffness of the sand increases at a higher rate with (confining) stress. This also means that stiffness decreases at a higher rate with decreasing stress. Generally, stiffness model parameters are expressed to a reference confining stress of 100 kPa. Confining stress is applied by the weight of the overlying sand fill, both increase with depth.

The secant stiffness values that were found for varying relative density and average shear strain level in the triaxial tests are used to calibrate a shear modulus reduction curve for sand to use it for the type of sand at the RWG container terminal. The modulus reduction curve is used to estimate the small strain stiffness and strain dependency of the stiffness. Uncertainty of the small strain stiffness and strain dependency of the stiffness is caused by uncertainty of the:

- secant stiffness;
- shear strain level corresponding to the secant stiffness;
- shear modulus reduction curve.

The shear strain level determines one point on the curve, here the sand has a stiffness equal to the secant stiffness. The relation between the stiffness and shear strain is described by the shear modulus reduction curve. Increase of the secant stiffness or the shear strain level corresponding to the secant stiffness used for the calibration of the shear modulus reduction curve result in an increase of the stiffness for any level of shear strain.

On a shear modulus reduction curve that lies to the left, like the curve for a well-graded gravel in Figure 3.7b, the secant stiffness values correspond to smaller values of the normalised shear modulus. This results in an increase of the stiffness for any level of shear strain. If the curve for well-graded gravel was used instead, the shear strain level in a triaxial test and secant stiffness correspond to a normalised shear modulus of around 0.10, instead of 0.17. At shear strain levels 0.1%, 0.01%, 0.001% and 0.0001% the stiffness becomes 2, 5, 9 and 10 times the secant stiffness, respectively. For the shear modulus curve for sands this is 2, 4, 5 and 6 times the secant stiffness, respectively. The shear modulus reduction curve for sand at the RWG container terminal might also lie to the right. That results in a decrease of the stiffness at any level of shear strain.

Behaviour of the sand in the first load cycle is characteristic for its behaviour in the subsequent load cycles, according to the C/L model for cyclic shear, seismic induced strain model, terminal density model and cumulative plastic strain model. Model parameters of these models are determined based on the response of the sand in the first load cycle. In the first load cycle the stiffness of the sand dominates the deformation behaviour of the sand. Consequently, the stiffness of the sand fill, parameter m and strain dependency of the stiffness influence the model predictions. Cyclic shear strain amplitude is determined in an FE computation that simulates the first load cycle. With increasing stiffness and decreasing parameter m the cyclic shear strain amplitude decreases. This results in a decrease of the settlement and depth of influence. Void ratio after one load cycle and vertical plastic strain after one load cycle are both estimated based on the vertical strain calculated with the improved Schmertmann method. With increasing stiffness and decreasing parameter m the void ratio after one load cycle increases and vertical plastic strain after one load cycle and settlement decrease. Model predictions of the C/L model for oedometer compression and the Hergarden model are not influenced by the stiffness of sand.

4.3.3. Minimum and maximum void ratio

The minimum and maximum void ratio represent a very dense and loose state of the sand, respectively. Minimum and maximum void ratio are soil properties. The void ratio of a sand and the relative density are related through the minimum and maximum void ratio.

The minimum and maximum void ratio are determined based on the minimum and maximum density measurements of sand samples taken from boreholes elsewhere at the RWG container terminal. The measurements do not indicate which standard was used to measure the loosest and densest state of the sand. This sand comparable to the sand underneath the ASC rail tracks. This data have a high correlation length. The minimum and maximum void ratio range from 0.472 - 0.680 and 0.721 - 1.032, respectively. This is inconsistent with Figure 3.4. For (sub-)rounded sand grains with a coefficient of uniformity of 2.0 the minimum and maximum void ratio are around 0.4 and 0.7, respectively. For sand underneath the ASC rail tracks the minimum and maximum void ratios are estimated at 0.5 and 0.8, respectively. These values lie within the range of measured values.

Settlement model prediction of the Hergarden model increases with decreasing minimum void ratio, as long as the gap between the minimum and maximum void ratio remains constant or increases. An increase of the gap between the minimum and maximum void ratio due to an increase of the maximum void ratio is (partially) cancelled out by the corresponding increase of the initial void ratio, according to Equation 2.11. For the C/L model for cyclic shear settlement model predictions increase with initial void ratio. Regardless of the gap between the minimum and maximum. The initial void ratio increases with increasing minimum and maximum void ratio. For the terminal density model influence of a change of the initial void ratio is negligible, according to Equation 2.13. Model predictions of the C/L model for cyclic oedometer compression, seismic induced strain model and cumulative plastic strain model are independent of the minimum and maximum void ratio.

4.3.4. Settlement measurements

The settlement measurements are not input data. They do not affect the cyclic settlement or model predictions of the cyclic settlement. Cyclic settlement model predictions are compared to the settlement measurements.

The settlement measurements consist of just one or two measurements of the rail tracks per location. The settlement is measured by comparing the rail tracks to their original level. Settlement is thus measured at the surface. Distribution of the cyclic settlement with depth is unknown. Furthermore, it is not indicated which technique was used to measure the , here the accuracy is unknown.

Locations 3 and 5 (CPT's 9R-4 and 12R-3) are discarded from the evaluation of the cyclic settlement models. Combination of the settlement measurements, CPT data and loading conditions indicate that some measurements are inconsistent. No settlement was measured at locations 3 and 5, however the sand has a lower relative density compared to locations where settlement was measured. It seems unlikely that no (or very small amount of) settlement occurred at these locations. Either settlement did occur but was not measured at locations 3 and 5, the initial relative density of the sand significantly increased at these locations or decreased at the other locations during construction of the ASC rail tracks, or the loading conditions at locations 3 and 5 were very different compared to the other locations.

The measured settlement is incomplete and contains too much uncertainty to validate the cyclic settlement models. An error in the settlement measurements could lead to agreement with a cyclic settlement model that incorrectly predicts the settlement. At the remaining locations 1, 2, 4 and 6 the settlement measurements are more consistent with the CPT data and loading conditions. The settlement measurements are used as an indication of the settlement that has occurred. Most settlement occurred at locations 2 and 4. At locations 1 and 6 less settlement occurred.

4.3.5. Volumetric threshold strain

Volumetric threshold strain is a soil property. It is a measure of the resistance of the sand against volumetric plastic strains. Plastic strain accumulates when the strain induced by an applied load is larger than the volumetric threshold strain.

The volumetric threshold strain of the sand at the RWG container terminal is estimated based on literature. Typical values of the volumetric threshold strain for clean sands range from 0.007% to 0.030% [55]. The volumetric threshold strain of the sand at the RWG container terminal is estimated at 0.01%. An increase of the volumetric threshold strain results in less permanent strain accumulation during a load cycle. Cyclic settlement decreases with increasing volumetric threshold strain.

In the seismic induced strain model the volumetric plastic strain decreases with increasing volumetric threshold strain. Additionally, depth of influence decreases with volumetric threshold strain. The depth at which the cyclic shear strain amplitude has a higher value decreases. Consequently, settlement decreases with increasing volumetric threshold strain. The same method is used to determine the depth of influence for the C/L model for cyclic shear.

4.3.6. Number of load cycles corresponding to the measured settlement

Due to the wide range of estimated number of load cycles that corresponds to the settlement measurements it is not possible to find reliable agreement with one cyclic settlement model. The number of load cycles that corresponds to the measured settlement at locations 1, 2, 4 and 6 is estimated between 10 and 50 thousand. An increase of number of load cycle means that it took more load cycles before the measured settlement occurred, i.e. rate of settlement decreases. Combination of the settlement measurements and estimated number of load cycles is used to evaluate which cyclic settlement model gives the best model predictions. For example, 14 mm settlement is measured at location 1. Two cyclic settlement models might predict 14 mm settlement at this location. One after 10 thousand another after 40 thousand load cycles. Although their prediction are significantly different, settlement predictions of both cyclic settlement models match to the settlement measurement.

All cyclic settlement models are affected by the number of load cycles, except the Hergarden model, which does not determine the settlement as function of the number of load cycles.

4.3.7. Amplitude of the load

Amplitude of the load is a load parameter. The amplitude of the load depends on the weight of an ASC (or heavier ASC-C) and container. Various model load parameters depend on the amplitude of the load: vertical stress, amplitude of the acceleration of the vibration and foundation stress.

The amplitude of the load varies due to the varying weight of the containers that are transported. Weight of a container can be up to 40 tonne, depending on its content. It is assumed that the combined weight is distributed equally over the four legs of an ASC. For an ASC the amplitude of the load is estimated to be equivalent to a vertical stress on the ballast bed-sand interface between 63 and 74 kPa, depending on whether the ASC is carrying a container and the weight of the container. For the heavier ASC-C this ranges from 78 and 89 kPa. However, in case a container is lifted more on one side of an ASC the combined weight is not distributed equally over its four legs. The amplitude of the load on that side increases. It is estimated that the load could become equivalent to a vertical stress of 100 kPa.

Settlement increases with increasing amplitude of the load for all cyclic settlement models. The cyclic shear strain amplitude increases with amplitude of the load. Consequently, depth of influence increases in the C/L model for cyclic shear and the seismic induced strain model. Further, amplitude of the acceleration of the vibration increases. The depth at which the amplitude of the acceleration is larger than the threshold acceleration increases, i.e. depth of influence in the Hergarden model increases. An increase of the depth of influence results in a further increase of the settlement.

4.3.8. Spreading of the load

Distribution of the load is a geometrical parameter and is related to the foundation type, in the current problem a shallow foundation. Loads applied to the ASC rail tracks are transferred by concrete railroad ties to the ballast bed underneath. In the ballast bed load decreases with depth due to spreading. The angle of spreading determines the rate at which the amplitude of the load decreases with depth. The load spreads out more in the sand underneath the ballast bed.

A larger angle, or wider spreading, in the ballast bed results in an increase of the loaded surface area at the ballast-bed sand interface. The load spreads out over a larger area which results in an increase of the rate of damping, i.e. the vertical stress and amplitude of the load decrease with depth at a higher rate. Consequently, settlement model predictions decrease for all cyclic settlement models with increasing angle of spreading. In the ballast bed a spreading under a 1:1 angle is assumed. This is a typical value for granular materials. A result is that the load of one leg of an ASC is spread out over a 4.6 m by 2.0 m surface area at the ballast bed-sand interface and the L/B ratio is 2.3. For a 1:2 angle for example, the load would spread out over a 5.6 m by 3.0 m surface area and the L/B ratio would become 1.9. With increasing angle of spreading in the ballast bed the foundation becomes more squared.

Depth of influence determined by the C/L model for cyclic shear, seismic induced strain model and Hergarden model decreases with decreasing amplitude of the load. This leads to an additional decrease of the cyclic settlement.

Most of the cyclic settlement models do not explicitly consider the spreading angle of the load in sand. The improved Schmertmann method and FE model computations inherently include spreading of the load. The Hergarden model uses an attenuation equation to determine the amplitude of the acceleration of the vibration with depth, plotted in Figure 3.12. Consequently, only predictions of the C/L model for cyclic oedometer compression decrease with increasing angle of spreading. The assumed distribution of the vertical stress in the sand underneath the ballast bed is given by the 2D spreading under a 1:1 angle plotted in Figure 3.11. In sands an increase of the spreading angle leads to an increased rate of damping and amplitude of the load decreases.

4.3.9. Maximum density

Maximum density is considered a soil property. However, its value also depends on the initial state of the sand and boundary conditions and it increases with amplitude of the load [39]. Sand evolves towards its maximum density with increasing number of load cycles. The difference between the initial and maximum density determines the settlement as $N \to \infty$.

It is difficult to determine the maximum density of the sand with depth. That explains why some cyclic settlement models do not consider the maximum density and instead assume cyclic settlement continues indefinitely. Maximum density of the sand can be determined in cyclic soil tests. Cyclic soil tests are not executed on sand samples from the RWG container terminal.

Both C/L models, seismic induced strain model and cumulative plastic strain model assume that cyclic settlement continues indefinitely. Maximum density is therefore not a model parameter. The Hergarden model assumes that the maximum density is reached. It predicts the maximum density. The terminal density model is the only cyclic settlement model with a model parameter representing the maximum density. With increasing maximum density model prediction of the settlement increases.

4.3.10. Cyclic densification properties

Cyclic densification properties are soil properties. They characterise densification of the sand. Cyclic densification properties are determined in cyclic soil tests. These tests are not executed on sand samples from the RWG container terminal.

The cyclic settlement models that assume indefinite densification do not have a maximum density. A high rate of densification will result in large model prediction of the settlement. These models are therefore especially sensitive to the cyclic densification properties. This comprises both C/L models, seismic induced strain model and cumulative plastic strain model. The maximum densification determined with the Hergarden model depends on the densification properties of sand. An overestimate of the maximum densification results in a large model prediction of the settlement. In the terminal density model the maximum density is defined. The cyclic densification properties determine the rate density of the sand evolves towards its maximum value. Model predictions are therefore bounded by the settlement related to the maximum density. The terminal density model is therefore less sensitive to the model parameters that determine the cyclic densification, especially for a large number of load cycles as it approaches the maximum density.

4.3.11. Reliability cyclic settlement models

Performance of each cyclic settlement model is affected differently by uncertainties of the input data. Table 4.1 summarises the uncertainty of relevant input data and sensitivity of the cyclic settlement models. Uncertainty about the input data are indicated by uncertain (-), less (un)certain (+/-) or certain (+). Information outlined in red are uncertain. Sensitivity of cyclic settlement models to the information is indicated by independent or negligible sensitivity (0), sensitive (1) or very sensitive (2). Cells highlighted in red indicate cyclic settlement models that are very sensitive to uncertain information. Model predictions of cyclic settlement models that are very sensitive to uncertain information can become unreliable in case uncertainties become too large.

Engineering parameters & input data / Cyclic settlement models	CPT data & relative density	Stiffness of the sand	Min. & max. void ratio	Volumetric threshold strain	Number of load cycles	Amplitude of the load	Spreading of the load	Maximum density	Cyclic densification properties
Uncertainty information	+/-	+/-	+	-	-	+	+/-	-	-
C/L model for cyclic shear	2	2	1	1	2	2	1	0	2
C/L model for cyclic oedometer compression	2	0	0	0	2	2	2	0	2
Hergarden model	2	0	2	0	0	2	1	0	2
Terminal density model	2	2	0	0	2	2	1	2	1
Seismic induced strain model	2	2	0	2	2	2	1	0	2
Cumulative plastic strain model	2	2	0	0	2	2	1	0	2

Table 4.1: Overview of the uncertainty of the input data and sensitivity of the cyclic settlement models. Uncertainty ranges from uncertain (-) to certain (+) and sensitivity from independent or negligible sensitivity (0) to very sensitive (2). Information that are uncertain are outlined in red. Red cells indicate cyclic settlement models that are sensitive to uncertain information.

C/L model for cyclic shear is very sensitive to the cyclic densification properties. The model parameters that describe the cyclic densification properties are defined as material constants. Ideally their values are measured in a cyclic soil test. These are not executed, their values are therefore uncertain. However, values for the material constants can be determined with a correlation [34]:

$$c_1 = 13.3 - 7.4 \cdot D_{R,0} \tag{4.1a}$$

$$c_2 = 0.13 \tag{4.1b}$$

This correlation is based on a large number of cyclic simple shear tests on different types of sand executed by several researchers. An overview of the values of the material constants of these sands is given in Appendix F. This improves the reliability of the model predictions of the C/L model for cyclic shear.

The C/L model for cyclic oedometer compression also defines material constants c_1 and c_2. It is not possible to use the correlation in Equation 4.1 to determine values of the material constants of the C/L model for cyclic oedomdeter compression. A similar correlation for this version does not exist. Their values remain uncertain. The C/L model for cyclic oedometer compression is very sensitive for these model parameters. Model predictions of the C/L model for cyclic oedometer compression are therefore unreliable.

Amplitude of the acceleration of the vibration depends not only on the amplitude of the load, but also on an ASC's velocity and acceleration. Its value is difficult to determine. Amplitude of the acceleration of the vibration is therefore uncertain. The Hergarden model is very sensitive to this model parameter. In Table 4.1 is indicated that the Hergarden model is also very sensitive to the cyclic densification properties. Model predictions of the Hergarden model are unreliable.

Model predictions of the terminal density model are very sensitive to the maximum density, which is uncertain. However, the terminal void ratio, a model parameter of the terminal density model that describes the maximum density, can be correlated to the void ratio after one load cycle [16]:

$$e_T = 0.987e_1 \tag{4.2}$$

The correlation has a good fit ($R^2 = 0.99$). This makes the estimate of the maximum density of sand in the terminal density model more certain and the model predictions more reliable.

The seismic induced strain model is very sensitive to the volumetric threshold strain, number of load cycles and cyclic densification properties, which are all uncertain. Model predictions with this cyclic settlement model are unreliable.

The cumulative plastic strain model calculates the cyclic settlement based on three model parameters, vertical plastic strain after one load cycle, number of load cycles and a material constant that describes the cyclic densification properties of the sand. The latter two are uncertain. Model predictions of the cumulative plastic strain model are very sensitive to all three model parameters. Model predictions of the cumulative plastic strain model are therefore unreliable.

Considering the available input data and uncertainty the C/L model for cyclic shear and terminal density model are the two cyclic settlement models that give reliable model predictions. They are indicated in grey in Table 4.1. The C/L model for cyclic shear and terminal density model are evaluated in this chapter. Their results are presented and discussed in Sections 4.8 and 4.9.

4.4. Assumptions and limitations

Assumptions to about the soil and loading conditions to apply the cyclic settlement models, FE computational model and improved Schmertmann method and obtain more reliable model predictions are discussed here. Limitations of the cyclic settlement models and assumptions are also discussed.

4.4.1. Modelling of the load and foundation

The dimensions of the foundation are estimated at 2.0 m by 4.6 m. It is therefore a 3D problem. Although the entire rail track is much longer, only part of the rail tracks that experiences the load applied by an ASC is modelled as the foundation. Distance between the legs of one ASC is large enough to model the load applied by each leg as an individual load and foundation. This means that each ASC is sitting on four small foundations. The foundations move with the ASC. The ballast bed-sand interface is taken as the bottom of the foundation.

The load is modelled as a static or a quasi-static (cyclic) load, either amplitude of the load is fully applied or no load is applied. However, the load applied by a moving ASC is best represented by a sinus-shape, like the vertical stress presented in Figure 4.2. The principal stresses rotate with the moving load. Principle stress rotation can lead to an increase of the settlement [23]. Principal stress rotation is neglected. In the FE computation and improved Schmertmann method the principal stress directions are vertical and horizontal.

In the FE computation, improved Schmertmann method and cyclic settlement models the load and foundation are modelled as a vertical stress equivalent to the amplitude of the load at a depth of 4.3 m NAP spread out over a surface area of 2.0 m by 4.6 m. This is the foundation stress. The ballast bed-sand interface is situated at 4.3 m NAP. Figure 4.2 shows that the horizontal stress under a passing wheel load is significantly smaller compared to the vertical stress. Horizontal stress applied by an ASC is neglected.

Dynamic effects related to the velocity and acceleration of an ASC and lifting of containers are neglected. Amplitude of the load could increase temporarily due to dynamic effects.

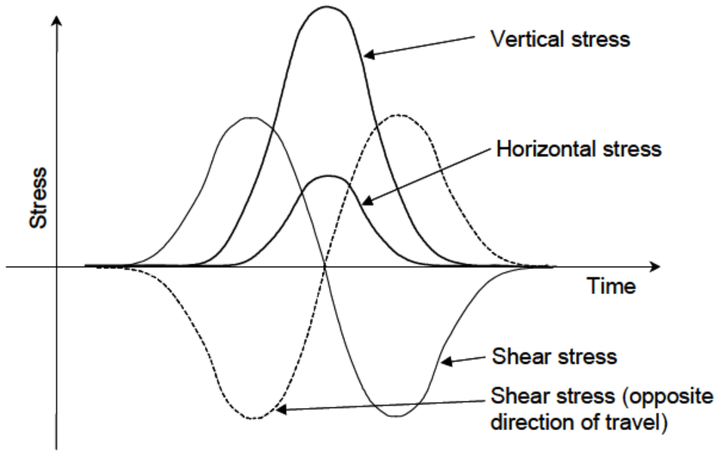

Figure 4.2: Induced stress conditions under a passing wheel load [23].

In this research the effect of the static load applied by the weight of the container in the container stack is neglected. During the settlement measurement period only a very small number of containers was stored in the container stacks. During operation of the container terminal a larger number of containers are stored. The static load applied by the containers influences the stress state in the sand. The confining stress underneath the adjacent ASC rail tracks increases. This is not investigated.

4.4.2. Soil profile

Assumptions specifically about soil data and model parameter values are discussed in Chapter 3 and in the previous section. Two significant assumptions about the soil profile are repeated below.

The compacted top layer of the sand fill and the ballast bed have a relative density of 100%. Extent of the compacted sand layer is estimated till 3.5 m NAP. Above this depth no settlement occurs.

Below the extent of the CPT data the relative density of the sand underneath the ASC rail tracks is estimated 65%. This is based on deeper CPT's executed elsewhere at the RWG container terminal.

4.4.3. FE computation and improved Schmertmann method

The FE simulation of the first load cycle is executed in PLAXIS 2D and assumes plane strain conditions, while this is a 3D problem. Under plane strain conditions vertical strain and cyclic shear strain amplitude increase. This could lead to an overestimate of the depth of influence and cyclic settlement.

Depth of influence estimated for the terminal density model is 6 m below the bottom of the foundation, independent of the soil and loading conditions. The depth of influence is estimated using the improved Schmertmann method and is equal to three times the width of the foundation, based on the foundation's dimensions $1 < L/B < 10$ (see Figure 2.6). The width of the foundation is determined at 2 m.

4.4.4. Cyclic settlement models

Cyclic settlement is predicted for a vertical through the center of the foundation. It is assumed that this represents settlement of the entire foundation.

Densification stops as soon as the relative density becomes 100%. To prevent indefinite plastic strain accumulation by the cyclic settlement models a maximum density corresponding to the minimum void ratio is implemented. A result is that at depths where the initial relative density of the sand is nearly at 100%, less settlement occurs. The terminal density model determines the maximum density using the correlation in Equation 4.2. This is the terminal void ratio. Accordingly, terminal void ratio cannot become lower than the minimum void ratio.

The terminal density model and C/L model for cyclic shear assume behaviour of sand in the first load cycle characterises its densification behaviour in the subsequent load cycles. Model parameters of both cyclic settlement models are determined by simulating the first load cycle with an FE computation or the improved Schmertmann method. In the first load cycle the stiffness of the sand dominates its behaviour. The cyclic shear strain amplitude and void ratio after one load cycle both depend on the stiffness of the sand.

According to the terminal density model settlement that occurs after the first load cycle is nearly homogeneously distributed with depth. This is a result of the correlation that is used to determine the terminal void ratio, given in Equation 4.2. Due to this correlation also the variation of model predictions of the cyclic settlement between different locations is relatively small, even between locations with large differences in initial relative density. This is illustrated with an example: the top part of a sand fill consist of a very loose sand layer. After one load cycle the void ratio is 0.75. The bottom part consists of a dense sand layer. The void ratio after one load cycle is 0.55. The terminal void ratio at the top and bottom part of the sand layer become 0.740 and 0.543, respectively. Difference between the void ratio after one load cycle and the terminal void ratio in the top and bottom part are 0.01 and 0.007, respectively. The corresponding volumetric plastic strain is 0.57% and 0.45%, respectively. For a one meter thick sand layer that is 5.7 mm settlement in the top part and 4.5 mm settlement in the bottom part as $N \to \infty$ (assuming vertical plastic strain is equal to the volumetric plastic strain). That is a small difference considering the large difference of the relative density. The correlation either implies that settlement occurs both in very loose and very dense sands. Increase of settlement related to decreasing relative density is limited. Or increase of settlement with decreasing relative density occurs primarily during the first load cycle.

Model predictions of the C/L model are very sensitive to the initial state of the sand, because Equation 4.1 correlates the initial relative density of the sand to the material constants. Model predictions of the C/L model are very sensitive to the material constants c_1 and c_2.

Cyclic settlement per load cycle decreases with number of load cycles. This is integrated in the cyclic settlement models by a natural logarithm or natural exponential function. Implicitly this incorporates a cyclic stress history dependency. This is illustrated with another example: sand at location A is medium dense. At location A 10 thousand load cycles are applied. Due to densification its relative density increases and becomes equal to the relative density of the sand at location B. No cyclic load has been applied at location B yet. From that moment the same number of load cycles with the same amplitude of the load are applied to locations A and B. According to the cyclic settlement models rate of settlement at location B is higher compared to location A. Rate of settlement decreases due to a 'cyclic load history'.

4.5. Increase reliability cyclic settlement prediction

It is recommended to carry out a more extensive site investigation program compared to Phase 1 of the RWG container terminal to make more reliable cyclic settlement predictions. To validate the cyclic settlement models more reliable settlement measurements are needed.

4.5.1. Recommended site investigation program

The recommended site investigation program for the construction of ASC rail tracks consists of:

- CPT measurements;
- borehole testing & sampling;
- minimum and maximum void ratio measurements;
- triaxial tests;

- cyclic soil tests.

The first four types of soil tests of the recommended site investigation program were executed in Phase 1 of the RWG container terminal. It is recommended to concentrate these measurements in the area of the ASC rail tracks, like the shallow CPT measurements in Phase 1, and measure the disturbance of the soil due to the construction works. In addition, it is recommended to execute cyclic soil tests to make more reliable predictions of the cyclic settlement.

Shallow CPT measurements have to be closely spaced to measure the strong variation of the relative density of the sand fill, laterally and vertically. Per 25 m along the ASC rail tracks one CPT measurement is sufficient. This is well done in Phase 1 of the RWG container terminal. Every CPT represents an area of 12.5 m from its location in both directions along the rail tracks. This area will need to be compacted around CPT's that show a low relative density. However a closer spacing would decrease the uncertainty about the relative density of the sand, it will become more intensive to execute such a large number of CPT's compared to compacting the area.

In Phase 1 shallow CPT's extent till a depth of around 6 m below the bottom of the foundation. It is recommended to execute shallow CPT's till a depth of at least 2 m below the estimated depth of influence, to measure the entire zone of influence. At the RWG container terminal that corresponds to about 8 m below the bottom of the foundation and 9 m below the surface. In Phase 2 of the RWG container terminal CPT's are executed till 10 m below the surface. Additionally, it is recommended to execute a few deeper CPT's, to determine the soil conditions below the sand fill. Deep CPT's in Phase 1 are executed till a depth of around 45 m below the surface.

Due to construction of the ASC rail tracks the sand at the RWG container terminal gets disturbed. In addition to the CPT measurements that are executed before construction of the ASC rail tracks, execute CPT measurements after construction of the ASC rail tracks nearby the settlement measurement locations. Five to ten additional CPT's should be sufficient to quantify the average disturbance caused by the construction works, this can be extrapolated to the other locations that have been disturbed.

Execute 5 to 10 boreholes distributed evenly over the RWG container terminal. Boreholes are executed to determine variation of the type of sand (or soil), which is small within a man-made sand fill like MV2. 5 to 10 boreholes are therefore sufficient. Extent of a borehole must be at least till a depth of 8 m below the bottom of the foundation, like the shallow CPT's. To get a complete image of the subsurface of the project site it is recommended to execute a few deeper boreholes. Because the recommended number of boreholes is relatively low, all boreholes should be deeper boreholes. Depth of the boreholes depends on the subsurface profile. At the RWG container terminal the first 20 m consists of sand. The boreholes should extent till a depth of around 25 m below the surface, to identify the soil layers underneath the sand fill.

Obtain multiple samples per borehole from various depths, primarily from the top part of the sand fill. These are used for laboratory testing such as minimum and maximum void ratio measurements, triaxial tests and cyclic soil tests.

Measure the minimum and maximum void ratio for around 25 samples taken from the top 8 meters of the sand fill. That is slightly more than in Phase 1 of the RWG container terminal. Variation of the sand type is small at the RWG container terminal. A relatively small number of measurements will therefore be sufficient.

Execute triaxial tests using sand samples taken from the boreholes from various depths within the zone of influence. Execute at least 60 triaxial tests. For every 2 m depth interval within the zone of influence, starting from the surface that are four intervals, prepare samples at 35, 65, 80, 90 and 100% relative density. For every sample a triaxial test is executed at three different levels of confining stress. Based on the measurements a correlation between the secant stiffness and relative density, between the unloading / reloading stiffness and relative density and parameter m can be determined. These are model parameters of the FE computation and improved Schmertmann method in which the first load cycle is simulated. Based on these model parameters the stiffness of the sand under the influence of a (cyclic) load can be determined at any depth and relative density.

Model parameters of the C/L model for cyclic shear and terminal density model determined in cyclic soil tests are the:

- material constants c_1 and c_2;
- volumetric threshold strain;
- void ratio after one load cycle;
- terminal void ratio;
- characteristic number of load cycles N^*.

Additionally, model parameter values that describe cyclic densification properties of the other cyclic settlement models can be determined.

Measure the densification properties in cyclic triaxial tests. This test mimics the loading and boundary conditions underneath ASC rail tracks better than a direct shear or simple shear test. Material constants c_1 and c_2 of the C/L model for cyclic shear are determined in cyclic shear tests. Strain-controlled cyclic triaxial tests are executed on multiple sand samples with varying relative density to determine a relation between the material constants and initial relative density of the sand. The volumetric threshold strain is determined as the largest applied strain level for which no plastic strain accumulate.

The remaining model parameters can be determined in cyclic triaxial or cyclic oedometer tests. Although their boundary conditions are different, both cyclic tests mimic to some degree the conditions underneath ASC rail tracks. The dominating force is a cyclic vertical stress. The void ratio after one load cycle is determined based on the volumetric plastic strain after one load cycle. The terminal void ratio is determined based on the volumetric plastic strain after plastic strain per load cycle becomes zero. In addition, stress-controlled cyclic triaxial or oedometer tests are executed on multiple samples to determine relations between the applied stress and the void ratio after one load cycle, terminal void ratio and characteristic number of load cycles.

Phase 1 of the RWG container terminal is a unique area to determine the terminal void ratio of the sand underneath ASC rail tracks. At some locations underneath ASC rail tracks of Phase 1 cyclic settlement stopped. Density of the sand has evolved towards its terminal void ratio, which can be measured with for example CPT's. To determine the influence of the initial relative density and applied stress CPT's must be executed at multiple locations and underneath rail tracks of ASCs and ASC-Cs, preferably nearby CPT's that were executed before construction of the ASC rail tracks. In this way reliable values of the terminal void ratio can be obtained without executing cyclic soil tests. The largest depth where the relative density has increased determines the depth of influence. The maximum density can also be used to predict cyclic settlement with the models that assume cyclic settlement continues indefinitely, instead of the minimum void ratio.

4.5.2. Validation of the cyclic settlement models

At Phase 1 of the RWG container terminal it is no longer possible to measure the cyclic settlement, because most of the settlement already occurred here. Cyclic settlement measurements for validation of the cyclic settlement models must be obtained in Phase 2 of the RWG container terminal, or another newly build container terminal constructed on sand.

Measure the settlement with depth and number of load cycles at multiple locations underneath ASC and ASC-C rail tracks to determine the influence of the initial state of the sand and amplitude of the load on the settlement with depth. Execute settlement measurements underneath ASC rail tracks within a few meters distance from a CPT measurement, preferably nearby CPT's executed after construction of the ASC rail tracks. Here the initial state of the sand and soil profile contain the least uncertainty. A match between the measurements and model predictions of the cyclic settlement, vertical plastic strain distribution with depth and depth of influence is required for the validation of a cyclic settlement model. Differences between the settlement measurements and predictions quantitatively describe the reliability of the cyclic settlement models.

4.6. Densification of the sand fill in the first load cycle

More settlement occurs in the first load cycle than in any of the subsequent load cycles. The terminal density model and C/L model for cyclic shear assume that densification behaviour of the sand during the first load cycle characterises its densification behaviour during the subsequent load cycles. The plastic strain after one load cycle is not measured. Instead, the first load cycle is simulated with the improved Schmertmann method and an FE computation in PLAXIS. Model predictions of these methods are used to estimate the void ratio after one load cycle and cyclic shear strain amplitude. Further, the depth of influence is estimated with both methods. The results and sensitivity of the improved Schmertmann method and FE computation to a few of their model parameters are presented and discussed in this section. More results are attached in Appendix C.

4.6.1. FE computation in PLAXIS

Main goal of the FE computations is to determine the cyclic shear strain amplitude, a model parameter of the C/L model for cyclic shear. The FE computations that were executed consist of two steps in which a quasi-static load cycle is applied. In the first step a vertical stress equivalent to the load of an ASC is applied onto the foundation and in the second step the stress is removed. Plane strain conditions are assumed in the FE computations. The sand layers are modelled with the hardening soil small strain (HSsmall) material model [40]. Model parameter values vary per layer, which are distinguished based on their relative density. In Appendix C is explained how the cyclic shear strain amplitude is determined.

The cyclic shear strain amplitude is significantly larger for locations 1 and 2 compared to locations 4 and 6. In Figure 4.3 the cyclic shear strain amplitude on a vertical through the center of the foundation is plotted for locations 1, 2, 4 and 6. The cyclic shear strain amplitude is calculated based on strains computed with the FE computation. At locations 1 and 2 the cyclic shear strain amplitude is induced by a load equivalent to a vertical stress of 89 kPa, which is applied to the bottom of the foundation at 4.3 m NAP. This corresponds to a heavier ASC-C carrying a 40 tonne container. The cyclic shear strain amplitude at locations 4 and 6 is induced by a load equivalent to a vertical stress of 73.5 kPa. This corresponds to a smaller ASC carrying a 40 tonne container. The cyclic shear strain amplitude decreases with depth. The cyclic shear strain amplitude is plotted from a depth of 3.5 till -3.5 m NAP. Above 3.5 m NAP densification does not occur, because the sand fill has a 100% relative density. Below -3.5 m NAP does not occur, because the cyclic shear strain amplitude is smaller compared to the minimum volumetric threshold strain of 0.007%. Plots of the cone tip resistance and estimated initial relative density of locations 1, 2, 4 and 6 (the same plots as in Figure 3.14) are also given. Variation of the cyclic shear strain amplitude caused by variation of the estimated initial relative density is negligible.

Depth of influence increases with foundation stress and decreasing volumetric threshold strain. Depth of influence is determined at the intersect between the cyclic shear strain amplitude and volumetric threshold strain. Above the intersect the cyclic shear strain amplitude is larger than the volumetric threshold strain, as a result densification occurs. The depths at which the cyclic shear strain amplitude intersects the 0.01% volumetric threshold strain match well to the distribution of the vertical stress for 2D stress spreading, plotted in Figure 3.11. At 6 m below the shallow foundation, corresponding to almost -2 m NAP, increase in vertical stress induced by a load on the foundation is 5% of its value directly below the foundation, that is less than 5 kPa. The vertical plastic strain induced by this vertical stress increase is assumed to be negligible.

In Figure 4.4a the cyclic shear strain amplitude on a vertical through the center of the rail track at location 2 are plotted for varying foundation stress and rate of stress dependency of the stiffness (parameter m). The foundation stress is 60, 73.5, 89 and 100 kPa and parameter m varies between 0.5 and 0.7. In Figure 4.4b the corresponding settlement on a vertical through the center of the rail track are plotted.

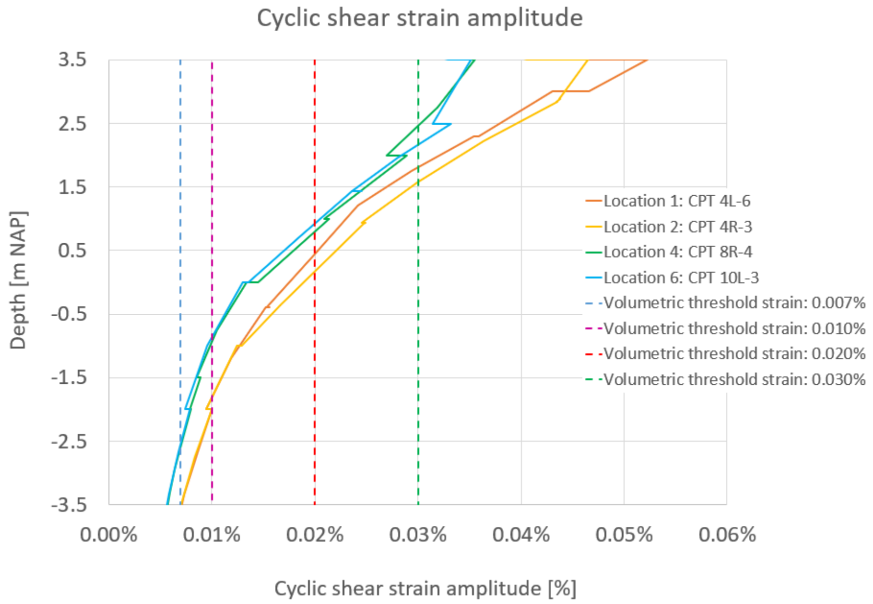

(a) Cyclic shear strain amplitude with depth.

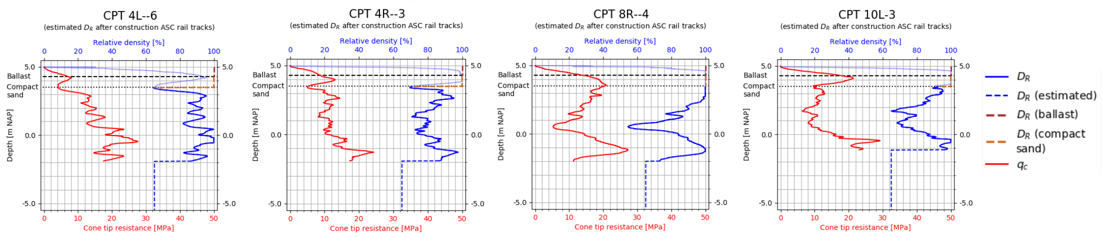

(b) Location 1: CPT 4L-6 (c) Location 2: CPT 4R-3 (d) Location 4: CPT 8R-4 (e) Location 6: CPT 10L-3

Figure 4.3: a) Cyclic shear strain amplitude with depth for locations 1, 2, 4 and 6 determined in an FE model and the volumetric threshold strain. At locations 1 and 2 a foundation stress of 89 kPa applied and at locations 4 and 6 a foundation stress of 73.5 kPa; and b-e) cone tip resistance and estimated relative density of the sand after construction of the ASC rail tracks of locations 1, 2, 4 and 6 (b-e).

The settlement at the end of the first load cycle, after the load is removed, increases with foundation stress and decreasing parameter m. At 3.5 m NAP the settlement after one load cycle varies between 3 and 6.5 mm, above 3.5 m NAP no settlement occurs. The cyclic shear strain amplitude and settlement after one load cycle increase almost linearly with the foundation stress.

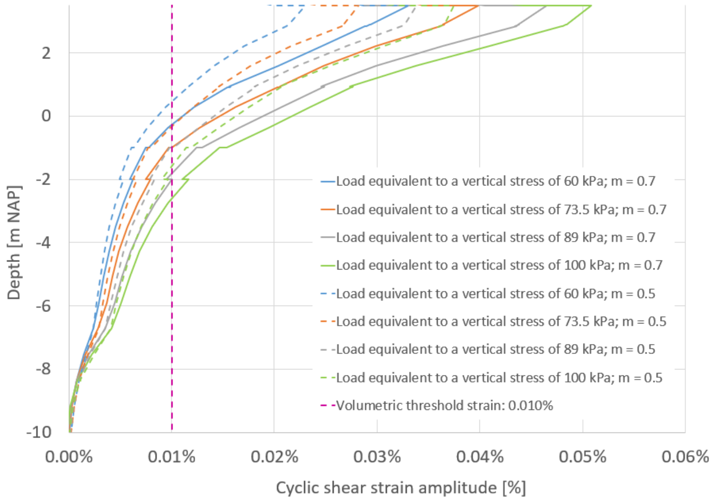

(a) Cyclic shear strain amplitude with depth

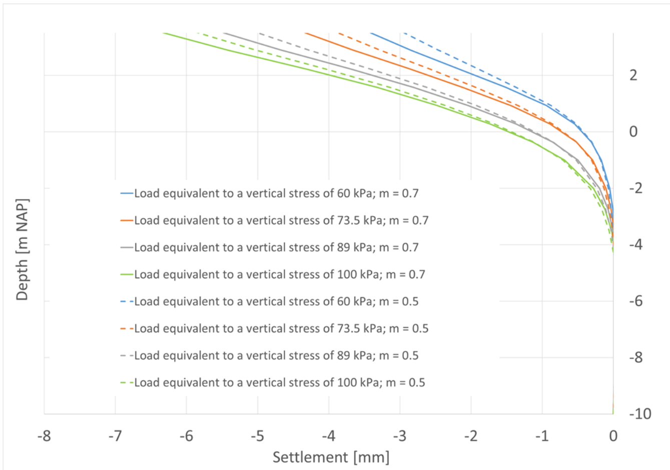

(b) Settlement with depth

Figure 4.4: Cyclic shear strain amplitude underneath and settlement of the rail tracks at location 2 (CPT 4R-3) after one load cycle for a rate of stress dependency of the stiffness of the sand of 0.5 and 0.7, for loads equivalent to a vertical stress of 60, 73.5, 89 and 100 kPa applied to the bottom of the foundation.

Figure 4.4 shows that the cyclic shear strain amplitude and settlement after one load cycle increase with decreasing stiffness of the sand fill. At depths where the confining stress is smaller than 100 kPa, i.e. within (almost) the entire zone of influence, stiffness of the sand is higher for $m = 0.5$ compared to $m = 0.7$. Within the zone of influence, increasing parameter m results in an increase of the cyclic shear strain amplitude and settlement after one load cycle. The increase of the depth of influence corresponding to the increase of the cyclic shear strain amplitude is about 0.5 m, indicating that the depth of influence increases with decreasing stiffness of the sand. The corresponding increase of the settlement is around 0.5 mm.

In Figure 4.5 vertical and horizontal plastic strains after one load cycle are plotted on a vertical through the center of the foundation for locations 1, 2, 4 and 6. The strains are determined with the FE computation and correspond to the cyclic shear strain amplitude plotted in Figure 4.3. Vertical plastic strain is larger at locations 1 and 2 compared to locations 4 and 6. At locations 1 and 2 the strains are induced by a load equivalent to a vertical stress of 89 kPa which is applied to the bottom of the foundation, at 4.3 m NAP. The strains at locations 4 and 6 are induced by a load equivalent to a vertical stress of 73.5 kPa. At location 1 the vertical plastic strain decreases with depth. In the FE model of location 1 directly below the compacted sand between 3.5 and 3.0 m NAP a medium dense sand layer is situated. At locations 2, 4 and 6 the vertical plastic strain increases till it reaches its maximum value at a depth around 2.5 to 2 m NAP. Deeper the vertical plastic strain decreases towards zero. Here dense sand layers are situated directly below the compacted sand layer. Horizontal strain is nearly equal at the four locations. It increases till it reaches its maximum value at a depth around 0.5 m NAP. Deeper the horizontal plastic strain decreases towards zero. The volumetric plastic strain is the sum of the horizontal and the vertical plastic strain. The ratio between the vertical plastic strain and the volumetric plastic strain after one load cycle, here called the vertical-volumetric strain ratio (VVSR), is plotted by the fine dashed lines for the four locations. The VVSR decreases with depth and is nearly equal for the four locations. The average value of the VVSR is determined at 0.66, indicated by the vertical fine dashed grey line.

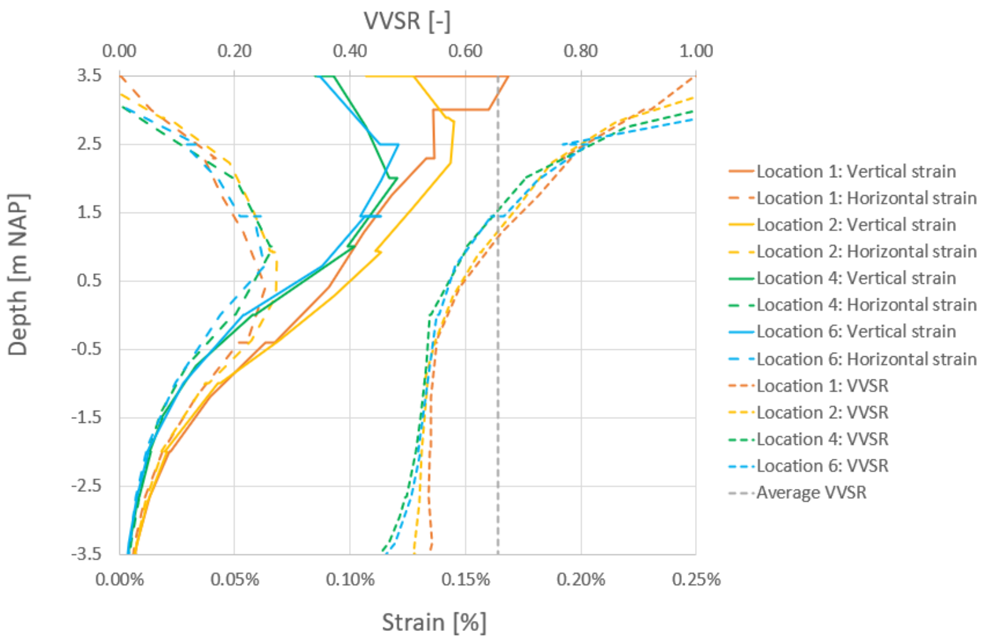

Figure 4.5: Vertical and horizontal plastic strains at locations 1, 2, 4 and 6 after the load is removed. At locations 1 and 2 the load is equivalent to a vertical stress of 89 kPa applied to the bottom of the foundation. At locations 4 and 6 the load is equivalent to a vertical stress of 73.5 kPa. The ratio between the vertical and the volumetric plastic strain for locations 1, 2, 4 and 6 and its average value are also plotted.

Vertical plastic strain in the first load cycle primarily increases with the foundation stress. Increase of the vertical plastic strain with decreasing relative density and stiffness of the sand, related to the layering of the sand fill, is less significant. The corresponding settlement determined with the FE computation at locations 1, 2, 4 and 6 is 5.3 mm, 5.5 mm, 4.2 mm and 4.2 mm, respectively. This is summarised in Table 4.2. The area underneath the graphs of the vertical plastic strain gives the settlement after one load cycle. Variation of the horizontal strain with foundation stress, relative density and stiffness of the sand is negligible.

Settlement is related to the vertical plastic strain. However, model predictions of the C/L model for cyclic shear, terminal density model and the Hergarden model are expressed as a change in void ratio or relative density as a function of the number of load cycles, which are related to volumetric plastic strain. To estimate the vertical plastic strain the volumetric plastic strain is multiplied by the VVSR. The

Computation	Location 1 (CPT 4L-6; p = 89 kPa)	Location 2 (CPT 4R-3; p = 89 kPa)	Location 4 (CPT 8R-4; p = 73.5 kPa)	Location 6 (CPT 10L-3; p = 73.5 kPa)
FE computation	5.3 mm	5.5 mm	4.2 mm	4.2 mm
Schmertmann	3.8 mm	3.8 mm	3.1 mm	3.2 mm

Table 4.2: Settlement at locations 1, 2, 4 and 6 calculated using the improved Schmertmann method and a FE computation in PLAXIS for a foundation stress of 73.5 kPa or 89.0 kPa.

average value of the VVSR is used, which is 0.66. The VVSR per location and the average value over the extent of the zone of influence is determined and plotted in Figure 4.5. It is assumed that this ratio remains constant with increasing number of load cycles, foundation stress, stiffness of the sand fill and that the estimated value of the VVSR for 3D conditions is the same.

4.6.2. The Schmertmann method

The improved Schmertmann method presented in Section 2.6 is used to estimate the vertical plastic strain and void ratio after one load cycle. Model parameters of the cumulative plastic strain model and terminal density model, respectively. The improved Schmertmann method determines the vertical strain induced by a static load.

In Figure 4.6 the vertical strain calculated with the improved Schmertmann method for locations 1, 2, 4 and 6 is plotted. For each location the vertical strain increases till a depth of 2.8 $m\ NAP$, which corresponds to 0.75B (B is the width of the foundation) below the bottom of the foundation. Deeper the vertical strain decreases and becomes zero at a depth of -1.7 $m\ NAP$, which corresponds to 3B or 6 m below the foundation. Meaning that the depth of influence is 6 m below the bottom of the foundation. The red dashed lines give the stiffness of the sand for a reference confining stress of 100 kPa. Its value increases with relative density. The stiffness of the sand for a reference confining stress of 100 kPa varies between 80 and 100 MPa. The stiffness values are obtained from the fifth column of Table 3.6, which corresponds to a vertical strain level of around 0.10%. The average level of vertical strain after one load cycle is determined at around 0.10%, according to the vertical strain plotted in Figure 4.5. The red solid line gives the stiffness at the in-situ confining stress. The stiffness of the sand increases with depth. This value is used to determine the vertical strain with Equation 2.20. At locations 1 and 2 strains are induced by a load equivalent to a vertical stress of 89 kPa which is applied to the bottom of the foundation. Strains at locations 4 and 6 are induced by a load equivalent to a vertical stress of 73.5 kPa. The vertical plastic strain is larger at locations 1 and 2 compared to locations 4 and 6. Consequently, the corresponding settlement is also larger at locations 1 and 2. The area underneath the blue graph gives the settlement. The settlement at locations 1 and 2 is 3.8 mm which is larger compared to locations 4 and 6 with 3.1 and 3.2 mm, respectively. The settlement is indicated on the right side of the graph and in Table 4.2.

An abrupt change of the value of the red lines indicates a separate sand layer. Layering of the sand fill does not exactly coincide with the FE models of the sand fill. In both cases the layers are distinguished based on the relative density determined with the CPT data, which is measured with a 2 cm interval. In the FE computations in PLAXIS it is not feasible to input a very large number of very thin sand layers. However, this is feasible in the implementation of the improved Schmertmann method. Especially at location 2 in Figure 4.6b this results in a relatively large number of thin sand layers. At locations 1 and 6 in Figures 4.6a and 4.6d only four layers are modelled.

Results from the improved Schmertmann method show similar relations and trends as the results from the FE computations. The vertical strain and settlement increase with the foundation stress.

Depth of influence does not increase with foundation stress, in contrast to the results from the FE computations. The depth of influence is based on the dimensions of the foundation, which are the same for both crane types and remain constant. Consequently, the estimated depth of influence is constant. However, the improved Schmertmann method indirectly considers increase of the depth of influence

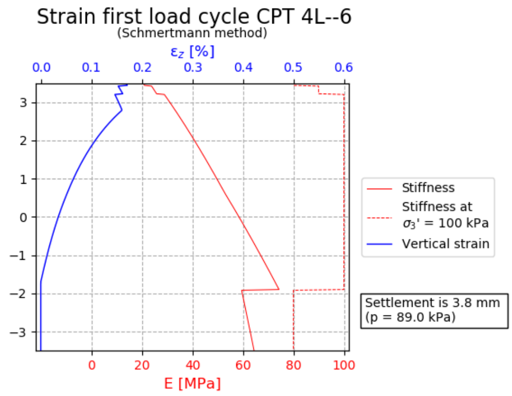

(a) Location 1: CPT 4L-6

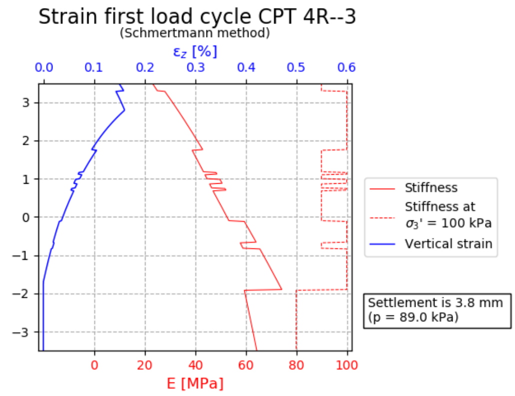

(b) Location 2: CPT 4R-3

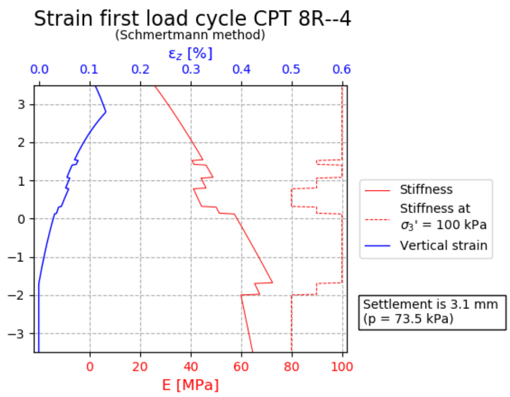

(c) Location 4: CPT 8R-4

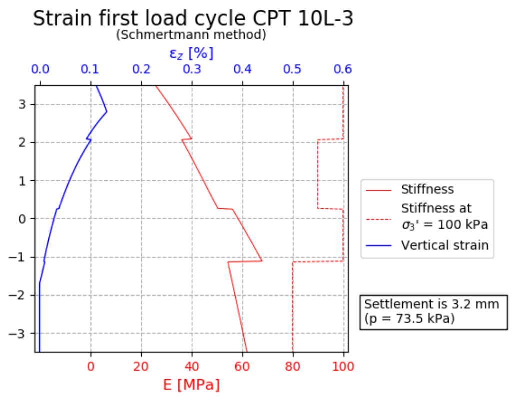

(d) Location 6: CPT 10L-3

Figure 4.6: Vertical strain at locations 1, 2, 4 and 6 calculated with the improved Schmertmann method. At locations 1 and 2 the load is equivalent to a vertical stress of 89 kPa applied to the bottom of the foundation. At locations 4 and 6 the load is equivalent to a vertical stress of 73.5 kPa. The red dashed line gives the estimated stiffness of the sand at a reference confining stress of 100 kPa. The red solid line gives the stiffness for the in-situ confining stress.

with the foundation stress. In geotechnical design size of a shallow foundation increases with increasing the foundation stress. Depth of influence estimated at -1.7 $m\ NAP$ matches well with the distribution of the vertical stress for 2D stress spreading in Figure 3.11 and depth of influence determined with the cyclic shear strain amplitude plotted in Figure 4.3 and a volumetric threshold strain of 0.01%, which varies between -1 and -2 $m\ NAP$ depending on the foundation stress.

It is assumed the model predictions of the improved Schmertmann method can be taken as the vertical plastic strain without subtracting the vertical elastic strain. The vertical strain calculated with the improved Schmertmann method contains vertical elastic and plastic strain. In Table 4.2 the corresponding settlements are summarised, together with the settlements determined with the FE computation. Settlement determined with the FE computations are larger, while that only consists of vertical plastic strain. The vertical plastic strain calculated with the improved Schmertmann method is zero beyond -1.7 $m\ NAP$. The vertical strain determined with the FE computation plotted in Figure 4.5 has a value larger than zero beyond -3.5 $m\ NAP$, i.e. settlement occurs at larger depths. This increase is (partially) caused by the plane strain conditions assumed by the FE computations. Furthermore, it is possible that the stiffness of the sand used for the improved Schmertmann method is higher than the stiffness of the sand determined with the FE computation.

In Figure 4.7 the vertical strain on a vertical through the center of the rail track at locations 1, 2, 4 and 6 are plotted. The foundation stress is 60, 73.5, 89 and 100 kPa. Parameter m of the sand is taken as 0.5 and 0.7. The stiffness of the sand for a reference confining stress of 100 kPa is plotted by the red dashed-dotted line. Stiffness corrected for the in-situ stress is plotted for $m = 0.5$ and $m = 0.7$ by the red dashed and solid lines, respectively.

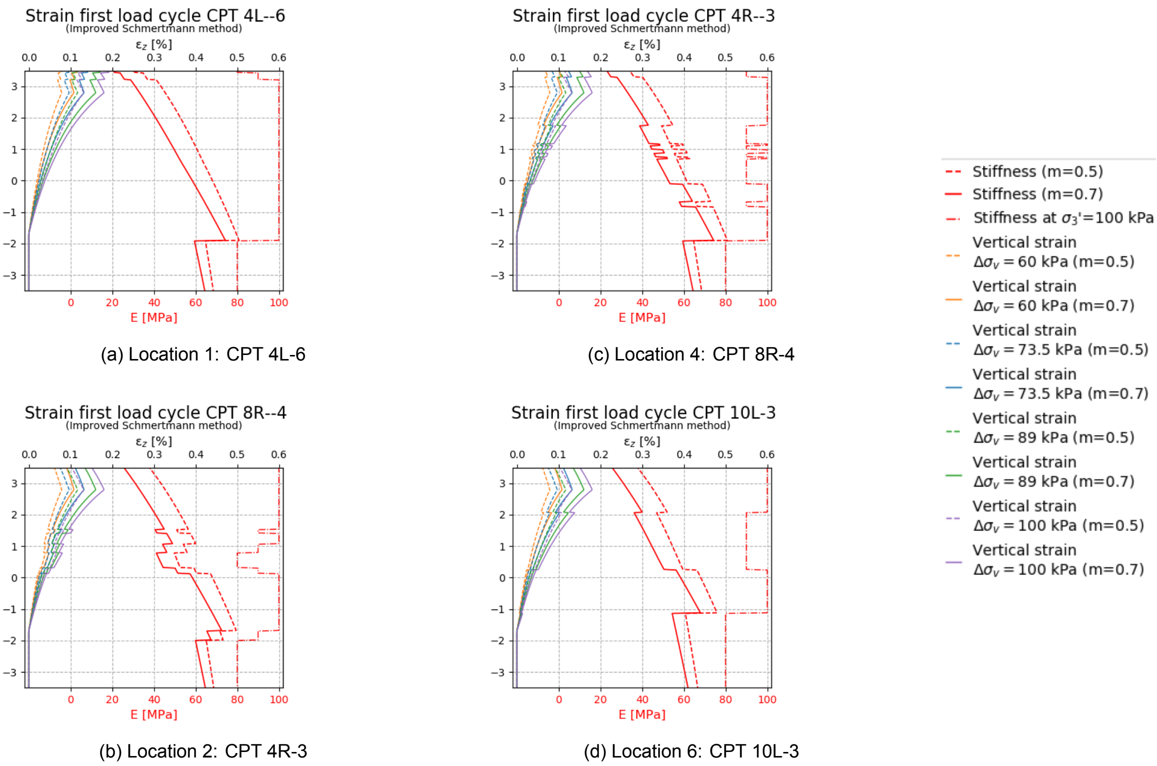

(a) Location 1: CPT 4L-6

(c) Location 4: CPT 8R-4

(b) Location 2: CPT 4R-3

(d) Location 6: CPT 10L-3

Figure 4.7: Vertical strain underneath the rail tracks at location 1, 2, 4 and 6 calculated with the improved Schmertmann method for a rate of stress dependency of the stiffness of the sand of 0.5 and 0.7, for loads equivalent to a vertical stress of 60, 73.5, 89 and 100 kPa applied to the bottom of the foundation.

Vertical strain increases with foundation stress. It is inversely related to the stiffness. Again, the stiffness of the sand layers is higher for $m = 0.5$ compared to $m = 0.7$. Consequently, the vertical strain calculated with $m = 0.5$ is smaller compared to $m = 0.7$. According to Equation 2.20 the vertical strain is linear related to the foundation stress.

4.6.3. Cyclic densification

Settlement after one load cycle determined with the FE computation and improved Schmertmann method are smaller than the measured settlement for the locations. It is concluded that (most) of the settlement of the rail tracks is a result of cyclic densification of the sand.

It is unlikely that no settlement occurred after a large number of load cycles at locations 3 and 5. Appendix C contains model predictions of locations 3 and 5 determined with the FE computations. Settlement at these locations after one load cycle is several millimeters. With better settlement observation and measurement methods these settlements would have been measured. It is correct to discard locations 3 and 5 from the evaluation.

4.7. Densification of the deeper sand layer

In Figure 4.8a the initial relative density profiles (after construction of the rail tracks) at locations 1 and 2 are shown. Here the heavier ASC-Cs are installed. The red horizontal dashed line indicates the domain in which the sand at the locations where most settlement was measured has a lower relative density. This domain extents from 2 to -1 $m\ NAP$. The relative density of the sand at location 2 is lower than at location 1. At location 2 more settlement is measured than at location 1 during the settlement measurement period. In Figure 4.8b the same is valid for locations 4 and 6, the domain extents from 1 to -1 $m\ NAP$. The relative density of the sand at location 4 is lower than at location 6, therefore more settlement is measured at location 4 during the settlement measurement period.

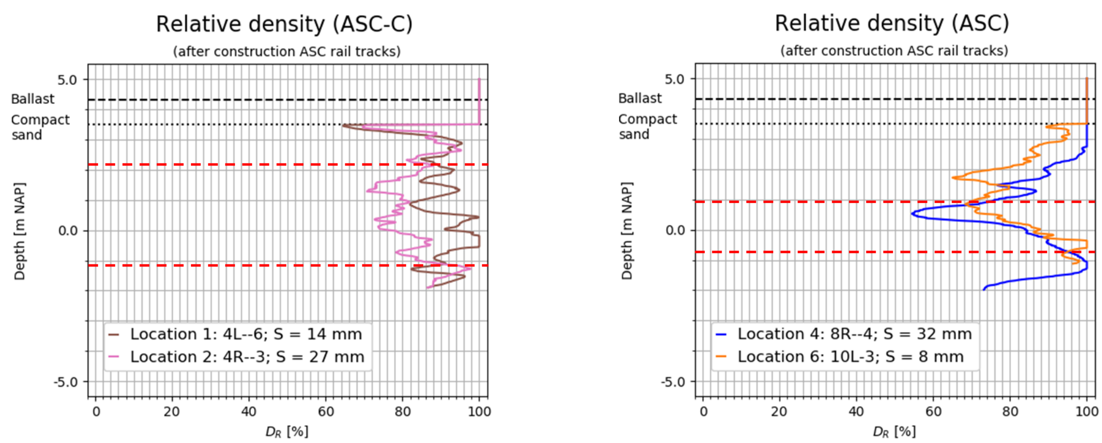

(a) Crane type: ASC-C

(b) Crane type: ASC

Figure 4.8: The relative density profiles of the sand at locations 1, 2, 4 and 6 after construction of the rail tracks. At locations 1 and 2 ASC-Cs and at locations 4 and 6 ASCs are installed. The red horizontal dashed lines indicate a domain in which the sand at the locations where most settlement was measured has a lower relative density.

Densification of the sand layer between 2 and -1 $m\ NAP$ primarily accounts for the total settlement of the ASC rail track at location 2. Densification of the sand inside the domain indicated by the red horizontal dashed lines primarily accounts for the settlement difference, which is about half of the total settlement at location 2. The relative density profiles of the sand at locations 1 and 2 are comparable. The sand is dense and their relative density with depth is more or less constant. Till a depth of 2 $m\ NAP$ the relative density of the sand at the two locations is nearly the same. Deeper the relative density at location 1 increases slightly and at location 2 it decreases slightly. Both locations are situated underneath the rail tracks of container stack 4. The loading conditions are therefore assumed to be equal, i.e. an equal number of load cycles (between 10 and 50 thousand) and foundation stress. The settlement difference is related to the lower relative density of the sand inside the domain indicated by the red horizontal lines.

Densification of the sand layer between 1 and -1 $m\ NAP$ primarily accounts for the total settlement of the ASC rail track at location 4. The settlement difference between locations 4 and 6 is related to the lower relative density of the sand at location 4 inside the domain indicated by the red horizontal dashed lines. Between 1 and -1 $m\ NAP$ the relative density of the sand at location 4 decreases to almost 50%. Relative density of the sand of the first 3 meters below the compact sand, till 1 $m\ NAP$, is higher at location 4. However, settlement measured at location 4 is significantly larger than at location 6. Both locations are situated below the rail tracks of the smaller ASC, the amplitude of the load cycles is therefore more or less equal. Note that although the estimated number of load cycles lies in the same range, the actual number of load cycles at one location can still be up to five times higher than at the other location (10 thousand vs. 50 thousand). Because most of the settlement occurs during the first load cycles this only partially justifies the difference in measured settlement between locations 4 and 6.

Vertical plastic strain concentrates in a sand layer with a significantly lower relative density. At location 4 vertical plastic strain primarily accumulates between 1 and 0 $m\ NAP$. Initially, after one load cycle, vertical plastic strain concentrates not directly below the foundation, but in the sand layer below that. The vertical strains after one load cycle plotted in Figures 4.5 and 4.6 both increase with depth until a maximum value is reached at around 2.5 and 2.8 $m\ NAP$, respectively. Deeper the vertical strains decrease towards zero.

4.7.1. Minimum depth of influence

Based on the CPT measurements in combination with the settlement measurements the depth of influence of an ASC is at least 0 $m\ NAP$, which is approximately 4 to 5 m below the bottom of the foundation. It is expected that the depth of influence of the heavier ASC-C is larger. At location 4 the largest settlement is measured. Here the sand fill contains a sand layer between 1 and 0 $m\ NAP$ with a significantly lower relative density. Densification of the sand in this layer primarily accounts for the total settlement measured at this location.

4.7.2. Shallow compaction is insufficient

Shallow compaction of the sand fill till a depth of around 2 $m\ NAP$, or 2 m below the bottom of the foundation, is insufficient to prevent settlement of ASC rail tracks. The data indicate that densification induced by an ASC of sand layers deeper than 2 $m\ NAP$ can result in significant cyclic settlement.

4.8. Cyclic settlement predictions

In this section results obtained with the six cyclic settlement models for locations 1, 2, 4 and 6 are presented. First, settlement as a function of the number of load cycles obtained with the best estimates of the model parameter values are presented for all cyclic settlement models. Secondly, vertical strain with depth of the C/L model for cyclic shear and terminal density model are presented. Finally, a sensitivity analysis of relevant input data on the cyclic settlement predictions of both cyclic settlement models is presented.

4.8.1. Settlement as a function of the number of load cycles

In Figure 4.9 settlement as a function of the number of load cycles is presented for locations 1, 2, 4 and 6 obtained with the six cyclic settlement models. This is the settlement at the surface. The blue vertical bands indicate the range of estimated load cycles during the settlement measurement period. At locations 1, 2, 4 and 6 this estimate lies between 10 and 50 thousand load cycles. The horizontal black lines indicate measured settlement. The C/L model for cyclic shear and terminal density model are plotted by the blue and red solid lines, respectively. The other cyclic settlement models are plotted with dashed lines. However most settlement is measured at location 4, all cyclic settlement models predict least settlement at location 4 and most settlement at location 2. Cyclic settlement predictions are plotted up till 100 million load cycles. The Hergarden model, plotted by the purple dashed lines, predicts zero settlement at the four locations.

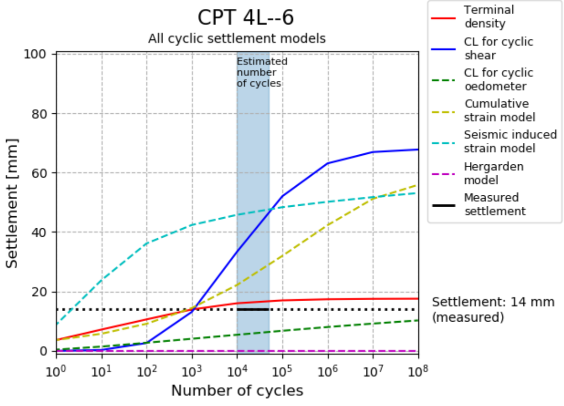

(a) Location 1: CPT 4L-6

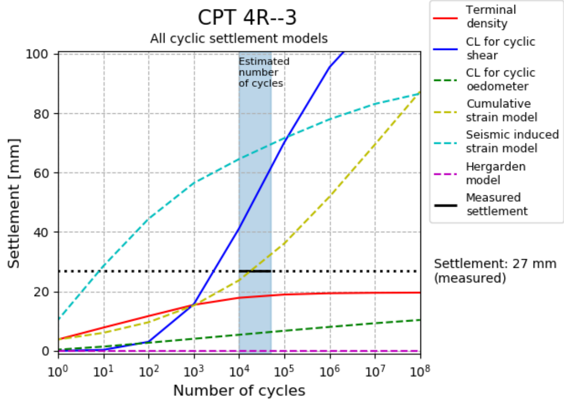

(b) Location 2: CPT 4R-3

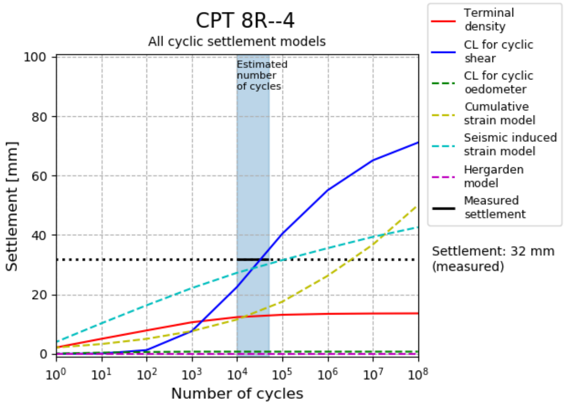

(c) Location 4: CPT 8R-4

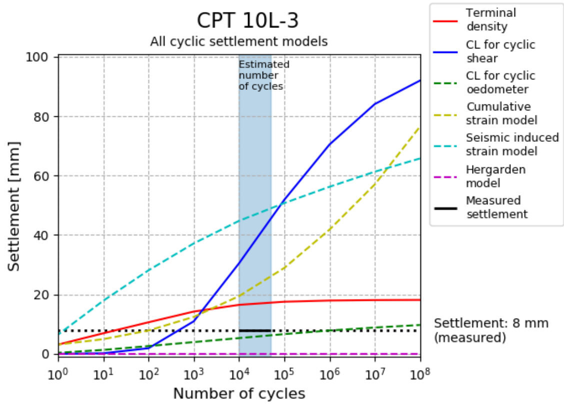

(d) Location 6: CPT 10L-3

Figure 4.9: Settlement vs. number of load cycles predicted by the six cyclic settlement models for locations 1, 2, 4 and 6. Cyclic settlement are predicted based on the best estimates of the model parameter values, summarised in Table 4.3.

Values of the best estimates of the model parameters are summarised in Table 4.3. These values are used to plot the settlement as a function of the number of load cycles. At locations 1 and 2 foundation stress is 89 kPa, which corresponds to a heavier ASC-C carrying a 40 tonne container. At locations 4 and 6 this is 73.5 kPa, which corresponds to an ASC carrying a 40 tonne container. Other model parameter values are obtained through correlation, (FE) modelling or based on estimates. References to the correlations, figures with plotted model parameter values and literature are also indicated in the table. Columns containing model parameter values of the terminal density model and C/L model for cyclic shear are highlighted in grey.

C/L model for cyclic shear (Equations 2.5 & 2.6)	C/L model for cyclic oedometer compression (Equation 2.8)	Hergarden model (Equations 2.9 - 2.11)	Terminal density model (Equations 2.12 & 2.13)	Cumulative plastic strain model (Equation 2.17)	Seismic induced strain model (Equation 2.19)
$e_0 \propto D_{R,0}$	$\sigma_z : \sigma_{z,0} = 73.5$ or 89 $[kPa]$; (Figure 3.11)	$D_{R,0}$ & $e_0 \propto D_{R,0}$	$e_0 \propto D_{R,0}$	$a = 5.38e^{-0.023D_{R,0}}$ [21]	$\varepsilon^p_{v,N=1}$ (Figure 4.6)
γ_0 (Figure 4.3)	$\sigma_x = (1/2)\sigma_z$ $[kPa]$	$e_{min} = 0.5$	$e_1 \propto \varepsilon^p_{v,N=1}$ (Figure 4.6)	$b = 1.2$ [21]	$b = 0.2$ [30]
c_1 & c_2 (Equation 4.1)	$c_1 = 0.776$ & $c_2 = 2.847$ [48]	$e_{max} = 0.8$	e_T (Equation 4.2)	$R = 0.25$ [21]	
		$a:\ a_0 = 1.6$ $[m/s^2]$; (Figure 3.12)	$N^* = 100$ [39]	γ_0 (Figure 4.3)	
		$\alpha_B = 3$ [34]	$m = 0.45$ [39]	$\gamma_{tv} = 0.01\%$ [55]	

Table 4.3: Best estimates of the values of the model parameters in Table 2.1. The equation numbers are of the six cyclic settlement models and reference to the parameter values are indicated.

Terminal density model

Settlement predictions made with the terminal density model are in the same order as the measured settlement. Predictions of the cyclic settlement vary between 12 and 19 mm after 10 to 50 thousand load cycles at the four locations. Variation of the predicted cyclic settlement is smaller compared to the variation of the settlement measurements. In the first 10 thousand load cycles most cyclic settlement is calculated. After 10 thousand load cycles the entire zone of influence is approaching the predicted terminal void ratio. Most settlement occurs in the first load cycle. After one load cycle settlement is between 3 and 4 mm. The first load cycle is determined with the improved Schmertmann method, plotted in Figure 4.6. After the first load cycle settlement continues to increase at a significantly slower rate. The predicted cyclic settlement after 50 thousand load cycles at location 4 is 13 mm, that is less than half of the measured settlement. The predicted cyclic settlement at location 2, after 50 thousand load cycles is about 19 mm.

Compaction / Liquefaction model for cyclic shear

The C/L model for cyclic shear predicts large settlement at all four locations after 10 to 50 thousand load cycles. Settlement continues to increase even beyond 10 million load cycles, corresponding to the estimated number of load cycles during the lifetime of a container terminal. In the first 100 load cycles a relatively small amount of settlement is predicted. Predicted settlement continues to increase after 100 load cycles at a relatively high rate. After 10 to 50 thousand load cycles the C/L model for cyclic shear predicts more settlement compared to the other cyclic settlement models, except the seismic induced strain model. Cyclic settlement predictions vary between 23 and 62 mm after 10 to 50 thousand load cycles at the four locations. At location 4 prediction of the settlement after 50 thousand load cycles matches well with the measured settlement, 35 vs. 32 mm. At location 6 cyclic settlement prediction is up to six times the measured settlement.

Hergarden model

The Hergarden model is not suitable for the current problem. It predicts no settlement at all four locations. Within the entire sand fill amplitude of the acceleration is below the acceleration threshold. Amplitude of the acceleration of the vibration at the bottom of the foundation is estimated at 1.6 m/s^2. That is around four times stronger compared to a vibration generated by a train that rolls into a train station. Amplitude of the acceleration decreases with depth, this is described by the attenuation of vibration plotted in Figure 3.12.

Cumulative plastic strain model

Model predictions of the cumulative plastic strain model are unreliable. The settlement predictions depend on the number of load cycles, vertical plastic strain after one load cycle and a material constant that describes densification of the sand. Its value is not measured in a cyclic soil test. Based on literature its value is estimated at 0.2, its value is therefore uncertain. Predictions of the cumulative plastic strain model, plotted in Figure 4.9 by the yellow dashed line, match better with the measurements compared to C/L model for cyclic shear for locations 1, 2 and 6.

Compaction / Liquefaction model for oedometer compression

The C/L model for cyclic oedometer compression is not suitable for the current problem. It underestimates cyclic settlement for most locations, except location 6. Cyclic settlement predicted with this model is plotted in Figure 4.9 by the green dashed line. The depth of influence is estimated to be less than one time width of foundation. That is less than two meters, significantly less compared to the depth of influence determined with the FE model, improved Schmertmann method and vertical stress increase with depth. It is also inconsistent with the CPT data in combination with the settlement measurements. The small zone of influence results in a small predictions of the settlement. At location 4 no settlement occurs because in the entire zone of influence the initial relative density is 100%. Furthermore, the C/L model for model is very sensitive to the material constants. This is observed in a global sensitivity analysis. Values of the material constants used for the model predictions are given in Table 4.3. This is the best estimate of the material constants, however the values represent a different sand type. Consequently, model predictions of the C/L model for cyclic oedometer compression are unreliable. Moreover, none of the model parameter values depend on the initial relative density, model predictions of the C/L model for cyclic oedometer compression are independent of the initial relative density.

Seismic induced strain model

At locations 1, 2 and 6 in the range 10 to 50 thousand load cycles the seismic induced strain model significantly overestimates the cyclic settlement, up to six times larger. However, at location 4 prediction of the settlement matches well with the measurement. Settlement prediction are plotted with the light blue dashed line in Figure 4.9. The seismic induced strain model is very sensitive to its densification properties and volumetric threshold strain, which are uncertain. Model predictions of the seismic induced strain model are therefore also unreliable.

Model predictions of the terminal density model and C/L model for cyclic shear are most reliable, because their input data and model parameters are most reliable. Model prediction of the terminal density model match best with the settlement measurements. At location 4 model prediction of the C/L model for cyclic shear matches better to the settlement measurement. The C/L model for cyclic oedometer compression, Hergarden model, cumulative plastic strain model and seismic induced strain model are discarded from further evaluation. Model predictions are unreliable for the available input data.

4.8.2. Vertical strain with depth

In Figure 4.10 the predicted vertical plastic strain with depth determined with the terminal density model (on the left) and C/L model for cyclic shear (on the right) together with the initial relative density are plotted for locations 1, 2, 4 and 6. Vertical plastic strain is calculated using the model parameter values in Table 4.3. The area underneath the graphs is equal to the predicted cyclic settlement plotted in Figure 4.9. The vertical axis starts at 3.5 $m\ NAP$ and ends at -3.5 $m\ NAP$. Above 3.5 $m\ NAP$ no vertical plastic strain accumulates, the sand is compacted here. Depth of influence varies between -1 and -2 $m\ NAP$, depending on the cyclic settlement model and location. Less vertical plastic strain accumulates at depths where the initial relative density of the sand is nearly 100%. For example, at around -0.5 $m\ NAP$ for location 1 (Figures 4.10a and 4.10b) and above 2.5 and at -1.5 $m\ NAP$ for location 4 (Figures 4.10e and 4.10f). Predicted settlement after 50 thousand load cycles and measured settlement are both indicated above the graphs.

The vertical plastic strain determined with the terminal density model is insensitive to the initial relative density. It is distributed evenly over the zone of influence for all four locations, despite varying initial relative density of the sand. For example at location 4 in Figure 4.10e, the increase of the vertical plastic strain corresponding to the significantly lower initial relative density between 1 and 0 $m\ NAP$ is almost unnoticeable. Variation of the cyclic settlement predictions is primarily related to the variation of the combined thickness of the sand layers with an initial relative density of nearly 100%. At location 4 this thickness is larger compared to the other locations, consequently the predicted settlement is smaller compared to the other locations. Largest settlement is predicted at location 2 due to the absence of a sand layer with an initial relative density of nearly 100%.

The vertical plastic strain predicted with the C/L model for cyclic shear is very sensitive to the initial relative density of the sand. Variation of the initial relative density with depth results in an uneven distribution of the vertical plastic strain over the zone of influence at all four locations. For a constant initial relative density with depth the vertical plastic strain decreases with depth. This is related to the cyclic shear strain amplitude which decreases with depth, plotted in Figure 4.3. This is best observed for locations 1 and 2 that have a more or less constant initial relative density with depth. Within the entire zone of influence the predicted vertical plastic strain has a large value, which results in an overestimate of the cyclic settlement at locations 1, 2 and 6. Similar to the terminal density model, predicted cyclic

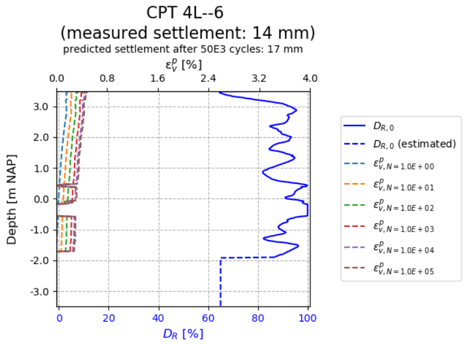

(a) Location 1: CPT 4L-6

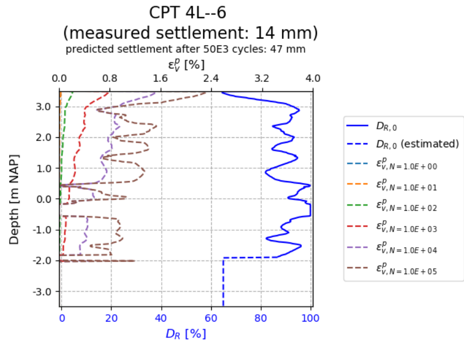

(b) Location 1: CPT 4L-6

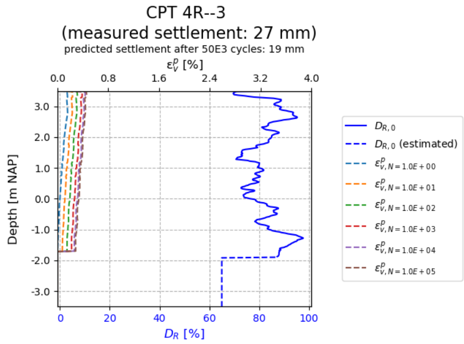

(c) Location 2: CPT 4R-3

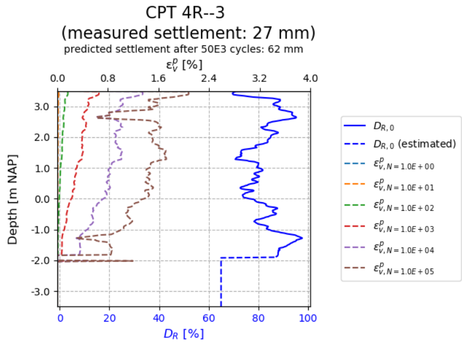

(d) Location 2: CPT 4R-3

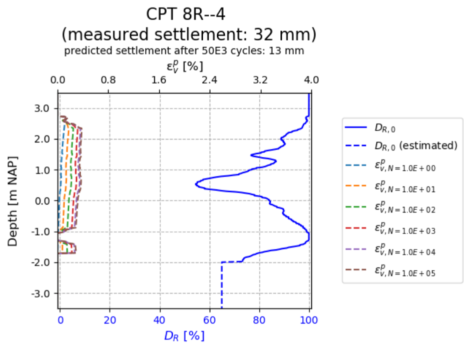

(e) Location 4: CPT 8R-4

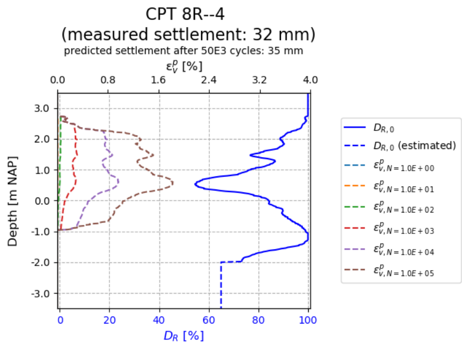

(f) Location 4: CPT 8R-4

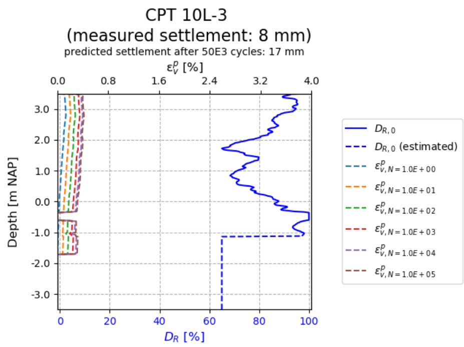

(g) Location 6: CPT 10L-3

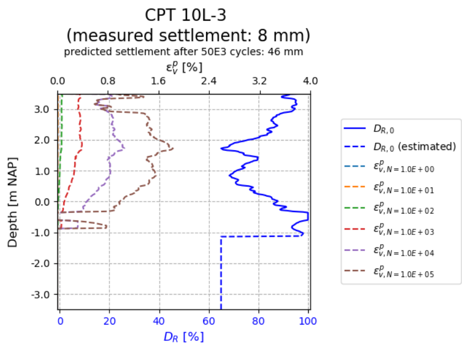

(h) Location 6: CPT 10L-3

Figure 4.10: Vertical plastic strain with depth with increasing number of load cycles determined with the terminal density model (on the left) and C/L model for cyclic shear (on the right) at locations 1, 2, 4 and 6.

settlement is related to the combined thickness of sand layers with an initial relative density of nearly 100%. At location 4 this thickness is larger compared to the other locations. Consequently, the predicted settlement is smaller compared to the other locations. Largest settlement is predicted at location 2 due to the absence of a sand layer with an initial relative density of nearly 100%.

Depth of influence estimated for the terminal density model is determined at 6 m below the shallow foundation, or -1.7 m NAP, for all four locations. Below -1.7 m NAP the vertical plastic strain predicted with the terminal density is zero. The C/L model for cyclic shear estimates a similar depth of influence between -1 and -2 m NAP. The cyclic shear strain amplitude increases with foundation stress. Depth of influence is therefore larger at locations 1 and 2 compared to locations 4 and 6. A significant amount of vertical plastic strain accumulates between -1 and -2 m NAP. Consequently, settlement predicted with the C/L model for cyclic shear is larger at locations 1 and 2 compared to locations 4 and 6.

4.8.3. Sensitivity terminal density model

In this section sensitivity of the terminal density model is evaluated. The following model parameters and input data are investigated:

- foundation stress;
- rate of stress dependency of the stiffness (parameter m);
- depth of influence;
- thickness of the compact sand layer underneath the foundation;
- initial relative density;
- terminal void ratio correlation (Equation 4.2).

In Figure 4.11 the predicted cyclic settlement at the four locations is plotted for a foundation stress between 60 and 100 kPa and for a rate of stress dependency of the stiffness (parameter m) of the sand between 0.5 and 0.7. Through the void ratio after one load cycle the foundation stress and stiffness of the sand fill influence model predictions of the terminal density model. Void ratio after one load cycle is related to vertical plastic strain after one load cycle, which is determined with the improved Schmertmann method. The vertical strain after one load cycle is plotted in Figure 4.7. With increasing foundation stress and decreasing parameter m vertical plastic strain increases and void ratio after one load cycle decreases. The terminal void ratio is correlated to the void ratio after the first load cycle in Equation 4.2. Its value decreases with decreasing void ratio after one load cycle. It results in a very small increase of the predicted settlement.

Model predictions of the cyclic settlement model are almost independent of the stiffness of the sand and foundation stress. The differences of the predicted cyclic settlement (primarily) occur in the first load cycle, this is shown in Figure 4.7. After the first load cycle the predicted cyclic settlement becomes insensitive to the foundation stress and stiffness of the sand. This difference remains constant with increasing number of load cycles, this is shown in Figure 4.11.

In Figure 4.12 cyclic settlement predicted with the terminal density model is plotted for the varying values of the depth of influence and thickness of the compacted sand layer. The predicted cyclic settlement corresponding to the estimated depth of influence and thickness of the compact sand layer is plotted with the red solid lines, which correspond to the red solid lines in Figure 4.9. Depth of influence varies between 2, 3 and 4 times the width of the foundation, which is 2 m wide. Depth of influence is thus 4, 6 or 8 m below the bottom of the ballast bed, which corresponds to 0.3, -1.7 or -3.7 m NAP, respectively. Thickness of the compacted sand layer varies between 0.3, 0.8 and 1.3 m. The bottom of the compacted sand layer is located at 4.0, 3.5 or 3.0 m NAP, respectively. The zone of influence is defined by the depth of influence and thickness of the compacted sand layer and varies from 2.7 to 7.7 m. At location 4 thickness of the sand layer does not influence the model prediction. The estimated

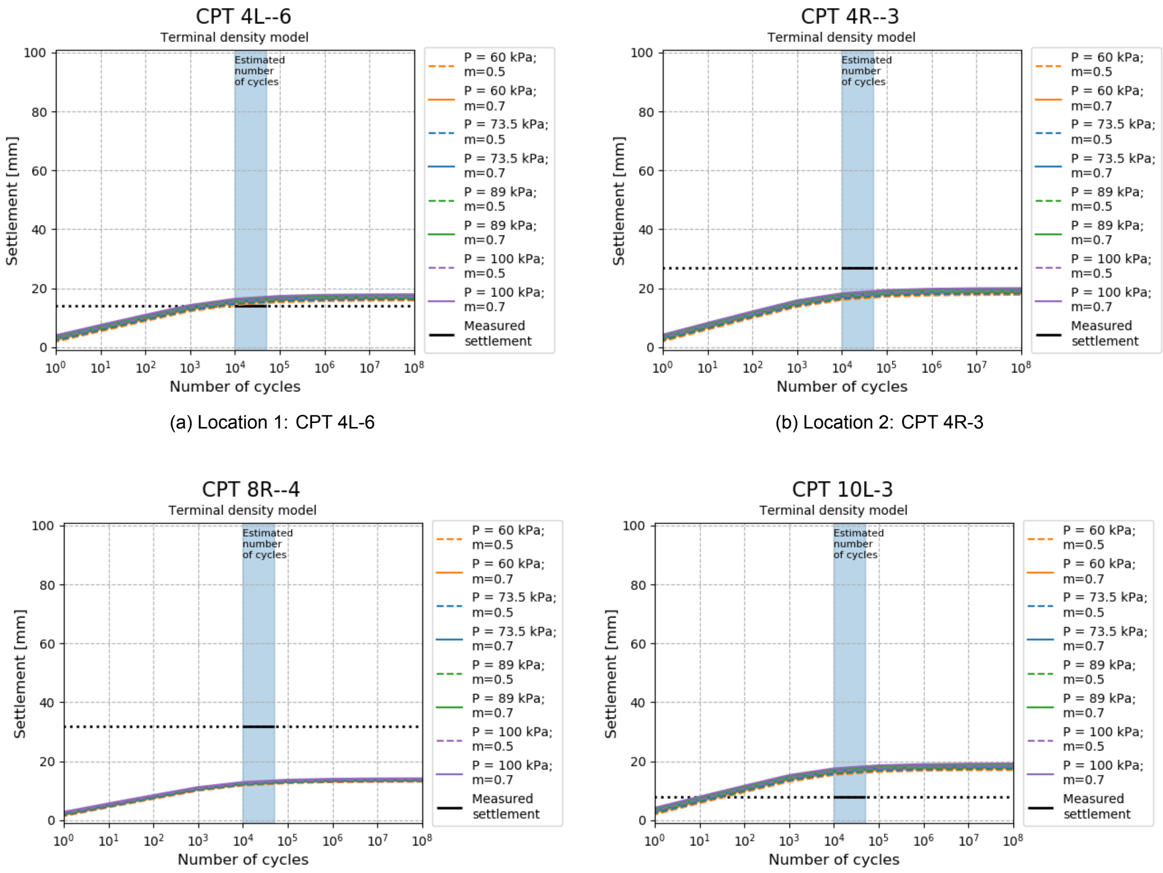

(a) Location 1: CPT 4L-6

(b) Location 2: CPT 4R-3

(c) Location 4: CPT 8R-4

(d) Location 6: CPT 10L-3

Figure 4.11: Cyclic settlement predicted with the terminal density model at locations 1, 2, 4 and 6 for a rate of stress dependency of the stiffness of the sand of 0.5 and 0.7 and for loads equivalent to a vertical stress of 60, 73.5, 89 and 100 kPa applied to the bottom of the foundation. The vertical strain after one load cycle used to calculate the void ratio after one load cycle to calculate the terminal void ratio and predict the settlement is plotted in Figure 4.7.

initial relative density above 3 m NAP is 100% at this location (see Figure 4.3d). No settlement is calculated above 3 m NAP, regardless of the thickness of the compacted sand layer.

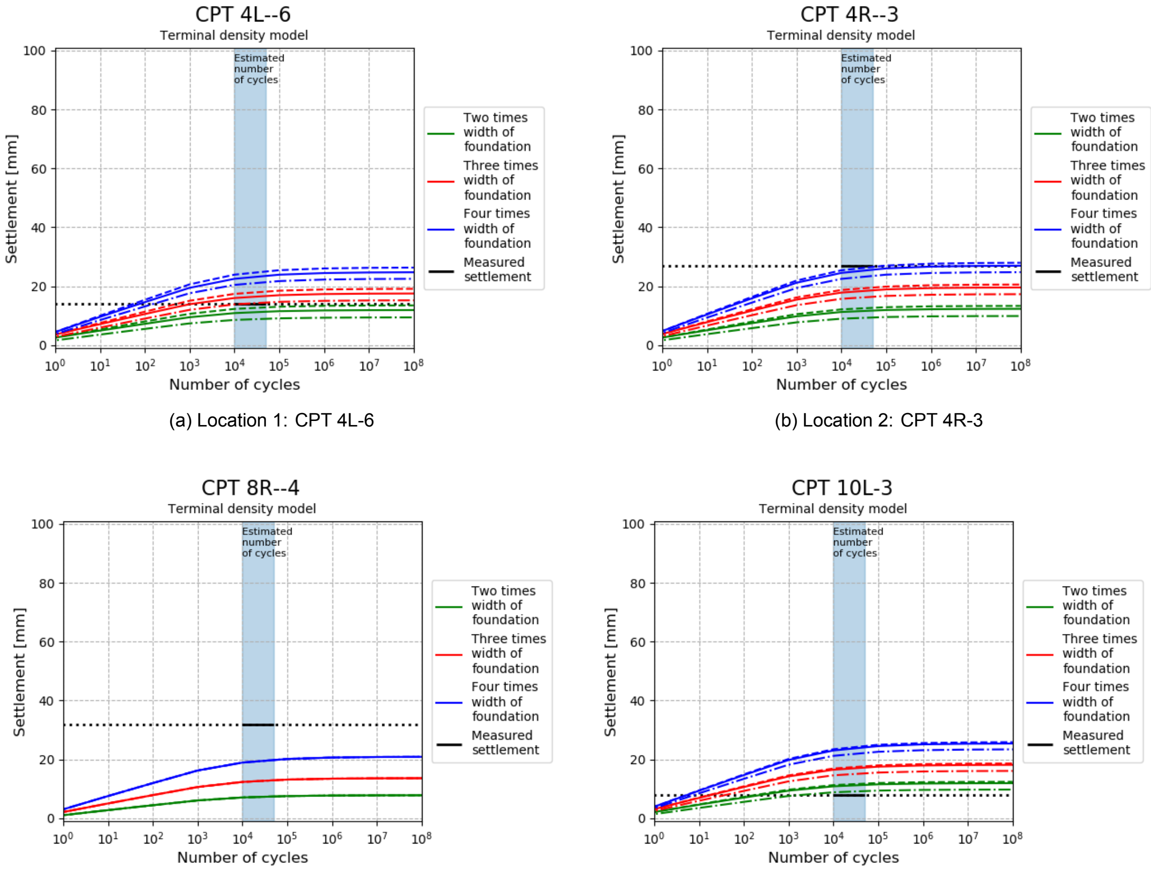

(a) Location 1: CPT 4L-6

(b) Location 2: CPT 4R-3

(c) Location 4: CPT 8R-4

(d) Location 6: CPT 10L-3

Figure 4.12: Cyclic settlement predicted with the terminal density model at locations 1, 2, 4 and 6 for varying depth of influence and thickness of the compacted sand layer. Depth of influence is estimated as two, three or four times the width of the foundation. That corresponds to 0.3, -1.7 and -3.7 m NAP, respectively. Thickness of the sand layer varies between 0.3 m (dashed lines), 0.8 m (solid lines) or 1.3 m (dashed-dotted lines). The bottom of the compacted sand layer is located at a depth of 4.0, 3.5 and 3.0 m NAP, respectively.

Predicted cyclic settlement increases (almost) linearly with increasing extent of the zone of influence. The green dashed-dotted lines and the blue dashed lines plotted in Figure 4.12 correspond to a zone of influence of 2.7 and 7.7 m, respectively. The blue dashed lines are almost three times larger compared to the green dashed-dotted lines. This is a result of the even distribution of the vertical plastic strain over the zone of influence predicted by the terminal density model, plotted in Figure 4.10.

Figure 4.13 presents the predicted cyclic settlement for varying initial relative density. The predicted cyclic settlement corresponding to the estimated initial relative density is plotted with the red lines, which correspond to the red solid lines in Figure 4.9. The initial relative density is increased and decreased by 10% and 25%.

An increase of the estimated initial relative density results in a relatively large decrease of the predicted cyclic settlement. An increase of the estimated initial relative density results in an increase of the combined thickness of the sand layer with an initial relative density of nearly 100%. In these sand layers less cyclic settlement is predicted. This is displayed in plots of the vertical plastic strain with depth predicted with the terminal density model in Figure 4.10. A result is that the predicted cyclic

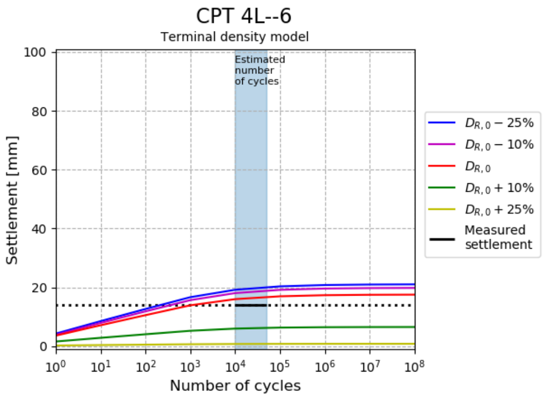

(a) Location 1: CPT 4L-6

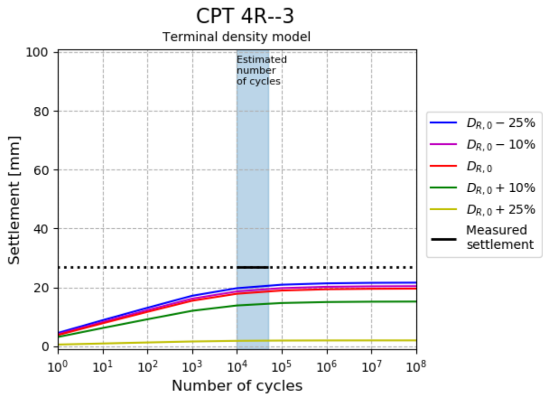

(b) Location 2: CPT 4R-3

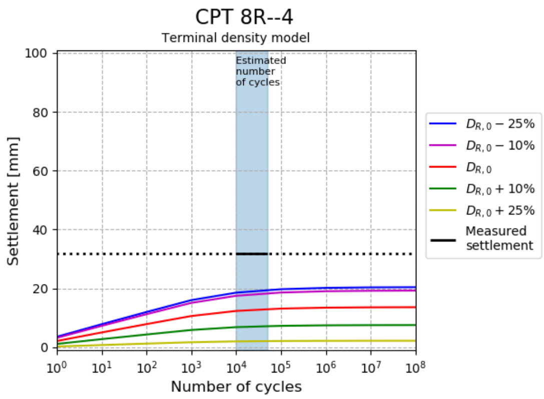

(c) Location 4: CPT 8R-4

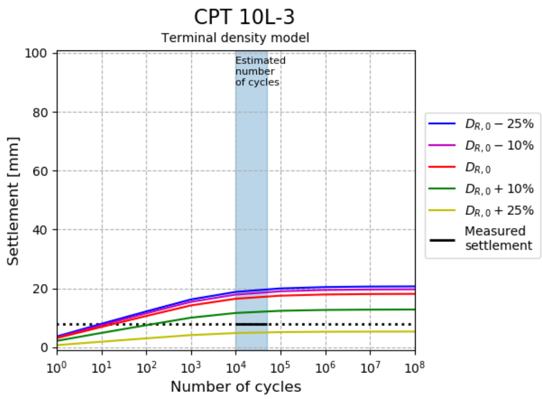

(d) Location 6: CPT 10L-3

Figure 4.13: Cyclic settlement predicted with the terminal density model at locations 1, 2, 4 and 6 for a varying initial relative density. The initial relative density is varied by subtracting 25% and 10% or adding 10% or 25% to the correlated initial relative density.

settlement decreases. By increasing the estimated initial relative density with 25% almost the entire zone of influence at all four locations reaches 100% initial relative density. Consequently, predicted cyclic settlement becomes almost zero.

A decrease of the estimated initial relative density by 10% results in a relatively small increase of the predicted cyclic settlement. Decreasing the initial relative density of the sand fill by 10% results in a zone of influence that has an initial relative density of 90% or lower. In the entire zone of influence there are no sand layers with an initial relative density of nearly 100%, i.e. within the entire zone of influence cyclic settlement occurs. This results in an increase of the predicted cyclic settlement. A decrease of the initial relative density of 25% results in a zone of influence that has an initial relative density below 75%. Similar to decreasing the initial relative density with 10%, in the entire zone of influence there are no sand layers with an initial relative density of nearly 100%. Cyclic settlement predicted for these two cases is therefore almost the same. The blue and purple lines almost coincide. At locations 2 and 6 the combined thickness of the sand layers with an estimated initial relative density of nearly 100% is small. At locations 1 and 4 the combined thickness of the sand layers with an estimated initial relative density of nearly 100% is larger. Increase of the predicted cyclic settlement related to a 10% decrease of the initial relative density is therefore larger at locations 1 and 4 compared to locations 2 and 6.

In Figure 4.14 the predicted cyclic settlement for a varying value of the empirical constant in Equation 4.2 is plotted, its original value is 0.987. Its value varies between 0.997, 0.987, 0.977, 0.937 and 0.887. The predicted cyclic settlement plotted by the red lines corresponds to the red solid lines in Figure 4.9. With decreasing value of the empirical constant the terminal void ratio decreases and difference between the initial void ratio increases. Consequently, model predictions of the cyclic settlement increases.

The plots in Figure 4.14 show that the correlation in Equation 4.2 with an empirical constant equal to 0.987 matches best with the settlement measurements. Decreasing the empirical constant results in an overestimate of the cyclic settlement. Model predictions of the terminal density model are very sensitive to the value of the empirical constant.

Model predictions of the cyclic settlement is primarily affected by the extent of the zone of influence and the thickness of the sand layer with an initial relative density of 100%. Cyclic settlement is (almost) linear related to the thickness of the sand layer within the zone of influence with an initial relative density is below 100%, i.e. thickness of the sand layer in which vertical plastic strain accumulates. Influence of changing the stiffness of the sand fill, foundation stress and decreasing initial relative density on model prediction of the cyclic settlement of the terminal density model are negligible.

4.8.4. Sensitivity compaction/liquefaction model for cyclic shear

In this section sensitivity of the C/L model for cyclic shear is evaluated. The following model parameters and input data are investigated:

- foundation stress;
- rate of stress dependency of the stiffness (parameter m);
- volumetric threshold strain;
- thickness of the compact sand layer underneath the foundation;
- initial relative density.

In Figure 4.15 predicted cyclic settlement at location 2 is plotted for a foundation stress that varying from 60 to 100 kPa and rate of stress dependency of the stiffness (parameter m) between 0.5 and 0.7. In Figure 4.4a the corresponding model parameter value of the cyclic shear strain amplitude is plotted for varying foundation stress and parameter m for location 2. Only at this location the cyclic shear strain amplitude is evaluated for varying foundation stress and parameter m.

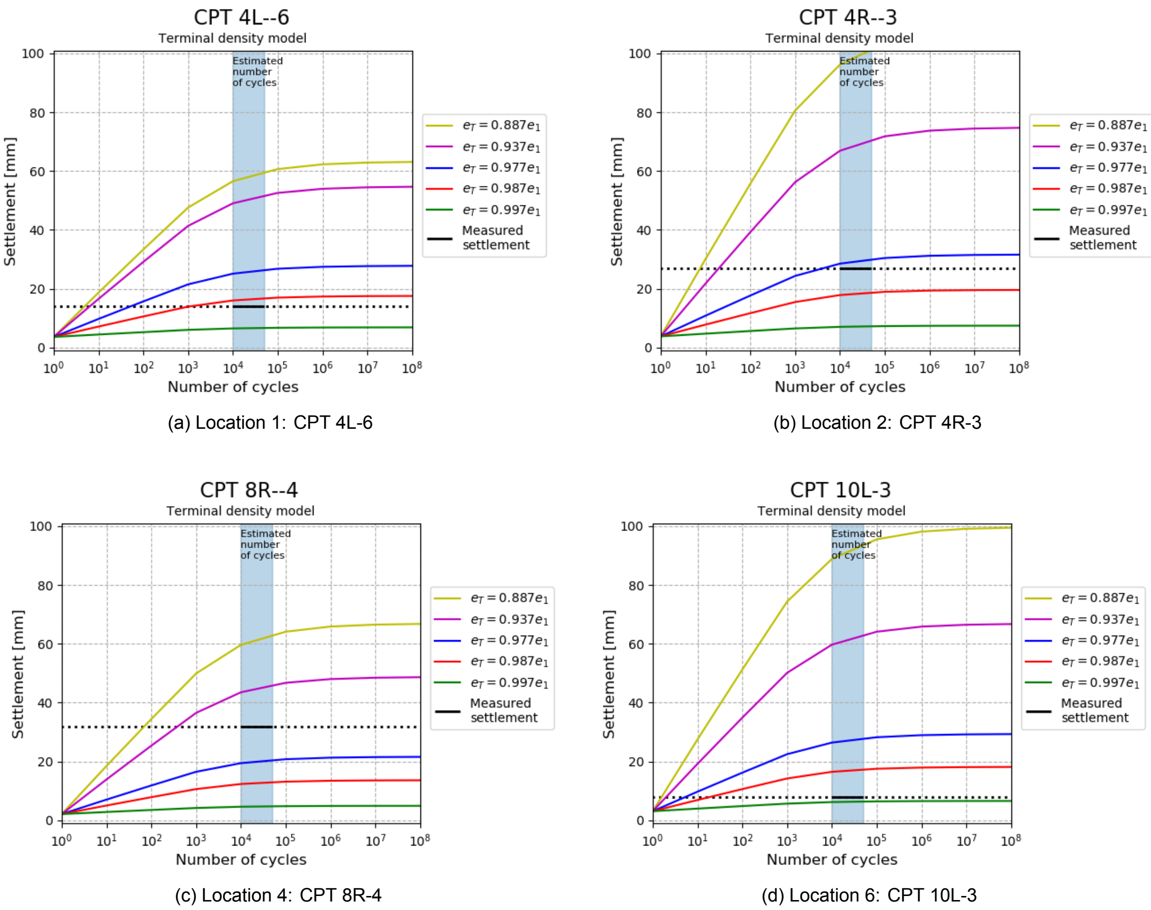

(a) Location 1: CPT 4L-6

(b) Location 2: CPT 4R-3

(c) Location 4: CPT 8R-4

(d) Location 6: CPT 10L-3

Figure 4.14: Cyclic settlement predicted with the terminal density model at locations 1, 2, 4 and 6 for a varying empirical constant of the correlation in Equation 4.2.

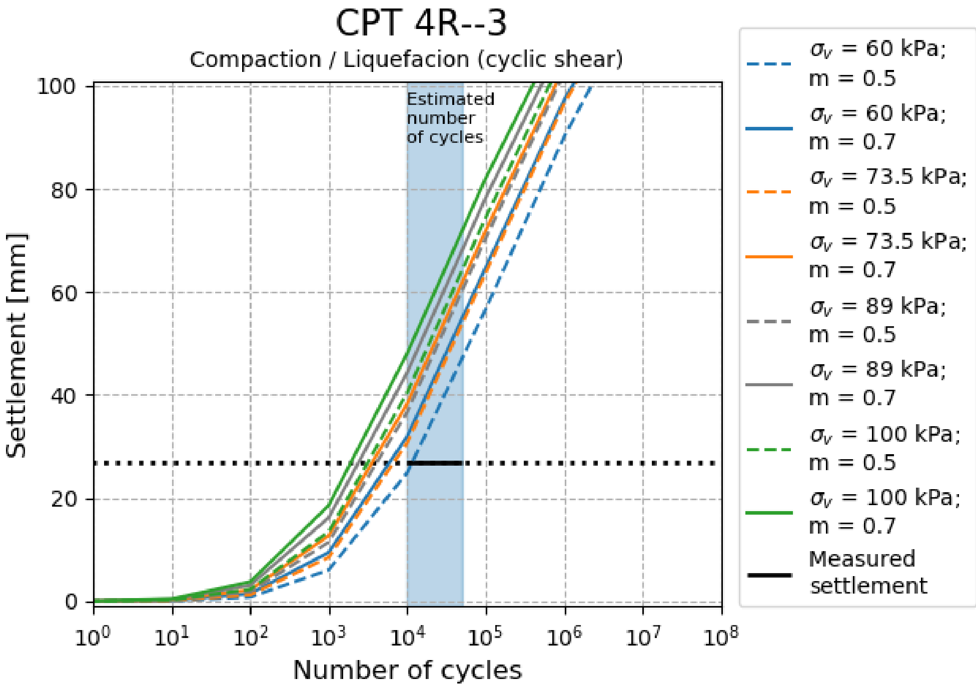

Figure 4.15: Cyclic settlement predicted with the C/L model for cyclic shear at location at location 2 for a rate of stress dependency of the stiffness of the sand of 0.5 and 0.7 and for loads equivalent to a vertical stress of 60, 73.5, 89 and 100 kPa applied to the bottom of the foundation. The cyclic shear strain amplitude used for these calculations of the cyclic settlement are plotted in Figure 4.4.

Model predictions of the cyclic settlement increase with cyclic shear strain amplitude, i.e. it increases with foundation stress and decreasing parameter m. Cyclic shear strain amplitude and depth of influence increase with foundation stress and decreasing parameter m.

In Figure 4.16 cyclic settlement is plotted for varying volumetric threshold strain and thickness of the compacted sand layer. The predicted cyclic settlement corresponding to the estimated volumetric threshold strain and thickness of the compact sand layer is plotted with the blue solid lines, which correspond to the blue solid lines in Figure 4.9. Thickness of the compacted sand layer varies between 0.3, 0.8 and 1.3 m. Bottom of the compacted sand layer is situated at 4.0, 3.5, and 3.0 m NAP, respectively. Volumetric threshold strain varies between 0.007% and 0.030%, corresponding to clean sands [55]. Depth of influence increases with decreasing volumetric threshold strain. In Figure 4.3 the cyclic shear strain amplitude and various values of the volumetric threshold strain are plotted. Depth of influence varies between 2.5 m NAP and -3.5 m NAP, that corresponds to about 2 to 8 m below the bottom of the foundation. Extent of the zone of influence increases with decreasing volumetric threshold strain and decreasing thickness of the compacted sand layer, it varies between 0.5 and 7.5 m.

Model predictions of the cyclic settlement increase with decreasing volumetric threshold strain and thickness of the sand layer, i.e. with increasing extent of the zone of influence. Model predictions of the C/L model for cyclic shear are very sensitive to the extent of the zone of influence. Plots of the vertical plastic strain predicted with the C/L model for cyclic shear in Figure 4.10 show that within the entire zone of influence a lot of vertical plastic strain accumulates. Varying the volumetric threshold strain has a significant influence at all locations. Varying the thickness of the compacted sand layer mainly affect the cyclic settlement predictions at locations 1 and 2. The estimated initial relative density of the top part of the sand fill at these locations is not nearly 100%. Varying the thickness of the compacted sand layer at location 4 does not influence the model predictions. The estimated initial relative density above 3 m NAP is 100% at this location (see Figure 4.3d). No settlement occurs above 3 m NAP, regardless of the thickness of the compacted sand layer.

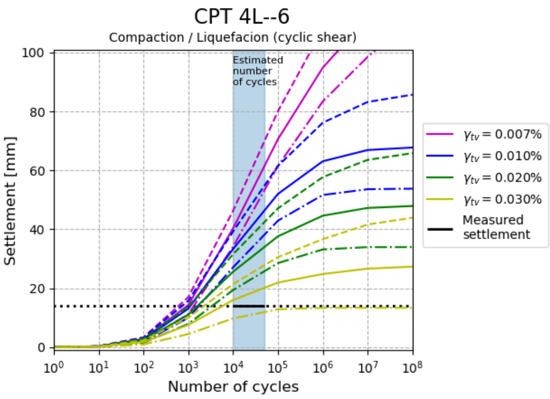

(a) Location 1: CPT 4L-6

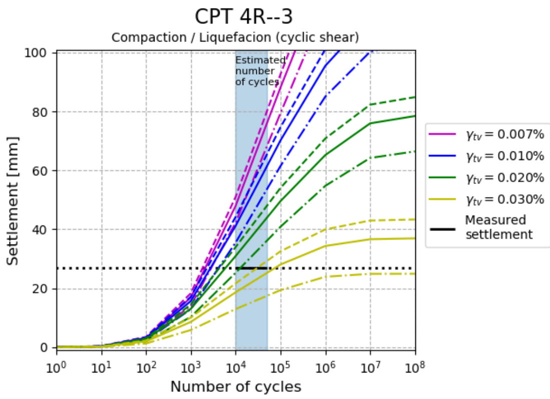

(b) Location 2: CPT 4R-3

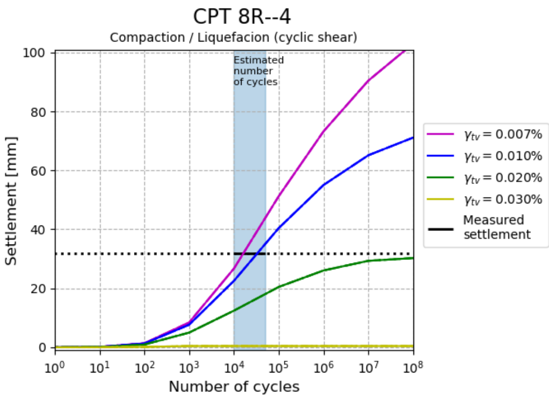

(c) Location 4: CPT 8R-4

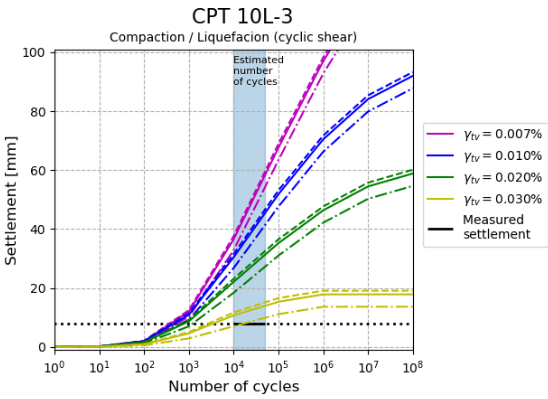

(d) Location 6: CPT 10L-3

Figure 4.16: Cyclic settlement predicted with the C/L model for cyclic shear at locations 1, 2, 4 and 6 for varying volumetric threshold strain and thickness of the sand layer. Thickness of the sand layer varies between 0.3 m (dashed lines), 0.8 m (solid lines) or 1.3 m (dashed-dotted lines). The bottom of the compacted sand layer is located at a depth of 4.0, 3.5 and 3.0 m NAP, respectively.

In Figure 4.17 the predicted cyclic settlement are plotted for varying initial relative density. The predicted cyclic settlement corresponding to the estimated initial relative density is plotted with the blue lines, which correspond to the blue solid lines in Figure 4.9. The initial relative density is increased and decreased by 10% and 25%.

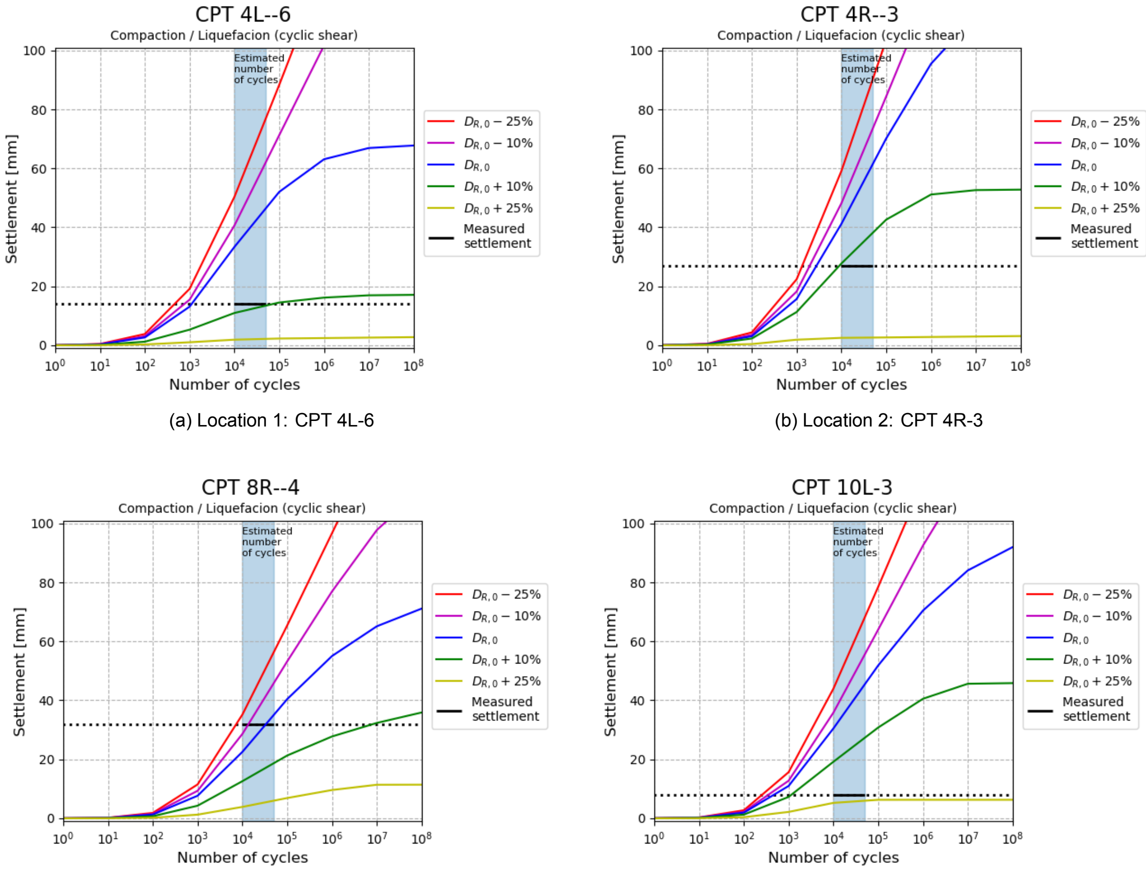

(a) Location 1: CPT 4L-6

(b) Location 2: CPT 4R-3

(c) Location 4: CPT 8R-4

(d) Location 6: CPT 10L-3

Figure 4.17: Cyclic settlement predicted with the C/L model for cyclic shear at locations 1, 2, 4 and 6 for a varying initial relative density. The initial relative density is varied by subtracting 25% and 10% or adding 10% or 25% to the correlated initial relative density.

Model predictions of the C/L model for cyclic shear are very sensitive to a decrease of the initial relative density, in contrast to the terminal density model which is not sensitive to a decrease of the initial relative density. Similar to the terminal density model, the C/L model for cyclic shear is sensitive to an increase of the initial relative density. This corresponds to the varying vertical plastic strain with relative density, plotted in Figure 4.10. Predicted cyclic settlement increases with decreasing relative density. According to the correlation in Equation 4.1, material constants increase with decreasing initial relative density. Furthermore, decreasing the initial relative density of the sand layer means that within the zone of influence there are no sand layers with an initial relative density of 100%. Vertical plastic strain accumulates over the entire zone of influence. Increasing the initial relative density by 25% almost the entire zone of influence reaches 100% initial relative density and almost no cyclic settlement occurs.

Model predictions of the C/L model for cyclic shear are very sensitive to the initial relative density extent of the zone of influence and the thickness of the sand layer with an initial relative density of 100%, i.e. thickness of the sand layer in which vertical plastic strain accumulates. Furthermore, it is also sensitive to the stiffness of the sand fill and foundation stress.

4.9. Discussion of the results

The cyclic settlement models discussed in this report are relatively easy to apply. Cyclic settlement can be evaluated at a large number of locations, for example one evaluation corresponding to each CPT measurement. The measurements show that the area has a strong variability of the relative density laterally and vertically, a large number of cyclic settlement predictions is required to analyse the cyclic settlement of all the rail tracks at the container terminal.

Figure 4.9 shows that model predictions of the C/L model for cyclic shear overestimate the cyclic settlement. Plots of the vertical plastic strain with depth in Figure 4.10 indicate that this is a result of the very sensitive response of the model to the initial relative density. Plots of the cyclic settlement in Figure 4.17 also show that the model predictions are very sensitive to the initial relative density. This is a result of the correlation in Equation 4.1 that is used to determine the material constants that describe the cyclic densification behaviour of the sand. At location 4 the model prediction of the C/L model for cyclic shear and the measured settlement match well. Here the sand fill contains a medium dense sand layer. The correlation seems to give better results for medium dense sand. However, at location 4 the model prediction is dominated by the combined thickness of the sand layers that have a 100% relative density. No densification is predicted in these layers which resulted in a smaller model prediction of the cyclic settlement.

Results plotted in Figure 4.9 show that the predictions of the terminal density model match best with the settlement measurements. However, Figures 4.10 and 4.13 demonstrate that the model predictions of the cyclic settlement and vertical plastic strain are insensitive to the initial relative density. Furthermore, Figure 4.11 shows that model predictions of the cyclic settlement are insensitive to the stiffness of the sand and amplitude of the load. It is a result of the correlation in Equation 4.2 used to determine the terminal void ratio. Model predictions with the terminal density model at location 1 in Figure 4.9a indicate that predictions are most reliable for dense to very dense sand layers. At location 1 the sand consists of dense to very dense sand layers and the model prediction and settlement measurement match well. At location 4 the sand fill contains a medium dense sand layer. The model prediction of the cyclic settlement at location 4 in Figure 4.9c shows that the terminal density model underestimates the cyclic settlement and is less reliable for locations where the sand fill also consists of less dense sand layers.

The zone of influence underneath the ASC rail tracks extents to a depth of approximately 6 m below the bottom of the foundation. This is based on the response of the first load cycle analysed with an FE model plotted in Figure 4.3, improved Schmertmann method plotted in Figure 4.7 and on the 2D-spreading of the load plotted in Figure 3.11. It is also consistent with the observation that the settlement measured at location 4 primarily occurred between 1 and 0 $m\ NAP$, which is around 4 m below the foundation. Three times the width of the foundation gives a good first estimate of the depth of influence underneath ASC rail tracks. Figures 4.3 and 4.4a show that depth of influence increases with the amplitude of the load and decreasing stiffness of the sand and decreasing volumetric threshold strain. Figures 4.12 and 4.16 show that model predictions of the cyclic settlement of the terminal density model and C/L model for cyclic shear increase with depth of influence.

Model predictions of the vertical plastic strain of the terminal density model and C/L model for cyclic shear in Figure 4.10 show that densification of the sand fill occurs in the entire zone of influence. Based on the responses determined with the FE computation and improved Schmertmann method in Figures 4.5 and 4.7, most densification in the first load cycle occurs between 0.5 and 2 m below the foundation. In the subsequent load cycles densification concentrates in the sand layers with a lower relative density. This is based on the larger settlement that was measured at location 4. It is expected that densification primarily occurred in the medium dense sand layer located at this location. This is consistent with the model predictions of the vertical plastic strain of the C/L model for cyclic shear in Figure 4.10. Cyclic settlement decreases with depth. This is indicated by model predictions of the vertical plastic strain of the C/L model for cyclic shear in Figure 4.10 and the response of the first load cycle in Figures 4.5 and

4.7. Deeper the stiffness of the sand is higher, due to the increasing confining stress and the amplitude of the load is smaller due to spreading of the load with depth.

According to the C/L model for cyclic shear densification stops when the relative density becomes 100%. The model predictions in Figure 4.9 show that this results in an overestimate of the cyclic settlement. The maximum densification therefore does not coincide with the minimum void ratio (or 100% relative density). Maximum densification is a property that depends on the soil conditions, initial state and loading conditions, i.e. the terminal void ratio.

Model predictions of the terminal density model in Figure 4.9 show that after 10^4 load cycles just a small amount of cyclic settlement will occur. Most densification occurs in the first load cycles. According to the terminal density model cyclic settlement will stop when the sand has reached its terminal density within the entire zone of influence. The terminal density model seems more theoretically based compared to the C/L model for cyclic shear. This model assumes that densification continues indefinitely. Model predictions of the C/L model for cyclic shear are in the right order of magnitude after order 10^4 load cycles, for higher number of load cycles the model predictions become unreliable. Cyclic settlement predictions with models that assume cyclic settlement continues indefinitely can be ‘cutoff’ after order 10^4 load cycles, i.e. the predicted cyclic settlement after about 10^4 load cycles is the maximum settlement.

Based on the combination of the measured settlement and initial relative density profile at location 4 (see Figure 3.14d), cyclic settlement will exceed the settlement requirement for ASC rail tracks for a sand fill that contains loose or medium dense sand layers within the zone of influence. The sand fill will have to be compacted at those locations, regardless of the model prediction.

To meet the 20 mm settlement requirement for ASC tracks, the sand fill underneath the rail tracks must have an average initial relative density of at least 85% and minimum initial relative density of at least 65% within the zone of influence. This is based on the combination of the measured settlement and initial relative density profile at location 1, given in Figure 3.14a. For these conditions the terminal density model gives most reliable predictions. Figure 4.9a shows that the terminal density model at location 1 predicts less than 20 mm settlement. At location 2 the average initial relative is less than 85%, here the settlement exceeded the settlement requirement for ASC rail tracks. For the smaller ASCs an average initial relative density of at least 80% is probably sufficient. This is based on the measured settlement and initial relative density profile at location 6, given in Figure 3.14f.

4.9.1. Terminal void ratio

Equation 4.2 correlates the void ratio after one load cycle to the terminal void ratio by an empirical constant. Figure 4.14 shows that the selected empirical constant gives the best match between the settlement predictions and measurements. However, the correlation makes the model prediction insensitive to the input data such as the stiffness of the sand, initial relative density and foundation stress. Even though, the void ratio after one load cycle is sensitive to the initial void ratio, foundation stress and stiffness of the sand. This empirical relation should only be used for a dense to very dense sand fill with a constant initial relative density. Therefore two different potentially interesting methods that can be used to estimate the terminal void ratio are presented below. Note that more reliable model predictions can be made if the terminal ratio of the sand is measured.

The terminal void ratio can be estimated by:

$$e_T = e_{min} + (e_0 - e_{min})(1.0 - a\frac{\Delta\sigma}{\sigma'_{v,0}}) \tag{4.3}$$

with

a = material constant, [-],
$\Delta\sigma$ = cyclic vertical stress increase, [kPa],
$\sigma'_{v,0}$ = initial vertical stress, [kPa].

It relates the terminal void ratio to the initial and minimum void ratio and the stress amplitude ratio [39]. Furthermore, the terminal void ratio cannot become smaller than the minimum void ratio. This was also assumed in the current research. For the sand at the RWG container terminal a is estimated at 0.05, which is based on another sand type that was evaluated [39]. The total vertical plastic strain corresponding to the terminal void ratio estimated with the correlation in Equation 4.3 is plotted in Figure 4.18 by the green line. The corresponding settlement at locations 1 and 4 are 1.2 and 0.4 mm, respectively. This is smaller compared to the vertical plastic strain after one load cycle determined with the improved Schmertmann method, which is plotted by the light blue lines. For the current problem the correlation underestimates the cyclic settlement, it will therefore not be used. However, the correlation takes into account the initial void ratio, minimum void ratio and vertical stress. It could be interesting to further investigate this type of correlation and the value of material constant a. With increasing value of a the terminal void ratio decreases and cyclic settlement increases.

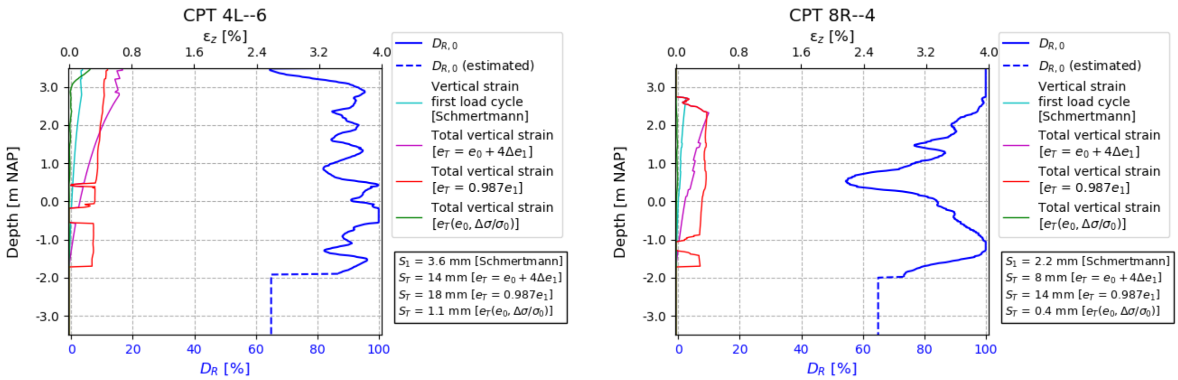

(a) Location 1: CPT 4L-6

(b) Location 4: CPT 8R-4

Figure 4.18: Vertical plastic strain after one load cycle (determined with the improved Schmertmann method) and vertical plastic strain related to the terminal density determined with the correlations in Equations 4.2, 4.3 and 4.5 plotted together with the initial relative density for locations 1 and 4.

Another option is to relate the vertical plastic strain after $N \rightarrow \infty$ load cycles to the vertical plastic strain in the first load cycle. This concept is based on the cumulative plastic strain model described in Section 2.5. In contrast, a maximum density is defined, the terminal density, or void terminal void ratio. Figure 4.19 shows two plots of the vertical plastic strain as a function of the vertical effective stress of a medium dense and a dense sand sample in a cyclic oedometer test applied to 10 thousand load cycles [39]. It is observed that the vertical plastic strain after 10 thousand load cycles is about three times the vertical plastic strain in the first load cycle. The vertical plastic strain associated with the amount of densification to reach the terminal void ratio, the maximum vertical plastic strain, is about four times larger than the vertical plastic strain in the first load cycle:

$$\varepsilon^p_{vol,N=\infty} = 4\varepsilon^p_{vol,N=1} \tag{4.4}$$

with

$\varepsilon^p_{vol,N=\infty}$ = maximum volumetric plastic strain to reach the terminal density, [-],
$\varepsilon^p_{vol,N=1}$ = volumetric plastic strain in the first load cycle, [-].

The terminal void ratio is the initial void ratio plus the change in void ratio after $N \rightarrow \infty$ load cycles:

$$e_T = e_0 + \Delta e_T = e_0 + 4\Delta e_1 \tag{4.5}$$

with

Δe_T = change in void ratio to reach the terminal void ratio, [-],
Δe_1 = change in void ratio in the first load cycle, [-].

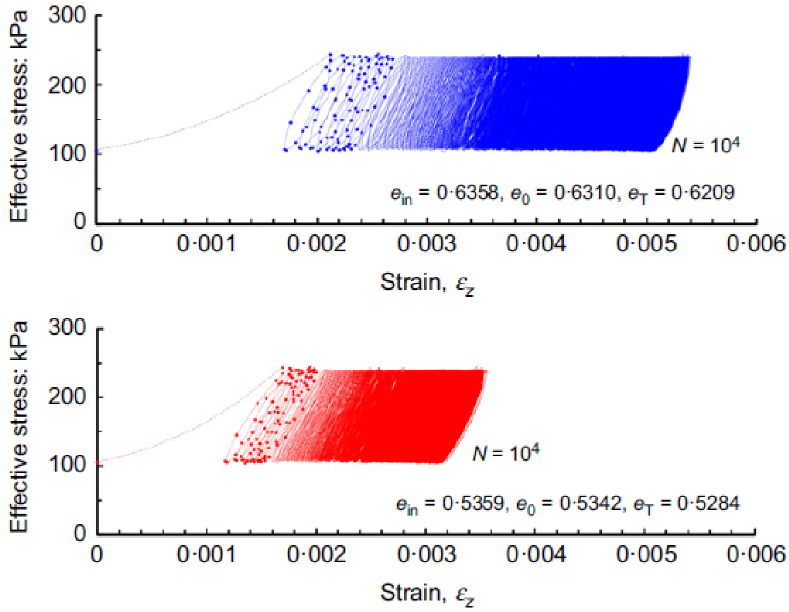

Figure 4.19: Results from two cyclic oedometer tests with an initial load of 105 kPa and applying 10^4 load cycles with a cyclic load amplitude of 138 kPa. The data plotted in blue is from a medium dense sand with a relative density of 44%, $e_{N=10.000} = 0.628$. The data plotted in red corresponds to a very dense sand with a relative density of 86%, $e_{N=10.000} = 0.532$ [39].

The vertical plastic strain related to the terminal void ratio determined with the correlation in Equation 4.5 is plotted by the purple line in Figure 4.18, for locations 1 and 4. Note that the vertical plastic strain is linear related to the vertical plastic strain in the first load cycle by a factor 4. Therefore the light blue and the purple lines in Figure 4.18 have a similar shape. Both the light blue and purple lines have the largest vertical plastic strain at 2.8 $m\ NAP$. The vertical plastic strain decreases with depth and becomes zero at -1.7 $m\ NAP$, corresponding to a depth of 0.75B and 3B below the shallow foundation. The increase of the vertical plastic strain at location 4 between 1 and 0 $m\ NAP$ related to the significantly lower initial relative density of the sand is negligible. The total settlement related to the vertical plastic strain is 14 and 8 mm for locations 1 and 4, respectively. Cyclic settlement predicted with the correlation in Equation 4.2 matches better with the cyclic settlement measurements.

To the author's knowledge, the latter correlation has not (yet) been described in literature in combination with the terminal density model. It is based on the data presented in Figure 4.19. The correlation of Equation 4.5 has never been evaluated or validated before and is based on the specific type of sand (Ottawa 20/30) that was used in the experiment presented in Figure 4.19.

4.10. RWG container terminal Phase 2

In the final section of this chapter is explained how the cyclic settlement is calculated in this research using the terminal density model. Then the cyclic settlement for two locations in Phase 2 of the RWG container terminal are predicted. Based on the model predictions a scenario for the compaction of the sand fill of Phase 2 of the RWG container terminal is presented.

4.10.1. Terminal density model recipe

The terminal density model is used to predict the cyclic settlement at Phase 2 of the RWG container terminal. It calculates the void ratio after N load cycles using Equation 2.12. The difference between the initial void ratio and void ratio after N load cycles defines the volumetric plastic strain, given by Equation 2.13. In order to determine the void ratio and volumetric plastic strain after N load cycles with the terminal density model, values of its model parameters need to be determined:

1. initial void ratio;
2. void ratio after one load cycle;
3. terminal void ratio;
4. characteristic number of load cycles;
5. fitting parameter.

Figure 4.20 gives a flowchart of the implementation of the terminal density model applied to this research.

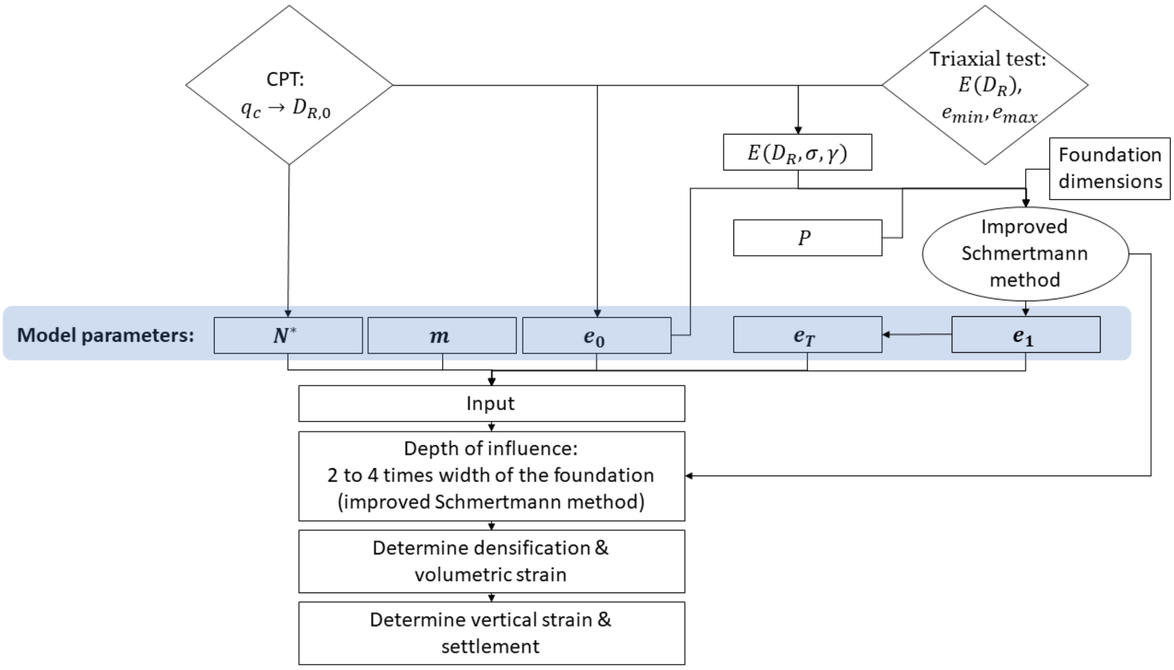

Figure 4.20: Flowchart of the implementation of the terminal density model in this research.

Initial void ratio (e_0)

The initial void ratio is the void ratio of the sand after construction of the rail tracks but before the ASCs start moving. The initial void ratio can be calculated based on the minimum and maximum void ratio and initial relative density:

$$e_0 = e_{max} - (e_{max} - e_{min}) \cdot D_{R,0} \tag{4.6}$$

with

e_0 = initial void ratio, [-],
$D_{R,0}$ = initial relative density, [-],
e_{min} = minimum void ratio, [-],
e_{max} = maximum void ratio, [-].

The minimum and maximum void ratios of the sand at the RWG container terminal are 0.5 and 0.8, respectively. The initial relative density is based on CPT measurements. The initial relative density of locations 1, 2, 4 and 6 are plotted in Figure 4.3.

Void ratio after one load cycle (e_1)

Void ratio after one load cycle is the initial void ratio plus the change in void ratio caused by the first load cycle, resulting in a decrease of the void ratio in case of densification (change in void ratio is negative for densification):

$$e_1 = e_0 + \Delta e_1 \tag{4.7}$$

with

e_1 = void ratio after one load cycle, [-],
Δe_1 = change in void ratio in the first load cycle, [-].

The change in void ratio in the first cycle corresponds to the volumetric plastic strain in the first load cycle:

$$\Delta e_1 = -\varepsilon^p_{vol,N=1}(1+e_0) \approx -\frac{\varepsilon^p_{v,N=1}}{VVSR}(1+e_0) \tag{4.8}$$

with

$\varepsilon^p_{vol,N=1}$ = volumetric plastic strain in the first load cycle, [-],
$\varepsilon^p_{v,N=1}$ = vertical plastic strain in the first load cycle, [-],
$VVSR$ = vertical-volumetric strain ratio, [-].

The volumetric plastic strain in the first load cycle is estimated based on the vertical plastic strain after one load cycle calculated with the improved Schmertmann method and the ratio between the vertical and volumetric plastic strain (VVSR). The VVSR is determined at 0.66 in Figure 4.5.

Terminal void ratio (e_T)

Considering cyclic loading conditions, the terminal void ratio is the void ratio of the sand at $N \to \infty$. That is the void ratio at the maximum density of the sand under the prevailing conditions. It is the void ratio of the sand at the moment plastic strain stops accumulating within a load cycle. Difference between the initial void ratio and the terminal void ratio gives the maximum possible densification of the sand for the given conditions. The terminal void ratio of the sand depends on the initial soil conditions, loading conditions and boundary conditions. The terminal void ratio is estimated with the correlation in Equation 4.2.

Characteristic number of load cycles (N^*)

The number of load cycles required to reach half of the total densification is equal to $N^* + 1$ and substitution of $N = N^* + 1$ into Equation 2.12 gives:

$$e_{N=N^*+1} = \frac{1}{2}(e_0 - e_T) \tag{4.9}$$

with

e_N = void ratio after N load cycles, [-],
N^* = characteristic number of load cycles, [-].

The rate of densification decreases with increasing characteristic number of load cycles. Considering compaction of sand under zero-lateral strain conditions, the characteristic number of load cycles decreases with increasing relative density. For a very dense sand $N^* \to 1$ and for a very loose sand $N^* \to 1000$ [39]. It seems to suggest that the rate of densification of very dense sands is higher than for loose sand, since half of the densification is reached after two load cycles. However, the difference between the initial and the terminal density will be very small in these cases. The rate of densification of a loose sand will therefore still be larger than for a dense sand. In this research $N^* = 100$ is used, independent of the relative density. The sand at the container terminal is medium to very dense so its actual value will not be constant.

Fitting parameter (m)

This parameter has been determined at $m = 0.45 \pm 0.05$ [39]. In this research $m = 0.45$ is used.

In Appendix D implementation of the C/L model for cyclic shear is described.

4.10.2. Cyclic settlement Phase 2

A large number of shallow CPT's are executed at Phase 2, around 400. The shallow CPT's at Phase 2 extent till -5 $m\ NAP$ (compared to -2 $m\ NAP$ at Phase 1). Soil conditions are assumed the same at Phase 2, because it is located adjacent to Phase 1. Two locations with different initial relative density profiles are selected. In Figure 4.21 the cone tipe resistance measured by CPT's 29 and 37, are plotted together with the estimated initial relative density. Similar to Phase 1, it is assumed that above 3.5 $m\ NAP$ the sand fill in Phase 2 is compacted due to construction works that will be carried out. Densification does not occur above that depth. Beyond -5 $m\ NAP$ the relative density is estimated at 65%. This lies outside the zone of influence and will not affect the model predictions.

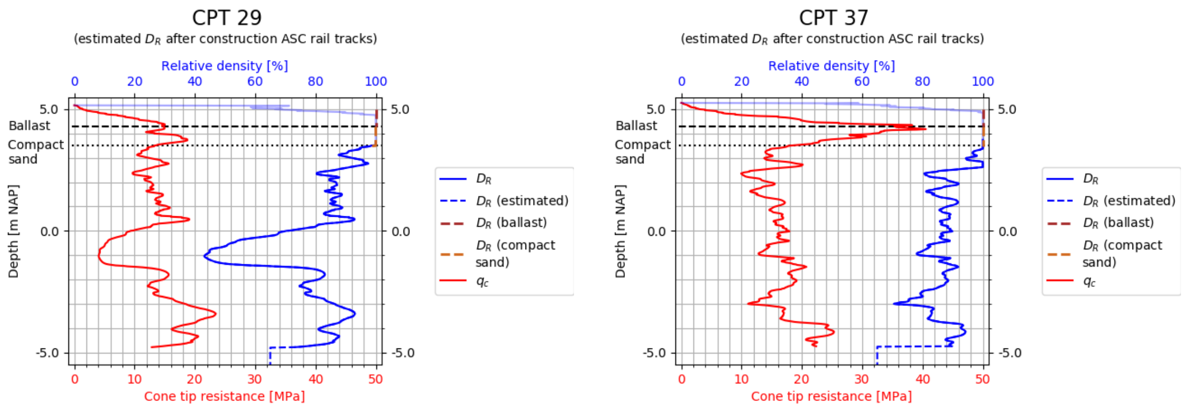

(a) (b)

Figure 4.21: Cone tip resistance and estimated initial relative density at two locations at Phase 2 of the RWG container terminal.

At Phase 2 the relative density of the sand fill varies laterally and vertically. The top part of the sand fill at both locations is dense, around 85% relative density. The sand fill at the location corresponding to CPT 37 has a constant relative density for the extent of the CPT. This is similar to the initial relative density profile at location 1 in Phase 1, plotted in Figure 4.3b. At the location corresponding to CPT 29 the relative density decreases significantly to almost 40% between 0 and -2 $m\ NAP$. This is similar to the initial relative density profile at location 4 in Phase 1, plotted in Figure 4.3d.

Figure 4.22 shows that at the location corresponding to CPT 29 the predicted cyclic settlement is 20 mm after around 100 thousand load cycles, according to the terminal density model. This is probably an underestimate of the cyclic settlement. Densification is expected to primarily occur in the sand layer with a significantly lower initial relative density. Similar to location 4 in Phase 1, the corresponding cyclic settlement will probably exceed 20 mm.

The terminal density model predicts around 17 mm settlement after 100 thousand load cycles at the location corresponding to CPT 37. Here the sand is dense to very dense. Under these conditions the terminal density model was found to give reliable model predictions. The depth of influence is estimated at three times the width of the foundation, that is till -1.7 $m\ NAP$. A more reliable estimate of the depth of influence and thickness of the compacted sand layer as a result of the construction works would further improve the reliability of the model prediction. Based on the model prediction for the location that corresponds to CPT 37 in Figure 4.22, cyclic settlement will probably not exceed the settlement requirements for ASC rail tracks.

4.10.3. Compaction of the sand fill

At phase 2 of the RWG container terminal there are many locations with varying initial relative density with depth or a low initial relative density. Conditions of the sand fill at these locations in terms of cyclic settlement are similar or worse compared to locations 2 and 4 at Phase 1. Here 27 and 32 mm cyclic settlement is measured, respectively. In order to meet the settlement requirement for ASC rail tracks,

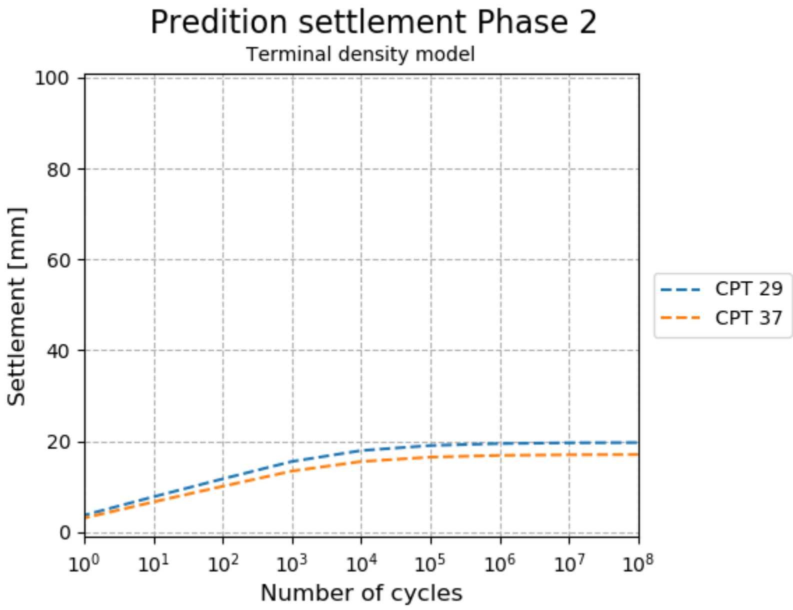

Figure 4.22: Predicted cyclic settlement with the terminal density model at two locations at Phase 2 of the RWG container terminal.

the sand fill will need to be compacted at these locations. At other locations, like CPT 37, the sand fill has a high initial relative density. Assuming that the initial relative density will not decrease due to construction works, cyclic settlement will probably meet the settlement requirements. The sand fill does not need to be compacted at locations with an initial relative density profile similar to CPT 37.

Extent and intensity of the compaction of the sand fill depends on the initial conditions. At locations with an initial relative density profile lower compared to CPT 37 in Phase 2 the sand fill needs to be compacted to meet the settlement requirement for ASC rail tracks. In case the top part of the sand fill, for example till a depth of 2 $m\ NAP$, consists of loose sand, while deeper it has a similar initial relative density profile as CPT 37, compaction of the sand till a depth of 1 $m\ NAP$ is sufficient. However, in case there are loose sand layers at larger depths, like CPT 29, the entire zone of influence must be compacted to meet the settlement requirements for ASC rail tracks. The average relative density of the sand fill must be compacted to at least 85% and the minimum relative density to at least 65%. For the smaller ASCs an average relative density of 80% is sufficient.

4.10.4. Alternative densification method

Most of the cyclic settlement occurs within the first load cycles. After 10 thousand load cycles almost all cyclic settlement has occurred, according to the terminal density model. That is regardless of the initial relative density. Instead of executing a pre-compaction, apply 10 thousand load cycles with the ASCs. Depending on the cyclic settlement that occurs the rail tracks must be maintained several times. With a reliable prediction of the cyclic settlement as function of the number of load cycles maintenance can be predicted and scheduled. Most densification occurs while an ASC is carrying a container with the maximum weight of 40 tonne and there are no containers stored in the container stack. That results in the maximum amplitude of the load while the stiffness of the sand, due to the lower confining stress, are minimal. It is therefore recommended to apply the load cycles before the container stack is operational, during the test phase of the ASCs.

5 Final conclusions and recommendations

The aim of the research that was carried out is to contribute to prevent unplanned downtime in Phase 2 of the RWG container terminal due to rail track settlements. Six cyclic settlement models were evaluated to predict the cyclic settlement of ASC rail tracks. Based on measurements of the soil and settlement in Phase 1 and model predictions the intensity and extent of the ground compaction that is necessary to meet the 20 mm settlement requirement for ASC rail tracks has been determined.

The relative density of the sand fill underneath the rail tracks varies, laterally and vertically. After the data were gathered construction of the ASC rail tracks disturbed the sand fill, especially its top part. The disturbance has not been quantified, which has hindered strong conclusions about the cyclic settlement (distribution) based on the data.

The sand fill is assumed to consist of one sand type, variation of relevant soil parameters is therefore not determined. Consequently, influence of the soil parameters on the densification of sand cannot be determined based on measurements. However, based on model predictions from the evaluated cyclic settlement models the influence of the relevant soil parameters on the densification of sand is predicted, including:

- decreasing initial relative density;
- decreasing volumetric threshold strain;
- amplitude of the load;
- decreasing stiffness;
- number of load cycles.

Rate of densification decreases with number of load cycles. By determining the maximum densification and depth of influence the maximum cyclic settlement can be determined. Maximum densification was found to be dependent on the first four points and depth of influence on the first three points.

The following cyclic settlement models were investigated for the evaluation of the cyclic settlement of ASC rail tracks at the RWG container terminal:

- terminal density model [39];
- compaction / liquefaction model for cyclic shear [45] [46];
- compaction / liquefaction model for oedometer compression [48] [49];
- Hergarden model [25];
- seismic induced strain model [21];

- cumulative plastic strain model [36].

The selected cyclic settlement models are engineering models that are easy to apply which allows them to make a large number of cyclic settlement predictions. To evaluate the settlement of all ASC rail tracks at the RWG container terminal a large number of cyclic settlement predictions is required, due to the strong variability of the relative density of the sand.

The main criteria used in this research to evaluate the performance of cyclic settlement models are:

- feasibility data recovery;
- availability data;
- reliability model prediction;
- match with the settlement measurements;
- theoretical and physical correctness.

The bottom four models listed above were found not to give reliable predictions of the cyclic settlement, due to incomplete input data their model parameter values contain uncertainty. These models have been discarded. More reliable results were obtained with the terminal density model and the compaction / liquefaction model for cyclic shear.

The terminal density model and compaction / liquefaction model for cyclic shear produce different responses of the cyclic settlement. Those models that assume cyclic settlement continues indefinitely do not seem to be the best choices. The terminal density model (and the compaction / liquefaction model for cyclic shear) gave better results of the cyclic settlement. However, model predictions of the terminal density model are not sensitive to the initial relative density – while the compaction / liquefaction model for cyclic shear is very sensitive to the initial relative density and assumes that cyclic settlement continues indefinitely. The terminal density model seems more physically based for this problem and gave reliable predictions of the cyclic settlement for sand with an initial relative density above 80% and can be used for these conditions.

The correlation in Equation 4.2 that is used to determine the maximum densification results in model predictions that are insensitive to the initial relative density, stiffness of the sand and amplitude of the load. The correlation in Equation 4.1 to determine the material constants for the compaction / liquefaction model for cyclic shear results in model predictions that are too sensitive for the initial relative density.

Cyclic settlement evolves with increasing number of load cycles towards a maximum value. After 10^4 load cycles the sand in the zone of influence has (nearly) reached its maximum densification, according to the terminal density model. Cyclic settlement predictions with models that assume cyclic settlement continues indefinitely can be ‘cut-off’ after order 10^4 load cycles, i.e. the predicted cyclic settlement after about 10^4 load cycles gives the maximum settlement. Model predictions of the compaction / liquefaction model for cyclic shear are in the right order of magnitude after 10^4 load cycles for the cases analysed. For higher number of load cycles the model predictions of the compaction / liquefaction model for cyclic shear become unreliable. The maximum densification of the sand underneath the ASC rail tracks was found not to coincide with the minimum void ratio. Maximum densification is a property that depends on the soil conditions, initial state and loading conditions. Taking the minimum void ratio as the maximum densification, i.e. densification stops when the sand reaches 100% relative density, results in an overestimate of the cyclic settlement.

The modelling approach showed the problem is 3D (not 1D) and affects a depth that depends on the amplitude of the load and geometry, i.e. dimensions of the loaded part of the rail track ballast bed (foundation). Further, depth of influence increases with decreasing volumetric threshold strain and slightly increases with decreasing stiffness of the sand. For the case analysed 6 m depth seems to comprise the volume that influences most of the cyclic settlement. This is consistent with the minimum depth of influence determined based on the measurements.

The measurements and modelling approach indicate that densification occurs within the entire zone of influence, except at depths where the maximum densification is reached. Although stress distributions show that the vertical stress decreases with depth, during the first load cycle most densification occurs between 0.5 and 2.0 m below the foundation. In the subsequent load cycles densification of the sand concentrates in the sand layers with a lower relative density. With depth densification is expected to decrease, which is related to the increasing stiffness of the sand, due to the increasing confining stress, and decrease of the amplitude of the load, due to spreading of the load.

The cyclic settlement of the rail tracks will probably not exceed the 20 mm settlement requirement if it is constructed on a sand fill with an average relative density above 85% and minimum relative density above 65% within the zone of influence. Densification increases with amplitude of the load. For the smaller ASCs the average relative density must be at least 80% to meet the settlement requirements. The depth of influence is determined at 6 m below the shallow foundation. Cyclic settlement increases with depth of influence. For a larger depth of influence the sand must be compacted to nearly its maximum densification to meet the settlement requirement for ASC rail tracks. The cyclic settlement is expected to exceed the settlement requirement for ASC rail tracks at locations where the sand fill contains loose or medium dense (<65%) layers within the zone of influence.

5.1. Answers to the research questions

Which parameters (soil properties, load parameters) affect densification of a sand layer (and resulting cyclic settlement) induced by a cyclic load as a result of the movements of automatic stacking cranes?

Densification of a sand layer increases with number of load cycles, amplitude of the applied load or strain and decreases with relative density, stiffness of the sand and volumetric threshold strain. In a sand fill that consists of sand layers with varying relative density more cyclic settlement seems to occur compared to a sand fill with a constant relative density, even when the average relative density at both locations is similar. Furthermore, cyclic settlement increases with extent of the zone of influence. This is defined by the depth of influence and combined thickness of sand layers within the zone of influence that reached maximum densification. Depth of influence increases with amplitude of the load and decreasing volumetric threshold strain and stiffness of the sand.

How reliable are the cyclic settlement predictions made by the evaluated model for the Rotterdam World Gateway container terminal Phase 2 and how do the results compare to the (differential) settlement requirements for automatic stacking crane rail tracks?

The terminal density model gives reliable model predictions of the cyclic settlement underneath ASC rail tracks for locations where the sand fill is dense to very dense ($D_{R,0}$ > 80%) within the zone of influence. With an average initial relative density above 85% and an estimated depth of influence of 6 m the predicted cyclic settlement probably does not exceed the 20 mm settlement requirement for ASC rail tracks. Reliability of the cyclic settlement can be improved by measuring the depth of influence. For a larger depth of influence the predicted cyclic settlement exceeds 20 mm.

For a sand fill that consists of sand layers with a lower relative density the terminal density model predicts almost the same amount of cyclic settlement as for a sand fill that consists of sand layers with a lower relative density. This is a result of the correlation in Equation 4.2 that is used to determine the terminal void ratio. The correlation is unsuitable for sand layers with a lower relative density. It underestimates the cyclic settlement. To improve the (reliability of the) model predictions for loose and medium dense sand measure the depth of influence and terminal void ratio.

Model predictions of the compaction / liquefaction model for cyclic shear overestimate the cyclic settlement of the sand fill. This is a result of the correlation in Equation 4.1 that is used to determine the material constants c_1 and c_2 which define the cyclic densification properties of the sand. The correlation is unsuitable to determine the cyclic densification properties of the sand fill underneath the ASC rail tracks. To improve the (reliability of the) model predictions measure the depth of influence and material constants. According to the compaction / liquefaction model for cyclic shear significant cyclic settlement continues to occur indefinitely, beyond order 10^4 load cycles model predictions become unreliable.

How should the cone penetration test profile of a sand fill look like in order to meet the (differential) settlement requirements for automatic stacking crane rail tracks?

The sand fill must consist of dense to very dense sand layers within the entire zone of influence to prevent that cyclic settlement exceeds the 20 mm settlement requirement for ASC rail tracks. The depth of influence is determined around 6 m, between -1 and -2 m NAP. Cyclic settlement is predicted to occur in the entire zone of influence. At locations where the sand fill consists of loose or medium dense sand layers, the relative density must be increased. The minimum relative density within the zone of influence must be at least 65% and the average relative density at least 85%. However, for a larger depth of influence the relative density should be increased (nearly) to its densest state to meet the settlement requirement for ASC rail tracks.

With the correlation of Baldi in Equation 3.1 the initial relative density profile can be expressed in terms of a cone tip resistance with depth. The sand fill at the location corresponding to CPT 37 in Phase 2 of the RWG container terminal (see Figure 4.21b) has a relative density above 85% within the zone of influence. The cone tip resistance of the entire sand fill till a depth of 2 $mNAP$ should be similar to this CPT.

5.2. Consequences for Phase 2 of the RWG container terminal

The settlement measured in Phase 1 of the RWG container terminal exceeded the settlement requirement for ASC rail tracks at multiple locations. This has led to (unplanned) downtime of the RWG container terminal.

In Phase 2 there are many locations where the sand fill has an initial relative density that is lower compared to locations 2 and 4 in Phase 1, where 27 and 32 mm settlement were measured, respectively. This suggests that also in Phase 2 at multiple locations settlement will exceed the settlement requirement for ASC rail tracks. Cyclic settlement can be minimised by increasing the initial relative density by means of ground compaction. This will contribute to prevent unplanned downtime in Phase 2 of the RWG container terminal.

Extent and intensity of the compaction works needed to meet the settlement requirement for ASC rail tracks depend on the initial state of the sand fill. The sand within the zone of influence must be compacted to a relative density of at least 85%. Under these conditions small amounts of densification can still occur within the entire zone of influence, for a zone of influence that extents to a maximum of 6 m below the foundation the cyclic settlement will probably not exceed 20 mm. However, if the depth of influence is larger it is recommended to compact the sand to a depth of 1 m NAP till its densest state. For the case analysed in Phase 2 given by CPT 37 it is not necessary to compact the sand fill at the corresponding location. The average initial relative density is about 85% within the zone of influence. In contrast, for the case analysed in Phase 2 given by CPT 29 the initial relative density is significantly. To meet the settlement requirement for ASC rail tracks at this location it is necessary to increase the initial relative density to 85% within the entire zone of influence. This means that the sand fill must be compacted below the water table. CPTs must be executed afterwards to control the effect of the compaction works.

Instead of carrying out ground compaction of the sand fill, densification of the sand can be induced by means of ASCs applying a cyclic load to the sand underneath their rail tracks, i.e. construct the ASC rail tracks, install the ASCs and let them ride along the entire ASC rail track to induce densification of the sand. At locations where the settlement requirements for ASC rail tracks are exceeded the rail tracks need to be maintained. Based on reliable predictions of the cyclic settlement a maintenance schedule can be suggested in order to prevent unplanned downtime. At locations with a low relative density maintenance must be scheduled more frequently, for example after 10^2, 10^3 and 10^4 load cycles. After 10^4 load cycles most of the settlement is expected to have occurred. It is recommended that the ASCs and ASC-Cs carry a 40 tonne container, to apply the maximum amplitude of the load. Further, it is recommended to execute this alternative densification method before the container terminal becomes operational. During operation containers are stored in the container stacks, causing an increases of the confining stress underneath the rail tracks. Consequently, the stiffness of the sand increases which could prevent maximum densification. Maximum densification might be reached at a later moment when less containers are stored in the container stack. It is an option to apply the alternative densification method in combination with the pre-compaction.

After the sand fill is disturbed by construction works, the sand must be compacted to its initial or higher relative density.

5.3. General recommendations

The relative density of the man-made sand fill has a strong variability vertically and laterally. To obtain a reliable estimate of the relative density of the entire area underneath the ASC rail tracks CPT measurements must be executed closely spaced. At Phase 1 and 2 of the RWG container terminal a 25 m spacing was adopted. This seems to be sufficient for the current problem. CPT data is then extrapolated over a maximum distance of 12.5 m.

To measure the cone tip resistance sand within the entire zone of influence CPT's must be executed till a depth of at least 2 m deeper than the estimated depth of influence. That is 8 m below the bottom of the foundation. In Phase 1 the bottom of the zone of influence lies beyond the extent of some of the CPT measurements. Beyond the extent of the CPT the data is estimated, which contributes to the uncertainty of the data. In Phase 2 CPT's are executed to 9 m below the bottom of the foundation, which is sufficient to measure the cone tip resistance for the entire zone of influence.

The calculations are based on parameters inferred from the literature and correlations. It would be better to have direct data to determine the volumetric threshold strain, maximum densification (terminal void ratio) and densification properties of the sand. These parameters are determined in cyclic load tests. Because the sand at the RWG container terminal consists of one sand type, maximum densification varies with the initial relative density and amplitude of the load and the densification properties vary with the initial relative density. To investigate their influence, it is recommended to execute at least twenty cyclic load tests. Execute cyclic triaxial tests or cyclic oedometer test for a vertical stress of 25, 50, 75 and 100 kPa on sand samples of 35, 65, 80, 90 and 100% relative density. Although their boundary conditions are very different, these two cyclic tests more or less mimic the conditions underneath the ASC rail tracks, as in both tests the vertical stress is dominant.

Cyclic load tests that apply over 10^4 load cycles are difficult to perform and expensive. Instead, the maximum densification can be determined by measuring the relative density underneath the ASC rail tracks in Phase 1 at locations where settlement stopped occurring. Here the sand has reached its maximum densification. The corresponding relative density can be determined based on CPT data. Execute CPT measurements underneath rail tracks of ASCs and ASC-Cs at five to ten locations nearby CPT's that were execute before, to determine the influence of the amplitude of the load and initial state of the sand. The deepest point where the relative density has increased is the depth of influence. It is recommended to limit this investigation to (parts of) a few rail tracks to minimise the downtime of the container terminal.

Disturbance of the sand due to construction works causes uncertainty of the initial state of the sand, especially in the top part of the sand fill. To increase reliability of the model predictions, multiple CPT's must be executed after the construction works to quantify the disturbance. Five to ten additional CPT's should be sufficient to quantify the average disturbance caused by the construction works, this can be extrapolated to the other locations that have been disturbed.

To validate (one of) the cyclic settlement models for the current problem measure the settlement with depth and number of load cycles. Model predictions of the cyclic settlement and vertical plastic strain distributions with depth can be compared to these measurements. At five to ten locations settlement measurements underneath rail tracks of ASCs and ASC-Cs must be executed to determine the influence of the amplitude of the load and initial state of the sand. Because (most) cyclic settlement already occurred in Phase 1, the settlement measurements need to be executed in Phase 2. The initial state of the sand must be determined and the sand cannot be compacted before and during the settlement measurements. Consequently, cyclic settlement will probably exceed the settlement requirements for ASC rail tracks at multiple locations. It is recommended to limit this investigation to (parts of) a few rail tracks to minimise the downtime of the container terminal. Additionally, the depth of influence of ASCs and the number of load cycles after which the maximum densification is reached can be determined.

To investigate the response of the sand for varying soil conditions a virtual reality of the container terminal can be created using a reliable advanced FE model that can simulate the problem for a large number of load cycles. The conditions are well defined in the FE model, which makes it possible to determine the model parameter values of the cyclic settlement models. In FE model simulations of cyclic soil tests model parameter values, such as densification properties and maximum densification of the sand can be determined. The values are used to make predictions with the cyclic settlement models. A match between the predictions for varying conditions indicates that the cyclic settlement model is reliable. Be aware that a numerical error will accumulate in the model predictions of FE models. After a large number of load cycles the numerical error can become too large and model predictions unreliable.

However the correlation in Equation 4.2 corresponds best with the data in Phase 1 of the RWG container terminal, the correlations in Equations 4.3 and 4.5 which seem more physically based. For the problem analysed the correlations in Equations 4.3 and 4.5 underestimate the cyclic settlement and therefore were not used. 4.3 takes into account the initial void ratio, minimum void ratio and vertical stress. It would be interesting to further investigate this type of correlation and the value of material constant a. With increasing value of a the terminal void ratio decreases and cyclic settlement increases.

Bibliography

[1] Iadc, 1965. URL https://www.iadc-dredging.com/. [Online; accessed March 19, 2021].

[2] Google earth, 2001. URL https://www.google.com/earth/. [Online; accessed November 30, 2020].

[3] Python, 2001. URL https://www.python.org/. [Online; accessed March 19, 2020].

[4] The scientific python development environment, 2018. URL https://www.spyder-ide.org/. [Online; accessed March 19, 2020].

[5] Cofra, 2019. URL https://cofra.com/. [Online; accessed November 4, 2019].

[6] Kalmar, 2020. URL https://www.kalmarglobal.com/. [Online; accessed March 10, 2020].

[7] Port of rotterdam, 2020. URL https://www.portofrotterdam.com/. [Online; accessed February 27, 2020].

[8] Rotterdam world gateway, 2020. URL https://www.rwg.nl/. [Online; accessed February 27, 2020].

[9] USDA soil texture triangle, 2020. URL https://www.nrcs.usda.gov/. [Online; accessed January 26, 2020].

[10] G. BALDI. Interpretation of cpt's and cptu's. 2nd part : Drained penetration of sands. *Proc. IV Int. Geotech. Sem., Singapore*, 1986.

[11] D D Barkan. Dynamics of bases and foundations. *McGraw-Hill Book Company, Inc., New York*, 1962. (original publication in Russian 1948).

[12] Thomas Benz. *Small-strain stiffness of soils and its numerical consequences*. PhD thesis, 2007.

[13] R. Bhanbhro, R. Knutsson, M. Zardari, T. Edeskär, and S. Knutsson. Mechanical properties of soft tailings from different depths of a swedish tailings dam: Results from triaxial tests. 27:1066–1074, 05 2018. doi: 10.24200/sci.2018.20418.

[14] L. Booster and R. de Jager. Zandlichaam: Zettingsgedrag, February 2008. [Designnote PUMA].

[15] Joseph Boussinesq. *Application des potentiels à l'étude de l'équilibre et du mouvement des solides élastiques*, volume 4. Gauthier-Villars, 1885.

[16] Song-hun Chong and J Carlos Santamarina. Sands subjected to repetitive vertical loading under zero lateral strain : accumulation models , terminal densities , and settlement. *Canadian Geotechnical Journal*, 2046:2039–2046, 2016.

[17] CUR publication 166: CUR 1993. Damwandconstructies (sheet pile structures). Standard, CUR Bouw & Infra, October 1993. (in Dutch).

[18] B.M. Das. *Principles of Foundation Engineering 6th Edition*. Thomson, 2007.

[19] B.M. Das. *Geotechnical engineering handbook*. J.Ross Publishing, 2010. ISBN 9788578110796. doi: 10.1017/CBO9781107415324.004.

[20] Bart Dirks. Rotterdam is alweer bijna te klein voor alle containers, 2019. URL https://www.volkskrant.nl/economie/rotterdam-is-alweer-bijna-te-klein-voor-alle-containers~b47d4703/. [Online; accessed February 27, 2020].

[21] Pendo M. Duku, Jonathan P. Stewart, Daniel H. Whang, and Eric Yee. Volumetric strains of clean sands subject to cyclic loads. *Journal of Geotechnical and Geoenvironmental Engineering*, 134 (8):1073–1085, 2008. doi: 10.1061/(ASCE)1090-0241(2008)134:8(1073).

[22] Mark Duursma. Megakranen voor megaschepen, 2015. URL https://www.nrc.nl/nieuws/2015/04/22/megakranen-voor-megaschepen-1486838-a563523. [Online; accessed November 4, 2019].

[23] PJ Gräbe and CR Clayton. Effects of principal stress rotation on permanent deformation in rail track foundations. *Journal of Geotechnical and Geoenvironmental Engineering*, 135(4):555–565, 2009.

[24] Bobby O Hardin and William L Black. Sand stiffness under various triaxial stresses. *Journal of Soil Mechanics & Foundations Div*, 92(ASCE# 4712 Proceeding), 1966.

[25] R.H. Hergarden. Gronddeformaties tijdens het trillend trekken van damwanden (Ground deformations during vibratory pull of sheet piles). Master's thesis, Delft University of Technology, Delft, the Netherlands, 2000. [in Dutch].

[26] ISO 12488-1. ISO 12488-1 - Cranes — Tolerances for wheels and travel and traversing tracks — Part 1: General. Standard, International Organization for Standardization, Geneva, CH, July 2012.

[27] M. Jamiolkowski, D. C. F. Lo Presti, and M. Manassero. *Evaluation of Relative Density and Shear Strength of Sands from CPT and DMT*, pages 201–238. 2003. doi: 10.1061/40659(2003)7.

[28] Azad Koliji. Geotechdata, 2008. URL https://www.geotechdata.info/index.html. [Online; accessed February 20, 2020].

[29] H.J. Lengkeek. Estimation of sand stiffness parameters from cone resistance. 01 2003.

[30] Dingqing Li and Ernest T Selig. Cumulative plastic deformation for fine-grained subgrade soils. *Journal of geotechnical engineering*, 122(12):1006–1013, 1996.

[31] Tom Lunne and H. P. Christoffersen. Interpretation of cone penetrometer data for offshore sands. *Proceedings of the Annual Offshore Technology Conference*, May:181–192, 1983. ISSN 01603663. doi: 10.4043/4464-ms.

[32] Nikolaos Mastoropoulos. Verdichting Kraanbanen ASC Kranen, May 2019. [Memo Arcadis Nederland B.V.].

[33] L.A. Meerdink. Analyse zakkingsproblematiek asc-kraanbanen, April 2015. [Report BT Geoconsult BV].

[34] Piet Meijers. *Settlement during vibratory sheet piling*. PhD thesis, Delft University of Technology, 2007.

[35] Piet Meijers and A.F. van Tol. Voorspelling maaiveldzakking door het in- en uittrillen van damwanden. *Geotechniek*, 2010.

[36] Carl L Monismith, N Ogawa, and CR Freeme. Permanent deformation characteristics of subgrade soils due to repeated loading. *Transportation research record*, (537), 1975.

[37] G. A. Narsilio and J. C. Santamarina. Terminal densities. *Géotechnique*, 58:669–674, 2008. doi: 10.1680/geot.2008.58.8.669. [Technical note].

[38] O Oung and HE Brassinga. Predicted and measured settlements due to installation and removal of sheet piles. *Proceedings of the 17th International Conference on Soil Mechanics and Geotechnical Engineering*, 2009. doi: 10.3233/978-1-60750-031-5-1425.

[39] J. Park and J. C. Santamarina. Sand response to a large number of loading cycles under zero-lateral-strain conditions: Evolution of void ratio and small-strain stiffness. *Geotechnique*, 69:501–513, 2019. doi: 10.1680/jgeot.17.P.124.

[40] *PLAXIS Material Models CONNECT Edition V20*. PLAXIS, 10 2019.

[41] M. Post. Maasvlakte 2: Zettingsparameters ophoogzand, February 2010. [Report PUMA].

[42] J. Rindertsma, W. Karreman, S. Engels, and K. Gavin. Cpt based settlement prediction of shallow footings on granular soils. In *Cone Penetration Testing 2018: Proceedings of the 4th International Symposium on Cone Penetration Testing (CPT'18), 21-22 June, 2018, Delft, The Netherlands*, June 2018.

[43] A. Sadrekarimi. Evaluation of cpt-based characterization methods for loose to medium-dense sands. *Soils and Foundations*, 56(3):460 – 472, 2016. ISSN 0038-0806. doi: https://doi.org/10.1016/j.sandf.2016.04.012.

[44] A. Sawicki. Modelling earthquake-induced phenomena in the izmit bay coastal area. *Proc. Cyclic behaviour of sand and liquefaction phenomena*, pages 431–440, 2004.

[45] A. Sawicki and P. Śliwiński. Compaction due to a cyclic force acting in the inside of a sandy subsoil. *Computers and Geotechnics*, 7(3):223–237, 1989.

[46] A. Sawicki and W. Świdziński. Mechanics of a sandy subsoil subjected to cyclic loadings. *International Journal for Numerical and Analytical Methods in Geomechanics*, 13(5):511–529, 1989. doi: 10.1002/nag.1610130505.

[47] A. Sawicki and W. Świdziński. Pore pressure generation, dissipation and resolidification in a saturated subsoil. *Soils and Foundations*, 29(4):62–74, 1989.

[48] A. Sawicki and W. Świdziński. Cyclic compaction of soils, grains and powders. *Powder Technology*, 85(2):97–104, 1995. doi: https://doi.org/10.1016/0032-5910(95)03013-Y.

[49] A. Sawicki, W. Świdziński, and B. Zadroga. Settlement of shallow foundation due to cyclic vertical force. *Soils and Foundations*, 38:35–43, 1998. doi: 10.3208/sandf.38.35.

[50] John H Schmertmann. Static cone to compute static settlement over sand. *Soil Mechanics and Foundations Division*, 1970.

[51] John H Schmertmann. *Guidelines for cone penetration test. (Performance and Design)*. 1978.

[52] John H. Schmertmann, John Paul Hartman, and Phillip R. Brown. Improved strain influence factor diagrams. *Journal of Geotechnical and Geoenvironmental Engineering*, 104(8):1131–1135, 1978. doi: 10.1061/AJGEB6.0000683.

[53] H Bolton Seed, Robert T Wong, IM Idriss, and Kohji Tokimatsu. Moduli and damping factors for dynamic analyses of cohesionless soils. *Journal of geotechnical engineering*, 112(11):1016–1032, 1986.

[54] K. Tokimatsu and H. B. Seed. Evaluation of Settlements in Sands. *Journal of Geotechnical and Geoenvironmental Engineering*, 113:861–878, 1987. doi: 10.1061/(ASCE)0733-9410(1987)113:8(861).

[55] Mladen Vucetic. Cyclic threshold shear strains in soils. *Journal of Geotechnical Engineering*, 120 (12):2208–2228, 1994. doi: 10.1061/(ASCE)0733-9410(1994)120:12(2208).

[56] R D Woods and L P Jedele. Energy-attenuation relationships from construction vibrations. *International Journal of Rock Mechanics and Mining Sciences & Geomechanics Abstracts*, 24, 1987. ISSN 0148-9062. doi: 10.1016/0148-9062(87)92406-5.

[57] T. L. Youd. Factors controlling maximum and minimum densities of sands. In *ASTM Special Technical Publication*, pages 98–112, 1973.

A

Soil data from the RWG container terminal

CPT's 8R-4, 9R-4, 4L-6, 4R-3, 10L-3 and 12R-3 (Phase 1)

CPT's executed at the six selected locations at Phase 1 of the RWG container terminal. CPT's are located underneath the ASC rail tracks of the RWG container terminal Phase 1. CPT data are plotted in Python. Original data in PDF are also presented.

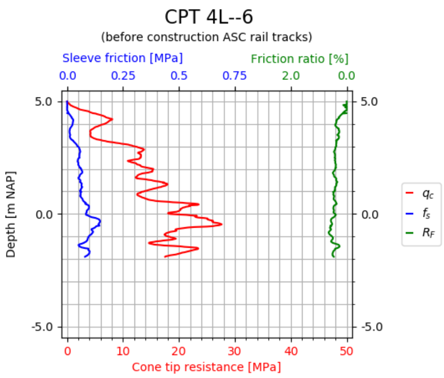

(a) Location 1: CPT 4L-6

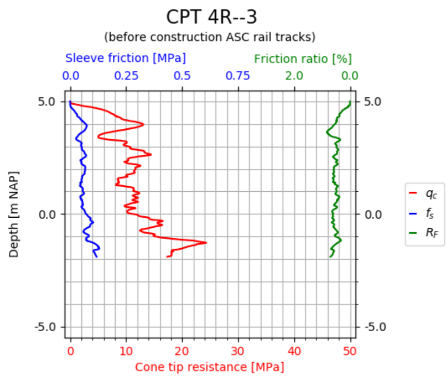

(b) Location 2: CPT 4R-3

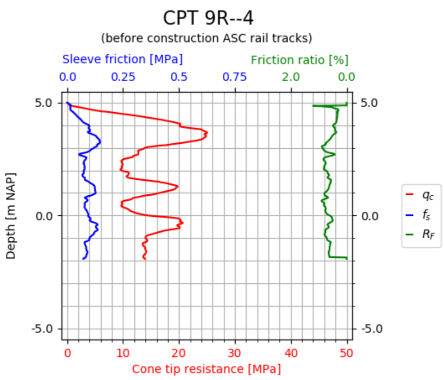

(c) Location 3: CPT 9R-4

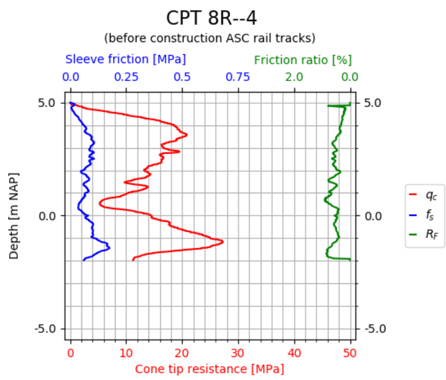

(d) Location 4: CPT 8R-4

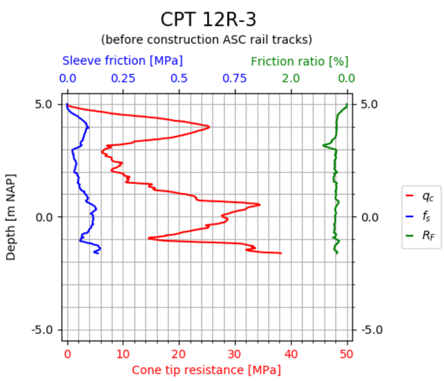

(e) Location 5: CPT 12R-3

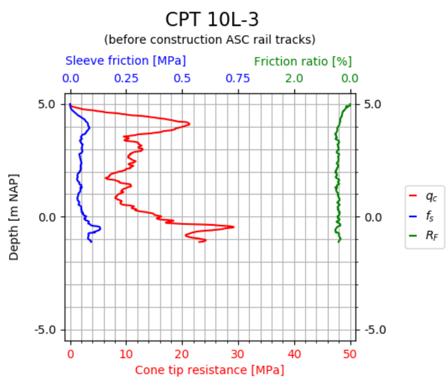

(f) Location 6: CPT 10L-3

Figure A.1: Measured cone tip resistance and sleeve friction and calculated friction ratio at the six selected locations at the RWG container terminal Phase 1.

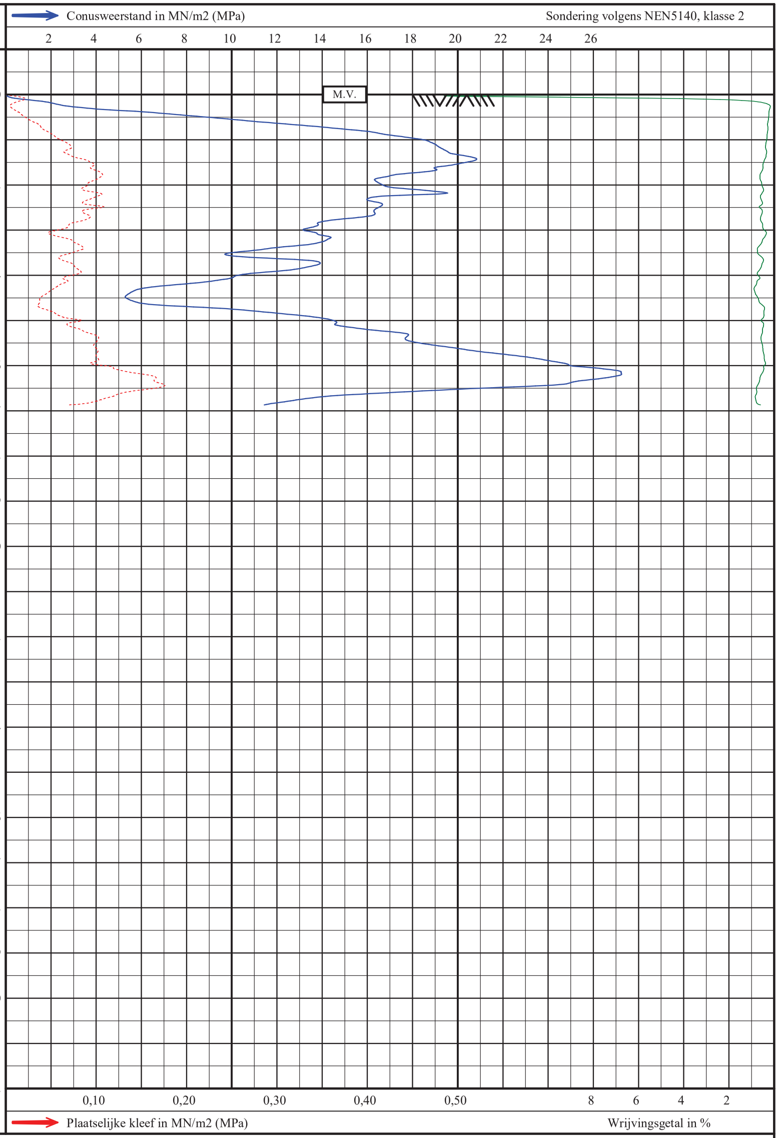

Conus-ID: S15-CFI.882 A-mantel: 20000 mm^2 A-conus: 1500 mm^2

HOOGVELD SONDERINGEN	Project aan de Amoerweg Rotterdam	mv : Maaiveld + 0,00 m uitv.: 06-03-2013 11:18 get. : 07-03-2013	Opdracht nummer: **HA-10543** Sondering nummer **8R4**

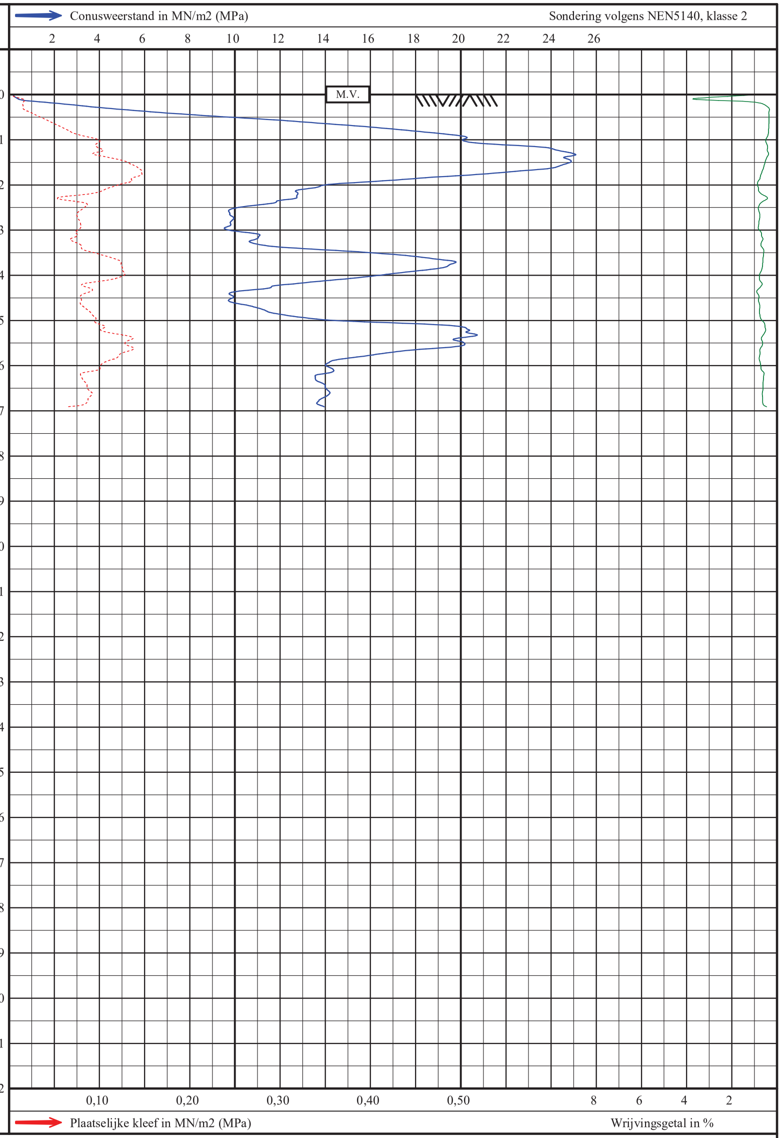

Conus-ID: S15-CFI.882 A-mantel: 20000 mm^2 A-conus: 1500 mm^2

HOOGVELD SONDERINGEN	Project aan de Amoerweg Rotterdam	mv : Maaiveld + 0,00 m uitv.: 06-03-2013 09:19 get. : 07-03-2013	Opdracht nummer: **HA-10543** Sondering nummer **9R4**

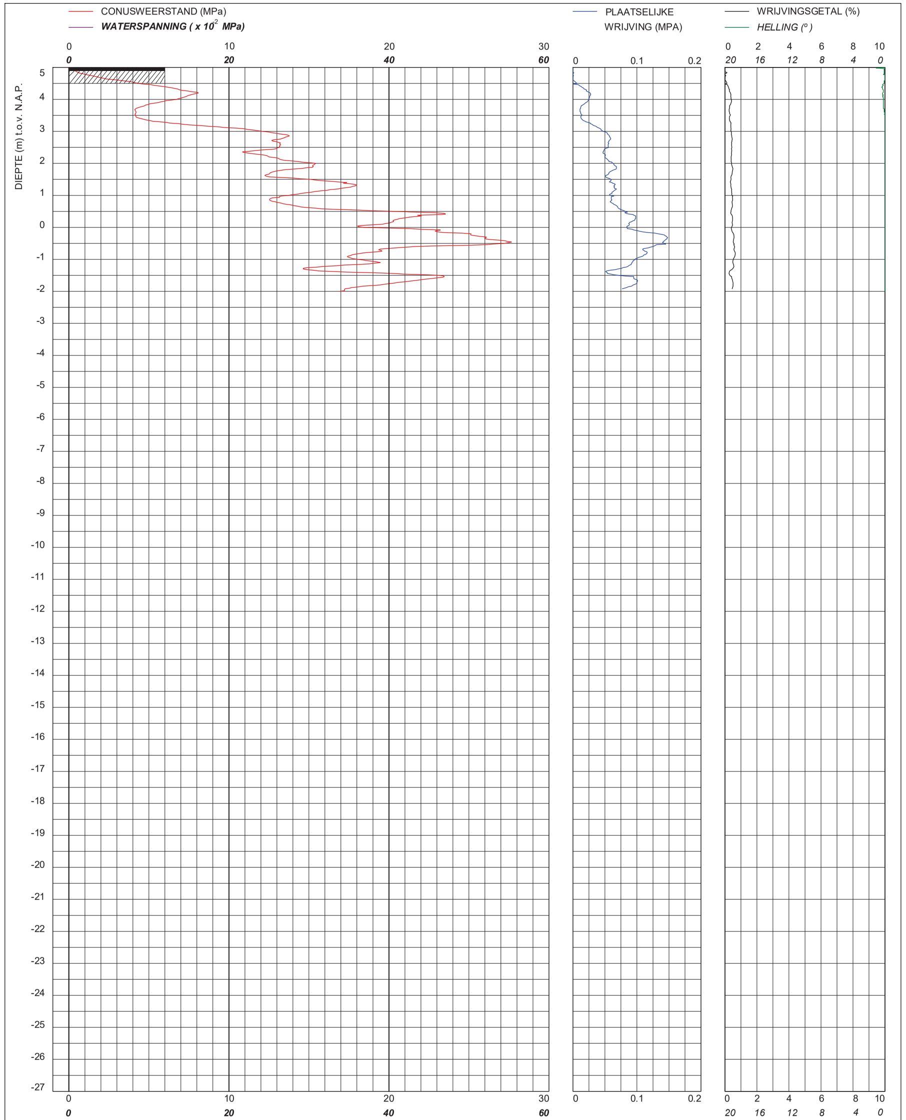

bam infra BAM Nelis De Ruiter Postbus 14 1160 AA Zwanenburg Telefoon (020) 4072222 / Fax (020) 4072223	Sondering CFI volgens NEN 5140 klasse 2 Conuspuntoppervlakte : 1000 mm² **BAVO Gateway-Wegen vof** **2e Maasvlakte Rotterdam**	MV	5.0 m N.A.P.	X	59099	Opdrachtnummer :
		Km		Y	441968	3350423
		Uitvoeringsdatum		15-3-2013		Locatiecode :
		Printdatum		18-3-2013		4L-6

PAGINA 1 van 1

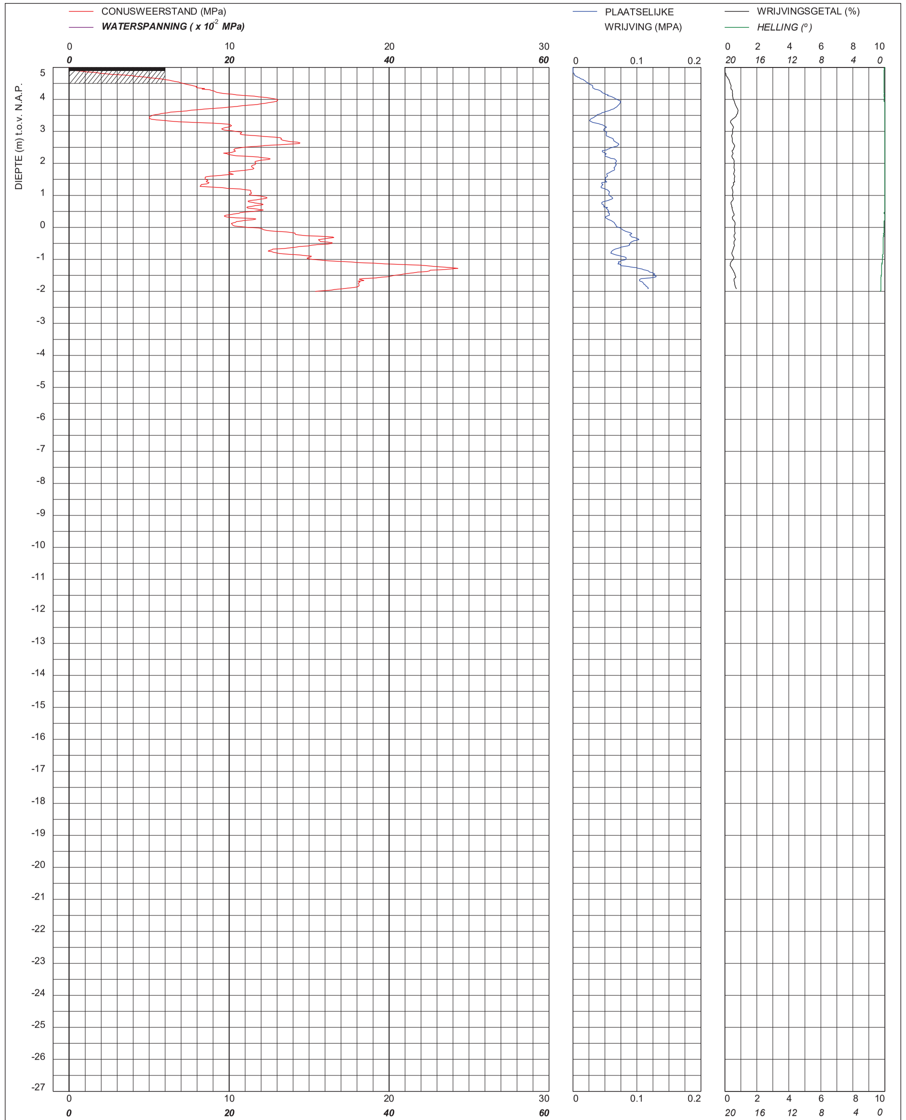

bam infra BAM Nelis De Ruiter Postbus 14 1160 AA Zwanenburg Telefoon (020) 4072222 / Fax (020) 4072223	Sondering CFI volgens NEN 5140 klasse 2 Conuspuntoppervlakte : 1000 mm² **BAVO Gateway-Wegen vof** **2e Maasvlakte Rotterdam**	MV	5.0 m N.A.P.	X	59120	Opdrachtnummer :
		Km		Y	441999	3350423
		Uitvoeringsdatum		15-3-2013		Locatiecode :
		Printdatum		18-3-2013		4R-3

PAGINA 1 van 1

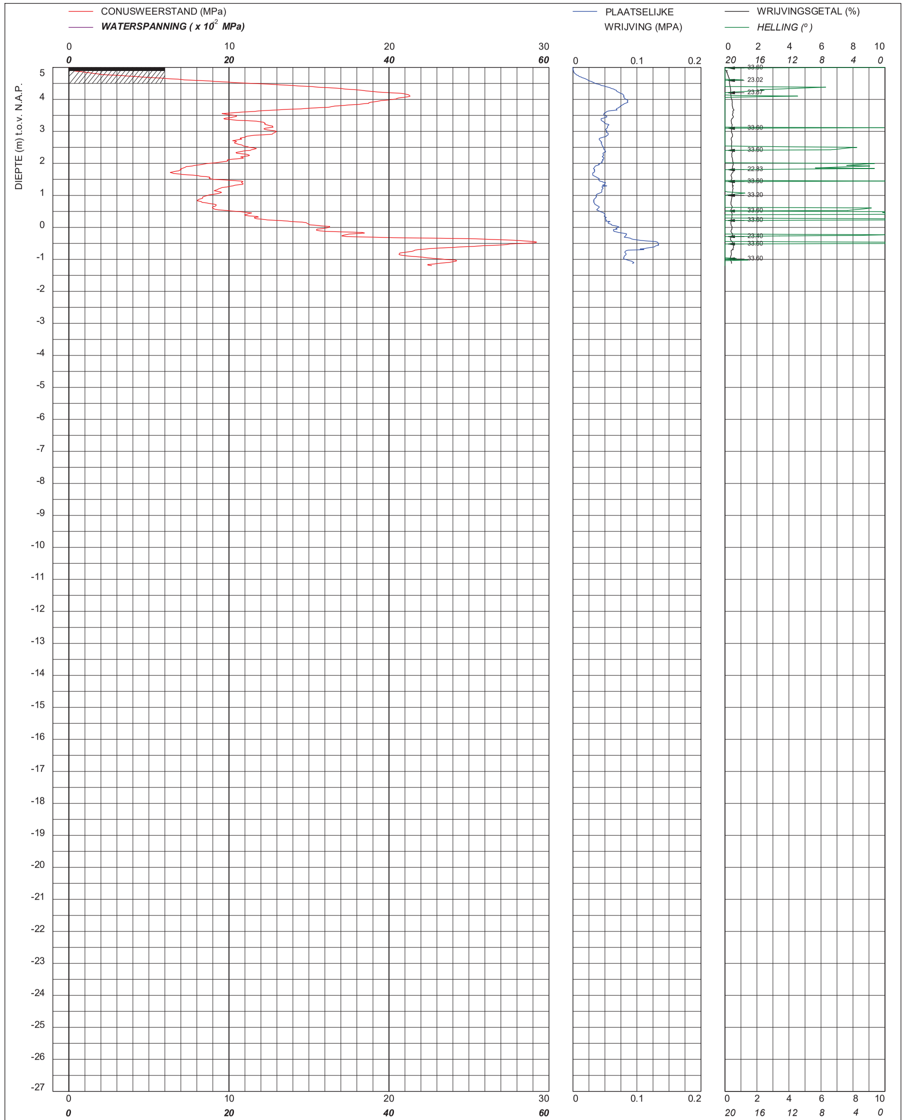

bam infra BAM Nelis De Ruiter	Sondering CFI volgens NEN 5140 klasse 2 Conuspuntoppervlakte : 1000 mm²	MV 5.0 m N.A.P.	X 58942	Opdrachtnummer :
Postbus 14 1160 AA Zwanenburg Telefoon (020) 4072222 / Fax (020) 4072223	BAVO Gateway-Wegen vof 2e Maasvlakte Rotterdam	Km	Y 441740	3350423
		Uitvoeringsdatum	7-3-2013	Locatiecode :
		Printdatum	11-3-2013	10L-3

PAGINA 1 van 1

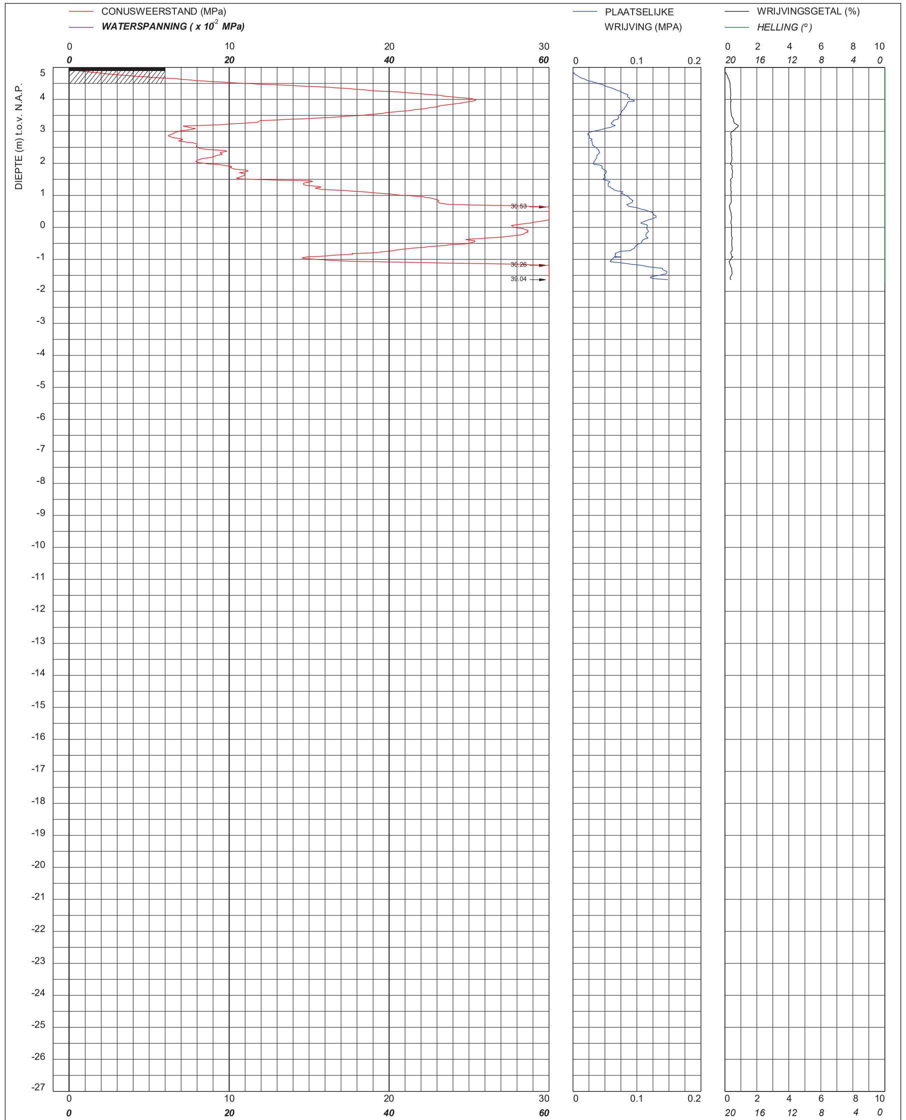

bam infra BAM Nelis De Ruiter	Sondering CFI volgens NEN 5140 klasse 2 Conuspuntoppervlakte : 1000 mm²	MV 5.0 m N.A.P.	X 58898	Opdrachtnummer :
Postbus 14 1160 AA Zwanenburg Telefoon (020) 4072222 / Fax (020) 4072223	BAVO Gateway-Wegen vof 2e Maasvlakte Rotterdam	Km	Y 441721	3350423
		Uitvoeringsdatum	7-3-2013	Locatiecode :
		Printdatum	11-3-2013	12R-3

PAGINA 1 van 1

CPT's 29 and 37 (Phase 2)

CPT's executed at the two selected locations at Phase 2 of the RWG container terminal. CPT's are located at the planned ASC rail tracks of the RWG container terminal Phase 2. CPT data are plotted in Python. Original data in PDF are also presented.

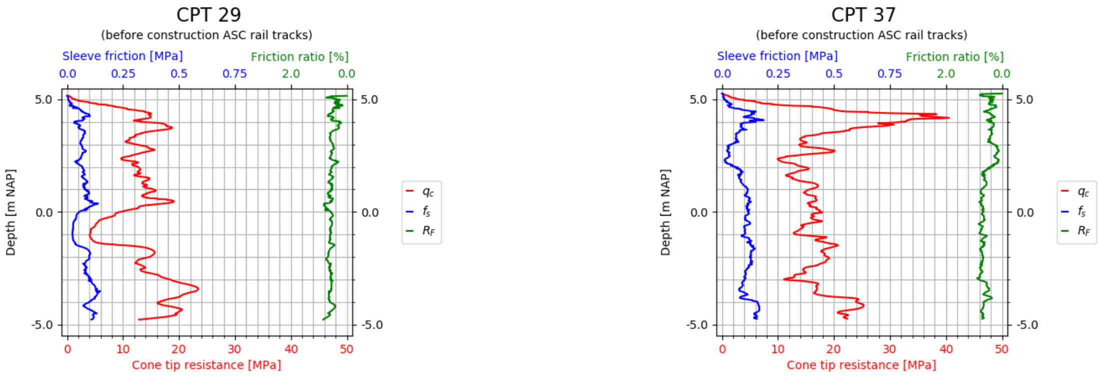

(a) CPT 29

(b) CPT 37

Figure A.2: Measured cone tip resistance and sleeve friction and calculated friction ratio at the six selected locations at the RWG container terminal Phase 2.

Sondering 29

Opdracht : 1803589
Plaats : Rotterdam - Maasvlakte
Datum : 21-02-2019
Project : Geotechnisch grondonderzoek RWG

Conus nummer : S15-CFII.1530
Soort conus : Elektrisch
Opp. conuspunt : 1500 mm²

NEN-EN-ISO-22476-1
Klasse 3, type TE1
Sondeerunit : SR2
Blad : 1 van 1

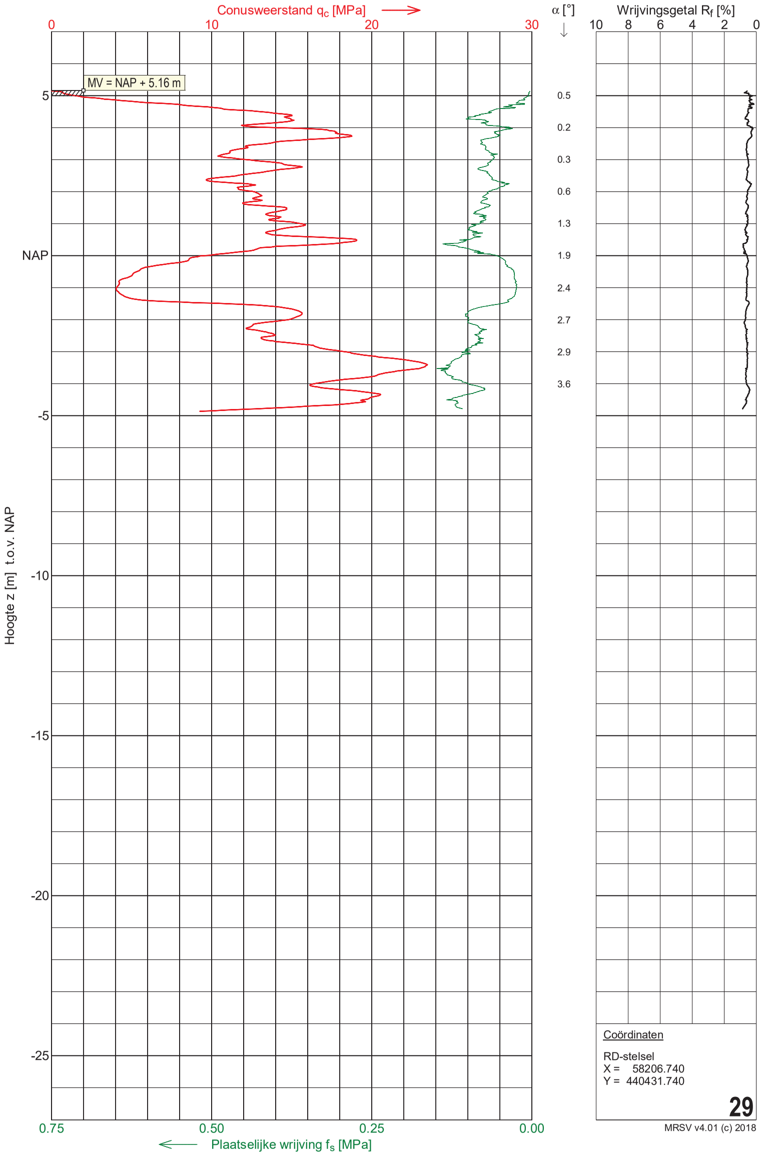

MOS GRONDMECHANICA

Sondering 37

Opdracht : 1803589
Plaats : Rotterdam - Maasvlakte
Datum : 20-02-2019
Project : Geotechnisch grondonderzoek RWG

Conus nummer : S15-CFII.1530
Soort conus : Elektrisch
Opp. conuspunt : 1500 mm²

NEN-EN-ISO-22476-1
Klasse 3, type TE1
Sondeerunit : SR2
Blad : 1 van 1

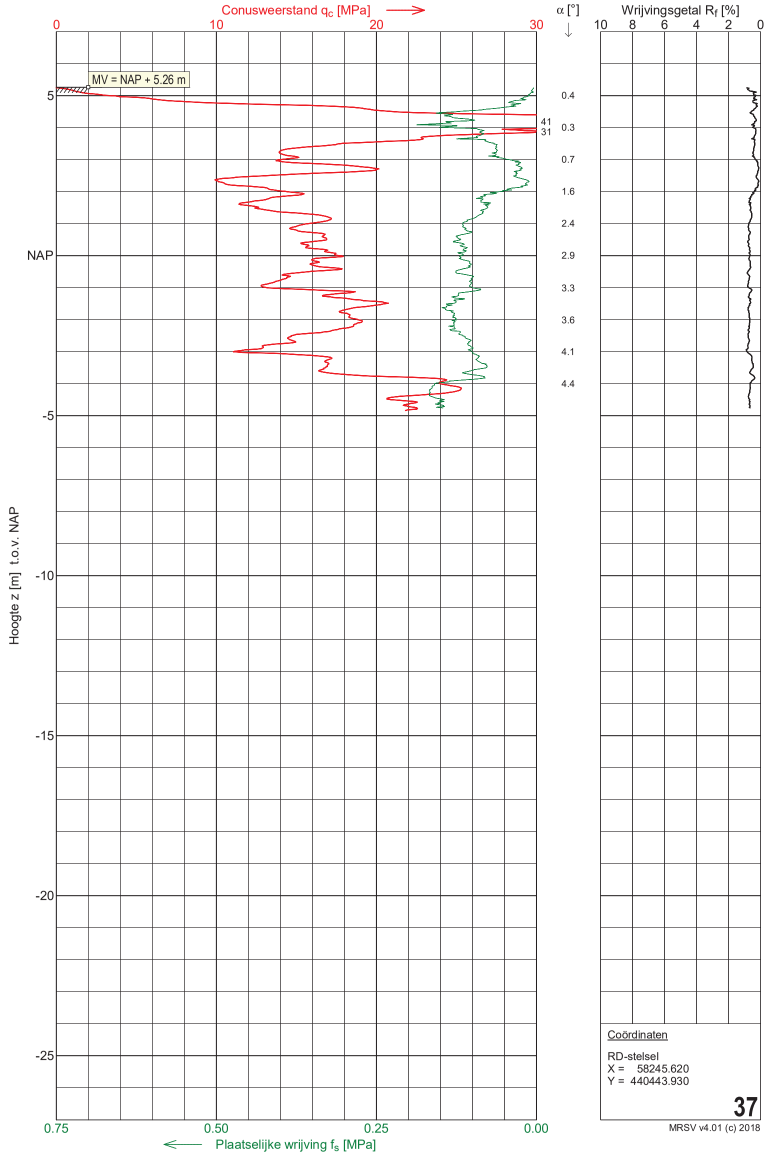

MOS GRONDMECHANICA

Deep CPT's 5.1-1, 5.1-48 and 5.2-25

Three deep CPT's executed in the area near the quay wall of the RWG container terminal. The CPT's have an extent till about -40 $m\ NAP$. CPT 5.1-1 shows the measured pore water pressure.

Sondering S5.1-1

Opdracht : 0045409
Plaats : Rotterdam-Maasvlakte
Datum : 11-08-2009
Project : Grondonderzoek kademuren

Conus nummer : C10CFIP461
Soort conus : Elektrisch

NEN 5140
Wagen : 11
Pagina : 1 van 2

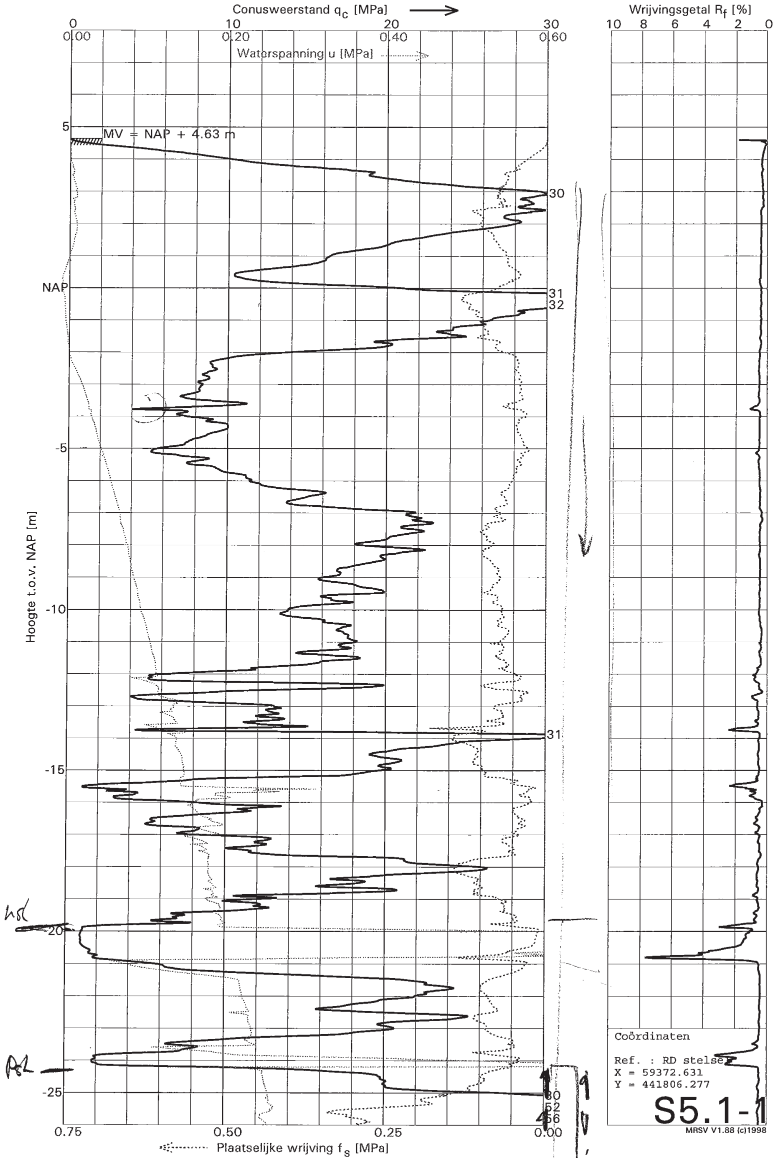

MOS GRONDMECHANICA Postbus 801, 3160 AA Rhoon - Telefoon (010) 5030200 - Fax (010) 5013656

MOS GRONDMECHANICA

Sondering S5.1-1

Opdracht : 0045409
Plaats : Rotterdam-Maasvlakte
Datum : 11-08-2009
Project : Grondonderzoek kademuren

Conus nummer : C10CFIP461
Soort conus : Elektrisch

NEN 5140
Wagen : 11
Pagina : 2 van 2

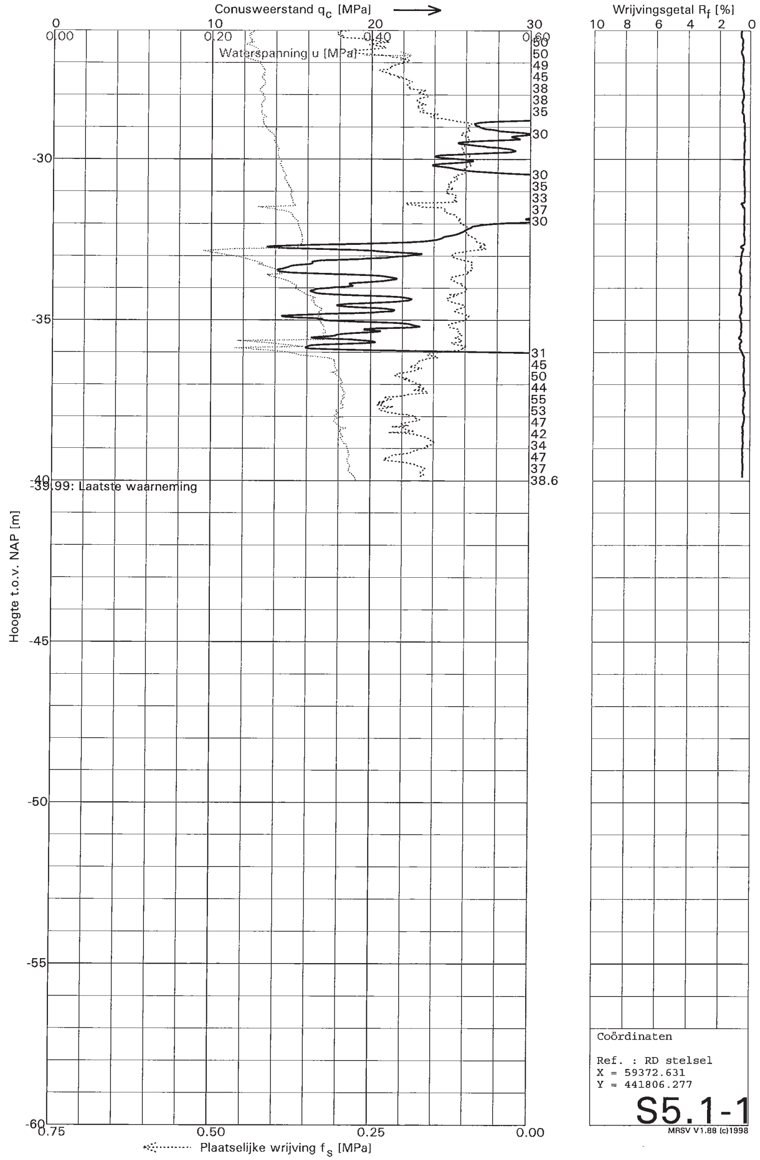

MOS GRONDMECHANICA Postbus 801, 3160 AA Rhoon - Telefoon (010) 5030200 - Fax (010) 5013656

MOS GRONDMECHANICA

Sondering S5.1-48

Opdracht : 0045409 Conus nummer : S15CFI468
Plaats : Rotterdam-Maasvlakte Soort conus : Elektrisch
Datum : 12-08-2009
Project : Grondonderzoek kademuren

NEN 5140
Wagen : 10
Pagina : 1 van 2

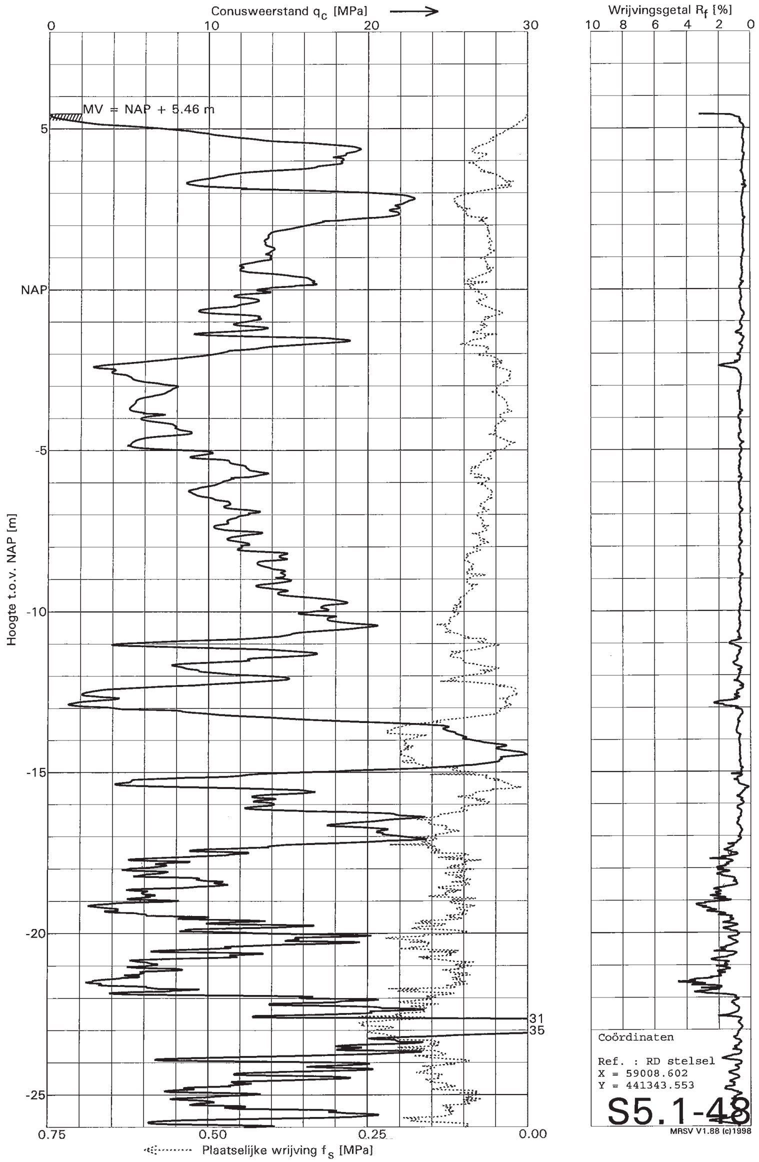

MOS GRONDMECHANICA Postbus 801, 3160 AA Rhoon - Telefoon (010) 5030200 - Fax (010) 5013656

MOS GRONDMECHANICA

Sondering S5.1-48

Opdracht : 0045409 Conus nummer : S15CFI468
Plaats : Rotterdam-Maasvlakte Soort conus : Elektrisch
Datum : 12-08-2009
Project : Grondonderzoek kademuren

NEN 5140
Wagen : 10
Pagina : 2 van 2

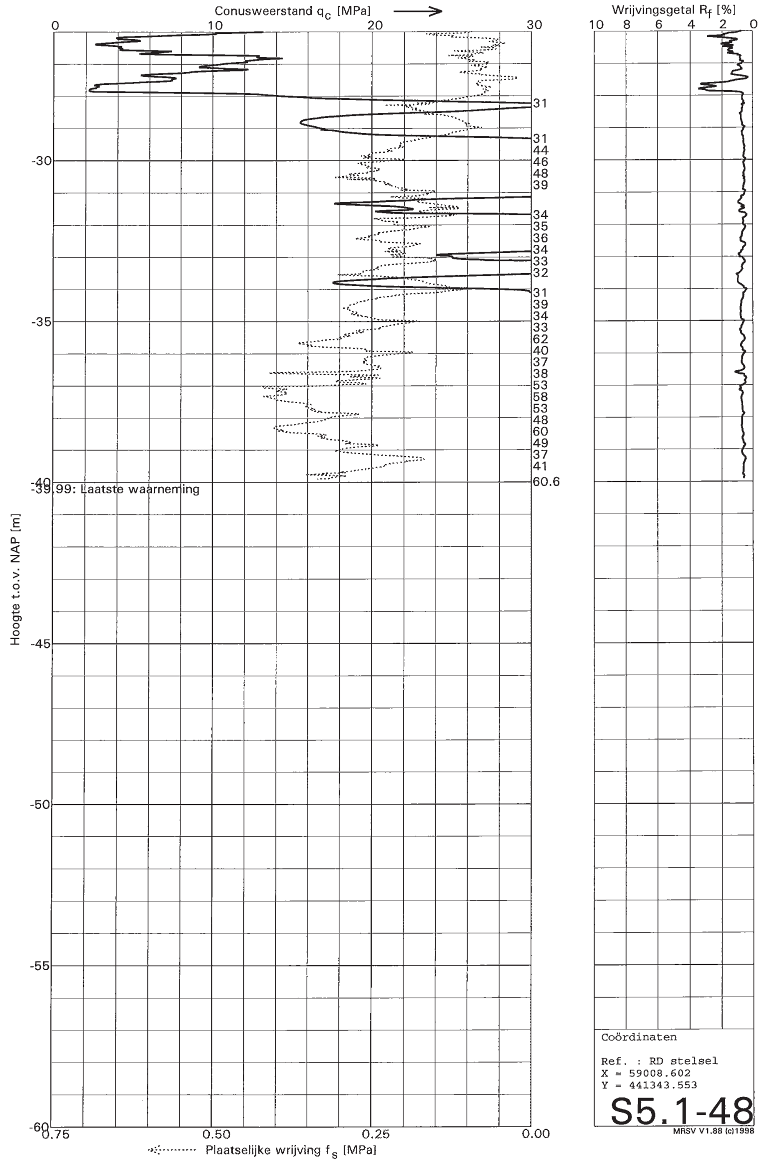

MOS GRONDMECHANICA Postbus 801, 3160 AA Rhoon - Telefoon (010) 5030200 - Fax (010) 5013656

MOS GRONDMECHANICA

Sondering S5.2-25

Opdracht : 0045409
Plaats : Rotterdam-Maasvlakte
Datum : 04-08-2009
Project : Grondonderzoek kademuren

Conus nummer : S15CFI256
Soort conus : Elektrisch

NEN 5140
Wagen : 5
Pagina : 1 van 2

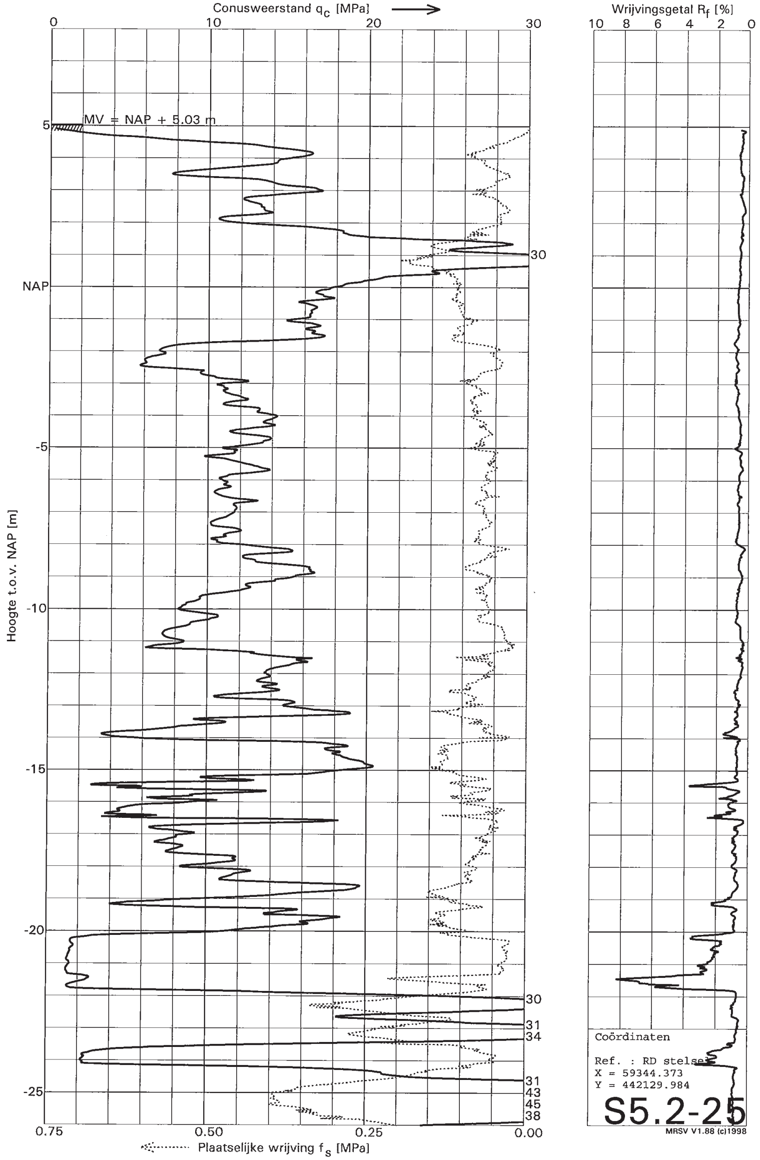

MOS GRONDMECHANICA Postbus 801, 3160 AA Rhoon - Telefoon (010) 5030200 - Fax (010) 5013656

MOS GRONDMECHANICA

Sondering S5.2-25

Opdracht : 0045409
Plaats : Rotterdam-Maasvlakte
Datum : 04-08-2009
Project : Grondonderzoek kademuren

Conus nummer : S15CFI256
Soort conus : Elektrisch

NEN 5140
Wagen : 5
Pagina : 2 van 2

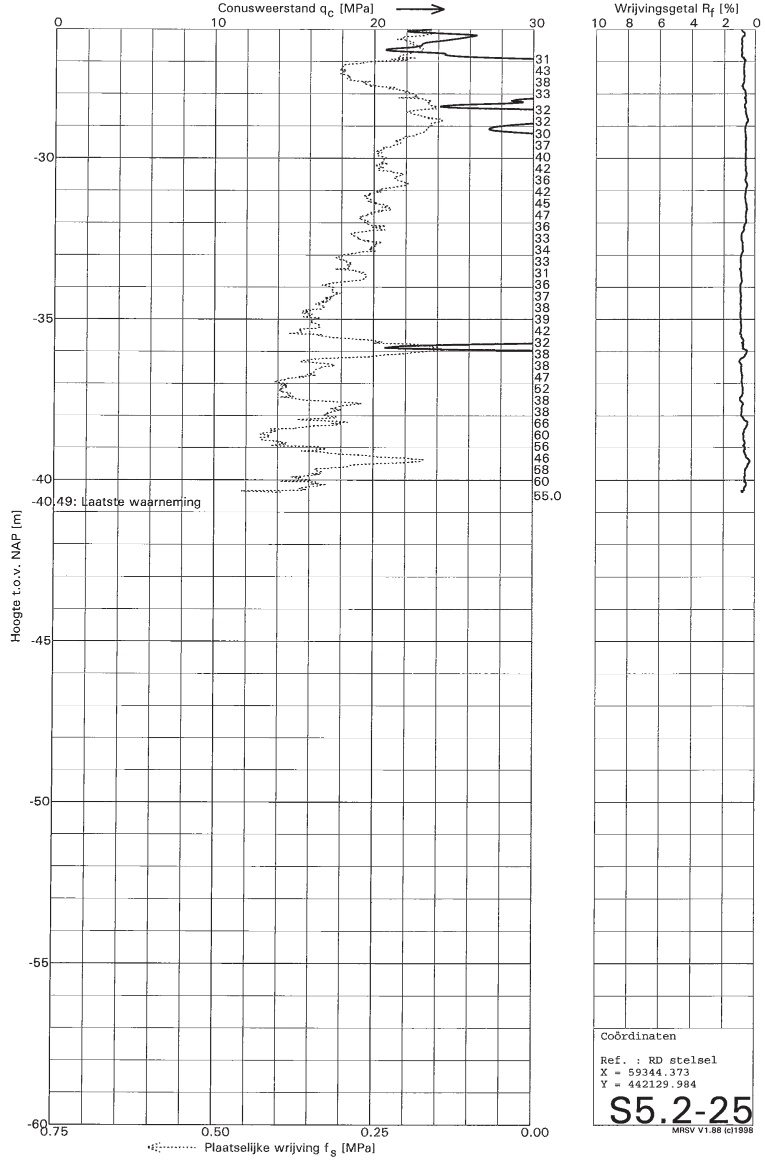

MOS GRONDMECHANICA Postbus 801, 3160 AA Rhoon - Telefoon (010) 5030200 - Fax (010) 5013656

MOS GRONDMECHANICA

Minimum and maximum dry unit weight of the sand

Opdracht : 0045409
Plaats : 2e Maasvlakte
Project : Kademuur.

Bor.	bus nummer	diepte t.o.v. NAP [m]		Dichtheden min. kN/m3	Dichtheden max kN/m3
B5.1-1	4351	0,27	0,02	15,30	17,91
B5.1-1	4352	-5,73	-6,13	14,18	16,68
B5.1-1	4353	-15,79	-16,09	13,44	15,95
B5.1-1	4358	-23,63	-23,93	15,10	17,29
B5.1-1	4359	-25,73	-26,13	15,06	17,56
B5.1-2	1607	1,43	1,03	14,49	16,77
B5.1-2	1609	-4,67	-5,02	14,54	16,72
B5.1-3	1610	1,34	1,02	15,40	18,00
B5.1-3	1611	-3,66	-3,92	14,34	16,95
B5.1-4	4370	-10,05	-10,45	14,66	16,91
B5.1-5	4382	-13,03	-13,33	13,04	15,77
B5.2-1	4361	-4,97	-5,31	14,54	16,73
B5.2-1	4362	-17,03	-17,33	13,84	16,74
B5.2-1	4367	-24,97	-25,32	14,79	17,05
B5.2-2	5559	-5,55	-5,95	15,27	17,86
B5.2-2	5560	-10,55	-10,95	15,14	17,52

Triaxial test data

Opdracht : 0045409
Plaats : 2e Maasvlakte
Betreft : Kademuur

TRIAXIAALPROEF

Boring : B5.1-1
Monster : 1
Bus : 4351
Datum : 24-08-2009
Opmerkingen :

Monsterklasse : 3
Diepte : 0.27 - 0.02 -NAP
Grondsoort : Zand mg. zwak siltig zw. grind sg. gs

Type proefstuk : Geprepareerd
Type proef : CD
Uitv. procedure : Enkeltraps
Uitgevoerd door :

Proefstuk	h_i [mm]	D_i [mm]	γ_i [kN/m³]	γ_{dr} [kN/m³]	w_i [%]	w_e [%]	f_{undr} [kPa]	$\varepsilon_{b;50}$ [%]	E'_{50}[MPa]	
1	79.00	38.40		16.13		24.50		0.10	65.42	
2	79.00	38.30		16.17		23.00		0.36	41.93	
3	78.80	38.40		16.18		23.20		0.25	82.54	
	Vóór de beproeving					Na de beproeving				

Proefstuk	h_c [mm]	V_c [cm³]	σ'_c [kPa]	u_{bk} [kPa]	v [%/h]	Stopcriterium
1	78.90	91.25	44.9	300.6	7.60	
2	78.83	90.53	89.6	300.3	7.61	
3	78.60	90.58	135.3	300.0	7.63	handmatig gestopt
	Consolidatie				Belasting	

ε_b [%]	Φ'_s [°]	c'_s [kPa]
1.0	35.7	1.43
2.0	37.4	0.82
3.0	37.7	-0.35
Bezwijken	37.7	0.09

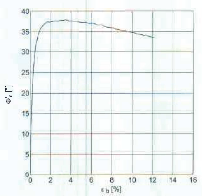

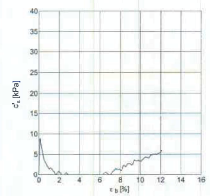

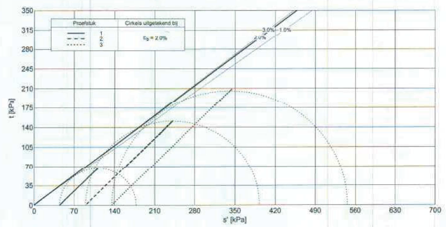

MOS GRONDMECHANICA bv Postbus 801, 3160 AA Rhoon - Telefoon (010) 5030200 - www.mosgeo.com

Opdracht : 0045409
Plaats : 2e Maasvlakte
Betreft : Kademuur

TRIAXIAALPROEF

Boring : B5.1-1
Monster : 1
Bus : 4351
Datum : 24-08-2009
Opmerkingen :

Monsterklasse : 3
Diepte : 0.27 - 0.02 -NAP
Grondsoort : Zand mg. zwak siltig zw. grind sg. gs

Type proefstuk : Geprepareerd
Type proef : CD
Uitv. procedure : Enkeltraps
Uitgevoerd door :

Proefstuk	h_i [mm]	D_i [mm]	γ_i [kN/m³]	γ_{dr} [kN/m³]	w_i [%]	w_e [%]	f_{undr} [kPa]	$\varepsilon_{b;50}$ [%]	E'_{50}[MPa]	
1	79.00	38.40		16.13		24.50		0.10	65.42	
2	79.00	38.30		16.17		23.00		0.36	41.93	
3	78.80	38.40		16.18		23.20		0.25	82.54	
	Vóór de beproeving					Na de beproeving				

Proefstuk	h_c [mm]	V_c [cm³]	σ'_c [kPa]	u_{bk} [kPa]	v [%/h]	Stopcriterium
1	78.90	91.25	44.9	300.6	7.60	
2	78.83	90.53	89.6	300.3	7.61	
3	78.60	90.58	135.3	300.0	7.63	handmatig gestopt
	Consolidatie				Belasting	

ε_b [%]	Φ'_s [°]	c'_s [kPa]
1.0	35.7	1.43
2.0	37.4	0.82
3.0	37.7	-0.35
Bezwijken	37.7	0.09

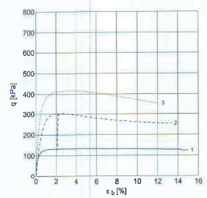

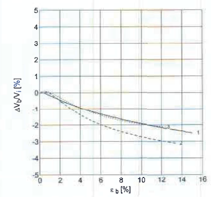

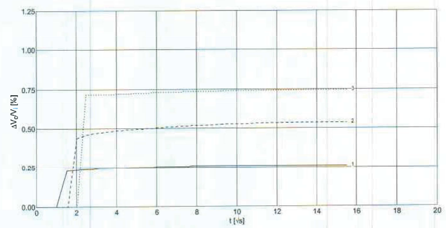

MOS GRONDMECHANICA bv Postbus 801, 3160 AA Rhoon - Telefoon (010) 5030200 - www.mosgeo.com

TRIAXIAALPROEF

Opdracht : 0045409
Plaats : 2e Maasvlakte
Betreft : Kademuur

Boring	: B5.1-4	Monsterklasse	: 3	Type proefstuk	: Geprepareerd
Monster	: 3	Diepte	: 10.05 - 10.45 -NAP	Type proef	: CD
Bus	: 4370	Grondsoort	: Zand mg. zwak siltig sg gs.	Uitv. procedure	: Enkeltraps
Datum	: 23-09-2009			Uitgevoerd door	:
Opmerkingen	:				

Proefstuk	h_i [mm]	D_i [mm]	γ_i [kN/m³]	γ_{dr} [kN/m³]	w_i [%]	w_e [%]	f_{undr} [kPa]	$\varepsilon_{b,50}$ [%]	E'_{50}[MPa]	
1	79.90	37.90		14.78		27.60		0.48	22.04	
2	80.00	38.00		14.69		27.00		0.73	29.64	
3	80.00	38.00		14.69		25.30		0.60	56.90	
	Vóór de beproeving					Na de beproeving				

Proefstuk	h_c [mm]	V_c [cm³]	σ'_c [kPa]	u_{bk} [kPa]	v [%/h]	Stopcriterium
1	79.30	89.27	99.2	401.1	7.57	
2	79.70	89.72	198.3	401.2	7.53	ε_b > 15.0%
3	79.60	89.10	300.3	399.9	7.54	ε_b > 15%
	Consolidatie				Belasting	

ε_i [%]	Φ'_ε [°]	c'_ε [kPa]
1.0	24.4	-1.13
2.0	27.3	1.03
12.0	32.7	-6.26
Bezwijken	32.7	-0.44

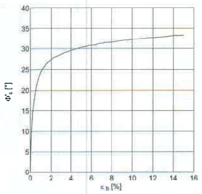

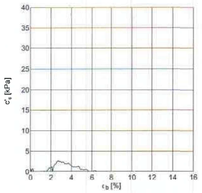

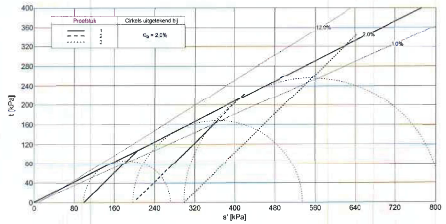

TRIAXIAALPROEF

Opdracht : 0045409
Plaats : 2e Maasvlakte
Betreft : Kademuur

Boring	: B5.1-4	Monsterklasse	: 3	Type proefstuk	: Geprepareerd
Monster	: 3	Diepte	: 10.05 - 10.45 -NAP	Type proef	: CD
Bus	: 4370	Grondsoort	: Zand mg. zwak siltig sg gs.	Uitv. procedure	: Enkeltraps
Datum	: 23-09-2009			Uitgevoerd door	:
Opmerkingen	:				

Proefstuk	h_i [mm]	D_i [mm]	γ_i [kN/m³]	γ_{dr} [kN/m³]	w_i [%]	w_e [%]	f_{undr} [kPa]	$\varepsilon_{b,50}$ [%]	E'_{50}[MPa]	
1	79.90	37.90		14.78		27.60		0.48	22.04	
2	80.00	38.00		14.69		27.00		0.73	29.64	
3	80.00	38.00		14.69		25.30		0.60	56.90	
	Vóór de beproeving					Na de beproeving				

Proefstuk	h_c [mm]	V_c [cm³]	σ'_c [kPa]	u_{bk} [kPa]	v [%/h]	Stopcriterium
1	79.30	89.27	99.2	401.1	7.57	
2	79.70	89.72	198.3	401.2	7.53	ε_b > 15.0%
3	79.60	89.10	300.3	399.9	7.54	ε_b > 15%
	Consolidatie				Belasting	

ε_i [%]	Φ'_ε [°]	c'_ε [kPa]
1.0	24.4	-1.13
2.0	27.3	1.03
12.0	32.7	-6.26
Bezwijken	32.7	-0.44

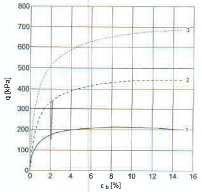

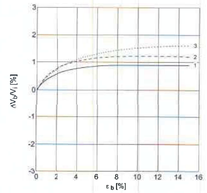

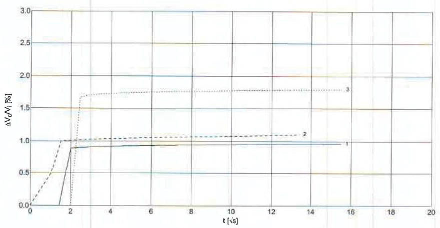

Opdracht : 0045409
Plaats : 2e Maasvlakte
Betreft : Kademuur

TRIAXIAALPROEF

Boring : B5.1-5
Monster : 4
Bus : 4382
Datum : 20-08-2009
Opmerkingen :

Monsterklasse : 1
Diepte : 13.03 - 13.33 -NAP
Grondsoort : Zand mf. zwak siltig gs.

Type proefstuk : Ongeroerd
Type proef : CD
Uitv. procedure : Enkeltraps
Uitgevoerd door :

Proefstuk	h_i [mm]	D_i [mm]	γ_i [kN/m³]	γ_{dr} [kN/m³]	w_i [%]	w_e [%]	f_{undr} [kPa]	$\varepsilon_{b;50}$ [%]	E'_{50}[MPa]	
1	77.20	37.50	19.18	15.59	23.00	26.30		0.71	41.99	
2	77.20	37.50	19.78	16.04	23.30	27.20		0.87	59.90	
3	77.20	37.50	19.61	16.19	21.10	25.90		0.76	84.17	
	Vóór de beproeving					Na de beproeving				

Proefstuk	h_c [mm]	V_c [cm³]	σ'_c [kPa]	u_{bk} [kPa]	v [%/h]	Stopcriterium
1	77.10	84.55	114.9	301.0	7.78	
2	77.00	84.17	229.5	301.0	7.79	handmatig gestopt
3	76.40	83.96	344.1	301.1	7.85	handmatig gestopt
	Consolidatie			Belasting		

ε_b [%]	Φ'_c [°]	c'_c [kPa]
1.0	26.2	69.45
2.0	32.6	84.70
3.0	35.8	75.06
Bezwijken	37.1	66.17

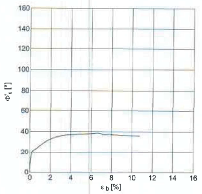

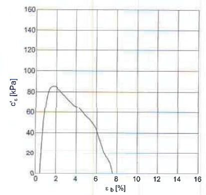

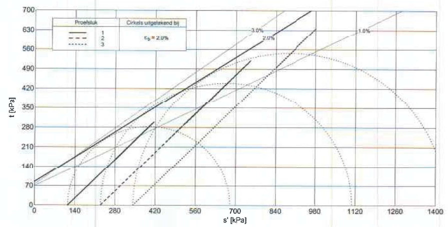

Opdracht : 0045409
Plaats : 2e Maasvlakte
Betreft : Kademuur

TRIAXIAALPROEF

Boring : B5.1-5
Monster : 4
Bus : 4382
Datum : 20-08-2009
Opmerkingen :

Monsterklasse : 1
Diepte : 13.03 - 13.33 -NAP
Grondsoort : Zand mf. zwak siltig gs.

Type proefstuk : Ongeroerd
Type proef : CD
Uitv. procedure : Enkeltraps
Uitgevoerd door :

Proefstuk	h_i [mm]	D_i [mm]	γ_i [kN/m³]	γ_{dr} [kN/m³]	w_i [%]	w_e [%]	f_{undr} [kPa]	$\varepsilon_{b;50}$ [%]	E'_{50}[MPa]	
1	77.20	37.50	19.18	15.59	23.00	26.30		0.71	41.99	
2	77.20	37.50	19.78	16.04	23.30	27.20		0.87	59.90	
3	77.20	37.50	19.61	16.19	21.10	25.90		0.76	84.17	
	Vóór de beproeving					Na de beproeving				

Proefstuk	h_c [mm]	V_c [cm³]	σ'_c [kPa]	u_{bk} [kPa]	v [%/h]	Stopcriterium
1	77.10	84.55	114.9	301.0	7.78	
2	77.00	84.17	229.5	301.0	7.79	handmatig gestopt
3	76.40	83.96	344.1	301.1	7.85	handmatig gestopt
	Consolidatie			Belasting		

ε_b [%]	Φ'_c [°]	c'_c [kPa]
1.0	26.2	69.45
2.0	32.6	84.70
3.0	35.8	75.06
Bezwijken	37.1	66.17

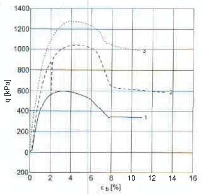

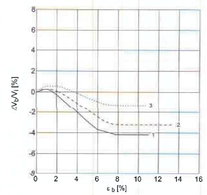

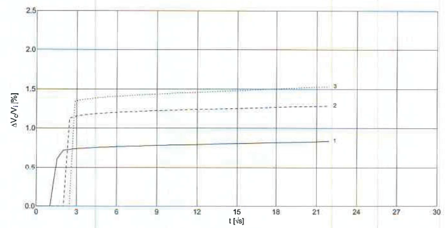

MOS GRONDMECHANICA bv Postbus 801, 3160 AA Rhoon - Telefoon (010) 5030200 - www.mosgeo.com

Two sieve analyses

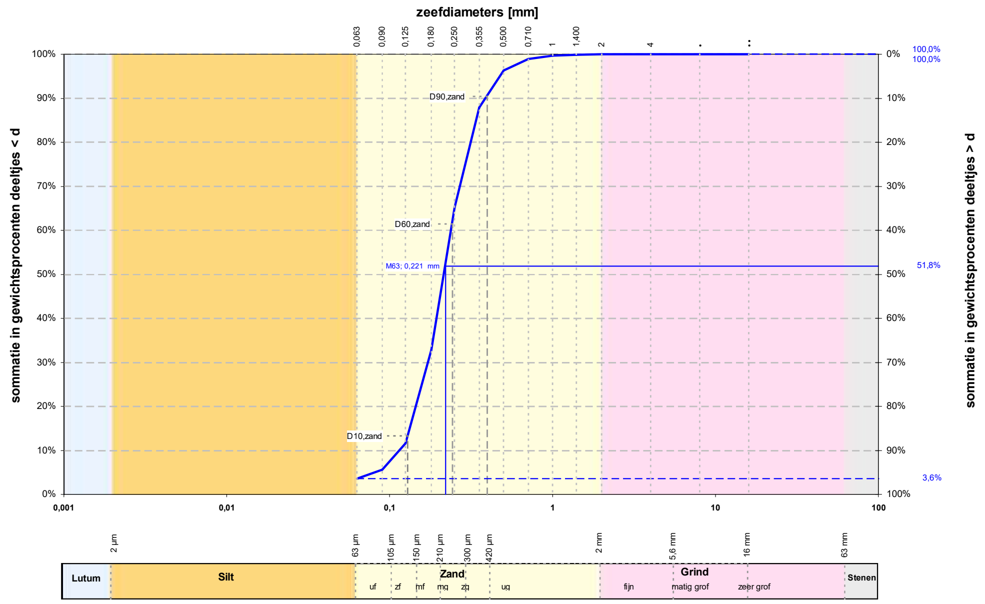

Alle fracties	
Kentallen	Waarde
d_{10} [mm]	0,115
d_{15} [mm]	0,134
d_{50} [mm]	0,217
d_{60} [mm]	0,239
$C_u = d_{60} / d_{10}$ [-]	2,1
d_{90} / d_{10} [-]	3,4
C_c [-]	1,08

	Bepaling fractie < 63 µm		Zand		Grind		Stenen	
	d [mm]	% < d	d [mm]	% < d	d [mm]	% < d	d [mm]	% < d
Lutum			0,075	-	2,8	-	125	-
Lutum	0,001	-	0,090	5,6	4,0	100,0		
Lutum	0,002	-	0,106	-	5,6	-		
Silt	0,004	-	0,125	11,6	8,0	100,0		
Silt	0,006	-	0,150	-	11,2	-		
Silt	0,008	-	0,180	32,8	16,0	100,0		
Silt	0,010	-	0,212	-	20,0	-		
Silt	0,016	-	0,250	65,2	22,4	-		
Silt	0,020	-	0,355	87,9	31,5	-		
Silt	0,030	-	0,500	96,3	45,0	-		
Silt	0,038	-	0,710	99,0	63,0	-		
Silt	0,045	-	1,000	99,7				
Silt	0,063	3,6	1,400	99,9				
Silt			2,000	100,0				

Karakteristieke waarden	
M_{63} [mm]	0,221
M_{2000} [mm]	-
D_m [mm]	0,230
F_m [-]	1,27
U_{16} [-] [16µm - 2mm]	-

Zandfractie	
Kentallen	Waarde
D_{10} [mm]	0,13
D_{15} [mm]	0,14
D_{60} [mm]	0,24
D_{90} [mm]	0,40
$C_u = D_{60} / D_{10}$ [-]	1,87
D_{90} / D_{10} [-]	3,08
U[-] [63µm - 2mm]	49,91

Beschrijving uitvoering proef	
Beschrijving volgens NEN 5104:	Zs1
kalkgehalte	niet bepaald
Methode bepaling fijn:	sedigraaf
Methode bepaling zand	zeven; nat
Methode bepaling grind	zeven; nat

Projectcode	**53029-1**
Projectnaam	2e Maasvlakte (uw projectnummer: 302664/T0063)
Boring	SZ015
Monster	2
Diepte	-2,00 m tot -4,00 m t.o.v. mv

versie: 1.3.0.15

AKKOORD LAB

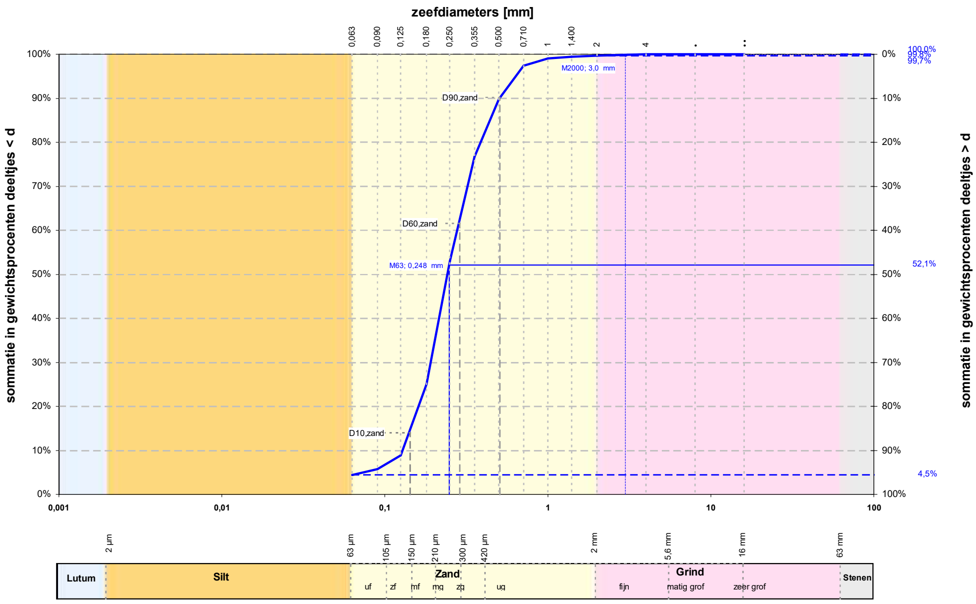

Alle fracties	
Kentallen	Waarde
d_{10} [mm]	0,129
d_{15} [mm]	0,146
d_{50} [mm]	0,243
d_{60} [mm]	0,281
$C_u = d_{60} / d_{10}$ [-]	2,2
d_{90} / d_{10} [-]	3,9
C_c [-]	1,02

Karakteristieke waarden	
M_{63} [mm]	0,248
M_{2000} [mm]	3,0
D_m [mm]	0,272
F_m [-]	1,50
U_{16} [-] [16µm - 2mm]	-

	Bepaling fractie < 63 µm		Zand		Grind		Stenen	
	d [mm]	% < d	d [mm]	% < d	d [mm]	% < d	d [mm]	% < d
Lutum			0,075	-	2,8	-	125	-
	0,001	-	0,090	5,8	4,0	100,0		
	0,002	-	0,106	-	5,6	-		
Silt	0,004	-	0,125	8,9	8,0	100,0		
	0,006	-	0,150	-	11,2	-		
	0,008	-	0,180	25,0	16,0	100,0		
	0,010	-	0,212	-	20,0	-		
	0,016	-	0,250	53,0	22,4	-		
	0,020	-	0,355	76,7	31,5	-		
	0,030	-	0,500	89,8	45,0	-		
	0,038	-	0,710	97,4	63,0	-		
	0,045	-	1,000	99,1				
	0,063	4,5	1,400	99,4				
			2,000	99,7				

Zandfractie	
Kentallen	Waarde
D_{10} [mm]	0,14
D_{15} [mm]	0,16
D_{60} [mm]	0,29
D_{90} [mm]	0,51
$C_u = D_{60} / D_{10}$ [-]	2,02
D_{90} / D_{10} [-]	3,57
U[-] [63µm - 2mm]	43,46

Beschrijving uitvoering proef	
Beschrijving volgens NEN 5104:	Zs1 met enkel spoor grind
kalkgehalte	niet bepaald
Methode bepaling fijn:	sedigraaf
Methode bepaling zand	zeven; nat
Methode bepaling grind	zeven; nat

Projectcode	**53029-1**	
Projectnaam	2e Maasvlakte (uw projectnummer: 302664/T0063)	
Boring	SZ017	
Monster	3	
Diepte	-4,00 m tot -6,00 m	t.o.v. mv

versie: 1.3.0.15

AKKOORD
LAB

B
Derivation of the soil properties and load parameters

Cone tip resistance - relative density correlations

Multiple correlations exist between the cone tip resistance measured by a CPT and relative density of a sand layer. In Figure B.1a five correlations are compared, two versions of the correlation of Baldi [10] and correlations of Jamiolkowski [27], Lunne & Christoffersen [31] and Schmertmann [51]. The correlations of Baldi, Lunne & Christoffersen and Schmertmann are described by Equation B.1a and the correlation of Jamiolkowski is described by Equation B.1b:

$$D_R = \frac{1}{C_2} ln(\frac{q_c}{C_0(\sigma'_{v0})^{C_1}} \tag{B.1a}$$

$$D_R = \frac{1}{C_2} ln(\frac{q_c}{(\sigma'_m)^{C_1}} - C_0 \tag{B.1b}$$

with

D_R = relative density, [-],
q_c = cone tip resistance, [MPa],
σ'_{v0} = vertical effective stress, [kPa],
σ'_m = mean effective stress, [kPa],
C_0, C_1, C_2 = material constants, [-].

Table B.1 presents the values of the material constants C_0, C_1 and C_2 of each correlation. In the correlations described by Equation B.1a the measured cone tip resistance is normalised by the vertical effective stress. In the correlations described by Equation B.1b the measured cone tip resistance is normalised by the mean effective stress.

Correlation	C_0	C_1	C_2	Equation
Baldi 1	**86**	**0.53**	**3.29**	**B.1a**
Baldi 2	157	0.55	2.41	B.1a
Lunne & Christoffersen	61	0.71	2.61	B.1a
Schmertmann	50	0.70	2.91	B.1a
Jamiolkowski	1.214	0.5	3.73	B.1b

Table B.1: Constants C_0, C_1 and C_2 of five commonly applied cone tip resistance-relative density correlations. Values of the constants of 'Baldi 1' are used to estimate the relative density of the sand fill at the RWG container terminal.

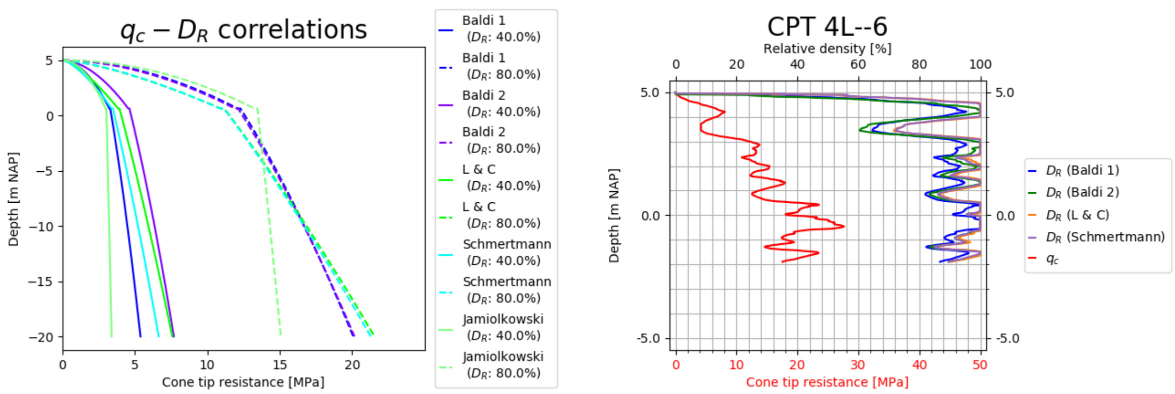

(a) (b)

Figure B.1: Comparison between the cone tip resistance - relative density correlations from Table B.1 a) for a hypothetical sand layer with a relative density of 40% or 80%; and b) described by Equation B.1a using CPT 4L-6 (location 1 of Phase 1 of the RWG container terminal). The effective vertical stress is calculated taking the unit weight of the sand above and below the ground water table at 18 and 20 kN/m^3, respectively. Surface is situated at 5 m NAP and water table at 0.63 m NAP.

In Figure B.1a an estimate of the cone tip resistance with depth is made for a hypothetical sand at 40% and 80% relative density with a water table at 0.63 $m\ NAP$. Surface of the sand layer is situated at 5 $m\ NAP$. The vertical effective stress is calculated taking the unit weight of the sand above the ground water table at 18 kN/m^3 (moist sand) and below the ground water table at 20 kN/m^3 (saturated). The mean stress is calculated based on the vertical effective stress:

$$\sigma_m^{'} = \frac{1}{2}(\sigma_{v0}^{'} + \sigma_{h0}^{'}) \approx \frac{3}{4}\sigma_{v0}^{'}. \tag{B.2}$$

with

$\sigma_m^{'}$ = mean effective stress, $[kPa]$,
$\sigma_{v0}^{'}$ = vertical effective stress, $[kPa]$,
$\sigma_{h0}^{'}$ = horizontal effective stress, $[kPa]$.

The correlation of Baldi described by Equation B.1a and the material constant values from the first row in Table B.1 are used to estimate the relative density of the sand fill at the RWG container terminal. Estimates of the relative density of a sand with similar minimum and maximum void ratio as the sand fill (0.5 vs. 0.490 and 0.8 vs. 0.821) corresponded well with the measured relative density [43]. Moreover, Figure B.1a shows that the other correlations described by Equation B.1a give similar estimates of the cone tip resistance for a dense sand layer with a relative density of 80%, especially in the first 10 m of the sand layer. Top part of the sand fill at the RWG container terminal consists primarily of dense and very dense sand layers. The zone of influence underneath the ASC rail tracks does not extent deeper than 10 m below the surface. The correlation of Jamiolkowski gives a significantly lower approximation of the relative density. This correlation uses the mean effective to correlate the cone tip resistance and relative density of the sand. The mean effective stress has not been measured, therefore it has to be estimated. This introduces an extra uncertainty into the correlation which makes its estimate of the relative density less reliable.

In Figure B.1b the first four correlations listed in Table B.1 are compared using data from CPT 4L-6. The differences between the correlations are relatively small. The differences become larger with decreasing relative density. Maximum difference between the correlations is around 10% relative density. For a relative density above 80%, correlation 'Baldi 1' estimates the lowest relative density. At lower relative densities, correlation 'Baldi 2' estimates a lower relative density.

Stiffness and unloading / reloading stiffness of the sand

To determine the stiffness of the sand fill, consolidated drained triaxial tests were executed on sand samples taken from boreholes executed near the quay wall of the RWG container terminal. Original documentation of the triaxial test results is attached in Appendix A.

Figure B.2 shows how the initial stiffness (E_i), secant stiffness (E_{50}) and the unloading/reloading stiffness (E_{UR}) are determined based on the deviatoric stress and the axial strain measurements. A steep slope of the secant or tangent line in the q, ε_a-plane indicates stiff behaviour. This means that the sand's resistance against deformation becomes larger. The secant stiffness is calculated by dividing the deviatoric stress at 50% of its maximum value to the corresponding axial strain:

$$E'_{50} = \frac{q_{max}}{2\varepsilon_a} \tag{B.3}$$

with

E'_{50} = secant stiffness in standard drained triaxial test, [kPa],
q_{max} = deviatoric stress at failure, [kPa],
ε_a = axial strain corresponding to half of the deviatoric stress at failure, [-].

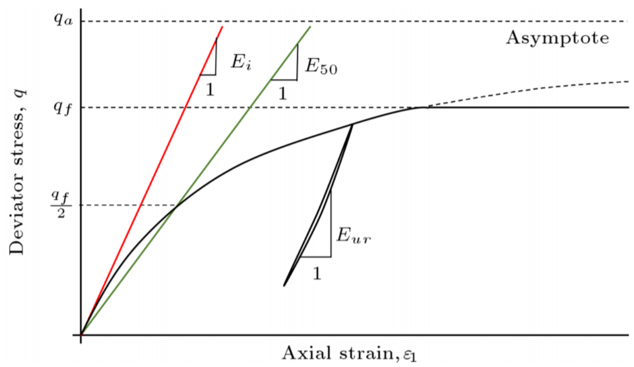

Figure B.2: Result from a triaxial test plotted in the q, ε_a-plane. Indicated are the secant stiffness (E_{50}), unloading / reloading stiffness (E_{ur}) and the initial stiffness (E_i) [13].

Stress dependency of the stiffness

Stiffness of sand increases with confining pressure. This dependency is described by a parameter m, rate of stress dependency of the stiffness. To determine parameter m, each sample from the sand fill was tested three times for varying confining pressures (σ'_3). The secant stiffness calculated with Equation B.3 and the confining stress are used to determine parameter m:

$$m = \frac{\ln\,(E'^{1}_{50}/E'^{2}_{50})}{\ln\,(\sigma'^{1}_{3}/\sigma'^{2}_{3})} \tag{B.4}$$

with

m = rate of stress dependency of the stiffness, [-],
E'^{1}_{50} = secant stiffness in standard drained triaxial at confining pressure σ'^{1}_{3}, [kPa],
E'^{2}_{50} = secant stiffness in standard drained triaxial at confining pressure σ'^{2}_{3}, [kPa],
σ'^{1}_{3} = confining pressure during the first triaxial test, [kPa],
σ'^{2}_{3} = confining pressure during the second triaxial test, [kPa].

$m = 0.7$ is used in this research to determine the stiffness of the sand fill at any confining stresses level. The average value of parameter m of all samples taken at the sand fill is determined at 0.7. A typical value of parameter m for sands is 0.5.

Parameter m is calculated using the triaxial test results from 'Boring 5.1-5 Monster 4'. This is a very dense sample. The original data is included in Appendix A. $E'^{1}_{50} = 41.99\ MPa$ measured at a confining stress of $\sigma'^{1}_{3} = 114.9\ kPa$; $E'^{2}_{50} = 59.90\ MPa$ measured at a confining stress of $\sigma'^{2}_{3} = 229.5\ kPa$; and $E'^{3}_{50} = 84.17\ MPa$ measured at a confining stress of $\sigma'^{3}_{3} = 344.1\ kPa$. Three values for parameter m can be obtained from the data, using Equation B.4. Data from tests 1 and 2 gives $m = 0.78$, tests 1 and 3 gives $m = 0.63$ and tests 2 and 3 gives $m = 0.39$.

Note that in some tests the measured stiffness was lower while the applied confining stress was higher. This results in negative values of parameter m. These measurements have been discarded from the data.

Secant stiffness of the sand fill at a confining pressure of 100 kPa is estimated as:

$$E'^{ref}_{50} = E'_{50}(\frac{100}{\sigma'_3})^{0.7} \tag{B.5}$$

with

E'^{ref}_{50} = secant stiffness at 100 kPa, [MPa],
E'_{50} = secant stiffness measured during triaxial test, [MPa],
σ'_3 = confining pressure during triaxial test, [kPa].

For the same sand sample mentioned above ('Boring 5.1-5 Monster 4') the stiffness at a reference confining stress of 100 kPa becomes 38, 33 and 35 MPa for tests 1, 2 and 3, respectively. The values of the stiffness correspond very well with each other. The secant stiffness at a reference confining stress of 100 kPa have been determined for all the samples from the RWG container terminal.

Stiffness of the sand fill at any confining pressure is estimated as:

$$E' = E'^{ref}_{50}(\frac{\sigma'_3}{100})^{0.7}. \tag{B.6}$$

Unloading / Reloading stiffness

The unloading / reloading stiffness is calculated by dividing the deviatoric stress increment in the unloading / reloading stage to the corresponding axial strain increment:

$$E'_{ur} = \frac{\Delta q}{\Delta \varepsilon_a} \tag{B.7}$$

with

E'_{ur} = unloading / reloading stiffness in a standard drained triaxial test, [kPa],
Δq = deviatoric stress increment unloading / reloading stage, [kPa],
$\Delta \varepsilon_a$ = axial strain increment unloading / reloading stage, [%].

The unloading / reloading stiffness at 100 kPa confining pressure is calculated in the same way as the secant stiffness. Replace the measured secant stiffness and the secant stiffness at a reference confining stress by the measured unloading / reloading stiffness and the unloading / reloading stiffness at a reference confining stress in Equations B.4 and B.5.

Minimum and maximum void ratios

Measurements of the minimum and maximum unit weights of dried sand samples taken from boreholes near the quay wall of the RWG container terminal are used to calculate the minimum and maximum void ratio. They were measured as part of triaxial testing. In Appendix A the original documentation of the measured unit weights is included.

The dried sand is used to build samples in their loosest and densest states. The corresponding void ratio gives the maximum and the minimum void ratio, respectively. Void ratio are calculated using the following formula:

$$e = G_s \frac{\gamma_w}{\gamma} - 1 = \frac{\gamma_s - \gamma}{\gamma} \tag{B.8}$$

with

e = void ratio, [-],
G_s = specific gravity of the sand particles, [-],
γ_s = unit weight of the sand particles, [-],
γ_w = unit weight of water, [kN/m^3],
γ = measured unit weight of the sand, [kN/m^3].

Unit weight of the sand particles is estimated at 26.5 kN/m^3. In Table B.2 the measured minimum and maximum unit weights of the samples are summarised together with their corresponding maximum and minimum void ratio.

Sample number	Minimum unit weight [kN/m^3]	Maximum void ratio [-]	Maximum unit weight [kN/m^3]	Minimum void ratio [-]
4351	15.30	0.732	17.91	0.480
4352	14.18	0.869	16.68	0.589
1607	14.49	0.829	16.77	0.580
1609	14.54	0.823	16.72	0.585
1610	15.40	**0.721**	18.00	**0.472**
1611	14.34	0.848	16.95	0.563
4370	14.66	0.808	16.91	0.567
4382	13.04	**1.032**	15.77	**0.680**
4361	14.54	0.823	16.73	0.584
5559	15.27	0.735	17.86	0.484
5560	15.14	0.750	17.52	0.513
average		**0.815**		**0.554**

Table B.2: Measured minimum and maximum unit weights of sand samples taken from the sand fill and corresponding maximum and minimum void ratio.

Spreading of the load beneath the foundation

The load applied by an ASC is transferred by the rail track and concrete railroad ties to the ballast bed. Due to spreading the amplitude of the applied load decreases with depth. In the ballast bed and sand a 1:1 spreading angle is assumed.

Figure B.3 shows a sketch of a cross-section of an ASC rail track through its center in longitudinal direction. The load of an ASC is divided over four ASC legs with each four wheels. Distance between the four legs is large enough to consider each leg as a separate linear load distributed between four wheels. The center-to-center (c.t.c.) distance between two adjacent wheels in the same leg is 1.2 m. The c.t.c. distance of the concrete railroad ties is 70 cm. The ballast bed-sand interface lies 40 cm below the bottom of the railroad ties.

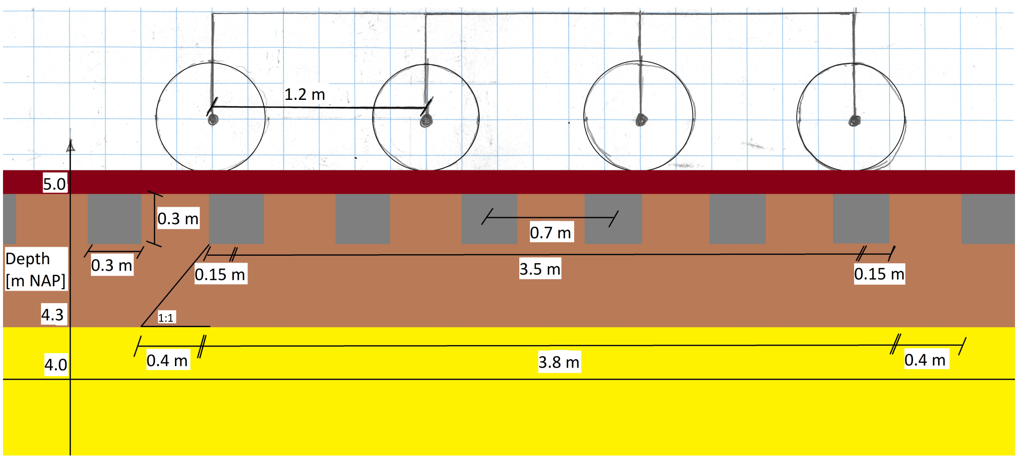

Figure B.3: Cross-section of an ASC rail track through its center in longitudinal direction. The length over which the load applied by one ASC leg spreads out increases with depth. A 1:1 spreading angle is assumed. one ASC leg consists of four wheels. The rail is indicated in red/brown, concrete railroad ties in grey, ballast bed in brown and sand in yellow.

Figure B.3 shows a sketch of a cross-section perpendicular to an ASC rail track. Length of a railroad tie is 1.2 m. The left rail track and right rail track of two adjacent container stacks share one ballast bed. On the right a small part of a railroad tie that belongs to the left ASC rail track of an adjacent container stack is visible.

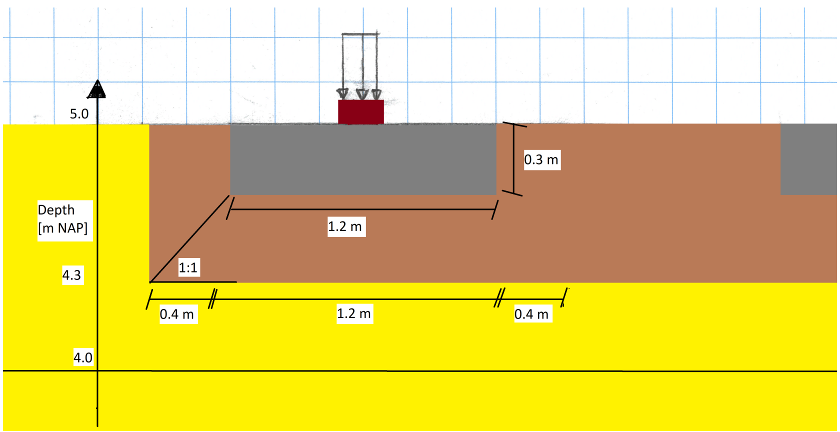

Figure B.4: Cross-section perpendicular to an ASC rail track. The width over which the load applied by one ASC leg spreads out increases with depth. A 1:1 spreading angle is assumed. On the right a small part of a railroad tie that belongs to the left ASC rail track of an adjacent container stack is visible. The rail is indicated in red/brown, concrete railroad ties in grey, ballast bed in brown and sand in yellow.

At the ballast bed-sand interface the applied load spreads out over a surface area of 2.0 m by 4.6 m.

The load of one ASC leg is supported by six railroad ties (see Figure B.3). At the depth corresponding to the bottom of the railroad ties the load spreads out over a length of 3.8 m. This length consists of five times the c.t.c. distance between the six railroad ties plus half of the widths of the two outer railroad ties, together 0.3 m. At this depth the load of one leg of an ASC is spread out over an area of 1.2 m by 3.8 m, including the area in between the railroad ties. In the ballast bed the load spreads out under a 1:1 angle. This means that at the ballast bed-sand interface, 40 cm below the bottom of the railroad ties, the surface area becomes two times 40 cm longer and wider. The length and width over which the load spreads out are indicated in Figures B.3 and B.4.

The vertical stress at the ballast bed-sand interface, at a depth of 4.3 m NAP, is estimated at 63 to 89 kPa, assuming an even distribution of the load over the 2.0 m by 4.6 m surface area. The load of one leg of an ASC varies between 579 and 822 kN, depending on the type of ASC and whether it is carrying a container and the weight of the container (see Table 3.10 in Chapter 3).

Estimate of the number of load cycles per year

The RWG container terminal handles 1.4 million containers annually. Capacity of the RWG container terminal is 2.35 million TEU (Twenty-foot equivalent), which consists of incoming and outgoing TEU 1 and TEU 2 containers [8]. Port of Rotterdam, including the RWG container terminal, handled in 2019 14.8 million TEU, corresponding to 8.8 million TEU 1 and 2 containers [7]. Assuming the same TEU-container ratio for the RWG container terminal, 2.35 million TEU corresponds to 1.4 million containers. 450.000 TEU 1 and 950.000 TEU 2 containers. TEU 1 containers are generally used for heavier cargo, they can therefore even be heavier compared to the larger TEU 2 containers.

200.000 load cycles are applied to the sand underneath the ASC rail tracks of the RWG container terminal per year. This comprises of 100.000 load cycles applied by an ASC that is carrying a container and 100.000 load cycles without container. The RWG container terminal is operating almost at its full capacity [20]. It is estimated it transports on average 1.25 million containers per year. This corresponds to 50.000 containers per container stack per year, assuming transport is distributed evenly over the 25 container stacks at the RWG container terminal. An ASC has two legs per rail track. That means that per container an ASC applies two load cycles carrying a container and two load cycles without a container.

C

Results PLAXIS computation

Results obtained with the FE computations executed in PLAXIS of the six selected locations are presented. In the FE computations the first load cycle is simulated. The computations consist of two steps. In the first step a vertical stress is applied onto the foundation. In the second step the stress is removed.

The results presented in this Appendix comprise of the settlement and cyclic shear strain amplitude with depth plotted for a vertical through the center of the foundation. The settlement and the cyclic shear strain amplitude are plotted from 3.5 $m\ NAP$ until a depth of -10 $m\ NAP$. Above 3.5 $m\ NAP$ the sand has a 100% relative density. Densification of the sand and settlement do not occur here. The volumetric threshold strain of the sand fill at the RWG container terminal is estimated at 10^{-4}, a typical value for sands. The volumetric threshold strain is plotted together with the cyclic shear strain amplitude. Densification of the sand occurs at depths where the cyclic shear strain amplitude lies above the volumetric threshold strain. It determines the depth of influence. Per location first the cone tip resistance and estimated initial relative density and the subsurface model in PLAXIS are presented.

Plane strain conditions are assumed in the PLAXIS computations. The sand layers are modelled with the hardening soil small strain (HSsmall) material model [40]. Model parameters of the HSsmall model:

- E_{50}^{ref}: secant stiffness in triaxial test at reference pressure;
- E_{oed}^{ref}: tangent stiffness in oedometer test at p^{ref};
- E_{ur}^{ref}: reference stiffness in unloading / reloading;
- G_0^{ref}: reference shear stiffness at small strains;
- $\gamma_{0.7}$: shear strain at which G has reduced to 72.2%;
- m: rate of stress dependency in stiffness behaviour;
- p^{ref}: reference pressure (100 kPa);
- ν_{ur}: Poisson's ratio in unloading / reloading;
- c': cohesion;
- ϕ': friction angle;
- ψ: dilatancy angle;
- R_f: failure ratio q_f/q_a (0.9);
- K_0^{NC}: stress ratio $\sigma'_{xx}/\sigma'_{yy}$ in 1D primary compression;

The sand layers are distinguished based on the relative density of the sand fill. In Table C.1 the model parameters and their estimated values of the HSsmall model for sands with a relative density of 35%, 65%, 80%, 90% and 100% are given. For other model parameters the default values were used.

Relative density sand		35% (loose)	65% (medium dense)	80% (dense)	90% (very dense)	100% (densified)
model parameter	unit					
γ_{unsat}	kN/m^3	17	18	19	19	19
γ_{sat}	kN/m^3	19	20	21	21	21
E_{50}^{ref}	kPa	35	40	45	50	55
E_{oed}^{ref}	kPa	35	40	45	50	55
E_{ur}^{ref}	kPa	150	160	165	170	175
G_0^{ref}	kPa	80	100	110	120	130
$\gamma_{0.7}$	[%]	0.015	0.015	0.015	0.015	0.015
ν_{ur}	[-]	0.2	0.2	0.2	0.2	0.2
c'	kPa	0	0	0	0	0
ϕ'	°	30	32.5	35	35	35
ψ	°	5	5	5	5	5
R_f	[-]	0.9	0.9	0.9	0.9	0.9
K_0^{NC}	[-]	0.4554	0.4554	0.4554	0.4554	0.4554

Table C.1: Values of the model parameters of the FE HSsmall model in PLAXIS. Sand layers are distinguished based on relative density of the sand.

Cyclic shear strain amplitude

The cyclic shear strain amplitude is a measure of the magnitude of the applied shear strain during a load cycle. It is defined as half of the difference between the maximum shear strain during loading and during unloading:

$$\gamma_0 = \frac{\gamma_{max,l} - \gamma_{max,u}}{2} \tag{C.1}$$

with

γ_0 = cyclic shear strain amplitude, [-],
$\gamma_{max,l}$ = the maximum cyclic shear strain during loading, [-],
$\gamma_{max,u}$ = the maximum cyclic shear strain after unloading, [-].

The maximum shear strain is calculated according to the equation below:

$$\gamma_{max} = ((\varepsilon_{xx} - \varepsilon_{yy})^2 + \gamma_{xy}^2)^{1/2} \tag{C.2}$$

with

ε_{xx} = strain in the x-direction, [-],
ε_{yy} = strain in the y-direction, [-],
γ_{xy} = shear strain in the y-direction in a plane perpendicular to the x-axis, [-].

The strains in the x- and y-direction and shear strain are computed by the FE model. After the load is removed the strains are computed again. With Equation C.2 the maximum shear strain is calculated during loading and unloading. With Equation C.1 the cyclic shear strain amplitude is calculated.

Location 1 - CPT 4L-6
FE PLAXIS model

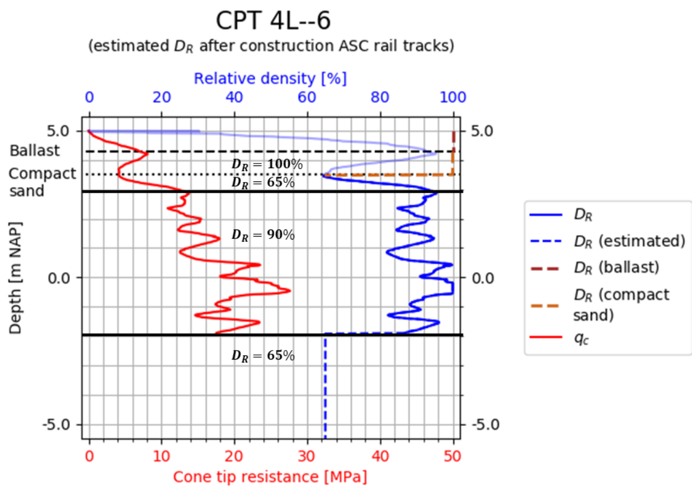

(a) CPT 4L-6

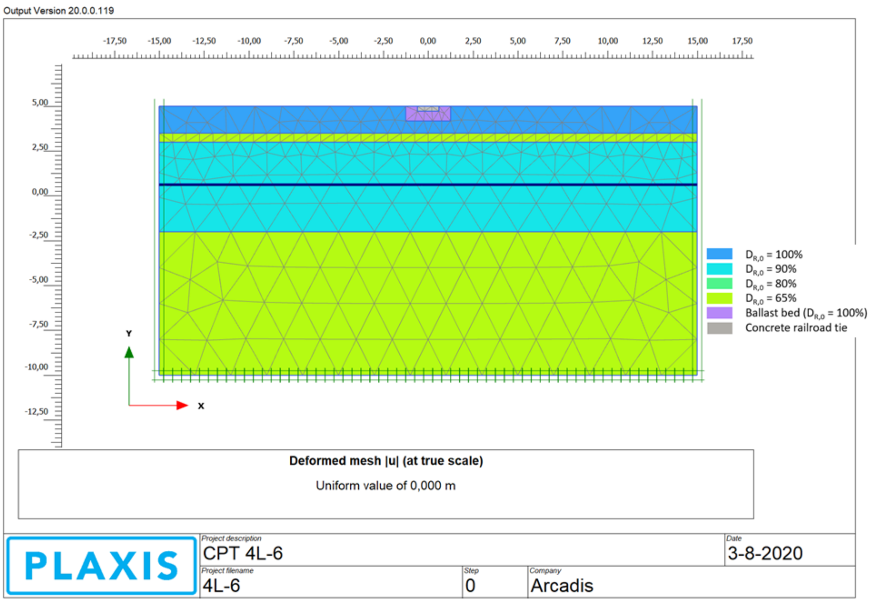

(b) PLAXIS subsurface model

Figure C.1: Cone tip resistance, estimated initial relative density and layering of the sand fill based on the initial relative density and the corresponding FE PLAXIS subsurface model.

Settlement after one load cycle

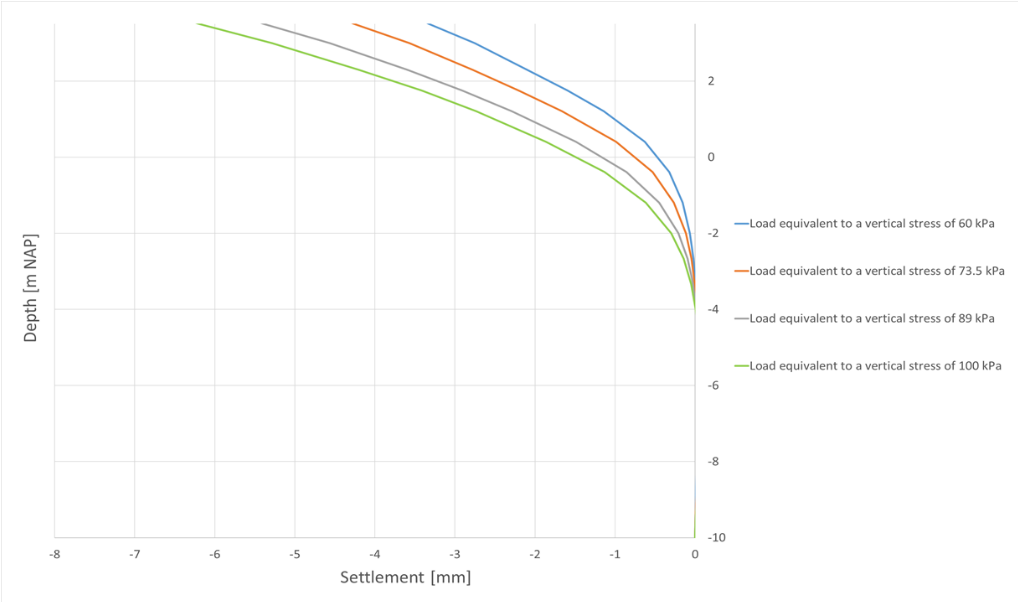

Figure C.2: Settlement after one load cycle for varying foundation stress computed with the FE PLAXIS model.

Cyclic shear strain amplitude

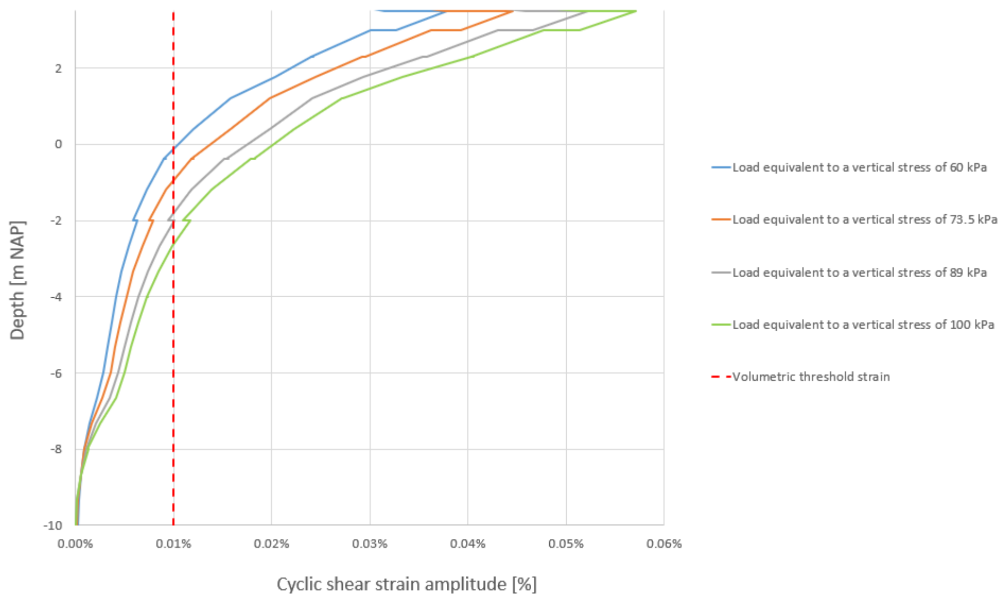

Figure C.3: Cyclic shear strain amplitude for varying foundation stress computed with the FE PLAXIS model and volumetric threshold strain.

Location 2 - CPT 4R-3

FE PLAXIS model

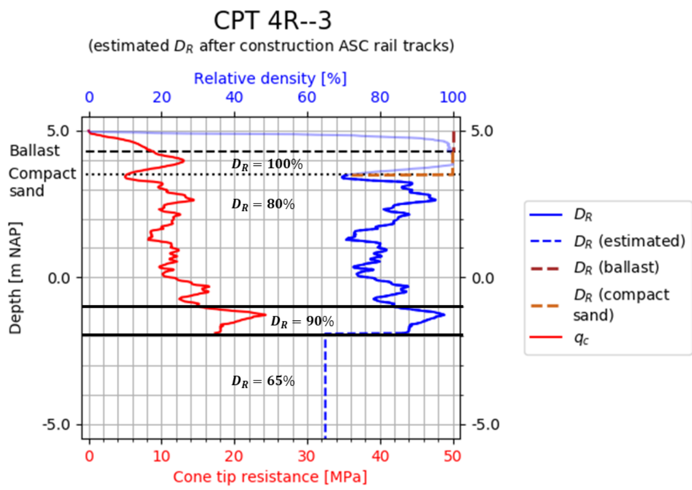

(a) CPT 4R-3

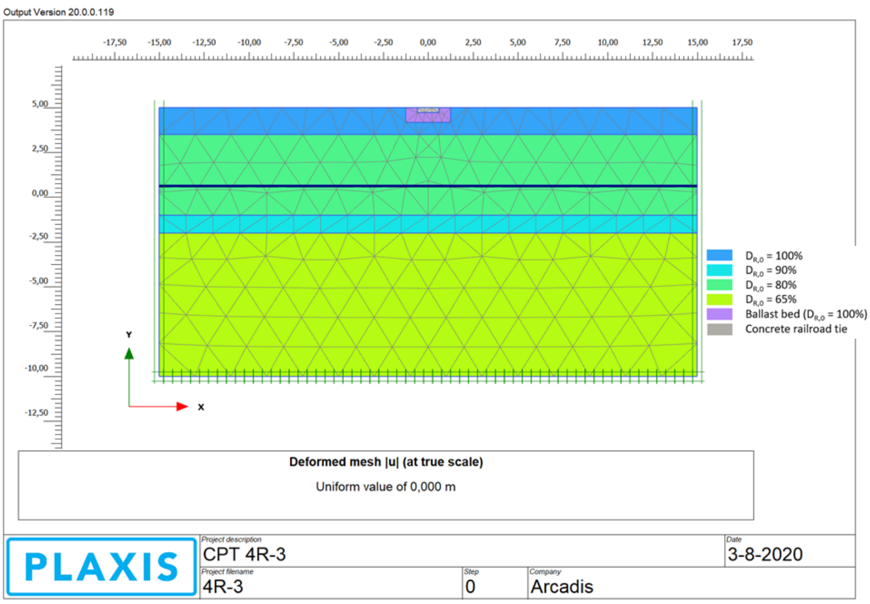

(b) PLAXIS subsurface model

Figure C.4: Cone tip resistance, estimated initial relative density and layering of the sand fill based on the initial relative density and the corresponding FE PLAXIS subsurface model.

Settlement after one load cycle

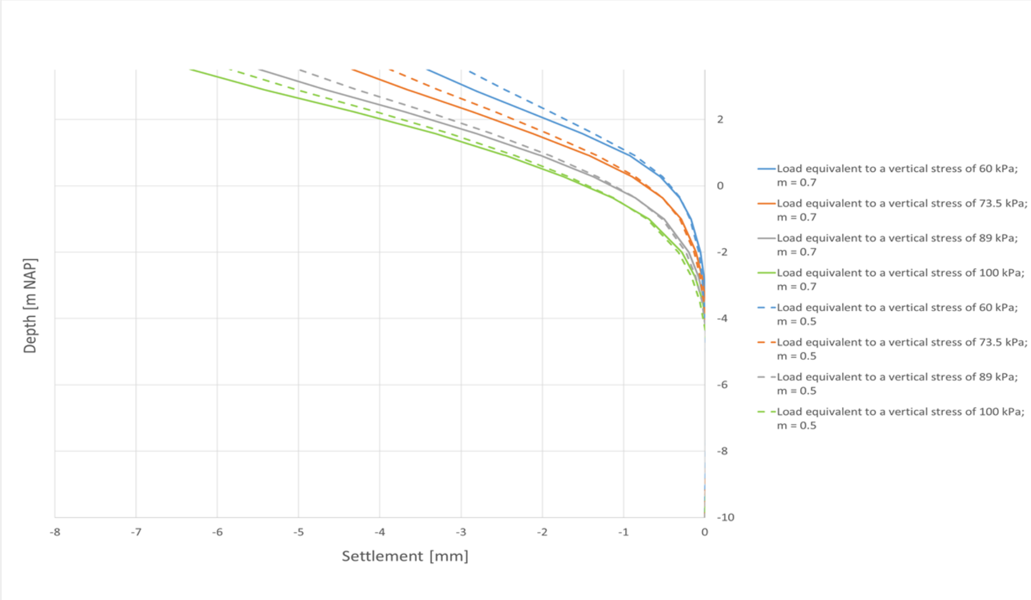

Figure C.5: Settlement after one load cycle for varying foundation stress computed with the FE PLAXIS model.

Cyclic shear strain amplitude

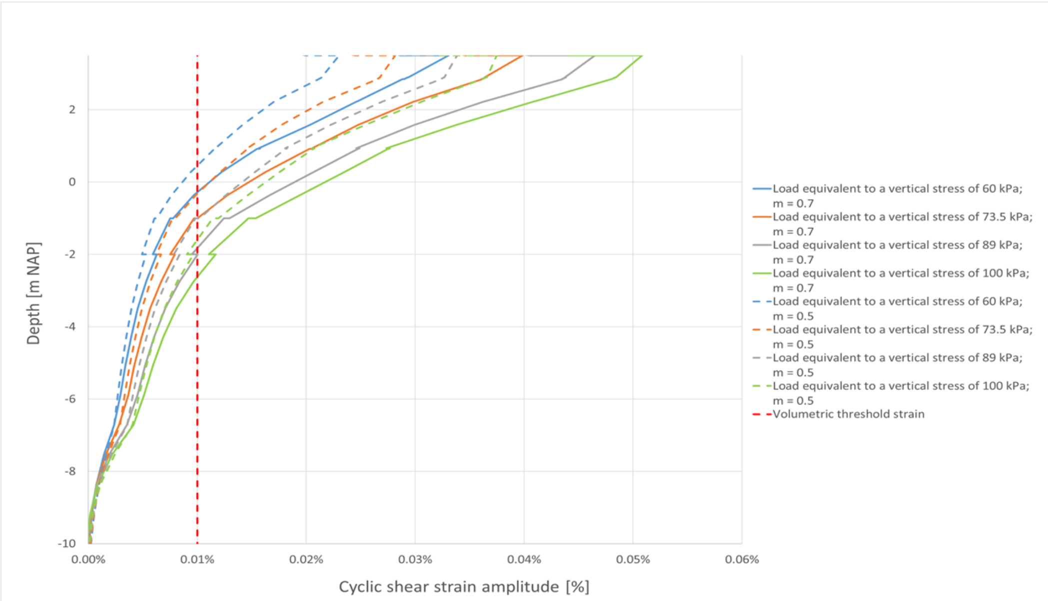

Figure C.6: Cyclic shear strain amplitude for varying foundation stress computed with the FE PLAXIS model and volumetric threshold strain.

Location 3 - CPT 9R-4

FE PLAXIS model

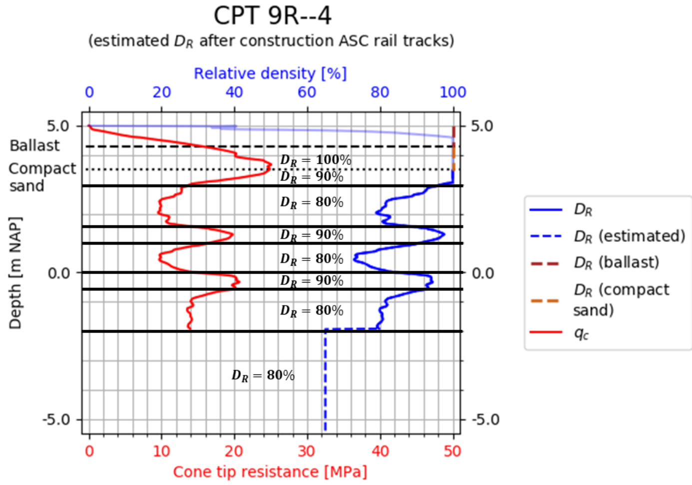

(a) CPT 9R-4

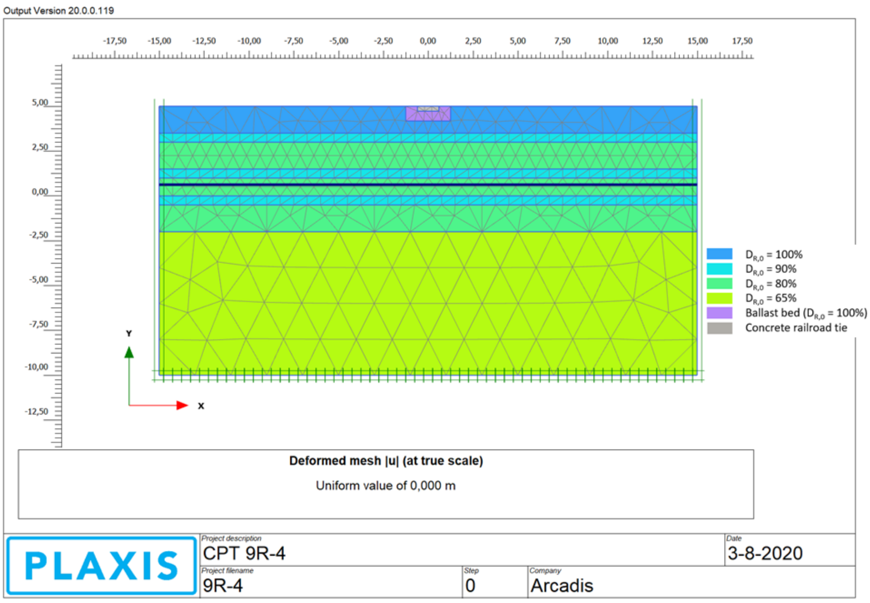

(b) PLAXIS subsurface model

Figure C.7: Cone tip resistance, estimated initial relative density and layering of the sand fill based on the initial relative density and the corresponding FE PLAXIS subsurface model.

Settlement after one load cycle

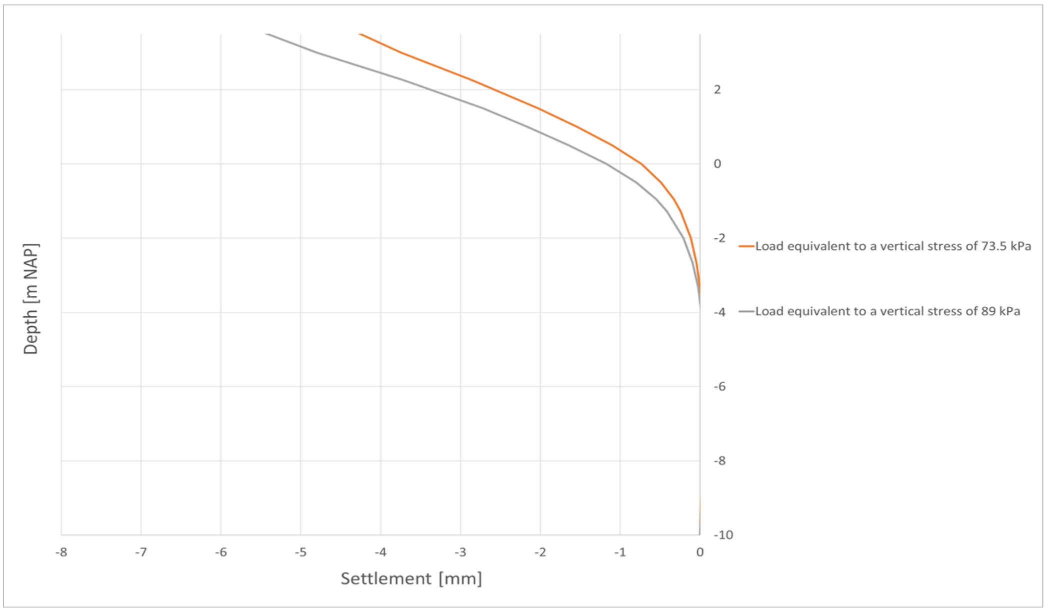

Figure C.8: Settlement after one load cycle for varying foundation stress computed with the FE PLAXIS model.

Cyclic shear strain amplitude

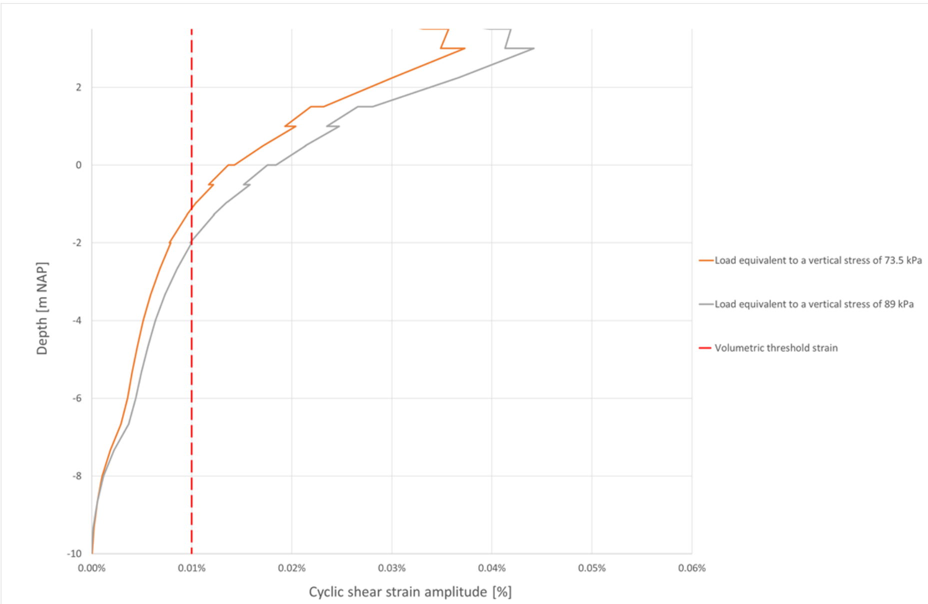

Figure C.9: Cyclic shear strain amplitude for varying foundation stress computed with the FE PLAXIS model and volumetric threshold strain.

Location 4 - CPT 8R-4
FE PLAXIS model

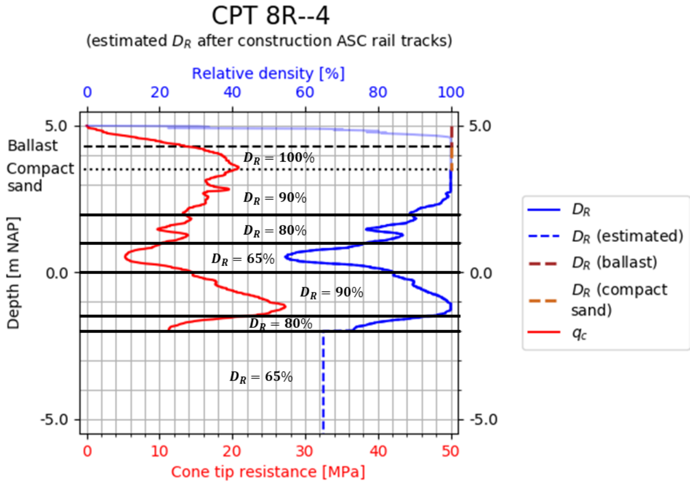

(a) CPT 8R-4

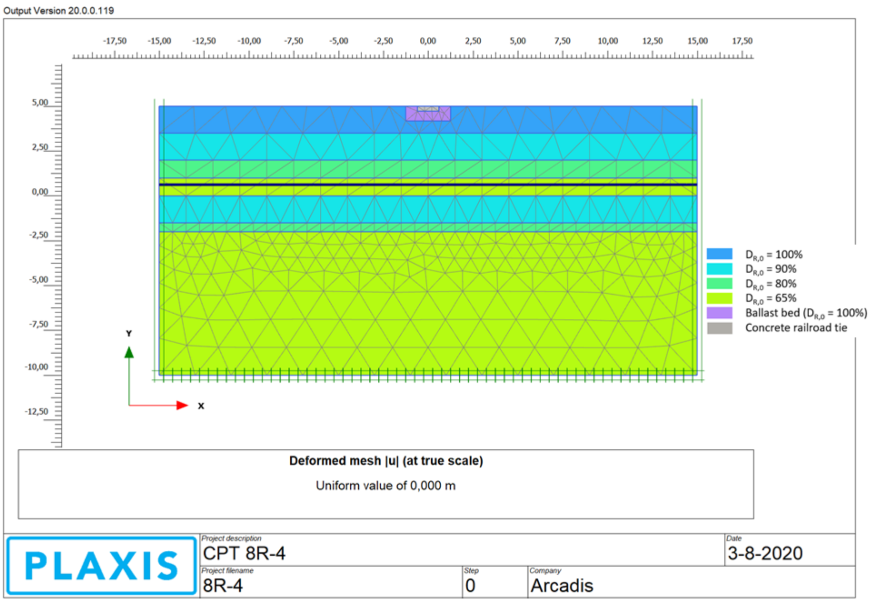

(b) PLAXIS subsurface model

Figure C.10: Cone tip resistance, estimated initial relative density and layering of the sand fill based on the initial relative density and the corresponding FE PLAXIS subsurface model.

Settlement after one load cycle

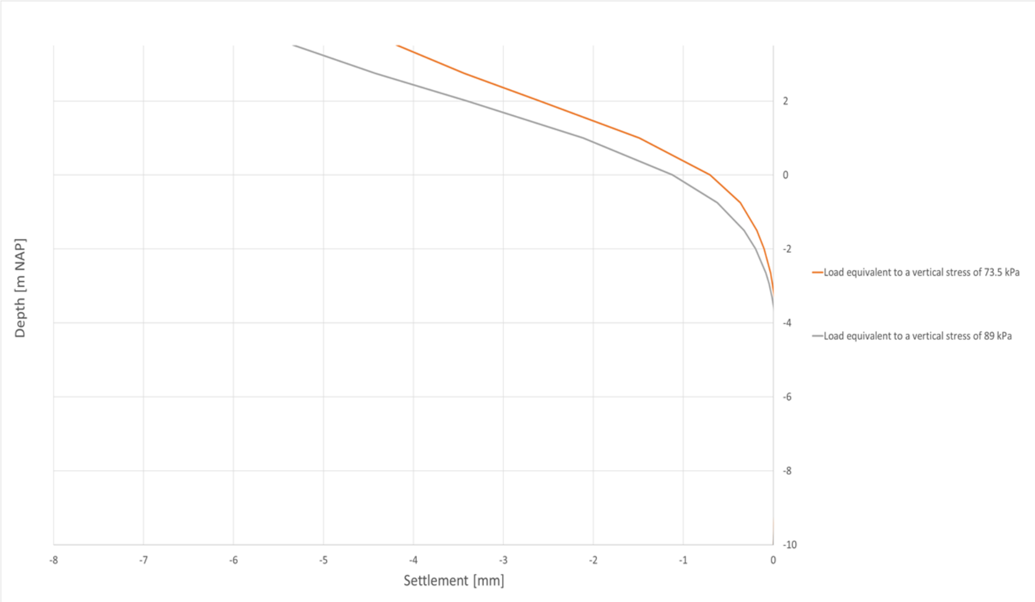

Figure C.11: Settlement after one load cycle for varying foundation stress computed with the FE PLAXIS model.

Cyclic shear strain amplitude

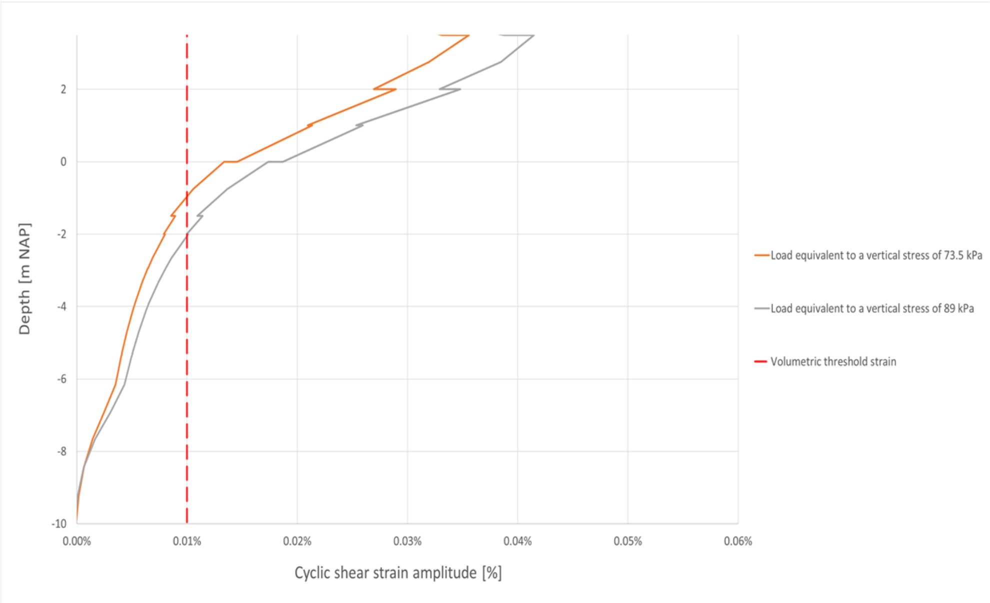

Figure C.12: Cyclic shear strain amplitude for varying foundation stress computed with the FE PLAXIS model and volumetric threshold strain.

Location 5 - CPT 12R-3
FE PLAXIS model

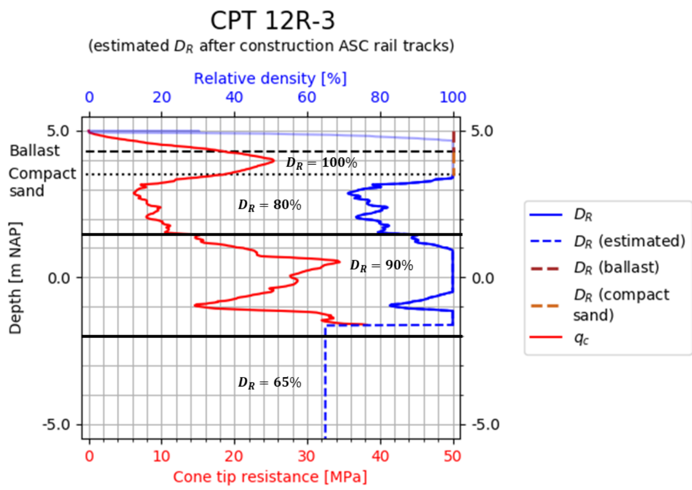

(a) CPT 12R-3

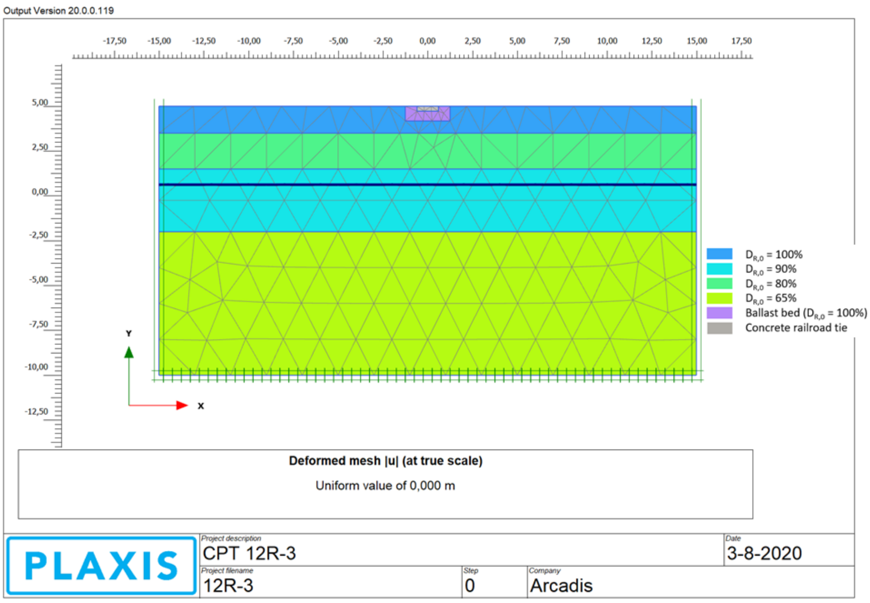

(b) PLAXIS subsurface model

Figure C.13: Cone tip resistance, estimated initial relative density and layering of the sand fill based on the initial relative density and the corresponding FE PLAXIS subsurface model.

Settlement after one load cycle

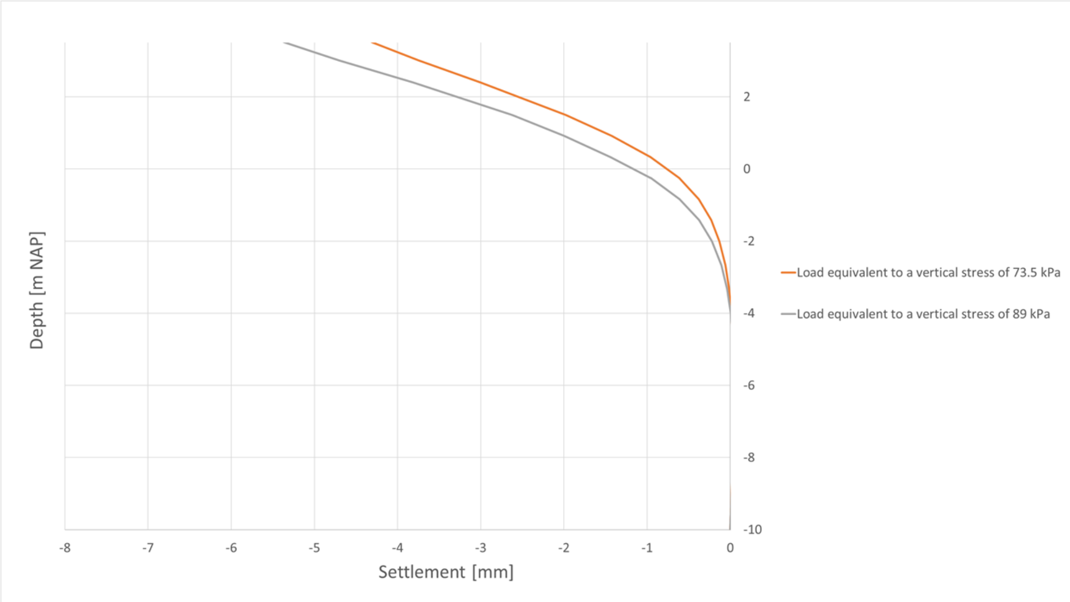

Figure C.14: Settlement after one load cycle for varying foundation stress computed with the FE PLAXIS model.

Cyclic shear strain amplitude

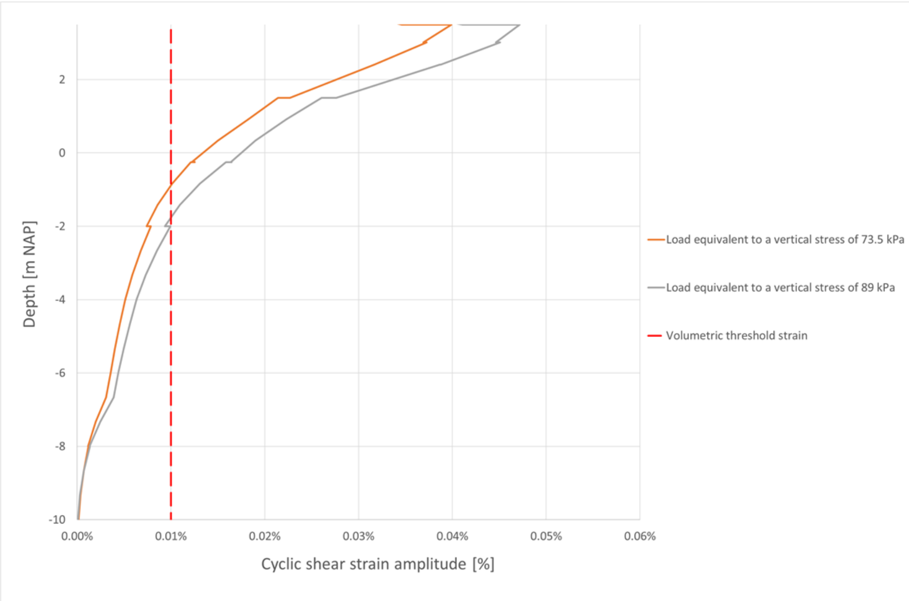

Figure C.15: Cyclic shear strain amplitude for varying foundation stress computed with the FE PLAXIS model and volumetric threshold strain.

Location 6 - CPT 10L-3

FE PLAXIS model

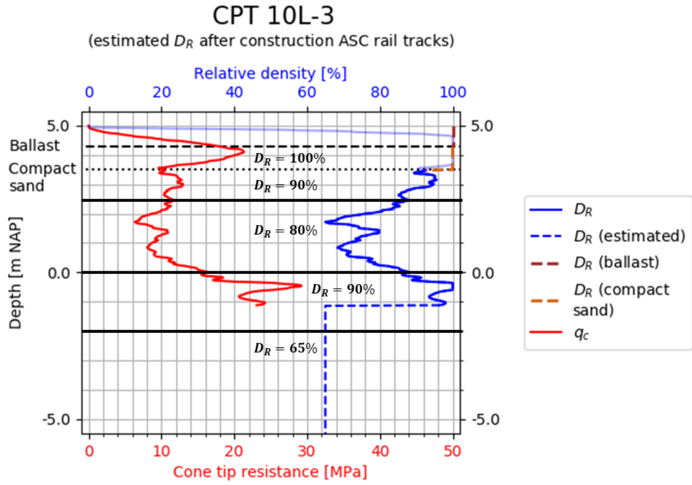

(a) CPT 10L-3

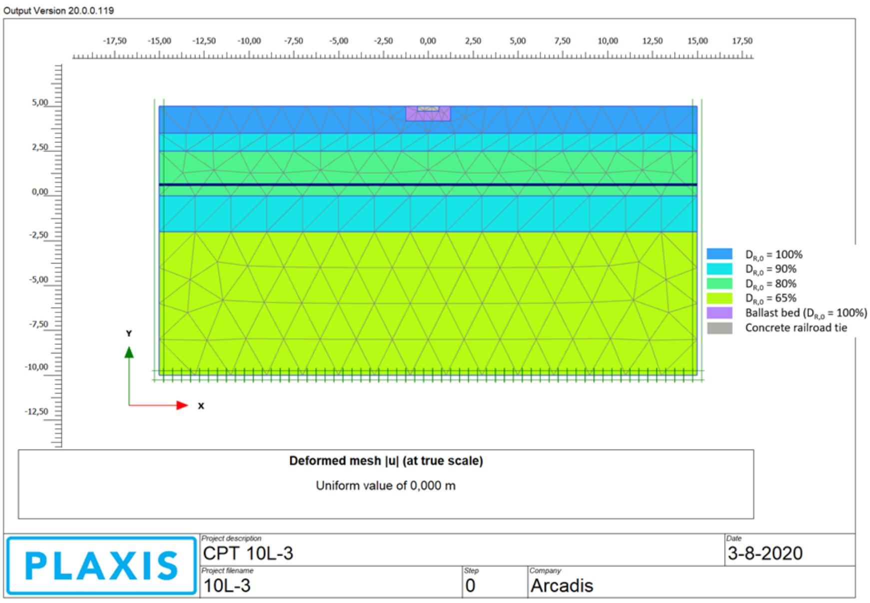

(b) PLAXIS subsurface model

Figure C.16: Cone tip resistance, estimated initial relative density and layering of the sand fill based on the initial relative density and the corresponding FE PLAXIS subsurface model.

Settlement after one load cycle

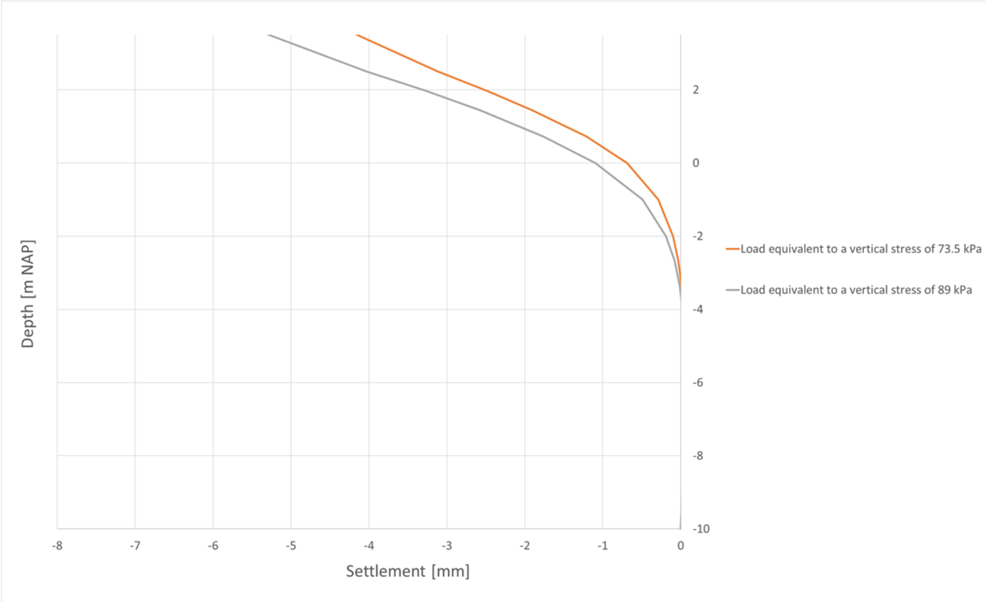

Figure C.17: Settlement after one load cycle for varying foundation stress computed with the FE PLAXIS model.

Cyclic shear strain amplitude

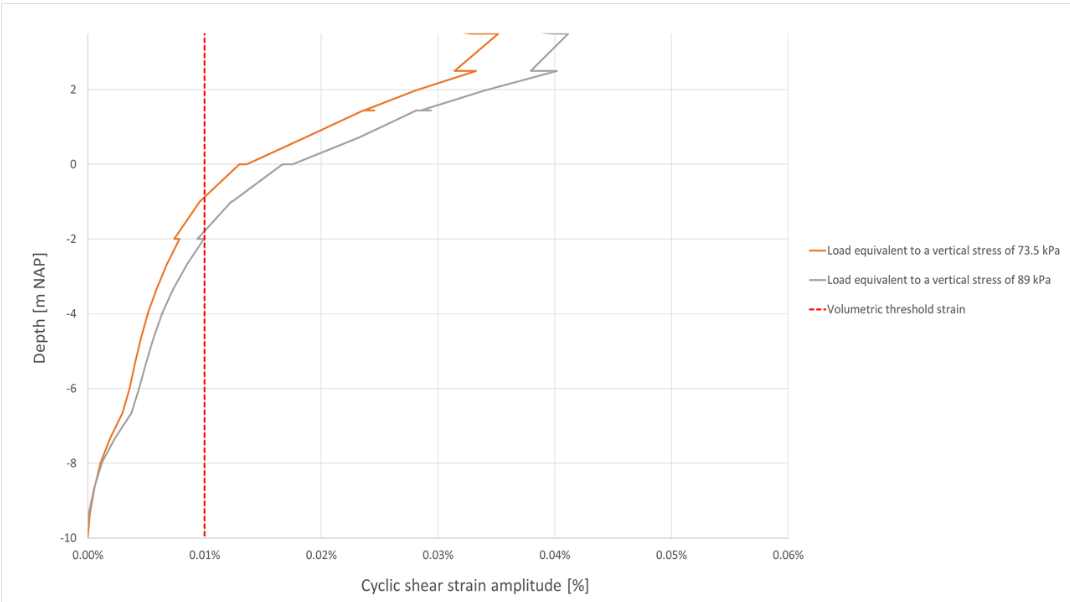

Figure C.18: Cyclic shear strain amplitude for varying foundation stress computed with the FE PLAXIS model and volumetric threshold strain.

D

Implementation of the compaction / liquefaction model for cyclic shear

The compaction / liquefaction model for cyclic shear is presented in Chapter 2. Implementation of this model in this research is described here. Implementation of the terminal density model is described in Section 4.10.

The C/L model for cyclic shear calculates densification of the sand after N load cycles induced by an applied cyclic shear strain. Densification of the sand is calculated with Equation 2.5 and the corresponding volumetric plastic strain with Equation 2.6. Values of the following model parameters have to be determined in order to calculate the densification and volumetric plastic strain after N load cycles with the C/L model for cyclic shear:

1. initial void ratio;
2. cyclic shear strain amplitude;
3. c_1 and c_2 for the C/L model for cyclic shear.

In addition, the volumetric threshold strain (γ_{tv}) is determined to estimate the depth of influence. It value is estimated at 0.010%, a typical value for sands.

Figure D.1 presents a flow chart of the implementation of the C/L model for cyclic shear. The relative density is correlated to the cone tip resistance. The material constants are correlated to the initial relative density. In triaxial tests the stiffness of the sand fill as function of the relative density, rate of stress dependency of the stiffness (parameter m) and minimum and maximum void ratio are determined. The initial void ratio is determined based on the minimum and maximum void ratio and initial relative density. Stiffness of the sand fill, unloading / reloading stiffness, shear modulus and parameter m are model parameters of the PLAXIS FE model. Together with the foundation stress the cyclic shear strain amplitude is determined.

Initial void ratio (e_0)

The initial void ratio is related to the initial relative density through the minimum and maximum void ratio:

$$e_0 = e_{max} - (e_{max} - e_{min}) \cdot D_{R,0} \tag{D.1}$$

with

e_0 = initial void ratio, [-],
$D_{R,0}$ = initial relative density, [-],
e_{min} = minimum void ratio, [-],
e_{max} = maximum void ratio, [-].

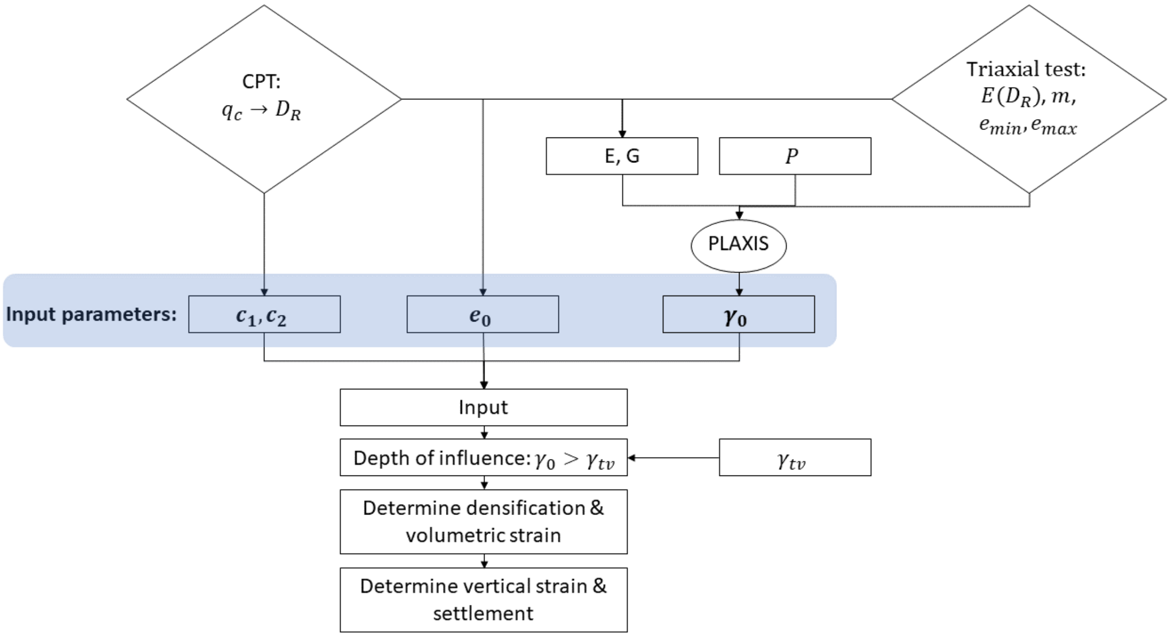

Figure D.1: Flowchart of the implementation of the C/L model for cyclic shear in this research.

The correlation of Baldi given in Equation 3.1 is used to correlate the cone tip resistance measured with a CPT to the relative density. In Appendix B is described how the relative density is correlated to the cone tip resistance. Other commonly applied cone tip resistance-relative density correlations are given and the decision to use the correlation of Baldi is explained.

The minimum and maximum void ratio of the sand have been determined as part of the triaxial tests that were executed on samples taken at the RWG container terminal. Based on the data the minimum and maximum void ratio are estimated at 0.50 and 0.80, respectively. This is described in Chapter 3. The data are attached in Appendix A.

In Figure D.2 the initial relative density with depth and the corresponding void ratio are displayed. Note that part of the data is displayed with a dashed line, to indicate that this is not based on a CPT measurement. It is assumed that between 5 and 3.5 $m\ NAP$ the sand is compacted to 100% relative density. This is a result of the compaction works that were carried out as part of the construction of ASC rail tracks. Beyond the extent of the CPT the sand is assumed to be medium dense with a relative density of 65%, this is based on deeper CPT measurements executed at different locations at the RWG container terminal.

Cyclic shear strain amplitude (γ_0)

The cyclic shear strain amplitude is a measure of the magnitude of the applied shear strain during a load cycle. In this research PLAXIS is used to create an FE model of the sand underneath the ASC rail tracks. The hardening soil small strain (HSsmall) material model is used to model the behaviour of the sand. In Appendix C is explained how the cyclic shear strain amplitude is determined and plotted for the six locations for varying foundation stress and varying stiffness for location 2. Depth of influence is determined where the cyclic shear strain amplitude intersects the volumetric threshold strain.

Material constants for the C/L cyclic shear model (c_1 and c_2)

The material constants c_1 and c_2 of a sand are correlated to the initial relative density in Equation 4.1. Preferably their values are determined in a cyclic (simple) shear test. These tests have not been executed on samples of the sand from the RWG container terminal.

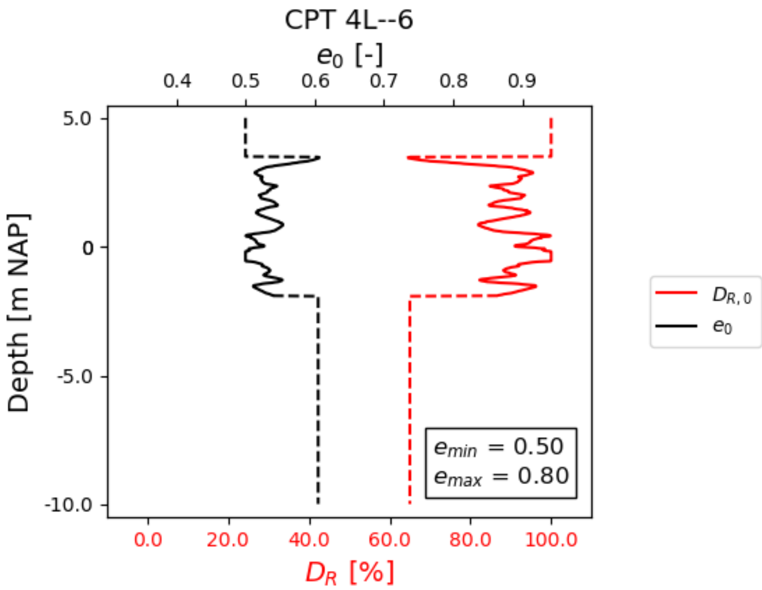

Figure D.2: The initial relative density and the initial void ratio at the location corresponding to CPT 4L-6. $e_{min} = 0.5$ and $e_{max} = 0.8$. The dashed line indicates that the data is estimated.

E
Python scripts

Geotechnical exchange format (GEF) files

This code is used to import the CPT data that are stored in a GEF-extension. Python code source: https://github.com/creepywaterbug?tab=repositories

```
# -*- coding: utf-8 -*-
"""

#!env/bin/python
# Datum:  1 Februari 2016
# Waterbug,waterbug@bitmessage.ch
"""


import re
import os
import time
import numpy as np

# Hulpfuncties
def is_number(s):
    try:
        float(s)
        return True
    except ValueError:
        return False


def removetrailers(string):
    d = re.sub('^[\t|\ ]*', '', string)
    e = re.sub('\r\n$', '', d)
    return e


class Gef2OpenClass:
    def __init__(self):
#        print ("init")
        return
```

```
    # Purpose: Of een BORE-Report file is (boring)
    def gbr_is_gbr(self):
        if 'PROCEDURECODE' in self.headerdict:
            if 'GEF-BORE-Report' in self.headerdict['PROCEDURECODE']:
                out = True
            else:
                out = False
        else:
            if 'REPORTCODE' in self.headerdict:
                if 'GEF-BORE-Report' in self.headerdict['REPORTCODE']:
                    out = True
                else:
                    out = False
            else:
                out = False
        try:
            return out
        except:
            return None

    # Purpose: Of een GEF-CPT-Report file is (sondering)
    def gcr_is_gcr(self):
        if 'PROCEDURECODE' in self.headerdict:
            if 'GEF-CPT-Report' in self.headerdict['PROCEDURECODE']:
                out = True
            else:
                out = False
        else:
            if 'REPORTCODE' in self.headerdict:
                if 'GEF-CPT-Report' in self.headerdict['REPORTCODE']:
                    out = True
                else:
                    out = False
            else:
                out = False
        try:
            return out
        except:
            return None

    # Purpose: Of #COMPANYID aanwezig
    def get_companyid_flag(self):
        if 'COMPANYID' in self.headerdict:
            if len(self.headerdict['COMPANYID']) > 0:
                out = True
            else:
                out = False
        else:
            out = False
        try:
            return out
        except:
            return None

    # Purpose: Geeft aantal kolommen in het data block
```

```python
def get_column(self):
    if 'COLUMN' in self.headerdict:
        if len(self.headerdict['COLUMN']) > 0:
            out = self.headerdict['COLUMN'][0]
        else:
            err = 'MissingValue'
    else:
        err = 'MissingKeyword'
    try:
        return out
    except:
        # return None
        return 'Error:%s' % (err)

# Purpose: Of #COLUMN aanwezig
def get_column_flag(self):
    if ('COLUMN' in self.headerdict):
        if len(self.headerdict['COLUMN']) > 0:
            out = True
        else:
            out = False
    else:
        out = False
    try:
        return out
    except:
        return None

# Purpose: Geeft nodata waarde voor geselecteerde kolom
def get_column_void(self, i_Kol):
    if 'COLUMNVOID' in self.headerdict:
        if len(self.headerdict['COLUMNVOID']) > i_Kol - 1:
            out = self.headerdict['COLUMNVOID'][i_Kol][1]
        else:
            err = 'MissingValue'
    else:
        err = 'MissingKeyword'
    try:
        return out
    except:
        # return None
        return 'Error:%s' % (err)

# Purpose: Of #COLUMNVOID aanwezig
def get_column_void_flag(self, i_Kol):
    if 'COLUMNVOID' in self.headerdict:
        if len(self.headerdict['COLUMNVOID']) > i_Kol - 1:
            out = True
        else:
            out = False
    else:
        out = False
    try:
        return out
    except:
        return None
```

```
    # Purpose: Geeft columninfo terug in een list
    def get_column_info(self, i_Kol):
        if 'COLUMNINFO' in self.headerdict:
            if len(self.headerdict['COLUMNINFO']) > i_Kol - 1:
                out = self.headerdict['COLUMNINFO'][i_Kol]
            else:
                err = 'MissingValue'
        else:
            err = 'MissingKeyword'
        try:
            return out
        except:
            # return None
            return 'Error:%s' % (err)

    # Purpose: Of #COLUMNINFO aanwezig
    def get_column_info_flag(self, i_Kol):
        if 'COLUMNINFO' in self.headerdict:
            if len(self.headerdict['COLUMNINFO']) > i_Kol - 1:
                out = True
            else:
                out = False
        else:
            out = False
        try:
            return out
        except:
            return None

    # Purpose: Geeft company naam
    def get_companyid_Name(self):
        if 'COMPANYID' in self.headerdict:
            if len(self.headerdict['COMPANYID']) > 0:
                out = self.headerdict['COMPANYID'][0]
            else:
                err = 'MissingValue'
        else:
            err = 'MissingKeyword'
        try:
            return out
        except:
            # return None
            return 'Error:%s' % (err)

    # Purpose: Geeft waarde uit bepaalde cel van data block
    def get_data(self, i_Kol, iRij):
        if 'datablok' in self.headerdict:
            if iRij in self.headerdict['datablok']:
                if len(self.headerdict['datablok'][iRij]) >= i_Kol - 1:
                    out = self.headerdict['datablok'][iRij][i_Kol - 1]
                else:
                    err = 'MissingKol'
            else:
                err = 'MissingRij'
        else:
```

```
            err = 'MissingDatablok'
        try:
            return out
        except:
            # return None
            return err

    # TODO continue get_data_iter
    # Purpose: geeft een iterator met alle waarden voor een bepaalde kolom
    ↪ in een data block
    def get_data_iter(self, i_Kol):
        try:
            if 'datablok' in self.headerdict:
                if len(self.headerdict['datablok'][1]) >= i_Kol - 1:
                    void = self.get_column_void(i_Kol)
                    for i_Rij in range(1, 1 + int(self.get_nr_scans())):
                        depth = self.get_data(1, i_Rij)
                        value = self.get_data(i_Kol, i_Rij)
                        if value == void:  #Replace nodata value for None
                            value = None
                        yield (depth, value)
                else:
                    err = 'MissingKol'
            else:
                err = 'MissingDatablok'
        except:
            yield err

    # Purpose: Of gegeven #MEASUREMENTTEXT index aanwezig
    def get_measurementtext_flag(self, i_Index):
        if 'MEASUREMENTTEXT' in self.headerdict:
            if i_Index in self.headerdict['MEASUREMENTTEXT']:
                out = True
            else:
                out = False
        else:
            out = False
        try:
            return out
        except:
            return None

    # Purpose: Of gegeven #MEASUREMENTVAR index aanwezig
    def get_measurementvar_flag(self, i_Index):
        if 'MEASUREMENTVAR' in self.headerdict:
            if i_Index in self.headerdict['MEASUREMENTVAR']:
                out = True
            else:
                out = False
        else:
            out = False
        try:
            return out
        except:
            return None
```

```
    # Purpose: Geeft measurementtext tekst
    def get_measurementtext_Tekst(self, i_Index):
        if 'MEASUREMENTTEXT' in self.headerdict:
            if i_Index in self.headerdict['MEASUREMENTTEXT']:
                if 1 in self.headerdict['MEASUREMENTTEXT'][i_Index]:
                    out = self.headerdict['MEASUREMENTTEXT'][i_Index][1]   #
                     ↪  ??
                else:
                    err = 'MissingValue'
            else:
                err = 'MissingIndex'
        else:
            err = 'MissingKeyword'
        try:
            return out
        except:
            # return None
            return 'Error:%s' % (err)

    # Purpose: Geeft measurementvar value
    def get_measurementvar_Value(self, i_Index):
        if 'MEASUREMENTVAR' in self.headerdict:
            if i_Index in self.headerdict['MEASUREMENTVAR']:
                if len(self.headerdict['MEASUREMENTVAR'][i_Index]) > 0:
                    out = self.headerdict['MEASUREMENTVAR'][i_Index][1]
                else:
                    err = 'MissingValue'
            else:
                err = 'MissingIndex'
        else:
            err = 'MissingKeyword'
        try:
            return out
        except:
            # return None
            return 'Error:%s' % (err)

    # Purpose: Geeft aantal rijen in het data block
    # neem aan waarde achter 'LASTSCAN', maar check dit!
    def get_nr_scans(self):
        if 'LASTSCAN' in self.headerdict:
            if len(self.headerdict['LASTSCAN']) > 0:
                out = self.headerdict['LASTSCAN'][0]
            else:
                err = 'MissingValue'
        else:
            err = 'MissingKeyword'
        try:
            return out
        except:
            # return None
            return 'Error:%s' % (err)

    # Purpose: Of #PARENT aanwezig
    # neeem aan dat er een par 'PARENT' aanwezig moet zijn. Check!
    def get_parent_flag(self):
```

```
    if ('PARENT' in self.headerdict):
        if len(self.headerdict['PARENT']) > 0:
            out = True
        else:
            out = False
    else:
        out = False
    try:
        return out
    except:
        return None  # test

# Purpose: Geeft referentie naar de parent, bv bestandsnaam
def get_parent_reference(self):
    if 'PARENT' in self.headerdict:
        if len(self.headerdict['PARENT']) > 0:
            out = self.headerdict['PARENT'][0]
        else:
            err = 'MissingValue'
    else:
        err = 'MissingKeyword'
    try:
        return out
    except:
        return 'Error:%s' % (err)

# Purpose: Of #PROCEDURECODE aanwezig
def get_procedurecode_flag(self):
    if 'PROCEDURECODE' in self.headerdict:
        if len(self.headerdict['PROCEDURECODE']) > 0:
            out = True
        else:
            out = False
    else:
        out = False
    try:
        return out
    except:
        return None

# Purpose: Geeft procedurecode code
def get_procedurecode_Code(self):
    if 'PROCEDURECODE' in self.headerdict:
        if len(self.headerdict['PROCEDURECODE']) > 0:
            out = self.headerdict['PROCEDURECODE'][0]
        else:
            err = 'MissingValue'
    else:
        err = 'MissingKeyword'
    try:
        return out
    except:
        # return None
        return 'Error:%s' % (err)

# Purpose: Of #PROJECTID aanwezig
```

```
    def get_projectid_flag(self):
        if 'PROJECTID' in self.headerdict:
            if len(self.headerdict['PROJECTID']) > 0:
                out = True
            else:
                out = False
        try:
            return out
        except:
            return None

    # Purpose: Geeft projectid nummer
    def get_projectid_Number(self):
        if 'PROJECTID' in self.headerdict:
            if len(self.headerdict['PROJECTID']) > 1:
                out = self.headerdict['PROJECTID'][1]
            else:
                err = 'MissingValue'
        else:
            err = 'MissingKeyword'
        try:
            return out
        except:
            # return None
            return 'Error:%s' % (err)

    # Purpose: Of #REPORTCODE aanwezig
    def get_reportcode_flag(self):
        if 'REPORTCODE' in self.headerdict:
            if len(self.headerdict['REPORTCODE']) > 0:
                out = True
            else:
                out = False
        else:
            out = False
        try:
            return out
        except:
            return None

    # Purpose: Geeft reportcode code
    def get_reportcode_Code(self):
        if 'REPORTCODE' in self.headerdict:
            if len(self.headerdict['REPORTCODE']) > 0:
                out = self.headerdict['REPORTCODE'][0]
            else:
                err = 'MissingValue'
        else:
            err = 'MissingKeyword'
        try:
            return out
        except:
            # return None
            return 'Error:%s' % (err)

    # Purpose: Of #STARTDATE aanwezig
```

```
    def get_startdate_flag(self):
        if 'STARTDATE' in self.headerdict:
            if len(self.headerdict['STARTDATE']) > 2:
                out = True
            else:
                out = False
        else:
            out = False
        try:
            return out
        except:
            return None

    # Purpose: Geeft startdate jaar (yyyy)
    def get_startdate_Yyyy(self):
        if 'STARTDATE' in self.headerdict:
            if len(self.headerdict['STARTDATE']) > 2:
                out = int(self.headerdict['STARTDATE'][0])
            else:
                err = 'MissingValue'
        else:
            err = 'MissingKeyword'
        try:
            return out
        except:
            # return None
            return 'Error:%s' % (err)

    # Purpose: Geeft startdate maand (mm)
    def get_startdate_Mm(self):
        if 'STARTDATE' in self.headerdict:
            if len(self.headerdict['STARTDATE']) > 2:
                out = int(self.headerdict['STARTDATE'][1])
            else:
                err = 'MissingValue'
        else:
            err = 'MissingKeyword'
        try:
            return out
        except:
            # return None
            return 'Error:%s' % (err)

    # Purpose: Geeft startdate dag (dd)
    def get_startdate_Dd(self):
        if 'STARTDATE' in self.headerdict:
            if len(self.headerdict['STARTDATE']) > 2:
                out = int(self.headerdict['STARTDATE'][2])
            else:
                err = 'MissingValue'
        else:
            err = 'MissingKeyword'
        try:
            return out
        except:
            # return None
```

```
            return 'Error:%s' % (err)

    # Purpose: Of #XYID aanwezig
    def get_xyid_flag(self):
        if 'XYID' in self.headerdict:
            if len(self.headerdict['XYID']) > 2:
                out = True
            else:
                out = False
        try:
            return out
        except:
            return None

    # Purpose: Geeft X coordinaat
    def get_xyid_X(self):
        if 'XYID' in self.headerdict:
            if len(self.headerdict['XYID']) > 0:
                out = self.headerdict['XYID'][1]
            else:
                err = 'MissingValue'
        else:
            err = 'MissingKeyword'
        try:
            return out
        except:
            # return None
            return 'Error:%s' % (err)

    # Purpose: Geeft Y coordinaat
    def get_xyid_Y(self):
        if 'XYID' in self.headerdict:
            if len(self.headerdict['XYID']) > 1:
                out = self.headerdict['XYID'][2]
            else:
                err = 'MissingValue'
        else:
            err = 'MissingKeyword'
        try:
            return out
        except:
            # return None
            return 'Error:%s' % (err)

    # Purpose: Of #ZID aanwezig
    def get_zid_flag(self):
        if 'ZID' in self.headerdict:
            if len(self.headerdict['ZID']) > 0:
                out = True
            else:
                out = False
        else:
            out = False
        try:
            return out
        except:
```

```
            return None

    # Purpose: Geeft Z coordinaat
    def get_zid_Z(self):
        if 'ZID' in self.headerdict:
            if len(self.headerdict['ZID']) > 1:
                out = self.headerdict['ZID'][1]
            else:
                err = 'MissingValue'
        else:
            err = 'MissingKeyword'
        try:
            return out
        except:
            # return None
            return 'Error:%s' % (err)

    # Purpose: Initialiseren interne geheugenstructuur
    # niet nodig
    def init_gef(self):
        True

    def qn2column(self, i_iQtyNumber, get_corrected_depth=False):
        """
       Geeft kolom nummer wat correspondeert met gegeven 'quantity number'.
        Geeft de corrected depth wanneer gevraagd en aanwezig bij opvragen
        quantity number = 1 (penetration depth)
        :param i_iQtyNumber: quantity number volgens GEF definitie
        :param get_corrected_depth: Wanneer TRUE en i_iQtyNumber = 1 word
↪   kolom
        voor quantity number 11 gezocht
        :return: index van waarde in data blok
        """
        try:
            i_iQtyNumber = int(i_iQtyNumber)
            for key, columninfo in
              ↪  self.headerdict['COLUMNINFO'].iteritems():
                if int(columninfo[3]) == i_iQtyNumber:
                    out = key
                if get_corrected_depth and i_iQtyNumber == 1:
                    if int(columninfo[3]) == 11:
                        out = key
            return int(out)
        except:
            # return None
            return 'Error: Quantity Number niet gevonden in GEF file'

    # Purpose: Leest een gegeven Gef bestand en zet alle info in een
      ↪  dictionary
    def read_gef(self, i_sBestandGef):
        EOH = False
        try:
            multipars = ['COLUMNINFO', 'COLUMNVOID', 'MEASUREMENTTEXT',
                         'MEASUREMENTVAR', 'SPECIMENVAR', 'SPECIMENTEXT']
            self.headerdict = {}
            f = open(i_sBestandGef, 'r')
```

```
tel = 0
for line in f.readlines():
    line = re.sub('\r\n', '', line)  # haal alle \r\n aan het
     ↪  einde van de regel weg
    linetmp = re.sub('(^[ \t]*)', '', line)  # remove trailing
     ↪  whitespace
    # if not re.sub('^[\ \t]*$','',line)=='': # lege regels
     ↪  uitsluiten. moet dit in test_gef?
    if not re.sub('^[\ \t]{0,}\n', '', linetmp) == '':  # lege
     ↪  regels uitsluiten. moet dit in test_gef?
        if 1 == 1:  # test1: begint line1 met '#' en komt '='
         ↪  minstens 1x voor
            line = linetmp.split('=', 1)
            par = re.sub('^#([^ \t]*)[ \t]*$', '\\1', line[0])
            # start test
            # if par == 'EOH': deel='data'
            if EOH is False and not re.sub('^[^#].*', '',
                                           linetmp) == '':  # er
                                             ↪  komen regels
                                             ↪  niet begin met
                                             ↪  # voor.
                # einde test
                if len(line) > 1:
                    keyinfo = line[1]
                    keyinfo = re.sub('(^[ \t]*)', '', keyinfo)
                     ↪  # remove trailing whitespace
                    keyinfo = re.sub('([,])([ \t])+', '\\1',
                                     re.sub('([ \t])+([,])', '\\2',
                                            keyinfo))  # haal eerst
                                              ↪  alle witruimte
                                              ↪  (spaties/tabs)
                                              ↪  rond de
                                              ↪  separators
                                              ↪  (',') weg.
                                              ↪  15-10-29
                    if keyinfo != '':
                        # print 'keyinfo: %s'%(keyinfo)
                        keyinfo = keyinfo.split(',')
                    else:
                        keyinfo = None
                else:
                    keyinfo = None
                b = keyinfo
                # print 'b: %s'%(b)
                if par in multipars:  # tabje hoger gezet zodat
                 ↪  conditie alleen geldt als een par bestaat.
                 ↪  2015-10-29
                    if is_number(b[0]):
                      parno = int(b[0]) # Gewijzigd in int voor
                         ↪  eenvoudiger keys in dictionaries
                    else:
                        parno = b[0]
                    # del keyinfo[0]
                    testpar = 'par1'
                    c = []
                    if keyinfo is not None:
```

```
                                for i in b:
                                    e = removetrailers(i)
                                    if is_number(e):
                                        c.append(float(e))
                                    else:
                                        c.append(e)
                                if par not in self.headerdict:
                                    self.headerdict[par] = {parno: c}
                                else:
                                    self.headerdict[par][parno] = c
                            else:
                                parno = None
                    if par == 'EOH':
                        self.headerdict['datablok'] = {}
                        EOH = True
                        self.headerdict[par] = {}
                    if EOH is True and par != 'EOH':
                        tel = tel + 1
                        data = par
                        data = re.sub(';!', '', data)   # einde
                         ↪ dataregel. moet hier een test op?
                        data = re.sub("'", "", data)
                        data = re.sub('"', '', data)
                        data = re.split(';|\ |\t|\n', data)
                        a2 = []
                        for i in data:
                            if is_number(i):
                                a2.append(float(i))
                            else:
                                a2.append(i)
                        self.headerdict['datablok'][tel] = a2
                    if (par != 'EOH') and (par not in multipars)\
                        and (EOH is not True):
                        testpar = 'par2'
                        c = []
                        if b is not None:
                            for i in b:
                                e = removetrailers(i)
                                if is_number(e):
                                    c.append(float(e))
                                else:
                                    c.append(e)
                            self.headerdict[par] = c

        return True

    except IndexError:
        print (
            """%s Headerdict() in UtlGefOpen.py geef IndexError:
                fout bij uitlezen gef""" % os.path.basename(
                i_sBestandGef))
        return False

# Purpose: Of een bestand geplot kan worden
def is_plotable(self):
    return 'datmoetenwenogeensuitzoeken'
```

```
    # Purpose: Of een bepaald aspect van een bestand correct is
    # Parms   : Toegestaan: 'HEADER', 'DATA',
      ↪  'GEF-CPT-Report','GEF-BORE-Report'
    def test_gef(self, i_sAspect):
        return 'datmoetenwenogeensuitzoeken'


def main(filename):
    # parse arguments using optparse or argparse or ...
    myGef = Gef2OpenClass()
    myGef.read_gef(filename)
    data = myGef.headerdict
    keys = ['COLUMNINFO', 'datablok', 'TESTID', 'XYID', 'ZID']
    return (data[keys[0]],data[keys[1]],[data[keys[2]][0],data[keys[3]][0],
            data[keys[3]][1],data[keys[3]][2],data[keys[4]][1]])


if __name__ == '__main__':
    # This is used for debugging. Using this separated structure makes it
      ↪  much
    # easier to debug using standard Python development tools.
    import sys
    main(sys.argv[1:])
```

F

Information

Material constants Compaction / Liquefaction model

Sand type	Relative density [-]	c_1	c_2	D_1	D_2	Source
Seymen	0.34	6.54	0.15	1.01	0.153	Sawicki [44]
Golcuk	0.41	9.26	0.25	2.28	0.108	
Eregli	0.38	9.52	0.17	1.6	0.105	
Derince	0.48	7.14	0.28	1.97	0.14	
Fine sand	0.91	7.52	0.03	0.212	0.133	Sawicki and Śliwiński [45]
	0.50	12.35	0.06	0.786	0.081	
	0.30	14.93	0.07	0.99	0.067	
Hostun2 sand	0.72	6.71	0.05	0.339	0.149	
	0.32	8.55	0.10	0.84	0.117	
	0.08	14.50	0.06	0.815	0.069	
Kozienice sand	medium dense	13.18	0.14	1.85	0.076	Sawicki and Świdziński [46]
	dense	4.87	1.26	6.14	0.205	
Silica sand	medium dense	8.7	0.2	1.74	0.14	
Lubiatowo sand	dense	7.52	0.19	1.41	0.133	Sawicki and Świdziński [47]

Table F.1: Values of the material constants c1, c2, D1 and D2 of the C/L model for cyclic shear for different types of sand and varying relative density obtained from literature. Values of the material constants apply to a strain unit 10^{-3}. Table is created by Meijers [34].

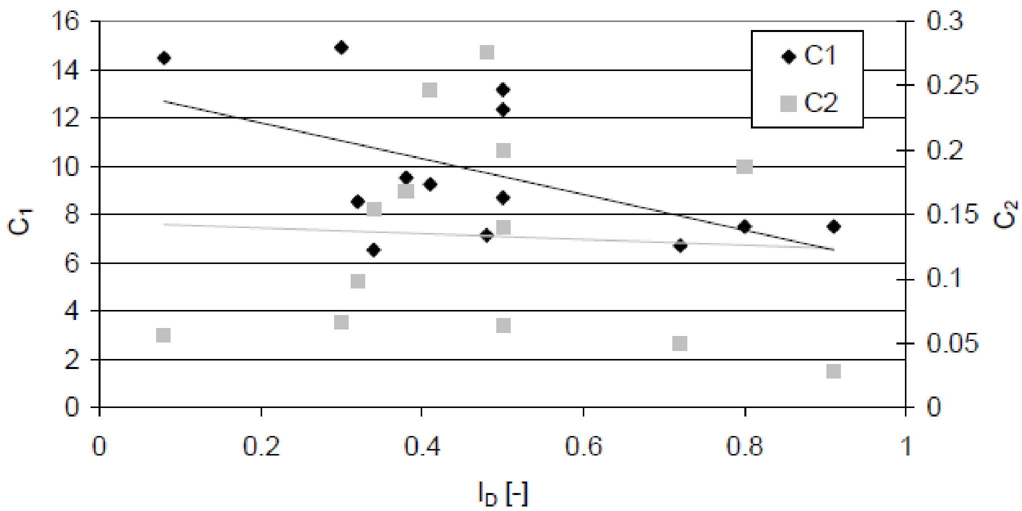

Figure F.1: Material constants c_1 and c_2 plotted against the relative density (D_R). Values of the material constants apply to a strain unit 10^{-3} [34].

Operational tolerances for crane rail tracks

Table 1 — Tolerance classes

Tolerance class	Limits of travelling and traversing distance km
1	$50\,000 \leq L$
2	$10\,000 \leq L < 50\,000$
3	$L < 10\,000$, for stationary erected tracks
4	Temporarily erected tracks for building and erection purposes
NOTE L is calculated as the product of the normal travel speed and the specified working time of the relevant travel/traverse mechanism, either by application of customer specified values or through reference to the classification of the mechanism (see ISO 4301-1).	

Table F.2: Table 1 in ISO 12488-1: the International Standard for Cranes - Tolerances for wheels and travel and traversing tracks [26].

Table 7 — Operational tolerances for travel and traverse tracks and crane and crab wheels of tolerances classes 1 to 4

Tolerance parameter			Tolerance				
Symbol	Description with respect to this table	Graphical representation	Class 1	Class 2	Class 3	Class 4	Unit
A_{w1}	Tolerance of span S of crane rails related to rail centre at each point of travelling track	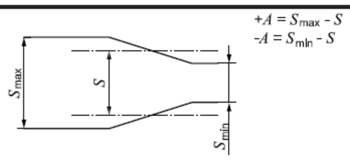	±10 Valid for all spans $S \leq 16$ m ±[10+ 0,25(S–16)] S in metres, valid for all spans $S > 16$ m	±16 Valid for all spans $S \leq 16$ m ±[16+ 0,25(S–16)] S in metres, valid for all spans $S > 16$ m	±25 Valid for all spans $S \leq 16$ m ±[25+ 0,25(S–16)] S in metres, valid for all spans $S > 16$ m	±40 Valid for all spans $S \leq 16$ m ±[40+ 0,25(S–16)] S in metres, valid for all spans $S > 16$ m	mm
B_{w1}	Tolerance of horizontal straightness of rail head at each point of travelling track	Position of crane rail in ground plan 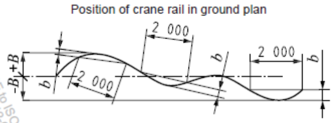	±10	±20	±40	±80	mm
E_{w1}	Tolerance of height related to opposite measuring points at right angles at each point of travelling track	Height of traversing track (lateral slope) 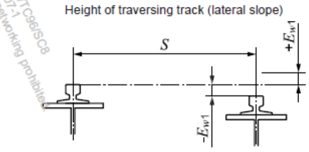	±10	±20	±40	±80	mm
A_{w2}	Tolerance of span S of crab rails related to rail centre at each point of traversing track	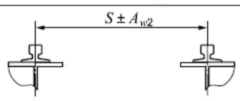	±6 Valid for all spans $S \leq 16$ m	±10 Valid for all spans $S \leq 16$ m	±16 Valid for all spans $S \leq 16$ m	±25 Valid for all spans $S \leq 16$ m	mm

Table F.3: Table 7 in ISO 12488-1: the International Standard for Cranes - Tolerances for wheels and travel and traversing tracks [26].

Infographic Rotterdam World Gateway container terminal

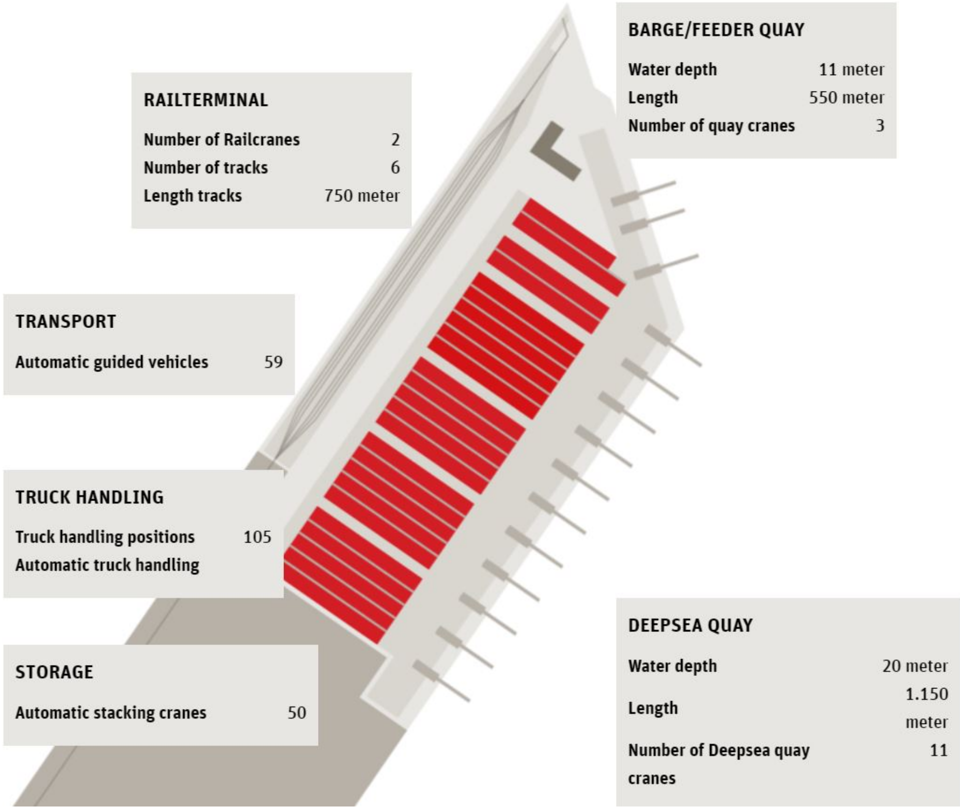

Figure F.2: Facts and numbers about the RWG container terminal phase 1 [8]. The area indicated in red are ASC rail tracks 3 to 27.

Infographic automatic stacking cranes
[6]

Building a fully automated solution.

End-to-end efficiency.
You can build a fully automated container terminal with the latest Kalmar ASC system at its heart. By adding Kalmar AutoShuttles™ to move containers between the quay and stacks, and Kalmar Automated Truck Handling System on the land side, you will have a complete automated solution that will operate in a safe and efficient manner.

Pre-integrated for instant use.
The Kalmar Terminal Logistics System (TLS) is the most flexible equipment control system on the market, as it can be integrated with any type of terminal operating system (TOS). Our TLS ensures that your automated equipment and TOS work together optimally at all times. The TLS comes fully pre-integrated with the equipment and Navis N4 TOS, meaning that much less time is needed for on-site testing.

Kalmar Insight

Turn your data into actionable insights.
Data is by far the most valuable asset when it comes to optimising your operations. Kalmar Insight takes the vast quantities of data you produce from multiple sources and turns it into actionable insights. With a real-time overview of your terminal's productivity and performance, you can take instant action that delivers instant impact.

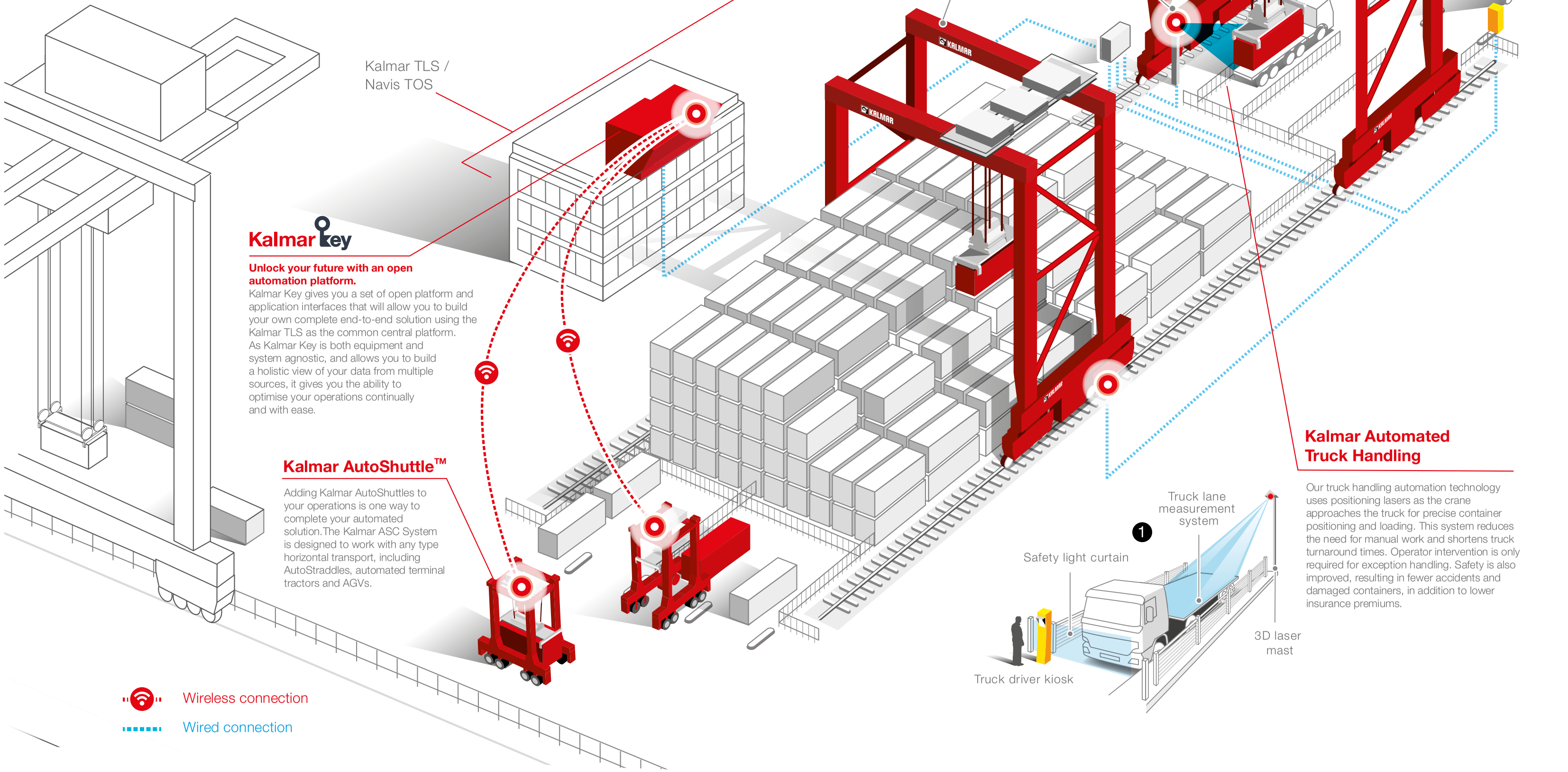

Kalmar Key

Unlock your future with an open automation platform.
Kalmar Key gives you a set of open platform and application interfaces that will allow you to build your own complete end-to-end solution using the Kalmar TLS as the common central platform. As Kalmar Key is both equipment and system agnostic, and allows you to build a holistic view of your data from multiple sources, it gives you the ability to optimise your operations continually and with ease.

Kalmar AutoShuttle™

Adding Kalmar AutoShuttles to your operations is one way to complete your automated solution.The Kalmar ASC System is designed to work with any type horizontal transport, including AutoStraddles, automated terminal tractors and AGVs.

Kalmar Automated Truck Handling

Our truck handling automation technology uses positioning lasers as the crane approaches the truck for precise container positioning and loading. This system reduces the need for manual work and shortens truck turnaround times. Operator intervention is only required for exception handling. Safety is also improved, resulting in fewer accidents and damaged containers, in addition to lower insurance premiums.